ISSN 0042-8469
e-ISSN 2217-4753
UDC 623 + 355/359

Vol. 74, Issue 1

2026

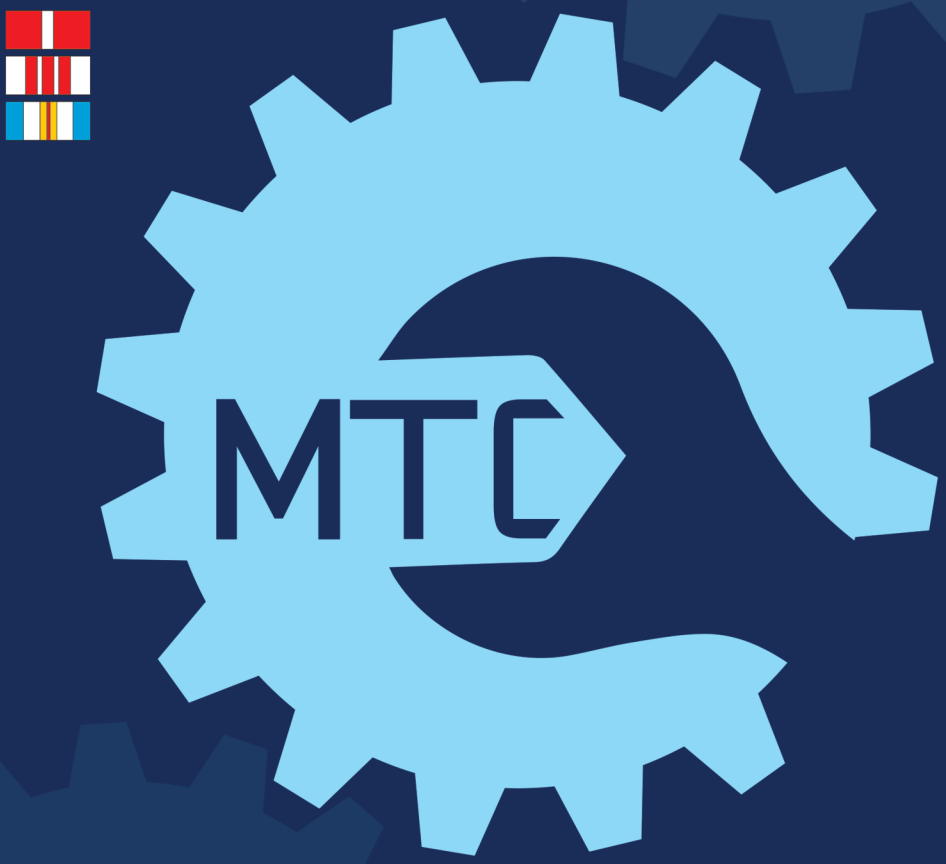

SCIENTIFIC JOURNAL OF THE MINISTRY OF DEFENCE AND THE SERBIAN ARMED FORCES

MILITARY TECHNICAL COURIER

www.vtg.mod.gov.rs

ISSN 0042-8469
e-ISSN 2217-4753
UDC 623 + 355/359

Vol. 74, Issue 1

2026

NAUČNI ČASOPIS MINISTARSTVA ODBRANE REPUBLIKE SRBIJE

VOJNOTEHNIČKI GLASNIK

www.vtg.mod.gov.rs

OWNERS:
Ministry of Defence and Serbian Armed Forces
PUBLISHER:
University of Defence in Belgrade, Military Academy
EDITORIAL TEAM (the pages of the Editorial Team's members in ORCID iD, Google Scholar, Web of Science ResearcherID, Scopus Author ID, and РИНЦ can be accessed at http://www.vtg.mod.gov.rs/editorial-team.html):
EDITOR IN CHIEF:
Dr. Dragan Trifković, University of Defence in Belgrade, Military Academy, Belgrade, Serbia,
e-mail: dragan.trifkovic@va.mod.gov.rs
EDITOR:
Dr. Vladan Anicijevic, University of Defence in Belgrade, Military Academy, Belgrade, Serbia,
e-mail: vojnotehnicki.glasnik@mod.gov.rs
Dr. Predrag Dobratic, University of Defence in Belgrade, Military Academy, Belgrade, Serbia,
e-mail: vojnotehnicki.glasnik@mod.gov.rs
Editor for Mathematics and Mechanics
Dr. Rale Nikolić, University of Defence in Belgrade, Military Academy, Belgrade, Serbia
Editor for Electronics, Telecommunications and Information Technology
Dr. Boban Bondžulić, University of Defence in Belgrade, Military Academy, Belgrade, Serbia
Editor for Mechanical Engineering
Dr. Branimir Krstić, University of Defence in Belgrade, Military Academy, Belgrade, Serbia
Editor for Materials and Chemical Technologies
Dr. Mihael Bučko, University of Defence in Belgrade, Military Academy, Belgrade, Serbia
EDITORIAL BOARD:
Dr. Gradimir Milovanović, Serbian Academy of Sciences and Arts, Belgrade, Serbia,
Dr. Ji-Huan He, Soochow University, College of Textile and Clothing Engineering, Soochow, China,
Dr. Madjid Tavana, La Salle University, Business Systems and Analytics Department, Philadelphia, USA,
Dr. Shankar Chakraborty, Jadavpur University, Department of Production Engineering, Kolkata, India,
Dr. Radu-Emil Precup, Politehnica University of Timisoara, Timisoara, Romania,
Dr. Jurgita Antuchevičienė, Vilnius Gediminas Technical University, Faculty of Civil Engineering, Vilnius, Lithuania,
Dr. Morteza Yazdani, ESIC Business and Marketing School, Madrid, Spain,
Dr. Prasenjit Chatterjee, MCKV Institute of Engineering, Department of Mechanical Engineering, Howrah, India,
Dr. Željko Stević, University of East Sarajevo, Faculty of Transportation, Doboj, Republic of Srpska, Bosnia and Herzegovina,
Dr. Hamed Fazlollahtabar, Damghan University, Department of Industrial Engineering, Damghan, Iran,
Dr. Jarosław Wątróbski, University of Szczecin, Faculty of Economics, Finance and Management, Szczecin, Poland,
Dr. Cristiano Fragassa, University of Bologna, Department of Industrial Engineering, Bologna, Italy,
Dr. Wojciech Sałabun, West Pomeranian University of Technology in Szczecin, Faculty of Computer Science and Information Technology, Szczecin, Poland,
Dr. Ieva Meidutė-Kavaliauskienė, General Jonas Žemaitis Military Academy of Lithuania, Research Group on Logistics and Defense Technology Management, Vilnius, Lithuania,
Dr. Šárka Mayerová, University of Defence in Brno, Department of Mathematics and Physics, Brno, Czech Republic,
Dr. Fatih Ecer, Afyon Kocatepe University, Faculty of Economics and Administrative Sciences, Afyonkarahisar, Turkey,
Dr. Ernesto D.R. Santibanez Gonzalez, Universidad de Talca, Talca, Chile,
Dr. Dragan Marinković, Technical University Berlin, Faculty of Mechanical and Transport Systems, Berlin, Germany,
Dr. Stefano Valvano, Kore University of Enna, Department of Aerospace Engineering, Enna, Italy,
Dr. Rafal Madonski, Jinan University, Energy Electricity Research Center, Guangzhou, China,
Dr. Milenko Andrić, University of Defence in Belgrade, Military Academy, Belgrade, Serbia,
Dr. Samarjit Kar, National Institute of Technology, Department of Mathematics, Durgapur, India,
Dr. Rosen Mitrev, Technical University of Sofia, Sofia, Bulgaria,
Dr. Bojan Milanović, University of Defence in Belgrade, Military Academy, Belgrade, Serbia,
Dr. Irik Mukhametzyanov, Ufa State Petroleum Technological University, Ufa, Russian Federation,
Dr. Pavel Otrisal, Palacký University, Olomouc, Czech Republic,
Dr. Radovan Radovanović, University of Criminal Investigation and Police Studies, Belgrade, Serbia,
Dr. Boško Rašuo, University of Belgrade, Faculty of Mechanical Engineering, Belgrade, Serbia,
Dr. Saad Aslam, Sunway University, Kuala Lumpu, Malaysia,
Dr. Nasreen Kausar, Yildiz Technical University, Istanbul, Turkey

VLASNICI:
Ministarstvo odbrane i Vojska Srbije
IZDAVAČ:
Univerzitet odbrane u Beogradu, Vojna akademija
UREDNIŠTVO (stranice članova uredništva u ORCID iD-u, Google Scholar-u, Web of Science ResearcherID-u, Scopus Author ID-u i RINC-u dostupni su na http://www.vtg.mod.gov.rs/urednistvo.html):
GLAVNI I ODGOVORNI UREDNIK:
Dr Dragan Trifković, Univerzitet odbrane u Beogradu, Vojna akademija, Beograd, Srbija,
e-mail: dragan.trifkovic@va.mod.gov.rs
UREDNIK:
Dr Vladan Anićijević, Univerzitet odbrane u Beogradu, Vojna akademija, Beograd, Srbija,
e-mail: vojnotehnicki.glasnik@mod.gov.rs
Dr Predrag Dobratić, Univerzitet odbrane u Beogradu, Vojna akademija, Beograd, Srbija,
e-mail: vojnotehnicki.glasnik@mod.gov.rs
Urednik za oblast matematike i mehanike
Dr Rale Nikolić, Univerzitet odbrane u Beogradu, Vojna akademija, Beograd, Srbija
Urednik za oblast elektronike, telekomunikacija i informacionih tehnologija
Dr Boban Bondžulić, Univerzitet odbrane u Beogradu, Vojna akademija, Beograd, Srbija
Urednik za oblast mašinstva
Dr Branimir Krstić, Univerzitet odbrane u Beogradu, Vojna akademija, Beograd, Srbija
Urednik za oblast materijala i hemijskih tehnologija
Dr Mihael Bučko, Univerzitet odbrane u Beogradu, Vojna akademija, Beograd, Srbija
UREĐIVAČKI ODBOR:
Dr Gradimir Milovanović, Srpska akademija nauka i umetnosti, Beograd, Srbija,
Dr Đi-Huan Hi, Univerzitet Sudžou, Fakultet za tekstilnu i odevnu tehniku, Sudžou, Kina,
Dr Mađid Tafana, Univerzitet La Sal, Odeljenje za poslovne sisteme i analitiku, Filadelfija, SAD,
Dr Šankar Čakraborti, Univerzitet Jadavpur, Odeljenje za proizvodno mašinstvo, Kalkuta, Indija,
Dr Radu-Emil Prekup, Univerzitet Politehnika u Temišvaru, Temišvar, Rumunija,
Dr Jurgita Antucheviči, Tehnički univerzitet Gediminas u Vilnjusu, Građevinski fakultet, Vilnjus, Litvanija,
Dr Srećko Joksimović, Univerzitet u Južnoj Australiji, Adelejd, Australija,
Dr Morteza Jazdani, Fakultet za biznis i marketing ESIC, Madrid, Španija,
Dr Prasendžit Čaterdži, Institut za inženjerstvo MCKV, Odeljenje za mašinstvo, Hovrah, Indija,
Dr Željko Stević, Univerzitet u Istočnom Sarajevu, Saobraćajni fakultet, Doboj, Republika Srpska, BiH,
Dr Hamed Fazlolahtabar, Univerzitet Damgan, Odeljenje za industrijsko inženjerstvo, Damgan, Iran,
Dr Jaroslav Vatrobski, Univerzitet u Ščećinu, Fakultet za ekonomiju, finansije i menadžment, Ščećin, Poljska,
Dr Kristiano Fragasa, Univerzitet u Bolonji, Odeljenje za industrijsko inženjerstvo, Bolonja, Italija,
Dr Vojčeh Salabun, Zapadnopomeranski tehnološki univerzitet u Ščećinu, Fakultet računarskih nauka i informacionih tehnologija, Ščećin, Poljska,
Dr Ieva Meidute-Kavaliauskiene, Vojna akademija Litvanije „General Jonas Žemaitis“, Viljnus, Litvanija,
Dr Šarka Majerova, Univerzitet odbrane u Brnu, Odeljenje za matematiku i fiziku, Brno, Češka Republika,
Dr Fatih Ecer, Univerzitet Afion Kođatepe, Fakultet za ekonomiju i administrativne nauke, Afionkarahisar, Turska,
Dr Ernesto D.R. Santibanez Gonzalez, Univerzitet u Talki, Talka, Čile,
Dr Dragan Marinković, Tehnički univerzitet u Berlinu, Fakultet za mašinske i transportne sisteme, Berlin, Nemačka,
Dr Stefano Valvano, Univerzitet Kore u Eni, Odeljenje za vazduhoplovni inženjering, Ena, Italija,
Dr Rafal Madonski, Univerzitet Đinan, Centar za istraživanje električne energije, Guangdžou, Kina,
Dr Milenko Andrić, Univerzitet odbrane u Beogradu, Vojna akademija, Beograd, Srbija,
Dr Samardžit Kar, Nacionalni institut za tehnologiju, Odeljenje za matematiku, Durgapur, Indija,
Dr Rosen Mitrev, Tehnički univerzitet u Sofiji, Sofija, Bugarska,
Dr Bojan Milanović, Univerzitet odbrane u Beogradu, Vojna akademija, Beograd, Srbija,
Dr Irik Muhamedzjanov, Državni naftni tehnološki univerzitet u Ufi, Ufa, Ruska Federacija,
Dr Pavel Otrisal, Univerzitet Palacki, Olomouc, Češka Republika,
Dr Radovan Radovanović, Kriminalističko-policijski univerzitet, Beograd, Srbija,
Dr Boško Rašuo, Univerzitet u Beogradu, Mašinski fakultet, Beograd, Srbija,
Dr Saad Aslam, Univerzitet Sunvai, Kuala Lumpur, Malezija,
Dr Nasrin Kausar, Tehnički univerzitet Jildiz, Fakultet umetnosti i nauke, Turska

C O N T E N T S / S A D R Ž A J

Cryptography using the Laplace transform for the Serbian language

Tatjana Mirković[a], *Nataša* Ćirović[b]

[a] School of Electrical Engineering, University of Belgrade (student)
e-mail: mt215030p@student.etf.bg.ac.rs
ORCID iD: https://orcid.org/0000-0002-8519-1955

[b] School of Electrical Engineering, University of Belgrade
e-mail: natasa@etf.bg.ac.rs
ORCID iD: https://orcid.org/0000-0001-8454-6688

https://doi.org/10.5937/vojtehg74-59148

FIELD: mathematics
ARTICLE TYPE: original scientific paper

Abstract:

Introduction/purpose: In this paper, the authors develop a new mathematical method for cryptography. The procedure was performed for messages written in the Serbian language, which consists of 30 phonemes.

Methods: The standard expansion of the inverse trigonometric function in a Taylor series was used. The Laplace transform was applied to encrypt the plaintext, while the corresponding inverse Laplace transform was used for decryption.

Results: A new cryptographic algorithm has been written to encrypt and decrypt a text message written in Serbian letters.

Conclusions: In the paper, the authors presented a new algorithm in which the Laplace transform was used for the encryption and decryption of a text message. The message is written in Serbian in Cyrillic letters.

Key words: cryptography, Laplace transform, inverse trigonometric function, Taylor series.

Introduction

Cryptography is a field of mathematics that deals with hiding secret text messages. It dates back to the time of Caesar, but most of the scientific work is devoted to modern digital cryptography. Numerous authors have dealt with this field, for example: Bhuvaneswari (2020), Gencoglu (2016), Gencoglu et al. (2019), Martin (2012), Delfs and Knebl (2007). Recently, several papers have been published in which the Laplace transform is implemented in cryptographic algorithms, for example: Al-Azzani et al. (2021), Briones (2018), Gencoglu (2017, 2019a), Gupta and Mishra (2014),

Hiwarekar (2012), Nagalakshmi et al. (2019, 2020). One of these works (Gencoglu, 2019a) motivated this paper. Namely, in the paper (Gencoglu, 2019a) the authors gave an algorithm for text messages in Turkish. In this paper, we have provided a new algorithm for encryption and decryption of text written in Serbian.

Considering that the mathematical model uses the Laplace transform, we first present the fundamental theory of this topic.

Definition 1. *Suppose that f is a real or complex-valued function of the time variable $t > 0$ and s is a real or complex parameter. We define the Laplace transform of f as follows:*

$$F(s) = \mathscr{L}\{f(t)\}(s) = \int_0^\infty e^{-st} f(t)\, dt,$$

whenever this integral converges for some values of s.

One of the most basic and useful properties of the Laplace operator $\mathscr{L}$ is that of linearity, namely, if $f_1 \in L$ for $Re(s) > \alpha$, $f_2 \in L$ for $Re(s) > \beta$, then $f_1 + f_2 \in L$ for $Re(s) > \max\{\alpha, \beta\}$, and

$$\mathscr{L}\{C_1 f_1(t) + C_2 f_2(t)\} = C_1 F_1(s) + C_2 F_2(s),$$

for arbitrary constants C_1 and C_2.

Definition 2. *If $\mathscr{L}\{f(t)\}(s) = F(s)$, then the inverse Laplace transform is denoted by*

$$\mathscr{L}^{-1}\{F(s)\} = f(t), \quad t \geq 0,$$

and it maps the Laplace transform of a function back to the original function.

Additionally, $\mathscr{L}^{-1}$ is linear, that is

$$\mathscr{L}^{-1}\{C_1 F_1(s) + C_2 F_2(s)\} = C_1 f_1(t) + C_2 f_2(t),$$

if $\mathscr{L}\{f_1(t)\}(s) = F_1(s)$ and $\mathscr{L}\{f_2(t)\}(s) = F_2(s)$, for arbitrary constants C_1 and C_2.

In our result we will use the values of Laplace and inverse Laplace transform for the function t^n, and these are $\mathscr{L}\{t^n\} = \frac{n!}{s^{n+1}}$; $\mathscr{L}^{-1}\left\{\frac{n!}{s^{n+1}}\right\} = t^n$.

Proposed mathematical model for encryption and decryption text message

In this section we present new algorithms for text encryption and decryption. The algorithm uses the Taylor series expansion of the arctg function, and then applies the Laplace transform to this series. We provide a detailed explanation of the text encryption.

Encryption:

Consider Tayler's expansion of these functions:

$$\operatorname{arctg} t = \int_0^t \frac{1}{1+t^2} dt = \int_0^t \left(\sum_{n=0}^{+\infty} (-1)^n t^{2n} \right) dt$$
$$= \sum_{n=0}^{+\infty} (-1)^n \int_0^t t^{2n} dt = \sum_{n=0}^{+\infty} (-1)^n \frac{t^{2n+1}}{2n+1}.$$

Each letter of the message is converted to an integer. M_l, $l = 0, ..., 29$, whereby $M_l = 0$ for $l > 29$. Thus, we must indicate that the letters take on the integer values, i.e. A = 0, B = 1, V = 2, Š = 29.

Let us consider

$$t \cdot \operatorname{arctg} rt = \sum_{n=0}^{+\infty} (-1)^n \frac{r^{2n+1} t^{2n+2}}{2n+1},$$

where r is a positive constant.

Using the previous Taylor series for $r = 2$, we observe the function:

$$f(t) = M_0 \tfrac{2t^2}{1} - M_1 \tfrac{2^3 t^4}{3} + M_2 \tfrac{2^5 t^6}{5} - M_3 \tfrac{2^7 t^8}{7} + ... + (-1)^{l-1} M_{l-1} \tfrac{2^{2l-1} t^{2l}}{2l-1}$$
$$= \sum_{n=0}^{l-1} M_n (-1)^n \tfrac{2^{2n+1} t^{2n+2}}{2n+1}.$$

Taking Laplace transformation to both sides of Taylor series we get the following.

$$\mathscr{L}\{f(t)\}(s)$$
$$= M_0 \tfrac{2 \cdot 2!}{1 s^3} - M_1 \tfrac{2^3 \cdot 4!}{3 s^5} + M_2 \tfrac{2^5 \cdot 6!}{5 s^7} - M_3 \tfrac{2^7 \cdot 8!}{7 s^9} + ... + (-1)^{l-1} M_{l-1} \tfrac{2^{2l-1}(2l)!}{(2l-1) s^{2l+1}}.$$

Let $\Phi_i = M_i \frac{2^{2i+1}(2i+2)!}{(2i+1)}$, $i = 0, 1, ..., l-1$.

The last relation takes a simpler form

$$\mathscr{L}\left\{f\left(t\right)\right\}\left(s\right)=\frac{\Phi_0}{s^3}-\frac{\Phi_1}{s^5}+\frac{\Phi_2}{s^7}-\frac{\Phi_3}{s^9}+...+\left(-1\right)^{l-1}\frac{\Phi_{l-1}}{s^{2l+1}}.$$

We transform the previous sum by multiplying each summand by $b_i=\frac{1}{(2i+2)!}$, $i=0,1,...,l-1$:

$$F_b(s)=\frac{b_0\Phi_0}{s^3}-\frac{b_1\Phi_1}{s^5}+\frac{b_2\Phi_2}{s^7}-\frac{b_3\Phi_3}{s^9}+...+\left(-1\right)^{l-1}\frac{b_{l-1}\Phi_{l-1}}{s^{2l+1}}.$$

Let us introduce the tags $R_i=\left\lfloor b_i\cdot\Phi_i\right\rfloor$, $i=0,1,2...,l-1$, thus getting

$$G_b(s)=\frac{R_0}{s^3}-\frac{R_1}{s^5}+\frac{R_2}{s^7}-\frac{R_3}{s^9}+...+\left(-1\right)^{l-1}\frac{R_{l-1}}{s^{2l+1}}. \tag{1}$$

The letters of the cipher text are obtained from the relation $M_i'=R_i-30k_i$, $i=0,1,2...,l-1$, and the key is given with $k_i=\frac{R_i-M_i'}{30}$, $i=0,1,2...,l-1$.

Decryption:

The reader receives the message as cipher text in terms of M_i; $i=0,1,...,l-1$, that is

$$R_i=30k_i+M_i'.$$

From (1), we have

$$G_b(s)=\frac{R_0}{s^3}-\frac{R_1}{s^5}+\frac{R_2}{s^7}-\frac{R_3}{s^9}+...+\left(-1\right)^{l-1}\frac{R_{l-1}}{s^{2l+1}}.$$

Multiplying each summand by b_i^{-1}, $i=0,1,...,l-1$, gives

$$\frac{b_0^{-1}R_0}{s^3}-\frac{b_1^{-1}R_1}{s^5}+\frac{b_2^{-1}R_2}{s^7}-\frac{b_3^{-1}R_3}{s^9}+...+\left(-1\right)^{l-1}\frac{b_{l-1}^{-1}R_{l-1}}{s^{2l+1}},$$

i.e.

$$\mathscr{L}\left\{f\left(t\right)\right\}\left(s\right)=\frac{\Phi_0}{s^3}-\frac{\Phi_1}{s^5}+\frac{\Phi_2}{s^7}-\frac{\Phi_3}{s^9}+...+\left(-1\right)^{l-1}\frac{\Phi_{l-1}}{s^{2l+1}}.$$

By taking the inverse Laplace transform to both sides we obtain

$$\mathscr{L}^{-1}\mathscr{L}\left\{f\left(t\right)\right\}\left(s\right)=\mathscr{L}^{-1}\left\{\frac{\Phi_0}{s^3}-\frac{\Phi_1}{s^5}+\frac{\Phi_2}{s^7}-\frac{\Phi_3}{s^9}+...+\left(-1\right)^{l-1}\frac{\Phi_{l-1}}{s^{2l+1}}\right\},$$

we obtain

$$f(t) = \Phi_0 \frac{t^2}{2!} - \Phi_1 \frac{t^4}{4!} + \Phi_2 \frac{t^6}{6!} - \Phi_3 \frac{t^8}{8!} + ... + (-1)^{l-1} \Phi_{l-1} \frac{t^{2l}}{(2l)!}.$$

The values of the plain text are obtained by using the formula:

$$M_i = \frac{(2i+1)\,\Phi_i}{2^{2i+1}\,(2i+2)!}, \quad i = 0, 1, ..., l-1.$$

The algorithms of encryption and decryption

The algorithm of encryption:

1. Convert the plain text to an integer number;
2. Embed the integer numbers as the coefficients of the Taylor series of the function $t \operatorname{arctg} rt$, $r \in N$;
3. Take the Laplace transform to both sides of the Taylor series;
4. The embedding coefficient of the Laplace transform is $\Phi_i = M_i \frac{2^{2i+1}(2i+2)!}{(2i+1)}, \quad i = 0, 1, ..., l-1$;
5. Multiply Φ_i by coefficients $b_i = \frac{1}{(2i+2)!}$, $i = 0, 1, ..., l-1$, and take the floor of these numbers to obtain R_i, $i = 0, 1, ..., l-1$;
6. Use the relation $M_i' = R_i - 30k_i$, $i = 0, 1, 2..., l-1$, to obtain the cipher text. The key is $k_i = \frac{R_i - M_i'}{30}, \quad i = 0, 1, ..., l-1$.

Algorithm of decryption:

1. Use the relation $R_i = 30k_i + M_i'$, $i = 0, 1, 2..., l-1$, to obtain R_i, from the cipher text;
2. Multiply coefficients R_i by b_i^{-1}, $i = 0, 1, ..., l-1$, to obtain Φ_i, $i = 0, 1, ..., l-1$;
3. Take the inverse of the Laplace transform to both sides of the Taylor series;
4. Use the relation $M_i = \frac{(2i+1)\Phi_i}{2^{2i+1}(2i+2)!}$, $i = 0, 1, 2..., l-1$, to obtain the plain text.

Application

We apply the above algorithm to a specific example for the Cyrillic alphabet. The Serbian word ЋИРИЛИЦА is first translated into a corrected message, after which the inverse procedure is performed

We assign values from 0 to 29 to each letter of this word, respectively, according to the alphabet, because the Serbian language consists of 30 letters.

Encryption:

$M_0 = 22;\ M_1 = 9;\ M_2 = 19;\ M_3 = 9;\ M_4 = 12;\ M_5 = 9;\ M_6 = 26;\ M_7 = 0.$

We apply the starting function from the algorithm:

$$f(t) = \operatorname{arctg} t = \sum_{n=0}^{+\infty} (-1)^n \frac{t^{2n+1}}{2n+1},$$

i.e.

$$t \operatorname{arctg} 2t = \sum_{n=0}^{+\infty} (-1)^n \frac{2^{2n+1} t^{2n+2}}{2n+1}.$$

We insert the given coefficients into the upper function:

$$f(t) = Mt \operatorname{arctg} 2t = \sum_{n=0}^{+\infty} (-1)^n \frac{2^{2n+1} t^{2n+2}}{2n+1} =$$
$$= 22\frac{2^1 t^2}{1} - 9\frac{2^3 t^4}{3} + 19\frac{2^5 t^6}{5} - 9\frac{2^7 t^8}{7} + 12\frac{2^9 t^{10}}{9} - 9\frac{2^{11} t^{12}}{11} + 26\frac{2^{13} t^{14}}{13} - 0\frac{2^{15} t^{16}}{15}$$

We implement the step from the algorithm in which the Laplace transform is applied:

$$\mathscr{L}\{f(t)\}(s)$$
$$= 22\frac{2^1 2!}{1 \cdot s^3} - 9\frac{2^3 4!}{3 \cdot s^5} + 19\frac{2^5 6!}{5 \cdot s^7} - 9\frac{2^7 8!}{7 \cdot s^9} + 12\frac{2^9 10!}{9 \cdot s^{11}} - 9\frac{2^{11} 12!}{11 \cdot s^{13}} + 26\frac{2^{13} 14!}{13 \cdot s^{15}} - 0\frac{2^{15} 16!}{15 \cdot s^{17}}.$$

From there, we obtained the coefficients $\Phi_0 = \frac{22 \cdot 2^1 \cdot 2!}{1}$; $\Phi_1 = \frac{9 \cdot 2^3 \cdot 4!}{3}$; $\Phi_2 = \frac{19 \cdot 2^5 \cdot 6!}{5}$; $\Phi_3 = \frac{9 \cdot 2^7 \cdot 8!}{7}$; $\Phi_4 = \frac{12 \cdot 2^9 \cdot 10!}{9}$; $\Phi_5 = \frac{9 \cdot 2^{11} \cdot 12!}{11}$; $\Phi_6 = \frac{26 \cdot 2^{13} \cdot 14!}{13}$; $\Phi_7 = \frac{0 \cdot 2^{15} \cdot 16!}{15}$.

We take the coefficients $b_i = \frac{1}{(2i+2)!},\ i = 0, 1, ..., l-1$, and multiply them by the coefficients Φ_i, so we obtain:

$$\mathscr{L}\{bf(t)\}(s)$$
$$= 22\frac{2^1}{1 \cdot s^3} - 9\frac{2^3}{3 \cdot s^5} + 19\frac{2^5}{5 \cdot s^7} - 9\frac{2^7}{7 \cdot s^9} + 12\frac{2^9}{9 \cdot s^{11}} - 9\frac{2^{11}}{11 \cdot s^{13}} + 26\frac{2^{13}}{13 \cdot s^{15}} - 0\frac{2^{15}}{15 \cdot s^{17}}.$$

We introduce the coefficients $R_i = \lfloor b_i \cdot \Phi_i \rfloor,\ i = 0, 1, ..., l-1$, from which we obtain:

$R_0 = 44$; $R_1 = 24$; $R_2 = \left\lfloor \frac{608}{5} \right\rfloor = 121$; $R_3 = \left\lfloor \frac{1152}{7} \right\rfloor = 164$; $R_4 = \left\lfloor \frac{6144}{9} \right\rfloor = 682$; $R_5 = \left\lfloor \frac{18432}{11} \right\rfloor = 1675$; $R_6 = \left\lfloor \frac{212992}{13} \right\rfloor = 16384$; $R_7 = 0$. We represent the numbers R_i, $i = 0, 1, ..., l-1$, in the form $R_i = 30k_i + M_i'$:

$$\begin{aligned} 44 &= 1 \cdot 30 + 14; \\ 24 &= 0 \cdot 30 + 24; \\ 121 &= 4 \cdot 30 + 1; \\ 164 &= 5 \cdot 30 + 14; \\ 682 &= 22 \cdot 30 + 22; \\ 1675 &= 55 \cdot 30 + 25; \\ 16384 &= 546 \cdot 30 + 4; \\ 0 &= 0 \cdot 30 + 0. \end{aligned}$$

The coefficients M_i; $i = 0, 1, ..., l-1$, determine the letters in the cipher message, and the values k_i, $i = 0, 1, ..., l-1$, determine the key. In this way, the word ĆIRILICA is translated into the word МФБМЋХДА, and the key is given by: $k_0 = 1$; $k_1 = 0$; $k_2 = 4$; $k_3 = 5$; $k_4 = 22$; $k_5 = 55$; $k_6 = 546$; $k_7 = 0$.

Decryption:

The reader receives the message МФБМЋХДА, and also the key $k_0 = 1$; $k_1 = 0$; $k_2 = 4$; $k_3 = 5$; $k_4 = 22$; $k_5 = 55$; $k_6 = 546$; $k_7 = 0$.

Firstly, we assign values from 0 to 29 to each letter of the cipher message:

$M_0' = 14$; $M_1' = 24$; $M_2' = 1$; $M_3' = 14$; $M_4' = 22$; $M_5' = 25$; $M_6' = 4$; $M_7' = 0$.

In the second step of the algorithm, we determine the coefficients:

$$R_i = 30k_i + M_i' :$$

$R_0 = 44$; $R_1 = 24$; $R_2 = 121$; $R_3 = 164$; $R_4 = 682$; $R_5 = 1675$; $R_6 = 16384$; $R_7 = 0$.

We multiply these coefficients by the coefficients $b_i^{-1} = (2i+2)!$, $i = 0, 1, ..., l-1$, to determine the coefficients Φ_i, $i = 0, 1, ..., l-1$ ($b_0^{-1} = 2!$; $b_1^{-1} = 4!$; $b_2^{-1} = 6!$; $b_3^{-1} = 8!$; $b_4^{-1} = 10!$; $b_5^{-1} = 12!$; $b_6^{-1} = 14!$; $b_7^{-1} = 16!$):

$$\begin{aligned} \Phi_0 &= b_0^{-1} \cdot R_0 = 2! \cdot 44; \\ \Phi_1 &= b_1^{-1} \cdot R_1 = 4! \cdot 24; \end{aligned}$$

$$\Phi_2 = b_2^{-1} \cdot R_2 = 6! \cdot 121;$$
$$\Phi_3 = b_3^{-1} \cdot R_3 = 8! \cdot 164;$$
$$\Phi_4 = b_4^{-1} \cdot R_4 = 10! \cdot 682;$$
$$\Phi_5 = b_5^{-1} \cdot R_5 = 12! \cdot 1675;$$
$$\Phi_6 = b_6^{-1} \cdot R_6 = 14! \cdot 16384;$$
$$\Phi_7 = b_7^{-1} \cdot R_7 = 16! \cdot 0.$$

In the last step, from the relation $M_i = \left[\frac{(2i+1)\Phi_i}{2^{2i+1}(2i+2)!} \right], i = 0, 1, 2..., l-1,$ we determine the coefficients M_i, $i = 0, 1, 2..., l-1,$, thus we obtain the coefficients $M_0 = 22$; $M_1 = 9$; $M_2 = 19$; $M_3 = 9$; $M_4 = 12$; $M_5 = 9$; $M_6 = 26$; $M_7 = 0$. The original message is ЋИРИЛИЦА.

Conclusion

This paper presents a new mathematical model for encryption and decryption of text messages. The model uses the inverse trigonometric function $\operatorname{arctg} t$ and its expansion in the Taylor series. Integers are included in this expansion and represent Cyrillic letters. The Laplace transform is applied to the resulting expression. Then, using the established congruence method, the encrypted message and the key are obtained. In this way, an algorithm for encrypting a text message is formulated. Using the inverse procedure, an algorithm for decrypting the text is derived. The theoretical part is illustrated in the final section through a concrete example.

References

Al-Azzani, M.A., Rageh, M. & Wang, G.H. 2021. A New Cryptography Scheme Based on Laplace Transform and a Substitution-Permutation Network, *International Journal of Advanced Trends in Computer Science and Engineering*, 10(4), pp.2658-2663. Available at: www.warse.org/IJATCSE/static/pdf/file/ijatcse01104 2021.pdf

Bhuvaneswari, R. & Bhuvaneswari, K. 2020. Application of Yang transform in cryptography, *Journal of Engineering, Science and Mathematics*, 9(3), pp.41-45. Available at: https://www.ijmra.us/project%20doc/2020/IJESM_MARCH2020/7111_pdf.pdf

Briones, R. P. 2018. Modification of an encryption scheme based on the Laplace transform, *International Journal of Current Research*, 10(7), pp.71759–71763. Available at: https://doi.org/10.24941/ijcr.31417.07.2018

Delfs, H., & Knebl, H. 2007. *Introduction to cryptography principles and applications*, Springer Science & Business Media. ISBN: 3540422781.

Gencogly, M. T. 2016. Use of integral transform in cryptology, *Sci Eng J Fırat Univ.*, 28(2), pp.217-220. Available at: https://scholar.google.com/scholar?hl=en&as_sdt=0,5&cluster=4164124505410972205

Gencogly, M. T. 2017. Cryptanalysis of a new method of cryptography using Laplace transform hyperbolic functions, *Communications in Mathematics and Applications*, 8(2), pp.183–189. Available at: https://doi.org/10.26713/cma.v8i2.708

Gencogly, M. T. 2019a. Embedded image coding using Laplace transform for Turkish letters, *Multimedia Tools and Applications*, 78(13), pp.17521–17534. Available at: https://doi.org/10.1007/s11042-018-7096-9

Gencogly, M. T. 2019. Importance of Cryptography in Information Security, *IOSR Journal of Computer Engineering*, 21(1), pp.65–68. Available at: https://doi.org/10.9790/0661-2101026568

Gupta, P., & Mishra, P.R. 2013. Cryptanalysis of a new method of cryptography using Laplace transform, *In Proceedings of the Third International Conference on Soft Computing for Problem Solving*, Springer, pp.539–546. Available at: https://www.semanticscholar.org/paper/Cryptanalysis-of-%22A-New-Method-of-Cryptography-Gupta-Mishra/b017b3b409bd3fbb73d6d1819780fc4d6eca2842

Hiwarekar, A.P. 2012. A new method of cryptography using Laplace transform, *International Journal of Mathematical Archive*, 3(3), pp.1193–1197. Available at: https://www.semanticscholar.org/paper/A-NEW-METHOD-OF-CRYPTOGRAPHY-USING-LAPLACE-Hiwarekar/c798fa28e9c03c0208e1be881890a2a0f73d80c3

Martin, K. M. 2012. *Everyday cryptography fundamental principles and applications*, Oxford University press. ISBN: 0199695598

Nagalakshmi, G., Sekhar, A.C. & Sankar, D.R. 2020. Asymmetric key cryptography using Laplace transform, *International Journal of Innovative Technology and Exploring Engineering*, 9(4), pp.3083-3087. Available at: https://doi.org/10.35940/ijitee.D2007.029420

Nagalakshmi, G., Sekhar, A.C., Sankar, N.R., Ravi, N., & Venkateswarlu, K. 2019. Enhancing the data security by using RSA algorithm with application of Laplace transform cryptosystem, *International Journal of Recent Technology and Engineering*, 8(2), pp.47–64. Available at: https://scholar.google.com/citations?view_op=view_citation&hl=en&user=4xY_RoIAAAAJ&citation_for_view=4xY_RoIAAAAJ:dfsIfKJdRG4C

Kriptografija Laplasovom transformacijom za srpski jezik

Tatjana Z. Mirković, **autor za prepisku**, *Nataša* A. Ćirović

Univerzitet u Beogradu, Elektrotehnički fakultet, Beograd, Srbija

OBLAST: matematika
KATEGORIJA (TIP) ČLANKA: originalni naučni rad

Sažetak:

Uvod/cilj: U ovom radu autori su dali novu matematičku metodu kriptografije. Procedura je sprovedena za poruke napisane na srpskom jeziku, koji se sastoji od 30 fonema.

Memođe: Metode: Koristili smo standardni razvoj inverzne trigonometrijske funkcije $\operatorname{arctg} t$ *u Tejlorov red. Takođe smo koristili Laplasovu transformaciju za šifrovanje početnog teksta i odgovarajuću inverznu Laplasovu transformaciju za dešifrovanje kodiranog teksta.*

Rezultati: Napisan je novi kriptografski algoritam za šifrovanje i dešifrovanje tekstualne poruke napisane na srpskom jeziku.

Zaključak: Autori su u radu predstavili novi algoritam u kome je korišćena Laplasova transformacija za šifrovanje i dešifrovanje tekstualne poruke. Poruka je na srpskom jeziku u ćiriličnom pismu.

Ključne reči: kriptografija, Laplasova transformacija, inverzna trigonometrijska funkcija, Tejlorov red.

Paper received on: 2 June 2025.
Manuscript corrections submitted on: 30 November 2025.
Paper accepted for publishing on: 2 December 2025.

© 2026 The Authors. Published by Vojnotehnički glasnik / Military Technical Courier (http://vtg.mod.gov.rs). This article is an open access article distributed under the terms and conditions of the Creative Commons Attribution license (http://creativecommons.org/licenses/by/4.0/rs/).

Some considerations on thermodynamics of quantum mechanics on a circle and Kałuża–Klein models

Nicola Fabiano

University of Belgrade, "Vinča" Institute of Nuclear Sciences - National Institute of the Republic of Serbia,
Belgrade, Republic of Serbia,
e-mail: nicola.fabiano@gmail.com,
ORCID iD: https://orcid.org/0000-0003-1645-2071

https://doi.org/10.5937/vojtehg74-58405

FIELD: mathematics
ARTICLE TYPE: original scientific paper

Abstract:

Introduction/purpose: Quantum mechanics on a circle has been investigated and applied to a Kałuża–Klein model with a compactified dimension.

Methods: Methods of quantum mechanics and statistical mechanics were employed. Additionally, a Kałuża–Klein toy model with compactified dimension was considered.

Results: The resulting partition function can be evaluated in a closed form, giving a special function. It presents a phase transition depending on the geometry. When used in a Kałuża–Klein model, it showed a phase transition regulated by the radius of the circle, and the transition disappears when the radius is infinite, that is in the flat space.

Conclusion: Quantum mechanics on a circle exhibits many peculiar characteristics. Energy levels are discrete because of the geometry, in contrast to the configuration space of the real line. It presents a phase transition depending on the circle radius, also when embedded in a Kałuża–Klein model. This characteristic disappears when the radius becomes infinite, in the flat space.

Keywords: quantum mechanics, statistical mechanics, phase transition, Jacobi theta function, Kałuża–Klein model.

Quantum mechanics on a circle

Consider the problem of one dimensional quantum mechanics on a circle of radius R with Hamiltonian

$$\mathcal{H}\psi = -\frac{\hbar^2}{2m}\left(\frac{d}{dx}\right)^2 \psi = E\psi \ . \tag{1}$$

Therefore, the Schrödinger equation (1) has the periodic boundary condition

$$\psi(x) = \psi(x + 2\pi R) \ . \tag{2}$$

It leads to the wavefunctions of the form

$$\psi_{\pm}(x) = \exp(\pm ikx) \tag{3}$$

where $+$ and $-$ represent the solutions for particles moving clockwise and anticlockwise respectively, while k is given by

$$k = \frac{\sqrt{2mE}}{\hbar} \ . \tag{4}$$

Imposing the periodic boundary conditions (2) for the motion on the circle, the following relation is obtained:

$$\exp(\pm ikx) = \exp[\pm ik(x + 2\pi R)] = \exp[\pm i(kx + 2\pi n)] \tag{5}$$

Therefore,

$$k = \frac{1}{R}n \ , \tag{6}$$

that leads to the following expression for the energy eigenvalues

$$E_n = \frac{\hbar}{2mR^2}n^2 = a^2n^2 \ , \tag{7}$$

where $n \in \mathbb{Z}$. Those eigenvalues have a double degeneracy, as the clockwise and anticlockwise motions have the same energy. The momentum is given by the expression $p = \hbar k$.

This problem is related to the model of Kałuża–Klein (Kaluza, 1921; Klein, 1926), which introduced an extra spatial dimension to extend general relativity in order to unify gravity and electromagnetism. This extra dimension is compactified on a circle with a radius so small that it is not

directly observable. Various extensions and variations of the model exist, starting from the ADD (Arkani-Hamed, Dimopoulos, Dvali) (Arkani-Hamed et al., 1998) model and the bulk scenario, where only gravity propagates to the extra dimension (Rizzo, 2010), to the UED (Universal extra dimensions) (Appelquist et al., 2001), in which all interactions of the Standard Model propagate into the extra dimension, among others (Kerner, 1968; Appelquist et al.; Randall & Sundrum, 1999; Zee, 2013). In (Fabiano & Panella, 2005, 2010) there are discussions and references to some of them.

To briefly illustrate this mechanism, consider what happens to gravitational interaction in a spatial dimension other than $D = 3$. Start with the Poisson's equation for the gravitational potential V generated by a single object of mass M located at the origin

$$\nabla^2 V = 4\pi G M \delta(r) \, . \tag{8}$$

From dimensional considerations, the delta has a dimension that is the inverse of length, because $\int \delta(x) \mathrm{d}x = 1$, therefore, $\delta \sim 1/r$, and $\delta \sim 1/r^D$ in D dimensions. Consequently, in D dimensions one obtains for the gravitational potential, integrating (8), the scaling relation

$$\nabla^2 V \sim \frac{V}{r^2} = 4\pi G M \delta(r) \sim \frac{1}{r^D} \, , \tag{9}$$

that provides the gravitational potential in D dimensions

$$V(r) \propto \frac{1}{r^{D-2}} \, . \tag{10}$$

Thanks to a theorem due to Bertrand (Bertrand, 1873), it is known that the only possible stable orbits (i.e., closed orbits) arising from a central potential are given by the Coulombic potential and the harmonic oscillator. This implies from (10) that Newtonian orbits are only stable in three dimensions, $D = 3$. Therefore, if further spatial dimensions exist beyond the usual three, they cannot be extended, but must instead be compactified on a circle of small radius, essentially a string, making it unobservable at low energies.

Thermodynamics

From the standard formula for the partition function (Landau & Lifshitz, 2013b; Huang, 2009)

$$Z = \text{tr}\, e^{-\beta\mathcal{H}} = \sum_{n=0}^{+\infty} \langle n|e^{-\beta\mathcal{H}}|n\rangle \tag{11}$$

where $\beta = \frac{1}{k_B T}$, and using the expression for the energy eigenvalues found in (7), one obtains the explicit form of the partition function

$$Z(a,\beta) = \sum_{n=-\infty}^{+\infty} e^{-\beta a^2 n^2} = \vartheta_3(0, e^{a^2\beta}) \,. \tag{12}$$

The function $\vartheta_3(z,q)$ is the elliptic theta function, also known as the Jacobi theta function (Whittaker & Watson). It is interesting to observe that the infinite series of this discrete Gaussian provides a known function, while its corresponding finite sum does not have a closed form.

The expected value of the energy, $\langle E\rangle$, also known as the internal energy U could be calculated using the expression

$$U(a,\beta) = -\frac{\partial}{\partial\beta}\log[Z(a,\beta)] \,, \tag{13}$$

and by means of (12) it is possible to write it in the following form

$$U(a,\beta) = \frac{a^2 e^{-a^2\beta}\cdot\vartheta_3^{(0,1)}(0, e^{a^2\beta})}{\vartheta_3(0, e^{a^2\beta})} \,, \tag{14}$$

where $\vartheta_3^{(0,1)}(z,q)$ is the derivative of ϑ_3 with respect to the second variable.

Other thermodynamics functions readily obtained from the partition function are the free energy

$$F(a,\beta) = -\frac{1}{\beta}\log[Z(a,\beta)] \tag{15}$$

and the entropy

$$S(a,T) = -\frac{\partial F(a,T)}{\partial T} \,. \tag{16}$$

Figures (1) and (2) represent the internal energy obtained as a function of the inverse radius circle a and the inverse of temperature β in two and

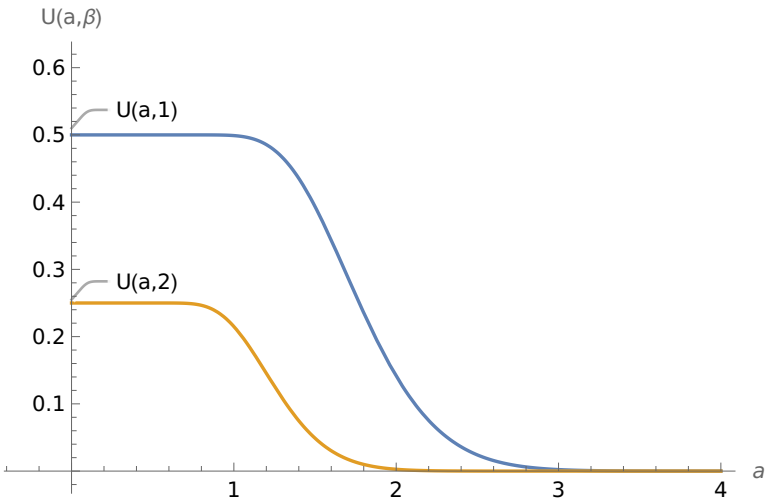

Figure 1 – Internal energy $U(a,\beta)$ as a function of energy parameter a for different values of β

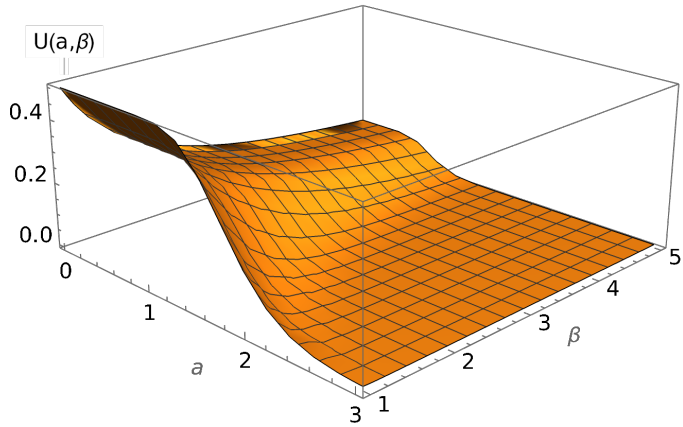

Figure 2 – Internal energy $U(a,\beta)$ as a function of a and β

three dimensions, respectively. From there, it is readily apparent that there is a phase transition driven by the variation of a at a fixed β, as it presents a sharp change. For example, Figure (1) for $\beta = 1$ indicates a critical value of a, that is, a_c, between 1.5 and 2, while for $\beta = 2$ it is found between 1 and 1.5.

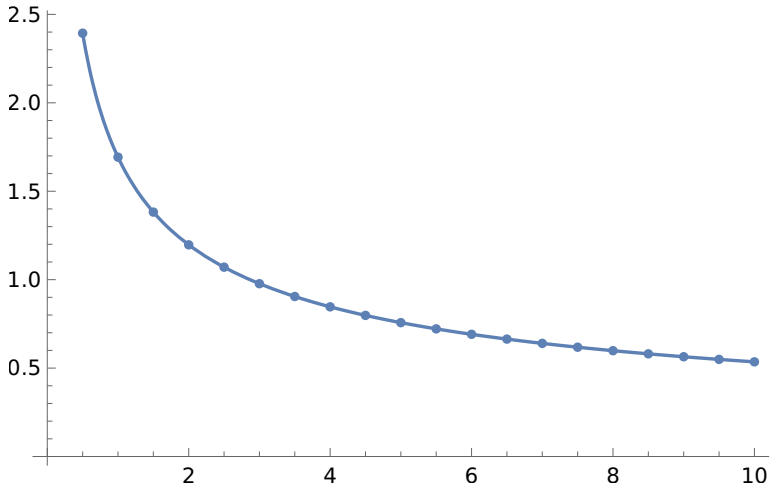

Figure 3 – Fit for critical values of a as function of β

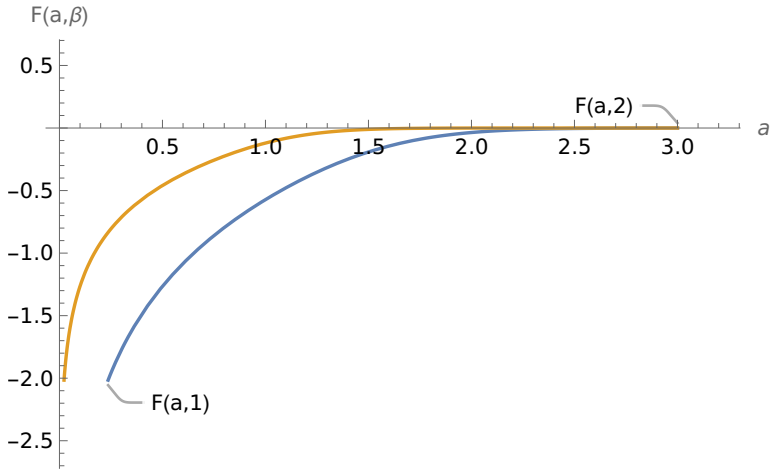

Figure 4 – Free energy $F(a,\beta)$ as a function of energy parameter a for different values of β

A careful numerical evaluation of those critical values as a function of β provides the following fit

$$a_c = \frac{1}{0.590782\sqrt{\beta} - 1.98913 \times 10^{-9}} , \tag{17}$$

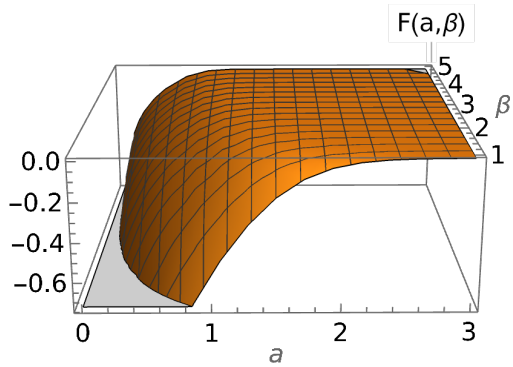

Figure 5 – Free energy $F(a, \beta)$ as a function of a and β

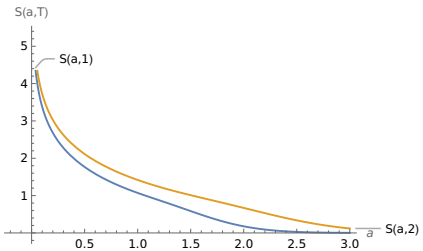

(a) Entropy 2d

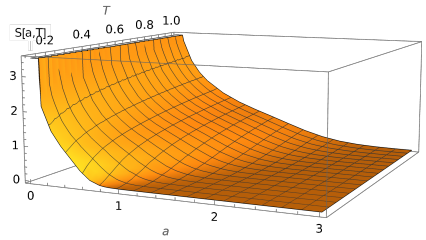

(b) Entropy 3d

Figure 6 – Entropy as a function of a and T

where both parameters at the denominator have a standard deviation error smaller than 10^{-9}.

The results are shown in Figure (3), and exhibit excellent agreement with the critical points, even at low temperatures. The formula (17) could be simplified in practice as $a_c \simeq 1.69267 \times \beta^{-1/2}$, that is the corresponding critical radius of the circle R_c from (7) behaves like

$$R_c \propto T^{-1/2} \, . \tag{18}$$

An observation is in order here. In (7), the energy increases with increasing a, whereas the results above show the opposite behavior for $U = \langle E \rangle$. This apparent paradox is resolved because U is calculated from the weighted average of energy E_n, and its weight, $\exp(-\beta E_n)$ decreases abruptly with E_n, that is a, so that only a few terms of the sum of the partition function actually contribute to $\langle E \rangle$.

Further evidence of the phase transition is seen in the free energy $F(a, \beta)$, which exhibits a pronounced variation for the neighborhood of a critical value of a, as shown in Figures (4) and (5). Less apparent, but still present, is the same critical behaviour of entropy $S(a, T)$ (16), presented in Figures (6a) and (6b). Numerical evaluation confirms that the critical values of a_c for F and S coincide with the ones found from U in formula (17) and shown in Figure (3).

This particular phase transition does not depend on temperature, unlike, for instance, melting - the transition from ice to water. There are many examples of hase transitions driven by parameters other than temperature, such as the circle radius in our example. To name a few:

- The Ising model, a lattice of spins, could have transitions driven by the coupling constant strength J. At a fixed temperature, when $J \gg kT$, the spins align to a ferromagnetic order, while when J decreases, the spins lose their alignment and undergo a phase transition to a paramagnetic state.
- A XY model with spin–orbit coupling has a phase transition when the α spin–orbit coupling strength changes.
- Ferromagnetic materials such as iron can have phase transitions when exposed to changing magnetic fields, which alter the material's magnetization.
- At low temperatures close to absolute zero, some materials can undergo phase transitions driven by quantum fluctuations, which become relevant at these energies: they can shift between distinct magnetic states, like antiferromagnetic and paramagnetic phases. High–temperature superconductors, cuprates such as $YBa_2Cu_3O_7$ or Bose–Einstein condensates such as Rubidium–87 Rb^{87} belong to this class of materials.

A Kałuża–Klein toy model

Consider the Hamiltonian of a one dimensional quantum harmonic oscillator

$$\mathcal{H}^{\text{ho}} = \frac{p^2}{2m} + \frac{m\omega^2}{2}x^2 \,, \tag{19}$$

the wavefunctions are given by a combination of a Gaussian and Hermite polynomials (Landau & Lifshitz, 2013a; Whittaker & Watson)

$$\psi_n^{\mathsf{ho}}(x) = \frac{1}{\sqrt{2^n n!}} \left(\frac{m\omega}{\pi\hbar}\right) \exp\left(-\frac{m\omega}{2\hbar}x^2\right) H_n\left(\sqrt{\frac{m\omega}{\hbar}}x\right) \ , \tag{20}$$

where

$$H_n(\xi) = (-1)^n \exp(\xi^2) \frac{d^n}{d\xi^n} \exp(-\xi^2) \ , \tag{21}$$

and the corresponding energy levels are given by the well–known formula

$$E_n^{\mathsf{ho}} = \hbar\omega \left(n + \frac{1}{2}\right) \ . \tag{22}$$

Proceeding in the same manner as in the section "Thermodynamics", one obtains

$$Z^{\mathsf{ho}}(a,\beta) = \sum_{n=0}^{+\infty} e^{-\beta a^2\left(n+\frac{1}{2}\right)} = \frac{\exp\left(\frac{a^2\beta}{2}\right)}{\exp(a^2\beta) - 1} \ , \tag{23}$$

having defined $a^2 = \hbar\omega$. Its internal energy is given by

$$U^{\mathsf{ho}}(a,\beta) = \frac{a^2}{2} \frac{\exp(a^2\beta) + 1}{\exp(a^2\beta) - 1} \ , \tag{24}$$

and is shown in Figures (7) and (8) in two and three dimensions respectively.

In contrast to the case of (1), there are no critical values for the energy parameter a that could be found, that is, there are not any phase transitions for the harmonic oscillator.

Introduce now a two dimensional system with coordinates x and y, where the x coordinate lives on a circle with radius R, while $y \in \mathbb{R}$. The Hamiltonian of this toy model is given by

$$\mathcal{H}^{\mathsf{KK}} = \mathcal{H}_x + \mathcal{H}_y^{\mathsf{ho}} \ , \tag{25}$$

where the Hamiltonian acting on the compactified coordinate x is described by (1) and its wavefunction obeys the boundary condition (2), while the Hamiltonian of the harmonic oscillator described in (19) acts on the coordinate y.

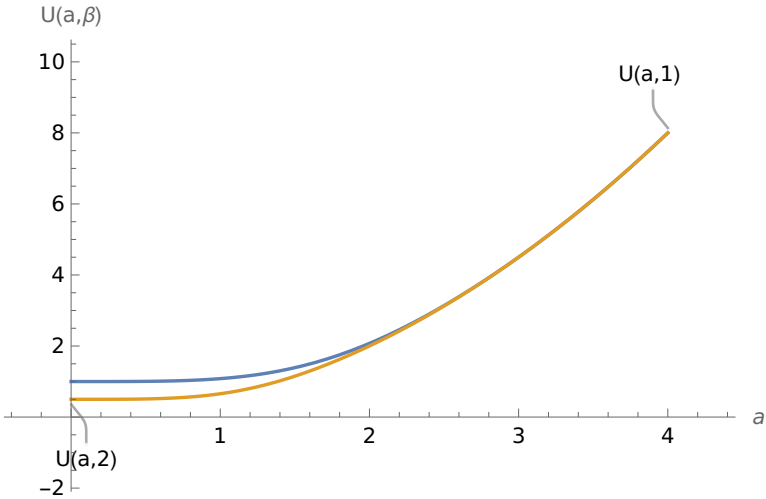

Figure 7 – Internal energy $U^{ho}(a,\beta)$ of harmonic oscillator as a function of energy parameter a for different values of β

The two components of the Hamiltonian do not interact with each other, and proceeding in the same fashion as before, one obtains

$$E^{\mathrm{KK}} = E_{n_x} + E^{\mathrm{ho}}_{n_y} = \frac{\hbar}{2mR^2} n_x^2 + \hbar\omega\left(n_y + \frac{1}{2}\right) \tag{26}$$

for the energy levels, and

$$\begin{aligned} Z^{\mathrm{KK}} &= \sum_{n_x,n_y} \langle n_x, n_y | e^{-\beta \mathcal{H}^{\mathrm{KK}}} | n_x, n_y \rangle = \\ &\sum_{n_x,n_y} \langle n_x, n_y | e^{-\beta \mathcal{H}_x} \otimes e^{-\beta \mathcal{H}^{\mathrm{ho}}_y} | n_x, n_y \rangle = \\ &\sum_{n_x} \langle n_x | e^{-\beta \mathcal{H}_x} | n_x \rangle \times \sum_{n_y} \langle n_y | e^{-\beta \mathcal{H}^{\mathrm{ho}}_y} | n_y \rangle \end{aligned} \tag{27}$$

for the partition function. This result is due to the fact that $\mathcal{H}_x$ acts on x and $\mathcal{H}^{\mathrm{ho}}_y$ on y, and they are independent. This implies that the eigenstates $|n_x, n_y\rangle$ of $\mathcal{H}^{\mathrm{KK}}$ can be written as tensor products $|n_x\rangle \otimes |n_y\rangle$, where $|n_x\rangle$ and $|n_y\rangle$ are eigenstates of $\mathcal{H}_x$ and $\mathcal{H}^{\mathrm{ho}}_y$, respectively. Using the explicit formulæ found in (12) and (23), with a slight change in notation to avoid

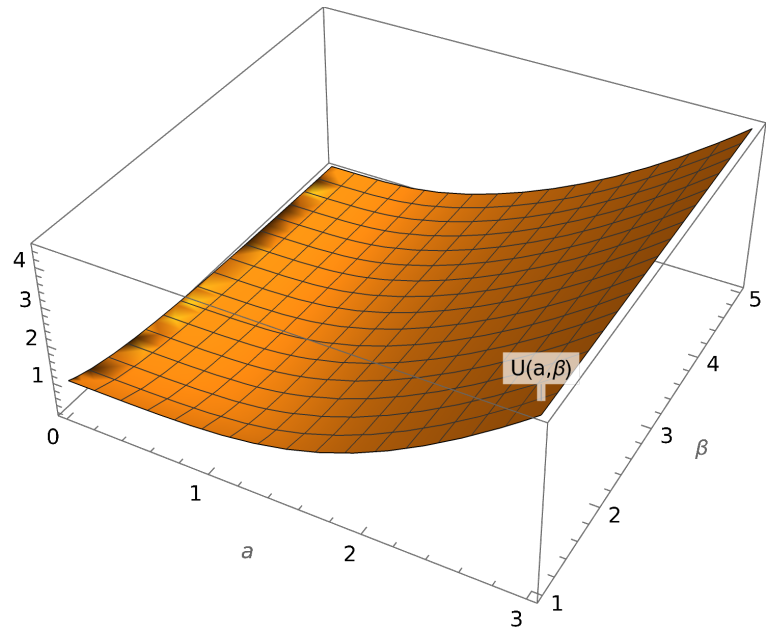

Figure 8 – Internal energy $U^{ho}(a,\beta)$ of harmonic oscillator as a function of energy parameter a and β

confusion between the two energies, one obtains the final result

$$Z^{\mathrm{KK}} = Z_x \times Z_y^{\mathrm{ho}} = \sum_{n_x=-\infty}^{+\infty} e^{-\beta E_{n_x}} \times \sum_{n_y=0}^{+\infty} e^{-\beta E^{\mathrm{ho}}_{n_y}} =$$

$$\sum_{n_x=-\infty}^{+\infty} e^{-\beta a_1^2 n_x^2} \times \sum_{n_y=0}^{+\infty} e^{-\beta a_2^2\left(n_y+\frac{1}{2}\right)} = \vartheta_3(0, e^{a_1^2\beta}) \times \frac{\exp\left(\frac{a_2^2\beta}{2}\right)}{\exp(a_2^2\beta)-1} \,. \qquad (28)$$

Using (13) and the explicit expressions of internal energies from (14) and (24) one arrives at the result

$$U^{\mathrm{KK}} = U + U^{\mathrm{ho}} = \frac{a_1^2 e^{-a_1^2\beta} \cdot \vartheta_3^{(0,1)}(0, e^{a_1^2\beta})}{\vartheta_3(0, e^{a_1^2\beta})} + \frac{a_2^2}{2}\frac{\exp(a_2^2\beta)+1}{\exp(a_2^2\beta)-1} \,, \qquad (29)$$

because the two Hamiltonians are independent from each other.

Therefore, this Kałuża–Klein model exhibits the same phase transition as observed previously with the Hamiltonian (1), with the only difference being higher values of internal energy. The a_2 parameter, which corresponds

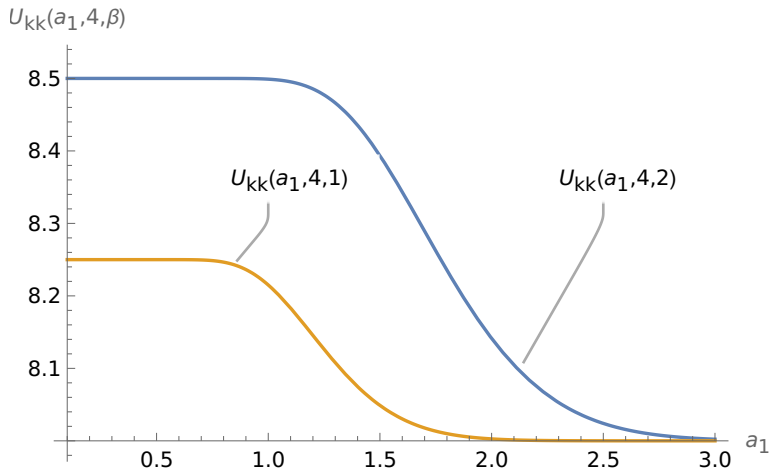

Figure 9 – Internal energy $U^{KK}(a_1, a_2, \beta)$ of toy KK model as a function of energy parameter a_1 and fixed a_2 for different values of β

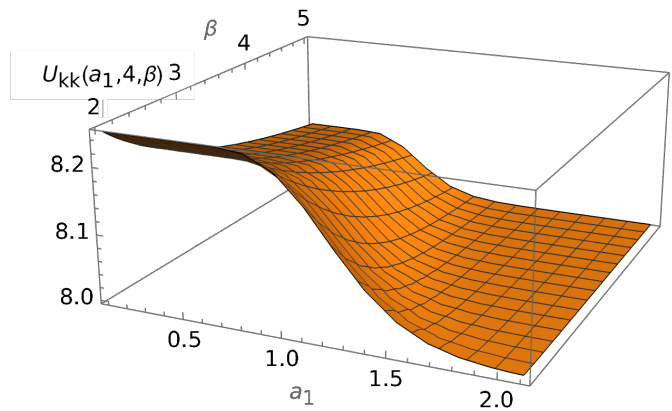

Figure 10 – Internal energy $U^{KK}(a_1, a_2, \beta)$ of toy KK model as a function of energy parameter a_1 and fixed a_2 for different values of β

to the harmonic oscillator component, is irrelevant for the existence of the phase transition. Figures (9) and (10) show the behaviour of the internal energy U^{KK} (29) as a function of the inverse radius circle a_1 for different values of the inverse temperature β, at a fixed harmonic oscillator frequency a_2, in two and three dimensions respectively. The critical value of the inverse radius circle is clearly the same as in (1), as seen in Figures (1) and (2). Therefore, the fit for its critical value found in formula (17) and shown in Figure (3) is the same. As expected, when the radius R of the circle is infinite, that is $a_1 = 0$, so that $x \in \mathbb{R}$, the internal energy U^{KK} does not present any kind of steep change with the variation of other parameters a_2 and β, therefore, there is not a phase transition anymore when the Kałuża–Klein model transforms to a model in the usual two dimensional space.

Conclusion

Quantum mechanics on a circle exhibits some surprising behaviour. Contrary to the case of the configuration space of the real line, its energy levels are discrete. The partition function can be expressed in closed form as a Jacobi theta function. It presents a phase transition, controlled by the geometry of the configuration space, specifically the radius of the circle. When considered in a simple two dimensional Kałuża–Klein model, it exhibits again a phase transition, that disappears in the limit of a flat space, for an infinite radius of the circle.

References

Appelquist, T., Cheng, H.C. & Dobrescu, B.A. 2001. Bounds on universal extra dimensions. *Physical Review D*, 64(3), p. 035002. Available at: https://doi.org/10.1103/PhysRevD.64.035002

Appelquist, T., Chodos, A. & Freund, P.*Modern Kaluza-Klein Theories*. Frontiers in Physics : a lecture note and reprint series. ISBN 9780201098297. Available at: https://archive.org/details/modern-kaluza-klein-theories, year=1987, publisher=Addison-Wesley Publishing Company.

Arkani-Hamed, N., Dimopoulos, S. & Dvali, G. 1998. The hierarchy problem and new dimensions at a millimeter. *Physics Letters B*, 429(3-4), pp. 263–272. Available at: https://doi.org/10.1016/S0370-2693(98)00466-3

Bertrand, J. 1873. Théoreme relatif au mouvement d'un point attiré vers un centre fixe. *CR Acad. Sci*, 77(16), pp. 849–853. Available at: https://gallica.bnf.fr/ark:/12148/bpt6k3034n/f849.item

Fabiano, N. & Panella, O. 2005. Sleptonium at the linear collider and the slepton co-next-to-lightest supersymmetric particle scenario in gauge mediated symmetry breaking models. *Physical Review D—Particles, Fields, Gravitation, and Cosmology*, 72(1), p. 015005. Available at: https://doi.org/10.1103/PhysRevD.72.015005

Fabiano, N. & Panella, O. 2010. Threshold production of metastable bound states of Kaluza-Klein excitations in universal extra dimensions. *Physical Review D—Particles, Fields, Gravitation, and Cosmology*, 81(11), p. 115001. Available at: https://doi.org/10.1103/PhysRevD.81.115001

Huang, K. 2009. *Introduction to statistical physics*. Chapman and Hall/CRC. Available at: https://doi.org/10.1201/9781439878132.

Kaluza, T. 1921. On the Unification Problem in Physics. *Sitzungsber. Preuss. Akad. Wiss. Berlin (Math. Phys.)*, 1921, pp. 966–972. Available at: https://doi.org/10.1142/S0218271818700017

Kerner, R. 1968. Generalization of the Kaluza-Klein theory for an arbitrary non-abelian gauge group. In: *Annales de l'institut Henri Poincaré. Section A, Physique Théorique*, vol. 9. pp. 143–152. Available at: https://www.numdam.org/article/AIHPA_1968__9_2_143_0.pdf.

Klein, O. 1926. Quantentheorie und fünfdimensionale Relativitätstheorie. *Zeitschrift für Physik*, 37, pp. 895–906. Available at: https://doi.org/10.1007/BF01397481

Landau, L.D. & Lifshitz, E.M. 2013a. *Quantum mechanics: non-relativistic theory*, vol. 3. Elsevier. Available at: https://archive.org/details/l-d-landau-e.-m.-lifshitz-quantum-mechanics-non-vol-3.

Landau, L.D. & Lifshitz, E.M. 2013b. *Statistical Physics: Volume 5*, vol. 5. Elsevier. Available at: https://ia802908.us.archive.org/31/items/ost-physics-landaulifshitz-statisticalphysics/LandauLifshitz-StatisticalPhysics.pdf.

Randall, L. & Sundrum, R. 1999. Large mass hierarchy from a small extra dimension. *Physical review letters*, 83(17), pp. 3370–3373.

Rizzo, T.G. 2010. Introduction to Extra Dimensions. In: *AIP Conf. Proc.*, vol. 1256. pp. 27–50. Available at: https://doi.org/10.1063/1.3473866.

Whittaker, E.T. & Watson, G.N.*A Course of Modern Analysis*. 5 edn. Cambridge University Press. Available at: https://doi.org/10.1017/9781009004091, year=2021.

Zee, A. 2013. *Einstein gravity in a nutshell*, vol. 14. Princeton University Press. Available at: http://www.stat.ucla.edu/~ywu/Einstein.pdf.

Neka razmatranja o termodinamici kvantne mehanike na krug i Kaluza-Klajn modeli

Nikola Fabiano

Univerzitet u Beogradu, Institut za nuklearne nauke „Vinča” –
Nacionalni institut Republike Srbije,
Beograd, Republika Srbija

OBLAST: matematika
KATEGORIJA (TIP) ČLANKA: originalni naučni rad

Sažetak:

Uvod/cilj: Kvantna mehanika na krugu je istražena i primenjena na Kaluza-Klajn model sa kompaktifikovanom dimenzijom.

Metode: Korišćene su metode kvantne mehanike i statističke mehanike. Takođe, razmatran je Kaluza-Klajn model igračke kompaktne dimenzije.

Rezultati: Rezultujuća particiona funkcija se može proceniti u zatvorenom obliku, dajući posebnu funkciju. Predstavlja fazni prelaz u zavisnosti od geometrije. Kada se koristi u modelu Kaluza-Klajn, pokazuje fazni prelaz regulisan poluprečnikom kruga, a prelaz nestaje kada je poluprečnik beskonačan, odnosno u ravnom prostoru.

Zaključak: Kvantna mehanika na krugu pokazuje mnoge neobične karakteristike. Nivoi energije su odvojeni usled geometrije, nasuprot konfiguracionom prostoru prave linije. Predstavlja fazni prelaz u zavisnosti od radijusa kruga, takođe kada je isti ugrađen u Kaluza-Klajn model. Ova karakteristika nestaje kada poluprečnik postane beskonačan, u ravnom prostoru.

Ključne reči: kvantna mehanika, statistička mehanika, fazni prelaz, Jakobijeva teta funkcija, Kaluza-Klajn model.

Paper received on: 23 April 2025.
Manuscript corrections submitted on: 9 June 2025.
Paper accepted for publishing on: 4 February 2026.

© 2026 The Authors. Published by Vojnotehnički glasnik / Military Technical Courier (http://vtg.mod.gov.rs). This article is an open access article distributed under the terms and conditions of the Creative Commons Attribution license (http://creativecommons.org/licenses/by/4.0/rs/).

A new iteration scheme for approximating fixed points of some generalized nonexpansive mappings

Penumarthy Parvateesam Murthy[a], *Chandra* Prakash Dhuri[b]

[a] Guru Ghasidas Vishwavidyalaya (A Central University), Department of Mathematics, Bilaspur, India, 495 009,
e-mail: ppmurthy@gmail.com, **corresponding author**,
ORCID iD: https://orcid.org/0000-0003-3745-4607

[b] Guru Ghasidas Vishwavidyalaya (A Central University), Department of Mathematics, Bilaspur, India, 495 009,
e-mail: cpdhuri@gmail.com,
ORCID iD: https://orcid.org/0000-0002-1431-4030

https://doi.org/10.5937/vojtehg74-52039

FIELD: mathematics,
ARTICLE TYPE: original scientific paper

Abstract:

Introduction/purpose: A new three-step iteration process, which converges faster than the Mann iteration and the S-iteration, is introduced, as well as some convergence results for approximation of fixed points of the Suzuki generalized nonexpansive mappings and nearly asymptotically nonexpansive mappings have been established.

Methods: The authors provide a specific three-step iterative method $\{x_n\}$ *in a Banach space, defined as a sequence of convex combinations of the current iterate and its images under the mapping T, with control sequences* $\{\alpha_n\}$, $\{\beta_n\}$, $\{\gamma_n\} \subseteq (0,1)$. *The results are proved in the setting of uniformly convex Banach spaces, where T is assumed to be either a Suzuki generalized nonexpansive mapping or a nearly asymptotically nonexpansive mapping. The authors obtain both weak and strong convergence theorems by using demiclosedness principles, Suzuki generalized nonexpansive mapping properties, and suitable lemmas on the behavior of the iterates. To compare the rates of convergence, they perform numerical experiments (usually implemented in MATLAB) where the proposed three-step iteration is run in parallel with the Thakur and S-iterations. The iterates are graphed to display the error convergence per iteration.*

ACKNOWLEDGMENT: The authors are thankful to the editor and referees of the journal for their valuable comments that helped improve the manuscript. The authors also thank the Department of Science and Technology, New Delhi, India, for approving the proposal under the FIST Program (Ref. No. SR/FST/MS/2022/122 dated 19 December 2022).

Results: The new iteration scheme converges faster than the S-iteration scheme if the mapping is a contraction. The new iteration scheme converges to a fixed point of a Suzuki generalized nonexpansive mapping under suitable conditions. The new iteration scheme converges to a fixed point of a nearly asymptotically nonexpansive mapping under suitable conditions.

Conclusions: The three-step iteration algorithm is proved, both theoretically and numerically, to converge faster than the Mann iteration and the S iteration (and sometimes faster than several other existing methods) for the considered types of mappings. The authors prove weak and strong convergence theorems for fixed points of the Suzuki generalized nonexpansive mappings and nearly asymptotically nonexpansive mappings in uniformly convex Banach spaces, thus generalizing, extending, and unifying several existing fixed-point approximation results in the literature.

Key words: fixed points, iteration, uniformly convex Banach space, nonexpansive mapping, Suzuki generalized nonexpansive mapping, nearly asymptotically nonexpansive mappings, reflexive Banach space.

Introduction

Let $(X, \|.\|)$ be a normed linear space, C a nonempty subset of X and $T : C \to C$ a mapping. Then T is said to be Lipschitzian if for any given $n \in \mathbb{N}$, there exists a real number $L_n \geq 0$ such that

$$\|T^n x - T^n y\| \leq L_n \|x - y\|, \text{ for all } x, y \in C$$

If $L_1 < 1$, then T is called contraction. If $L_1 = 1$, then it is called nonexpansive mapping. If $L_n \geq 1$ for all $n \in \mathbb{N}$ and $\lim_{n\to\infty} L_n = 1$, then it is called asymptotically nonexpansive (Goebel & Kirk, 1972, p.172). If $x = Tx, x \in X$, then x is called a fixed point of T. To approximate the fixed points of different kinds of mappings, the following iteration schemes are used:

The Picard Iteration Scheme:

$$\begin{aligned} x_1 &\in C, \\ x_{n+1} &= Tx_n, \quad n \in \mathbb{N}. \end{aligned}$$

The Mann iteration scheme: C is a convex subset of X,

$$\begin{aligned} x_1 &\in C, \\ x_{n+1} &= (1-\alpha_n)x_n + \alpha_n T x_n, \\ \alpha_n &\in [0,1), \quad n \in \mathbb{N}. \end{aligned}$$

The S-iteration scheme: In 2007, Agarwal et al. introduced this iteration scheme, which is as follows:
C is a convex subset of X. Choose $w_1 \in C$ and define a sequence $\{w_n\}$ in C as follows:

$$\begin{aligned} w_{n+1} &= \alpha_n T y_n + (1-\alpha_n) T w_n, \\ y_n &= (1-\beta_n)w_n + \beta_n T w_n, \ \ n \in \mathbb{N}. \end{aligned} \tag{1}$$

where $\{\alpha_n\}$ and $\{\beta_n\}$ are real sequences in $(0,1)$.

They showed that the rate of convergence of this process is the same as that of the Picard iteration but that it converges faster than the Mann iteration process (Mann, 1953) for contraction mappings.
Thakur et al. introduced the following iteration scheme in 2016 and showed that it has a faster rate of convergence than the Picard, Mann, S-iteration and some other iterations.

The Thakur Iteration Scheme:

$$\begin{aligned} x_1 &\in C, C \text{ is convex} \\ x_{n+1} &= \alpha_n T y_n + (1-\alpha_n) T z_n, \\ z_n &= (1-\gamma_n)y_n + \gamma_n T y_n, \\ y_n &= (1-\beta_n)x_n + \beta_n T x_n, \\ \alpha_n, \beta_n, \gamma_n &\in (0,1), \quad n \in \mathbb{N}. \end{aligned}$$

Our aim is to introduce an iteration process whose rate of convergence is faster than that of the S-iteration process, and hence faster than the Mann iteration. The new iteration scheme will also be compared numerically with the the Thakur iteration scheme. In addition, we prove some convergence results using this iteration process for Suzuki generalized nonexpansive mappings and nearly asymptotically nonexpansive mappings.

Preliminaries

Sahu introduced the class of nearly Lipschitzian mappings (Sahu, 2005, p. 654), which is a generalization of the class of Lipschitzian mappings.

Definition 1. *Let C be a nonempty subset of a normed linear space X and $\{a_n\}$ be a sequence in $[0,\infty)$ converging to zero. A mapping $T : C \to C$ is said to be nearly Lipschitzian with respect to $\{a_n\}$ if for any given $n \in \mathbb{N}$, there exists a real number $L_n \geq 0$ such that*

$$\|T^n x - T^n y\| \leq L_n(\|x - y\| + a_n) \text{ for all } x, y \in C \tag{2}$$

For any fixed n, the infimum of constants L_n for which (2) holds is called the nearly Lipschitz constant and will be denoted by k_n.

Definition 2. *the nearly Lipschitzian mapping T with sequence $\{(a_n, k_n)\}$ is said to be nearly asymptotically nonexpansive (Sahu, 2005, p. 654) if $k_n \geq 1$ for all $n \in \mathbb{N}$ and $\lim_{n\to\infty} k_n = 1$.*

In 2008, Suzuki (Suzuki, 2008, p.1089) generalized the nonexpansive mapping as follows:

Definition 3. *Let T be a mapping on a subset C of a Banach space E. Then T is said to satisfy the condition (C) if*

$$\frac{1}{2}||x - Tx|| \leq ||x - y|| \text{ implies } ||Tx - Ty|| \leq ||x - y||$$

for all $x, y \in C$.

Let us call a mapping satisfying the above condition a Suzuki generalized nonexpansive mapping.

Definition 4. *A self mapping T defined on a nonempty subset C of a Banach space E is said to be a quasi-nonexpansive mapping if $F(T) \neq \emptyset$ and*

$$\|Tx - p\| \leq \|x - p\|, \text{ for all } x \in C, p \in F(T).$$

Definition 5. *Let E be a Banach space and $S = \{x \in E : \|x\| = 1\}$, then the norm of E is said to be Fréchet differentiable if for each $x \in S$, the limit*

$$\lim_{t\to 0} \frac{\|x + ty\| - \|x\|}{t}$$

Murthy, P.P.. et al., A new iteration scheme for approximating fixed points of some generalized nonexpansive mappings, pp.26–49

is attained uniformly for $y \in S$.

Definition 6. *A Banach space* E *is said to satisfy the Opial condition (Opial, 1967, p.592) if for each sequence* $\{x_n\}$ *converging weakly to a point* $x \in E$, *we have*

$$\liminf_{n\to\infty} \|x_n - x\| < \liminf_{n\to\infty} \|x_n - y\|$$

for all $y \in X$ *such that* $y \neq x$.

Definition 7. *A Banach space* E *is said to have the Kadec-Klee property if the following condition holds:*
If $\{x_n\}$ *is a sequence in* E *such that* $\{x_n\}$ *converges weakly to* x *and* $\|x_n\|$ *converges strongly to* $\|x\|$, *then* $\{x_n\}$ *converges strongly to* x.

Definition 8. *Let* C *be a nonempty subset of a Banach space* E, *then a mapping* $T : C \to E$ *is called demiclosed (Opial, 1967, p.591) if its graph in* $C \times E$ *is closed in the topology of a Cartesian product induced in* $C \times E$ *by the weak topology in* C *and the strong topology in* E. *That is, if* $\{x_n\}$ *is a sequence in* C, *converging weakly to an* $x_0 \in C$ *and* $\{Tx_n\}$ *converging strongly to a* $y_0 \in X$, *then* $Tx_0 = y_0$.

Definition 9. *A Banach space* E *is said to be uniformly convex if for given* $\epsilon \in (0, 2]$, *there exists a* $\delta = \delta(\epsilon) > 0$ *such that*

$$\|\tfrac{x+y}{2}\| \leq 1 - \delta \text{ whenever } \|x\| \leq 1, \|y\| \leq 1 \text{ and } \|x - y\| \geq \epsilon.$$

Throughout this paper, $\omega_w(\{x_n\})$ will denote the set of all weak subsequential limits of $\{x_n\}$, $\mathbb{N}$ will denote the set of all natural numbers and $F(T)$ will denote the set of all fixed points of mapping T.
The following proposition and lemmas will be used in our theorems later on.

Proposition 1. *(2008) Let* E *be a Banach space,* $\phi \neq C \subseteq E$ *and* $T : C \to C$ *be a mapping.*

(i) If T *is a nonexpansive mapping, then it is a Suzuki generalized nonexpansive mapping.*

(ii) If T *is a Suzuki generalized nonexpansive mapping and has a fixed point, then it is a quasi-nonexpansive mapping.*

(iii) If T is a Suzuki generalized nonexpansive mapping, then

$$\|x - Ty\| \leq 3\|Tx - x\| + \|x - y\| \text{ for all } x, y \in C.$$

Lemma 1. *(Schu, 1991, p. 1555) Let $(E, ||.||)$ be a uniformly convex Banach space, $0 < b < c < 1, a > 0, \{t_n\}$ is a sequence in $[b, c]$, $\{x_n\}, \{y_n\}$ are sequences in E such that $\limsup_{n\to\infty} ||x_n|| \leq a$, $\limsup_{n\to\infty} ||y_n|| \leq a$ and $\lim_{n\to\infty} ||t_n x_n + (1 - t_n)y_n|| = a$. Then $\lim_{n\to\infty} ||x_n - y_n|| = 0$.*

Lemma 2. *(Suzuki, 2008, p.1093) Let T be a mapping on a weakly closed subset C of a Banach space E with the Opial property. Assume that T is a Suzuki generalized nonexpansive mapping. Then $I - T$ is demiclosed at zero.*

Lemma 3. *(Sahu & Beg, 2008, p.141) Let E be a uniformly convex Banach space satisfying the Opial condition, C a nonempty closed convex subset of E and T: C $\to$ C a uniformly continuous nearly asymptotically nonexpansive mapping. Then I-T is demiclosed at zero.*

Lemma 4. *(Agarwal et al., 2007, pp. 65-66) Let C be a non-empty convex subset of a Banach space E and let $H_n : C \to E$ $(n = 1, 2, ...)$ be mappings with $\bigcap_{n\in\mathbb{N}} F(H_n) \neq \phi$ satisfying*

$$||H_n x - H_n y|| \leq L_n||x - y|| + \rho_n$$

for all $x, y \in C$ and $n \in \mathbb{N}$, where $\{L_n\}$ and $\{\rho_n\}$ are sequences of real numbers such that

(i) $L_n \geq 1$ for all $n \in \mathbb{N}$ and $\sum_{n=1}^{\infty}(L_n - 1) < \infty$,

(ii) $\rho_n \geq 0$ for all $n \in \mathbb{N}$ and $\sum_{n=1}^{\infty} \rho_n < \infty$.

Let $\{x_n\}$ be a sequence in C defined by

$$x_{n+1} = H_n x_n \text{ for all } n \in \mathbb{N}.$$

Then the following holds:

(a) $\lim_{n\to\infty} \|x_n - p\|$ exists for all $p \in \bigcap_{n\in\mathbb{N}} F(H_n)$;

(b) If E is uniformly convex, then $\lim_{n\to\infty} \|tx_n + (1 - t)q_1 - q_2\|$ exists for all $q_1, q_2 \in \bigcap_{n\in\mathbb{N}} F(H_n)$ and $t \in [0, 1]$;

(c) If E is a real uniformly convex Banach space with Fréchet differentiable norm, then $\lim_{n\to\infty}\langle x_n, J(q_1-q_2)\rangle$ exists for all $q_1, q_2 \in \bigcap_{n\in\mathbb{N}} F(H_n)$, where J is a normalized duality mapping.

Lemma 5. *(Agarwal et al., 2007, pp. 68-69) Let E be a reflexive Banach space satisfying the Opial condition, C a nonempty, closed, convex subset of E and $T : C \to E$ a mapping such that*

1. $F(T) \neq \emptyset$,

2. $I - T$ is demiclosed at zero.

Let $\{x_n\}$ be a sequence in C satisfying the following properties:

(D_1) $\lim_{n\to\infty} ||x_n - p||$ exists for all $p \in F(T)$;

(D_2) $\lim_{n\to\infty} ||x_n - Tx_n|| = 0$.

Then $\{x_n\}$ converges weakly to a fixed point of T.

Lemma 6. *(Agarwal et al., 2007, p. 69) Let C be a nonempty, closed, convex subset of a real Banach space E and $T : C \to C$ a mapping such that*

(a) $F(T) \neq \emptyset$

(b) $I - T$ is demiclosed at zero.

Let $\{x_n\}$ be a sequence in C which satisfies property (D_2) and one of the following conditions:

(i) E is uniformly convex with the Fréchet differentiable norm and

$$\lim_{n\to\infty}\langle x_n, J(q_1-q_2)\rangle \text{ exists for all } q_1, q_2 \in F(T)$$

(ii) E is reflexive, E^* has the Kadec-Klee property and

$$\lim_{n\to\infty} \|tx_n + (1-t)q_1 - q_2\| \text{ exists}$$

for all $q_1, q_2 \in \omega_w(\{x_n\})$ and for all $t \in [0, 1]$.

Then $\{x_n\}$ converges weakly to a fixed point of T.

The following theorem regarding the existence of a fixed point of a nonexpansive mapping was proved independently by Browder, Kirk and Göhde in 1965.

Theorem 1. *Let C be a nonempty, closed, bounded and convex subset of a uniformly convex Banach space and $T : C \to C$ a nonexpansive mapping. Then T has a fixed point.*

The above theorem was generalized by Goebel and Kirk in 1972, which follows.

Theorem 2. *Every asymptotically nonexpansive self-mapping of a nonempty closed bounded and convex subset of a uniformly convex Banach space has a fixed point.*

The following theorem regarding the existence of a fixed point of the Suzuki generalized nonexpansive mapping was proved by Suzuki in 2008.

Theorem 3. *Let C be a weakly compact convex subset of a uniformly convex Banach space and $T : C \to C$ a Suzuki generalized nonexpansive mapping. Then T has a fixed point.*

C-iteration scheme and convergence analysis

We introduce the following iteration scheme:
Let C be a convex subset of a linear space X and T be a mapping from C into itself. Choose $x_1 \in X$ and define a sequence $\{x_n\}$ as follows

$$\begin{aligned} x_{n+1} &= \alpha_n T y_n + (1-\alpha_n) T z_n, \\ y_n &= (1-\beta_n) x_n + \beta_n T x_n, \\ z_n &= (1-\gamma_n) T x_n + \gamma_n T^2 x_n, \quad n \in \mathbb{N}. \end{aligned}$$

where $\{\alpha_n\}, \{\beta_n\}$ and $\{\gamma_n\}$ are sequences in $(0, 1)$. We will call it the C-iteration scheme. x_{n+1} can be written as

$$x_{n+1} = C(x_n, \alpha_n, \beta_n, \gamma_n, T), n \in \mathbb{N} \tag{3}$$

where

$$\begin{aligned} C(x_n, \alpha_n, \beta_n, \gamma_n, T) =& \alpha_n T[(1-\beta_n)x_n + \beta_n T x_n] + (1-\alpha_n) T[(1-\gamma_n) T x_n \\ &+ \gamma_n T^2 x_n]. \end{aligned}$$

If $\{x_n\}$ and $\{w_n\}$ are two iteration schemes converging to the same fixed point p, then according to Rhoades (1976), $\{x_n\}$ is better than $\{w_n\}$ if $||x_n - p|| \leq ||w_n - p||$ for all $n \in \mathbb{N}$

Proposition 2. *Let C be a nonempty closed convex subset of a Banach space E and $T : C \to C$ a contraction mapping with Lipschitz constant*

Murthy, P.P.. et al., A new iteration scheme for approximating fixed points of some generalized nonexpansive mappings, pp.26–49

k and a unique fixed point p. Let $\{w_n\}$ and $\{x_n\}$ are sequences obtained by S-iteration and C-iteration schemes respectively, where $w_1 = x_1$. Then $||x_n - p|| \leq ||w_n - p||$ for all $n \in \mathbb{N}$, i.e. C iteration is better than the S iteration.

Proof. Agarwal et al. (2007) proved that $||w_{n+1} - p|| \leq k[1 - (1 - k)\alpha_n\beta_n]||w_n - P||$ for all $n \in \mathbb{N}$. If $a_n = k[1 - (1 - k)\alpha_n\beta_n]$ then the above inequality can be rewritten as

$$\begin{aligned} ||w_{n+1} - p|| &\leq a_n||w_n - p|| \\ &\leq a_n a_{n-1}....a_1||w_1 - p|| \end{aligned} \tag{4}$$

As $y_n = (1 - \beta_n)x_n + \beta_n Tx_n$, we obtain

$$\begin{aligned} ||y_n - p|| &= ||(1 - \beta_n)(x_n - p) + \beta_n(Tx_n - p)|| \\ &\leq (1 - \beta_n)||(x_n - p)|| + \beta_n||(Tx_n - p)|| \\ &\leq (1 - \beta_n)||(x_n - p)|| + k\beta_n||(x_n - p)|| \\ &= \{(1 - \beta_n) + k\beta_n\}||(x_n - p)|| \\ &= \{1 - (1 - k)\beta_n\}||(x_n - p)|| \end{aligned} \tag{5}$$

As $z_n = (1 - \gamma_n)Tx_n + \gamma_n T^2 x_n$, we obtain

$$\begin{aligned} ||z_n - p|| &= ||(1 - \gamma_n)(Tx_n - p) + \gamma_n(T^2 x_n - p)|| \\ &\leq (1 - \gamma_n)||(Tx_n - p)|| + \gamma_n||(T^2 x_n - p)|| \\ &\leq k(1 - \gamma_n)||(x_n - p)|| + k^2\gamma_n||x_n - p)|| \\ &= \{1 - (1 - k)\gamma_n k\}||x_n - p||. \end{aligned} \tag{6}$$

Now

$$\begin{aligned} ||x_{n+1} - p|| &= ||\alpha_n(Ty_n - p) + (1 - \alpha_n)(Tz_n - p)|| \\ &\leq \alpha_n k||(y_n - p)|| + k(1 - \alpha_n)||(z_n - p)|| \end{aligned} \tag{7}$$

From (5), (6) and (7), we obtain

$$\begin{aligned} ||x_{n+1} - p|| \leq & \alpha_n k[\{1 - (1 - k)\beta_n\}||(x_n - p)||] \\ & + k(1 - \alpha_n)[\{1 - (1 - k)\gamma_n k\}||x_n - p||] \\ \leq & k[1 - (1 - k)\{\alpha_n\beta_n + (1 - \alpha_n)\gamma_n k\}]||x_n - p|| \end{aligned} \tag{8}$$

If $b_n = k[1-(1-k)\{\alpha_n\beta_n + (1-\alpha_n)\gamma_n k\}]$, then above inequality can be written as

$$\begin{aligned} ||x_{n+1} - p|| &\leq b_n||x_n - p|| \\ &\leq b_n b_{n-1}.....b_1||x_1 - p|| \end{aligned} \tag{9}$$

It is clear that $b_n \leq a_n$, thus from (4) and (9), we obtain

$$||x_{n+1} - p|| \leq ||w_{n+1} - p|| \tag{10}$$

Thus, the C - iteration converges better than the S-iteration. □

In the following example, we compare the rate of convergence of various iteration processes.

Example 1. Let $E = \mathbb{R}, C = [1, 100]$ and $T : C \to C$ be a mapping defined by $T(x) = \sqrt{x^2 - 10x + 30}$. Choosing $\alpha_n = \beta_n = \gamma_n = \frac{1}{2}$ and starting with the initial value 30, the successive iterations of various schemes are shown in the following table:

All the three sequences converge to 3, which is the fixed point of T. The table shows that the C iteration converges fastest among the others mentioned in the table.

Table 1 – Comparison of the rate of convergence

Step	Thakur Iteration	S-Iteration	C-Iteration
1	30	30	30
2	21.4448278	23.88014761	20.23163969
3	13.01007821	17.804770146	10.66340962
4	5.068991397	11.81891627	3.19808755
5	2.762120635	6.09946412	2.99531744
6	3.014495235	2.41807081	3.00008615
7	2.99905689	3.23583758	2.99999840
8	3.00006111	2.91017776	3.00000003
9	2.999996039	3.03518482	2.99999999
10	3.000000257	2.98635715	3.00000000
11	2.99999998	3.00531152	3.00000000
12	3.000000001	2.99793532	3.00000000
13	3.00000000	3.00080307	3.00000000
14	3.00000000	2.99968772	3.00000000
15	3.00000000	3.00012145	3.00000000
16	3.00000000	2.99995277	3.00000000
17	3.00000000	3.00001837	3.00000000
18	3.00000000	2.99999286	3.00000000
19	3.00000000	3.00000278	3.00000000
20	3.00000000	2.99999892	3.00000000
21	3.00000000	3.00000042	3.00000000
22	3.00000000	2.99999984	3.00000000
23	3.00000000	3.00000006	3.00000000
24	3.00000000	2.99999998	3.00000000
25	3.00000000	3.00000001	3.00000000
26	3.00000000	2.999999996	3.00000000
27	3.00000000	3.000000001	3.00000000
28	3.00000000	2.999999999	3.00000000
29	3.00000000	3.00000000	3.00000000

Remark 1. In Proposition 2, if T is quasi-nonexpansive with a fixed point p, then inequalities (5), (6) and (8) become

$$||y_n - p|| \leq ||x_n - p||, \tag{11}$$

$$||z_n - p|| \leq ||x_n - p|| \text{ and} \tag{12}$$

$$||x_{n+1} - p|| \leq ||x_n - p|| \tag{13}$$

respectively.

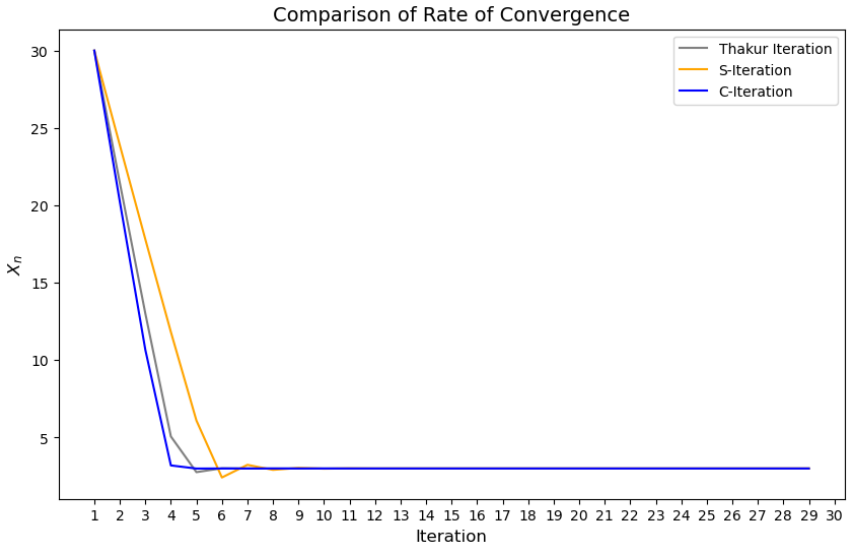

Figure 1 – Comparison of the rate of convergence

Now we will define the modified C-iteration as follows:
Let C be a convex subset of a normed linear space X and T be a mapping from C into itself. Choose $x_1 \in C$ and define a sequence $\{x_n\}$ in C as follows:

$$x_{n+1} = C(x_n, \alpha_n, \beta_n, \gamma_n, T^n), n \in \mathbb{N}. \tag{14}$$

That is

$$x_{n+1} = \alpha_n T^n[(1-\beta_n)x_n + \beta_n T^n x_n] + (1-\alpha_n)T^n[(1-\gamma_n)T^n x_n + \gamma_n T^{n+1} x_n]$$

where $\{\alpha_n\}, \{\beta_n\}$ and $\{\gamma_n\}$ are sequences in $(0, 1)$. Equivalently, it can be written as

$$\begin{aligned} x_{n+1} &= \alpha_n T^n y_n + (1-\alpha_n)T^n z_n & (15)\\ y_n &= (1-\beta_n)x_n + \beta_n T^n x_n & (16)\\ z_n &= (1-\gamma_n)T^n x_n + \gamma_n T^{n+1} x_n, \quad n \in \mathbb{N} & (17) \end{aligned}$$

Fixed point results for the Suzuki generalized nonexpansive mappings

The following Proposition and Lemma will be used to prove our main results in this section.

Proposition 3. *Let E be a Banach space, C a nonempty, convex subset of E, $T : E \to E$ be a quasi nonexpansive mapping with $F(T) \neq \emptyset$.$\{x_n\}$ be a sequence in E defined by C-iteration scheme. Then $\lim_{n\to\infty} ||x_n - p||$ exists for all $p \in F(T)$.*

Proof. If T is a quasi nonexpansive mapping with a fixed point p, then from (13), we obtain

$$||x_{n+1} - p|| \leq ||x_n - p||$$

for all $n \in \mathbb{N}$. That is, the sequence of real numbers $\{||x_n - p||\}$ is non-increasing and bounded below, so $\lim_{n\to\infty} ||x_n - p||$ exists for all $p \in F(T)$. □

Lemma 7. *Let E be a uniformly convex Banach space, C a nonempty, convex subset of E, T be a Suzuki generalized nonexpansive self mapping of C. Let $\{x_n\}$ be defined by the C-iteration scheme, given by (3), where $\{\alpha_n\}, \{\beta_n\}, \{\gamma_n\}$ are sequences in $[a, b]$ for some $a, b \in \mathbb{R}$ with $0 < a \leq b < 1$. If $F(T) \neq \phi$, then $\lim_{n\to\infty} ||x_n - Tx_n|| = 0$.*

Proof. Since T is a Suzuki generalised nonexpansive mapping with $F(T) \neq \phi$, it is a quasi-nonexpansive by Proposition 1. Hence, by Propostion 3, $\lim_{n\to\infty} ||x_n - p||$ exists for all $p \in F(T)$. Let this limit be l. From (11) and (12), we obtain

$$\lim_{n\to\infty} \sup ||y_n - p|| \leq l \text{ and} \tag{18}$$

$$\lim_{n\to\infty} \sup ||z_n - p|| \leq l. \tag{19}$$

Since $||Tx_n - p|| \leq ||x_n - p||, ||Ty_n - p|| \leq ||y_n - p||, ||Tz_n - p|| \leq ||z_n - p||$, we obtain

$$\lim_{n\to\infty} \sup ||Tx_n - p|| \leq l; \tag{20}$$

$$\lim_{n\to\infty} \sup ||Ty_n - p|| \leq l; \tag{21}$$

$$\lim_{n\to\infty} \sup ||Tz_n - p|| \leq l. \tag{22}$$

Now

$$l = \lim_{n\to\infty} \sup ||x_{n+1} - p|| = \lim_{n\to\infty} ||\alpha_n(Ty_n - p) + (1 - \alpha_n)(Tz_n - p)||$$

thus, by Lemma 1, we obtain

$$\lim_{n\to\infty} ||Ty_n - Tz_n|| = 0. \tag{23}$$

Now

$$\begin{aligned} ||x_{n+1} - p|| &= ||Tz_n - p + \alpha_n(Ty_n - Tz_n)|| \\ &\leq ||Tz_n - p|| + \alpha_n||(Ty_n - Tz_n)||. \end{aligned}$$

This implies

$$l \leq \lim_{n\to\infty} \inf ||Tz_n - p|| \tag{24}$$

This implies using (22) that

$$\lim_{n\to\infty} ||Tz_n - p|| = l.$$

Now, we have

$$\begin{aligned} ||Tz_n - p|| &\leq ||Tz_n - Ty_n|| + ||Ty_n - p|| \\ &\leq ||Tz_n - Ty_n|| + ||y_n - p||. \end{aligned}$$

This implies

$$l \leq \lim_{n\to\infty} \inf ||y_n - p||$$

This inequality with (18) yields

$$\lim_{n\to\infty} ||y_n - p|| = l. \tag{25}$$

Moreover

$$l = \lim_{n\to\infty} ||y_n - p|| = \lim_{n\to\infty} ||(1-\beta_n)(x_n - p) + \beta_n(Tx_n - p)|| \tag{26}$$

Thus, by Lemma 1, we obtain

$$\lim_{n\to\infty} ||x_n - Tx_n|| = 0.$$

□

Theorem 4. *Let E be a uniformly convex Banach space satisfying the Opial condition, C a nonempty, weakly closed, convex subset of E. T is a Suzuki generalized nonexpansive self mapping of C. Let $\{x_n\}$ be defined by the C-iteration scheme, given by (3), where $\{\alpha_n\}, \{\beta_n\}, \{\gamma_n\}$ are sequences in $[a, b]$ for some $a, b \in \mathbb{R}$ with $0 < a \leq b < 1$. If $F(T) \neq \emptyset$, then $\{x_n\}$ converges weakly to a fixed point of T.*

Proof. Since T is a Suzuki generalized nonexpansive with $F(T) \neq \emptyset$, it is a quasi nonexpansive mapping by Proposition 1 and hence $\{x_n\}$ has the property (D_1) and (D_2) by Proposition 3 and Lemma 7 respectively. $I-T$ is demiclosed by Lemma 2. Since E is uniformly convex, it is reflexive; hence, using Lemma 5, we conclude that sequence $\{x_n\}$ converges weakly to a fixed point of T. □

Corollary 1. *Let E be a uniformly convex Banach space satisfying the Opial condition, C a nonempty, closed, bounded and convex subset of E. T be a nonexpansive self mapping of C. Let $\{x_n\}$ be defined by the C-iteration scheme, given by (3), where $\{\alpha_n\}, \{\beta_n\}, \{\gamma_n\}$ are sequences in $[a, b]$ for some $a, b \in \mathbb{R}$ with $0 < a \leq b < 1$. Then $\{x_n\}$ converges weakly to a fixed point of T.*

Proof. $F(T) \neq \phi$ by Theorem 1. C is closed, therefore it is weakly closed. T is nonexpansive, therefore it is a Suzuki generalized nonexpansive map. Thus, the result follows from Theorem 4. □

Theorem 5. *Let E be a uniformly convex Banach space, C a nonempty, compact, convex subset of E. Let T be a Suzuki generalized nonexpansive self mapping of C. Let $\{x_n\}$ be defined by the C-iteration scheme, given by (3), where $\{\alpha_n\}, \{\beta_n\}, \{\gamma_n\}$ are sequences in $[a, b]$ for some $a, b \in \mathbb{R}$ with $0 < a \leq b < 1$. Then $\{x_n\}$ converges strongly to a fixed point of T.*

Proof. $F(T) \neq \phi$ by Theorem 3, therefore by Lemma 7, we obtain $\lim_{n\to\infty} \|Tx_n - x_n\| = 0$. Since C is compact, the sequence $\{x_n\}$ has a subsequence $\{x_{n_k}\}$ strongly converging to a point $p \in C$. By Proposition 1, we obtain

$$\|x_{n_k} - Tp\| \leq 3\|Tx_{n_k} - x_{n_k}\| + \|x_{n_k} - p\| \text{ for all } k \geq 1$$

Letting $k \to \infty$, we obtain $Tp = p$. Since $\lim_{n\to\infty} \|x_n - p\|$ exists by Proposition 3, $\{x_n\}$ converges strongly to p. □

Fixed point results for nearly asymptotically nonexpansive mappings

The following Lemma will be used to prove our main results in this section.

Lemma 8. *Let E be a uniformly convex Banach space, C a nonempty, closed, convex subset of E. Let $T : C \to C$ be a nearly asymptotically nonexpansive mapping with a sequence $\{(a_n, k_n)\}$ and $F(T) \neq \phi$ such that $\sum_{n=1}^{\infty} a_n < \infty$ and $\sum_{n=1}^{\infty} (k_n\sqrt{k_1} - 1) < \infty$. Let $\{x_n\}$ be defined by the modified C-iteration given by (14), where $\{\alpha_n\}, \{\beta_n\}, \{\gamma_n\}$ are sequences in $[a, b]$ for some $a, b \in \mathbb{R}$ with $0 < a \leq b < 1$. Then*

(i) $\lim_{n\to\infty} ||x_n - p||$ *exists;*

(ii) $\lim_{n\to\infty} ||x_n - T^n x_n|| = 0$;

(iii) $\{x_n\}$ *satisfies property* (D_2)*, if T is uniformly continuous.*

Proof. (i) We define a mapping $H_n : C \to C$ by

$$H_n(x) = \alpha_n T^n[(1-\beta_n)x + \beta_n T^n x] + (1-\alpha_n)T^n[(1-\gamma_n)T^n x + \gamma_n T^{n+1}x]$$

where $n \in \mathbb{N}$. Now

$$\begin{aligned}
||H_n x - H_n y|| \leq & \alpha_n[k_n(||(1-\beta_n)(x-y) + \beta_n(T^n x - T^n y)|| + a_n)] \\
& + (1-\alpha_n)[k_n(||(1-\gamma_n)(T^n x - T^n y) + \gamma_n(T^{n+1}x - T^{n+1}y)|| \\
& + a_n)] \\
\leq & \alpha_n[k_n\{(1-\beta_n)||x-y|| + \beta_n k_n(||x-y|| + a_n) + a_n\}] \\
& + (1-\alpha_n)[k_n\{(1-\gamma_n)k_n(||x-y|| + a_n) + \gamma_n k_{n+1}(||x-y|| \\
& + a_{n+1}) + a_n\}] \\
\leq & [k_n(1-\beta_n) + \beta_n k_n^2 + k_n\{(1-\gamma_n)k_n + \gamma_n k_{n+1}\}]||x-y|| \\
& + 2k_n^2 a_n + a_n k_n + k_n k_{n+1} a_{n+1} \\
\leq & [\alpha_n k_n^2 + (1-\alpha_n)k_n \max\{k_n, k_{n+1}\}]||x-y|| + 2k_n^2 a_n + a_n k_n \\
& + k_n k_{n+1} a_{n+1} \\
\leq & [\max\{k_n^2, k_n \max\{k_n, k_{n+1}\}\}]||x-y|| + 2k_n^2 a_n + a_n k_n \\
& + k_n k_{n+1} a_{n+1} \\
\leq & [\max\{k_n^2, k_n k_{n+1}\}]||x-y|| + 2k_n^2 a_n + a_n k_n + k_n k_{n+1} a_{n+1} \\
= & L_n||x-y|| + \rho_n
\end{aligned}$$

Murthy, P.P.. et al., A new iteration scheme for approximating fixed points of some generalized nonexpansive mappings, pp.26–49

where $L_n = \max\{k_n^2, k_n k_{n+1}\}$ and $\rho_n = 2k_n^2 a_n + a_n k_n + k_n k_{n+1} a_{n+1}$
If $K = \sup\{k_n : n \in \mathbb{N}\}$ then

$$\begin{aligned}\sum_{n=1}^{\infty}(L_n - 1) &= \sum_{n=1}^{\infty}(\max\{k_n^2, k_n k_{n+1}\} - 1)\\ &\leq \sum_{n=1}^{\infty}(\max\{k_n^2, k_n^2 k_1\} - 1)\\ &\leq \sum_{n=1}^{\infty}(k_n^2 k_1 - 1)\\ &\leq (K\sqrt{k_1} + 1)\sum_{n=1}^{\infty}(k_n\sqrt{k_1} - 1)\\ &< \infty\end{aligned}$$

and

$$\sum_{n=1}^{\infty}\rho_n = (2K^2 + K)\sum_{n=1}^{\infty}a_n + K^2\sum_{n=1}^{\infty}a_{n+1} < \infty.$$

It can be easily shown that $F(T) \subseteq F(H_n)$ for all $n \in \mathbb{N}$. Therefore by Lemma 4 $\lim_{n\to\infty}||x_n - p||$ exists where $p \in F(T)$.
(ii) Let $\lim_{n\to\infty}||x_n - p|| = l$.
Since

$$\begin{aligned}||y_n - p|| &\leq (1-\beta_n)||x_n - p|| + \beta_n||T^n x_n - p||\\ &\leq (1-\beta_n)||x_n - p|| + \beta_n k_n(||x_n - p|| + a_n)\\ &\leq k_n||x_n - p|| + k_n a_n.\end{aligned}$$

Therefore we obtain

$$\lim_{n\to\infty}\sup||y_n - p|| \leq l. \tag{27}$$

This implies

$$\lim_{n\to\infty}\sup||T^n y_n - p|| \leq \lim_{n\to\infty}\sup\{k_n(||y_n - p|| + a_n)\} \leq l \tag{28}$$

Moreover,

$$||z_n - p|| \leq (1-\gamma_n)||T^n x_n - p|| + \gamma_n||T^{n+1}x_n - p||$$

$$\begin{aligned} &\leq (1-\gamma_n)k_n(||x_n-p||+a_n)+\gamma_n k_{n+1}(||x_n-p||+a_n) \\ &\leq \max\{k_n,k_{n+1}\}||x_n-p||+a_n\max\{k_n,k_{n+1}\} \end{aligned}$$

which gives

$$\lim_{n\to\infty}\sup||z_n-p||\leq l \tag{29}$$

and hence

$$\lim_{n\to\infty}\sup||T^n z_n-p||\leq\lim_{n\to\infty}\sup\{k_n(||z_n-p||+a_n)\}\leq l. \tag{30}$$

Since

$$l=\lim_{n\to\infty}||x_{n+1}-p||=\lim_{n\to\infty}||\alpha_n(T^n y_n-p)+(1-\alpha_n)(T^n z_n-p)||,$$

therefore by Lemma 1, we obtain

$$\lim_{n\to\infty}||T^n y_n-T^n z_n||=0. \tag{31}$$

Now, since

$$||x_{n+1}-p||\leq\alpha_n||T^n y_n-T^n z_n||+||T^n z_n-p||,$$

thus

$$l\leq\lim_{n\to\infty}\inf||T^n z_n-p||. \tag{32}$$

From (30) and (32), we obtain

$$\lim_{n\to\infty}||T^n z_n-p||=l. \tag{33}$$

Since

$$||T^n z_n-p||\leq||T^n z_n-T^n y_n||+||T^n y_n-p||\leq||T^n z_n-T^n y_n||+k_n(||y_n-p||+a_n),$$

we obtain

$$l\leq\lim_{n\to\infty}\inf||y_n-p||. \tag{34}$$

From (27) and (34), we obtain

$$\lim_{n\to\infty}||y_n-p||=l.$$

Since

$$l=\lim_{n\to\infty}||y_n-p||=\lim_{n\to\infty}||(1-\beta_n)(x_n-p)+\beta_n(T^n x_n-p)||$$

therefore by Lemma 1, we obtain

$$\lim_{n\to\infty} ||x_n - T^n x_n|| = 0. \tag{35}$$

(iii) Since $||T^n x_n - p|| \leq k_n(||x_n - p|| + a_n)$,

$$\lim_{n\to\infty} \sup ||T^n x_n - p|| \leq l \text{ and } \lim_{n\to\infty} \sup ||T^{n+1} x_n - p|| \leq l. \tag{36}$$

Since $||T^n z_n - p|| \leq k_n(||z_n - p|| + a_n)$, using (33), we obtain

$$l \leq \lim_{n\to\infty} \inf ||z_n - p||. \tag{37}$$

(29) and (37) give

$$\lim_{n\to\infty} ||z_n - p|| = l.$$

This gives using (17) that

$$l = \lim_{n\to\infty} ||z_n - p|| = \lim_{n\to\infty} ||(1-\gamma_n)(T^n x_n - p) + \gamma_n(T^{n+1} x_n - p)$$

This gives using (36) and Lemma 1 that

$$\lim_{n\to\infty} ||T^n x_n - T^{n+1} x_n|| = 0. \tag{38}$$

Now

$$\begin{aligned} ||z_n - x_n|| &= ||(1-\gamma_n)T^n x_n + \gamma_n T^{n+1} x_n - x_n|| && (39)\\ &\leq ||x_n - T^n x_n|| + \gamma_n ||T^n x_n - T^{n+1} x_n||. && (40) \end{aligned}$$

This implies using (35) and (38) that

$$\lim_{n\to\infty} ||z_n - x_n|| = 0 \tag{41}$$

Thus

$$\lim_{n\to\infty} ||T^n z_n - T^n x_n|| \leq \lim_{n\to\infty} k_n(||z_n - x_n|| + a_n) = 0$$

This implies

$$\lim_{n\to\infty} ||T^n z_n - T^n x_n|| = 0 \tag{42}$$

Now from (15), we have

$$||x_{n+1} - T^n x_n|| = ||\alpha_n T^n y_n + (1-\alpha_n)T^n z_n - T^n x_n||$$

$$\leq \quad \alpha_n||T^n y_n - T^n z_n|| + ||T^n z_n - T^n x_n||$$

This gives using (31) and (42)

$$\lim_{n\to\infty} ||x_{n+1} - T^n x_n|| = 0. \tag{43}$$

By (35) and (43), we have

$$0 = \lim_{n\to\infty} ||x_{n+1} - x_n|| \leq \lim_{n\to\infty} ||x_{n+1} - T^n x_n|| + \lim_{n\to\infty} ||T^n x_n - x_n|| = 0 \tag{44}$$

By uniform continuity of T and (35), we have

$$\lim_{n\to\infty} ||T^{n+1} x_n - T x_n|| = 0. \tag{45}$$

Now

$$\begin{aligned} ||x_n - Tx_n|| \leq & ||x_n - x_{n+1}|| + ||x_{n+1} - T^{n+1}x_{n+1}|| + ||T^{n+1}x_{n+1} - T^{n+1}x_n|| \\ & + ||T^{n+1}x_n - Tx_n|| \\ \leq & ||x_n - x_{n+1}|| + ||x_{n+1} - T^{n+1}x_{n+1}|| + k_{n+1}(||x_{n+1} - x_n|| + a_n) \\ & + ||T^{n+1}x_n - Tx_n||. \end{aligned}$$

This implies using (35), (44) and (45), that

$$\lim_{n\to\infty} ||x_n - Tx_n|| = 0.$$

□

Theorem 6. *Let E be a uniformly convex Banach space satisfying the Opial condition, C a nonempty, closed, convex subset of E. $T : C \to C$ be a uniformly continuous nearly asymptotically nonexpansive mapping with the sequence $\{(a_n, k_n)\}$ and $F(T) \neq \phi$ such that $\sum_{n=1}^{\infty} a_n < \infty$ and $\sum_{n=1}^{\infty} (k_n\sqrt{k_1} - 1) < \infty$. Let $\{x_n\}$ be defined by the modified C-iteration given by (14) where $\{\alpha_n\}, \{\beta_n\}, \{\gamma_n\}$ are sequences in $[a, b]$ for some $a, b \in \mathbb{R}$ with $0 < a \leq b < 1$. Then $\{x_n\}$ converges weakly to a fixed point of T.*

Proof. E is uniformly convex, so it is reflexive. The sequence $\{x_n\}$ has properties (D_1) and (D_2) by Lemma 8. $I - T$ is demiclosed at zero by Lemma 3 and $F(T) \neq \emptyset$ by assumption. Therefore, by Lemma 5, $\{x_n\}$ converges weakly to a fixed point of T. □

Corollary 2. *Let E be a uniformly convex Banach space satisfying the Opial condition, C a nonempty, closed, convex subset of E. $T : C \to C$ be a uniformly continuous asymptotically nonexpansive mapping with sequence $\{k_n\}$ such that $\sum_{n=1}^{\infty}(k_n\sqrt{k_1} - 1) < \infty$. Let $\{x_n\}$ be defined by the modified C-iteration given by (14) where $\{\alpha_n\}, \{\beta_n\}, \{\gamma_n\}$ are sequences in $[a, b]$ for some $a, b \in \mathbb{R}$ with $0 < a \leq b < 1$. Then $\{x_n\}$ converges weakly to a fixed point of T.*

Proof. Since $F(T) \neq \phi$ by Theorem 2 and every asymptotically nonexpansive mapping is nearly asymptotically nonexpansive mapping, the proof follows by Theorem 6. □

Theorem 7. *Let E be a real uniformly convex Banach space. Let E has the Fréchet differentiable norm or E^* has the Kadec-Klee property, C a nonempty, closed, convex subset of E. $T : C \to C$ be a uniformly continuous nearly asymptotically nonexpansive mapping with sequence $\{(a_n, k_n)\}$ such that $\sum_{n=1}^{\infty} a_n < \infty$, $\sum_{n=1}^{\infty}(k_n\sqrt{k_1} - 1) < \infty, I - T$ is demiclosed at zero and $F(T) \neq \phi$. Let $\{x_n\}$ be defined by the modified C-iteration given by (14) where $\{\alpha_n\}, \{\beta_n\}, \{\gamma_n\}$ are sequences in $[a, b]$ for some $a, b \in \mathbb{R}$ with $0 < a \leq b < 1$. Then $\{x_n\}$ converges weakly to a fixed point of T.*

Proof. $\{x_n\}$ has properties (D_1) and (D_2) by Lemma 8. By Lemma 4, we have

(a) $\lim_{n\to\infty} \|tx_n + (1-t)q_1 - q_2\|$ exists for all $q_1, q_2 \in F(T)$, $t \in [0, 1]$;

(b) $\lim_{n\to\infty} \langle x_n, J(q_1 - q_2)\rangle$ exists for all $q_1, q_2 \in F(T)$ if E has Fréchet differentiable norm.

$I - T$ is demiclosed by assumption. E is reflexive as it is uniformly convex. Hence the result follows from Lemma 6. □

References

Agarwal, R.P., O'Regan D. & Sahu D.R. 2007. Iterative construction of fixed points of nearly asymptotically nonexpansive mappings. *Journal of Nonlinear Convex Analysis* 8(1), pp. 61-79. Available at: http://www.ybook.co.jp/online-p/JNCA/vol8/jncav8n1p61.pdf

Browder, F. E. 1965. Nonexpansive nonlinear operators in a Banach space. *Proceedings of the National Academy of Sciences, U.S.A.* 54(4) , pp. 1041-1044. Available at: https://www.pnas.org/doi/pdf/10.1073/pnas.54.4.1041.

Goebel, K. & Kirk, W.A. 1972. A fixed point theorem for asymptotically nonexpansive mappings. *Proceedings of the American Mathematical Society* 35(1), pp. 171-174. Available at: https://doi.org/10.1090/S0002-9939-1972-0298500-3

Gӧhde, D. 1965. Zum Prinzip der kontraktiven Abbildung. *Mathematische Nachrichten.* 30, pp. 251-258 (in German). Available at: https://doi.org/10.1002/mana.19650300312.

Kirk, W. A. 1965. A fixed point theorem for mappings which do not increase distance. *The American mathematical monthly.* 72(9), pp. 1004-1006. Available at: https://doi.org/10.2307/2313345.

Mann, W. R. 1953. Mean value methods in iteration. *Proceedings of the American Mathematical Society,* 4, pp. 506-510. Available at: https://doi.org/10.2307/2032162

Opial, Z. 1967. Weak convergence of the sequence of successive approximations for nonexpansive mappings. *Bulletin of American Mathematical Socety,* 73, pp. 591-597. Available at: https://www.ams.org/journals/bull/1967-73-04/S0002-9904-1967-11761-0/?active=current

Rhoades, B.E. 1976. Comments on two fixed point iteration methods. *Journal of Mathematical Analysis and Applications.* 56(3), pp. 741-750. Available at: https://doi.org/10.1016/0022-247X(76)90038-X

Sahu, D.R. 2005. Fixed points of demicontinuous nearly Lipschitzian mappings in Banach spaces. *Commentationes Mathematicae Universitatis Carolinae.* 46(4), pp. 653-666. Available at: http://dml.cz/dmlcz/119557

Sahu, D.R. & Beg I. 2008. Weak and strong convergence for fixed points of nearly asymptotically non-expansive mappings. *International*

Journal of Modern Mathematics. 3(2), pp. 135-151. Available at: https://www.researchgate.net/publication/233878799

Schu, J. 1991. Weak and strong convergence to fixed points of asymptotically nonexpansive mappings. *Bulletin of the Australian Mathematical Society.* 43, pp. 153-159. Available at: https://doi.org/10.1017/S0004972700028884

Suzuki, T. 2008. Fixed point theorems and convergence theorems for some generalized nonexpansive mappings. *Journal of mathematical analysis and applications.* 340, pp. 1088-1095. Available at: https://www.sciencedirect.com/science/article/pii/S0022247X07010955

Thakur, B.S., Thakur D., & Postolache M. 2016. A new iteration scheme for approximating fixed points of nonexpansive mappings. *Filomat*, 30(10), pp. 2711-2720. Available at: https://doi.org/10.2298/FIL1610711T

Nova iteraciona šema za aproksimaciju fiksnih tačaka nekih generalizovanih neekspanzivnih preslikavanja

Penumarthy Parvateesam Murthy, **autor za prepisku**, *Chandra* Prakash Dhuri

Guru Ghasidas Vishwavidyalaya (A Central University), Department of Mathematics, Bilaspur, India, 495 009

OBLAST: matematika
KATEGORIJA (TIP) ČLANKA: originalni naučni rad

Sažetak:

Uvod/cilj: U radu je predstavljen novi trostepeni iterativni postupak koji konvergira brže od Manove iteracije i S-iteracije, a utvrđeni su i rezultati konvergencije za aproksimaciju fiksnih tačaka generalizovanih Suzukijevih neekspanzivnih preslikavanja i skoro asimptotski neekspanzivnih preslikavanja.

Metode: Autori daju specifičnu trostepenu iterativnu metodu $\{x_n\}$ *u Banahovom prostoru, definisanu kao niz konveksnih kombinacija trenutnog iterata i njegovih slika pod preslikavanjem T, sa kontrolnim nizovima* $\{\alpha_n\}$, $\{\beta_n\}$, $\{\gamma_n\} \subseteq (0,1)$. *Rezultati su dokazani u okviru uniformno konveksnih Banahovih prostora gde se pretpostavlja da je T Suzukijevo generalizovano neekspanzivno preslikavanje ili skoro asimptotski neekspanzivno preslikavanje. Autori su dobili teoreme o slaboj i jakoj konvergenciji*

koristeći principe demizatvorenosti, osobine Suzukijevih generalizovanih neekspanzivnih preslikavanja i odgovarajuće leme o ponašanju iterata. Za poređenje brzine konvergencije sprovedeni su numerički eksperimenti (obično implementirani u MATLAB-u) u kojima se predložena trostepena iteracija vrši paralelno sa Takurovom i S-iteracijom. Iterati su grafički prikazani kako bi se pokazala konvergencija greške po iteraciji.

Rezultati: Nova iteraciona šema konvergira brže od S-iteracione šeme ako je preslikavanje kontrakcija. Nova iteraciona šema konvergira ka fiksnoj tački Suzukijevog generalizovanog neekspanzivnog preslikavanja pod odgovarajućim uslovima. Šema takođe konvergira ka fiksnoj tački skoro asimptotski neekspanzivnog preslikavanja pod odgovarajućim uslovima.

Zaključci: Dokazano je, i teorijski i numerički, da trostepeni iteracioni algoritam konvergira brže od Manove iteracije i S-iteracije (a ponekad i brže od nekoliko drugih postojećih metoda) za razmatrane tipove preslikavanja. Autori su dokazali teoreme o slaboj i jakoj konvergenciji za fiksne tačke Suzukijevih generalizovanih neekspanzivnih preslikavanja i skoro asimptotski neekspanzivnih preslikavanja u uniformno konveksnim Banahovim prostorima, čime se generalizuju, proširuju i objedinuju brojni postojeći rezultati aproksimacije fiksnih tačaka u literaturi.

Ključne reči: fiksne tačke, iteracija, uniformno konveksan Banahov prostor, neekspanzivno preslikavanje, Suzukijevo generalizovano neekspanzivno preslikavanje, skoro asimptotski neekspanzivna preslikavanja, refleksivni Banahov prostor.

Paper received on: 13 July 2024.
Manuscript corrections submitted on: 12 November 2024.
Paper accepted for publishing on: 6 November 2025.

© 2026 The Authors. Published by Vojnotehnički glasnik / Military Technical Courier (http://vtg.mod.gov.rs). This article is an open access article distributed under the terms and conditions of the Creative Commons Attribution license (http://creativecommons.org/licenses/by/4.0/rs/).

Selection of 3D printer for racing car spoilers using Entropy - CRADIS model

Rajeev Ranjan[a], *Sonu* Rajak[b], *Prasenjit* Chatterjee[c]

[a] Department of Mechanical Engineering, National institute of Technology, Patna, India,
e-mail: rajeevr.phd19.me@nitp.ac.in,
ORCID iD: https://orcid.org/0009-0006-3392-392X

[b] Department of Mechanical Engineering, National institute of technology, Patna, India,
e-mail: sonu.me@nitp.ac.in,
ORCID iD: https://orcid.org/0000-0002-4334-8010

[c] Department of Mechanical Engineering, MCKV Institute of Engineering, Howrah, West Bengal, India,
e-mail: chatterjee.drprasenjit@gmail.com, **corresponding author,**
ORCID iD: https://orcid.org/0000-0002-7994-4252

https://doi.org/10.5937/vojtehg74-58269

FIELD: mechanical engineering
ARTICLE TYPE: original scientific paper

Abstract:

Introduction/purpose: This study aims to identify the most suitable 3D printer for manufacturing racing car spoilers.

Methods: Sixteen different 3D printing machines are evaluated based on eight selection criteria including print volume, maximum print speed, layer thickness, number of extruders, machine cost, manufacturer filament price, maximum extruder temperature, and maximum bed temperature. The criteria weights are determined using the Entropy method, while the Compromise Ranking of Alternatives from Distance to Ideal Solution (CRADIS) method is applied to rank the machines and identify the best option for spoiler production. Sensitivity analysis is conducted using various methods to validate the results.

Results: Ultimaker 2 is identified as the most suitable 3D printer, followed by Delta Non-Turbo WASP 2040, while UP Plus 2 ranks as the least favorable.

Conclusion: By using the Entropy and CRADIS methods, Ultimaker 2 is identified as the best-performing 3D printer, followed by Delta Non-Turbo WASP 2040, while UP Plus 2 is ranked the lowest. Various MCDM methods are applied for performance comparison and sensitivity analysis, with the Spearman Rank Correlation Coefficient applied to assess the correlation between different MCDM methods.

Key words: additive manufacturing, 3D Printing, multi-criteria decision making, entropy, CRADIS, densitivity analysis.

Introduction

3D printing, also known as additive manufacturing, is a cutting-edge technology that enables the creation of three-dimensional objects by layering materials based on digital models. This innovation has transformed industries by offering enhanced design flexibility, reduced material waste, and cost-effective production, with applications spanning from prototyping and custom manufacturing to aerospace, healthcare, and the automotive sector (Gibson et al, 2015). Beyond revolutionizing traditional design and manufacturing processes, 3D printing has profoundly influenced various fields, including economics, geopolitics, sociology, environmental sustainability, demography, and security (Matias & Rao, 2015). A group of digital manufacturing technologies combined to create components layer by layer while using all available materials is known as 3D printing (West &Kuk, 2016; Sandström, 2016).

The true potential of 3D printing lies in its ability to drastically reduce the time required for large-scale production line adjustments while enabling continuous innovation during the manufacturing process. Simultaneously, this technology allows for mass production that is far more customizable to individual needs (Rayna & Striukova, 2016). The advancement and growth of manufacturing, retail, healthcare, and other industries are among the economic advantages of this technology (Jia et al, 2017). According to a recent survey by Allied Industry Research (AMR), the global 3D printing industry was estimated to be worth US $8.6 billion in 2020 and is expected to expand to US $15.6 billion by 2030, at a compound annual growth rate (CAGR) of 20.6%.

Although 3D printing has many benefits for businesses, its application is still rather limited. According to relevant studies, for instance, fewer than 2% of the manufacturing market still uses 3D printing (Wohlers et al, 2016). Furthermore, a lot of manufacturing companies are still having trouble optimizing their production lines and goods using this promising technology. In general, it appears that companies are facing significant challenges as a result of the widespread use of 3D printing.

Selecting a 3D printer for a specific industrial application is a complex decision-making problem that requires evaluating multiple conflicting criteria, such as cost, print quality, material compatibility, speed, reliability, ease of maintenance, and environmental impact (Gibson et al, 2015; Berman, 2012; Guo & Leu, 2013). Since no single 3D printer excels in all these aspects simultaneously, trade-offs must be made based on user

priorities. Multi-criteria decision-making (MCDM) methods provide structured frameworks to systematically assess these criteria, assign appropriate weights, and rank alternatives objectively, ensuring a balanced and rational selection process (Zavadskas et al, 2014). Without such an approach, decisions risk being subjective, inconsistent, or inefficient, potentially leading to suboptimal selections that may fail to meet operational requirements (Mardani et al, 2015). By using MCDM methods, decision-makers can quantify preferences, minimize biases, and align their selection with both technical and economic constraints, ultimately enhancing transparency and improving the likelihood of meeting long-term operational goals (Ford & Despeisse, 2016; Huang et al, 2013).

MCDM methods have emerged as indispensable tools in addressing complex decision problems that involve multiple conflicting criteria, particularly in engineering, business, sustainability, and industrial domains. These methods support decision-makers by offering systematic frameworks for evaluating alternatives based on diverse quantitative and qualitative factors. As highlighted by Kumar and Pamucar (2025), MCDM methods have evolved significantly over the past two decades, enabling better structuring, analysis, and resolution of real-world decision problems. MCDM methods have been widely applied across diverse sectors, demonstrating their adaptability to complex decision-making contexts. They have been used for personnel selection in the tourism industry (Genç et al, 2024), selection of automotive equipment (Komatina, 2025), evaluation of smog mitigation strategies in environmental and public health contexts (Kousar et al, 2025), and procurement decisions in defense, such as assault rifle selection (Radovanovic et al, 2024). Further applications include combat system selection (Tesic and Marinkovic, 2023), sustainability evaluations (Sahoo et al, 2025), financial performance assessments (Yalçın et al, 2025), and sensitivity analysis under uncertainty modeling (Więckowski & Sałabun, 2025). These developments highlight the importance of MCDM as a robust tool for intricate technical and strategic decisions, enabling transparent, data-driven choices in applications like high-performance 3D printer selection.

Despite the growing use of 3D printing in a variety of industries, current research on 3D printer selection is sometimes lacking in application specificity and depends primarily on subjective decision-making methods. Most previous studies have focused on general-purpose use cases or prototyping requirements, with little attention paid to high-performance, end-use applications such as the production of racing car spoiler components that require a unique balance of precision, speed, material compatibility, and temperature stability. Furthermore, many of

these studies use standalone MCDM approaches without incorporating objective weighting mechanisms, which might contribute to bias or inconsistency in criteria prioritisation. The market for 3D printers and related services, while still relatively small, is growing rapidly, making it increasingly important to select the most suitable option based on key factors such as cost efficiency, customization capabilities, and performance effectiveness. This study fills these gaps by proposing an integrated Entropy-Compromise Ranking of Alternatives from Distance to Ideal Solution (CRADIS) model for identifying the best 3D printer for manufacturing racing car spoilers. In the proposed model, the Entropy method has been used to evaluate the objective weights of criteria based on data variability. This approach reduces subjectivity and improves the reliability of the decision-making process. The CRADIS method is then employed to rank the 3D printers by calculating their distances from the ideal and anti-ideal solutions, providing a systematic and robust ranking framework. These two methods ensure a comprehensive evaluation, enabling decision-makers to balance technical requirements and economic constraints effectively. In addition, this study also conducts a comparative analysis with other prevalent MCDM methods to assess the stability and consistency of the rankings generated. This multi-method validation increases the trustworthiness of the results. To demonstrate the practical application of this approach, a case study is considered involving 16 alternative 3D printers evaluated against eight key selection criteria. This systematic methodology enhances decision-making transparency and ensures the selection of a 3D printer that optimally meets the specific needs of industrial applications, such as the production of high-performance racing car spoilers. This study makes a significant contribution to the literature by aligning the selection framework with the specific performance demands of racing car components and applying a rigorous, objective, and comparative MCDM approach. It also serves as a practical decision-support tool for engineers and practitioners in the automotive and motorsport industries.

Literature review

Paul et al. (2015) evaluated three MCDM methods for selecting 3D printers. The analytical Network Process (ANP) was used to determine criteria weights. The ranking methods included Technique for Order of Preference by Similarity to Ideal Solution (TOPSIS), Deng's Similarity-Based Approach, and Preference Ranking Organization Method for Enrichment Evaluations and Geometrical Analysis for Interactive Aid

(PROMETHEE-GAIA). Vinodh and Shinde (2018) optimized process parameters for Fused Deposition Modeling (FDM) in 3D printing. The multi-Objective Optimization on the Basis of Ratio Analysis (MOORA) method was used for optimization. Yeh and Chen (2018) developed a hybrid approach integrating Analytic Hierarchy Process (AHP) with the Technology-Organizational-Environment (TOE) framework to evaluate 3D printing adoption in Taiwanese manufacturing enterprises. The findings provided decision-makers with key insights for strategic adoption. Wang et al. (2018) introduced a system framework enabling customers to explore 3D printer alternatives based on their preferences. A case study demonstrated the benefits of allowing users to define acceptable levels, showing that a modified TOPSIS method achieved greater accuracy than the traditional approach. Khamhong et al. (2019) evaluated 3D printer selection criteria using Fuzzy AHP. The study analyzed decision-making perspectives of technical experts and users to determine optimal criteria weights. Prabhu et al. (2020) developed an MCDM model for selecting 3D printers based on criteria such as print volume, speed, and cost. The Preference Selection Index (PSI) method was employed, with Wanhao Duplicator 4 emerging as the best choice for racing car applications. Raigar et al. (2020) developed a decision support system for selecting an additive manufacturing process. A hybrid MCDM model was applied, combining Best Worst Method (BWM) for criteria weighting and Proximity Indexed Value (PIV) method for ranking. A spur gear model was fabricated using four AM processes, and sensitivity analysis validated the results. Lai and Chang (2021) proposed a two-stage evaluation approach for technology adoption. The first stage identified criteria using expert interviews and fuzzy Delphi, while the second stage used ANP for decision-making. Raja and Rajan (2022) examined the selection of an FDM machine for an Indian nongovernment organization based on nine criteria. The study recommended a suitable FDM machine among nine alternatives based on expert suggestions, aiding in machine selection for prototype production. Chatterjee and Chakraborty (2023) applied Evaluation Based on Distance from Average Solution (EDAS) method for selecting 3D printing nozzle materials. They considered eight alternative materials and nine criteria, incorporating sensitivity analysis to measure the robustness of the methodology. Nagarajan et al. (2023) proposed a group decision-making method for selecting 3D printing technologies. The study used neutrosophic ensembles to handle uncertainty and ambiguity, enabling efficient group decision-making. Wang et al. (2023) proposed a nonlinear Fuzzy Graph Model (FGM) combined with a dependency-

considered fuzzy VIseKriterijumska Optimizacija I Kompromisno Resenje (VIKOR) method.

Table 1 - Researcher contributions in 3D printer selection

Study	Methodology Used	Key Findings & Contributions
Paul et al. (2015)	ANP, TOPSIS, Deng's Similarity, PROMETHEE, GAIA	Compared MCDM techniques for 3D printer selection
Vinodh & Shinde (2018)	MOORA	Optimized FDM process parameters
Yeh & Chen (2018)	AHP, TOE framework	Examined 3D printing adoption in manufacturing
Wang et al. (2018)	Modified TOPSIS	Enhanced customer decision-making for 3D printer selection
Khamhong et al. (2020)	Fuzzy AHP	Assessed criteria for 3D printer selection
Prabhu et al. (2020)	PSI method	Identified optimal 3D printer for specific applications
Raigar et al. (2020)	BWM, PIV, sensitivity analysis	Developed a decision support system for AM selection
Lai & Chang (2021)	Fuzzy Delphi, ANP	Proposed a two-stage evaluation model for technology adoption
Raja & Rajan (2022)	Expert opinion-based ranking	Selected FDM machine for NGO use
Chatterjee & Chakraborty (2023)	EDAS, sensitivity analysis	Selected 3D printing nozzle materials
Nagarajan et al. (2023)	Neutrosophic ensembles	Addressed uncertainty in AM decision-making
Wang et al. (2023)	FGM, fuzzy VIKOR	Developed a dependency-considered 3D printer evaluation model
Sellamuthu et al. (2024)	MCDM, MEREC, MABAC	3D printer nozzle material selection
Yildirim & Ayyildiz,(2025)	MCDM, BWM, FF-WASPAS	Selecting the most suitable 3D printing technology for custom manufacturing

The proposed method incorporated interdependencies between criteria for comprehensive 3D printer evaluation. Sellamuthu et al. (2024) introduced an MCDM approach for selecting optimal materials for 3D printer nozzles by applying an integrated method based on the removal effects of criteria (MEREC)-multi-attributive border approximation area

comparison (MABAC) methods to determine both the criteria weights and material performance. Yildirim and Ayyildiz (2025) proposed the first hybrid Fermatean fuzzy MCDM framework to evaluate six leading 3D printing technologies based on nine criteria, combining BWM for criteria weighting with fuzzy weighted aggregated sum product assessment (WASPAS) for alternative ranking. Table 1 shows the researcher's contributions in 3D printer selection by MCDM methods.

Methods

In this paper, the Entropy method is employed to determine the weights of the criteria, while the CRADIS method is used to rank the alternatives based on the established criteria. The entropy method is a widely accepted technique for calculating objective weights, as it measures the uncertainty or dispersion in the data, ensuring that the weights are derived based on the intrinsic information of the criteria (Shannon, 1948). This approach is particularly useful in MCDM problems, as it minimizes subjective bias in weight assignment.

CRADIS, on the other hand, is a well-established MCDM method that ranks alternatives by evaluating their distances from both the ideal and anti-ideal solutions. This method is highly regarded among decision-makers due to its ability to provide a balanced and comprehensive assessment of alternatives (Puška et al, 2022). To apply the CRADIS method, it is essential to first construct a decision-making matrix that evaluates the performance of each alternative against the selected criteria. This matrix serves as the foundation for subsequent calculations, enabling a systematic comparison of alternatives.

The integration of the Entropy method for weight determination and the CRADIS method for ranking offers a robust framework for addressing complex decision-making problems. By combining these methods, the study ensures that the criteria weights are objectively derived, while the ranking of alternatives is conducted in a structured and transparent manner. This approach not only enhances the reliability of the decision-making process but also provides a clear and defensible rationale for the final rankings.

The Entropy method

Shannon (1948) introduced the concept of entropy in the context of communication theory as a measure of uncertainty or information loss in data transmission, particularly to address issues related to missing and ambiguous data. This mathematical formulation of entropy quantifies the

unpredictability or randomness in a system, making it a powerful tool for analyzing information systems. Zeleny (2012) highlighted the effectiveness of entropy as a tool for determining objective weights in decision-making processes. By measuring the dispersion or variability of data, entropy helps to assign weights to criteria in a way that minimizes subjective bias, ensuring a more balanced and rational evaluation of alternatives. The adaptability of the entropy concept to decision-making problems lies in its ability to quantify the relative importance of criteria based on the inherent information contained within the data. This makes it particularly useful in scenarios where decision-makers must evaluate multiple conflicting criteria and alternatives. The entropy method involves the following key steps:

Step 1: The method begins by establishing a decision matrix consisting of m alternatives and n criteria. Each element in the matrix represents the performance value (x_{ij}) of an alternative (i) with respect to a specific criterion (j).

Step 2: Normalize the decision matrix to ensure that all criteria values are on a comparable scale. For beneficial criteria (where higher values are better), normalization is done by dividing each value by the maximum value in that criterion (Equation 1). This scales all values between 0 and 1, preserving the relative performance and ensuring comparability across criteria. For non-beneficial criteria (where lower values are preferred), normalization is performed by dividing the minimum value by each value (Equation 2). This inversely scales the values so that better (lower) original values correspond to higher normalized scores. This step is particularly important when criteria are measured in different units.

$$n_{ij} = \frac{x_{ij}}{x_{jmax}}, \text{ for Beneficial Criteria} \quad (1)$$

$$n_{ij} = \frac{x_{jmin}}{x_{ij}}, \text{ for Non Beneficial Criteria} \quad (2)$$

Step 3: Calculate the entropy value for each criterion j as follows:

$$E_j = -\frac{\sum_{i=1}^{m} (P_{ij} * \ln P_{ij})}{\ln m} \quad (3)$$

The entropy value for each criterion j is calculated to measure the degree of disorder or uncertainty in the decision data. For the sake of ease of calculation, $(P_{ij} * \ln P_j)$ is defined as zero whenever $P_{ij} = 0$ in the actual evaluation using entropy method. The entropy value E_j ranges between 0 and 1. A higher entropy value indicates greater uncertainty or less useful

information in criterion j, while a lower entropy value suggests that the criterion provides more discriminative information for decision-making.

Step 4: Calculate the weight (W_j) of each criterion as follows:

$$W_j = \frac{1-E_j}{\sum_{j=1}^{n}(1-E_j)} \quad (4)$$

where ($1-E_j$) indicates degree of diversification for criterion j. A higher ($1-E_j$) value indicates that the criterion carries more useful information for distinguishing among alternatives.

The CRADIS method

CRADIS, developed by Puška et al. (2022), is a robust MCDM method that merges the core advantages of Additive Ratio ASsessment (ARAS), Measurement of Alternatives and Ranking according to COmpromise Solution (MARCOS), and TOPSIS methods. Its design aims to reduce the possibility of rank reversal and presents a balanced mechanism for selecting optimal alternatives by accounting for deviations from both ideal and anti-ideal solutions. This dual-reference perspective offers a more comprehensive understanding of the relative performance of alternatives. CRADIS also enables flexible integration of various distance and weighting strategies, allowing it to be tailored to diverse decision-making environments (Wang et al, 2022). Additionally, it provides a simplified and interpretable structure compared to more complex models, enhancing its applicability across industrial applications (Zhang & Esangbedo, 2025). The CRADIS Method has been proven useful in complex domains like occupational risk assessment and sustainable infrastructure investment (Chakraborty et al, 2023). The CRADIS method has the following eight simple steps:

Step 1: Development of the decision matrix. The values of the alternatives according to the observed criteria make up the initial decision matrix.

Step 2: Normalization of the decision matrix. Normalization is performed based on equations (1) and (2).

Step 3: Weighting the normalized decision matrix. Aggravation of decision-making matrices. The aggravated decision matrix is obtained by multiplying the value of the normalized decision matrix by corresponding weights, based on the following expression:

$$V_{ij} = n_{ij} * w_j \quad (5)$$

Step 4: Determination of ideal (T_i) and anti-ideal (T_{ai}) solutions for each criterion. T_i corresponds to the highest value in the weighted decision matrix, whereas T_{ai} corresponds to the lowest value.

$$t_i = \max V_{ij} \quad (6)$$

$$t_{ai} = \min V_{ij} \quad (7)$$

Step 5: Calculation of deviations from T_i and T_{ai}. In this step, the weighted normalized values are subtracted from the maximum or minimum value.

$$d^+ = t_i - V_{ij} \quad (8)$$

$$d^- = V_{ij} - t_{ai} \quad (9)$$

Step 6: Calculation of the deviation score of individual alternatives from T_i and T_{ai}. Here, deviations are summed up and optimal alternatives are determined by the following expression:

$$S_i^+ = \sum_{j=1}^{n} d^+ \quad (10)$$

$$S_i^- = \sum_{j=1}^{n} d^- \quad (11)$$

Step 7: Calculation of the utility function for each alternative in relation to the deviations from the optimal alternatives. In this step, each alternative is compared with respect to the optimal alternatives:

$$K_i^+ = \frac{S_O^+}{S_i^+} \quad (12)$$

$$K_i^- = \frac{S_i^-}{S_O^-} \quad (13)$$

where S_o^+ is an optimal alternative from T_i, while S_O^- is an optimal alternative from T_{ai}.

Step 8: Ranking alternatives, the final order is obtained by looking for the average deviation of the alternatives from the degree of utility:

$$Q_i = \frac{K_i^+ + K_i^-}{2} \quad (14)$$

The best alternative is the one that has the highest value of Q_i.

Case study

A spoiler, in the context of racing cars, is a device designed to disrupt and manage airflow over the vehicle. Figure 1 shows a high-performance rear spoiler designed to enhance aerodynamic efficiency by generating downforce at high speeds. It features a dual-bracket support structure for stability and adjustable mounting, commonly used in motorsport and performance vehicles for improved control. The primary purpose is to improve aerodynamic performance and increase stability at high speeds (Eftekhari et al, 2023). The main function of a spoiler is to generate

downforce, which is a downward aerodynamic force that helps increase the grip and traction of the tires on the road (Zhang et al, 2006). This effect is particularly crucial when racing cars are traveling at high speeds or when cornering at high g-forces. Downforce improves overall handling and stability, allowing drivers to maintain control and achieve faster lap times (Katz, 2006). While spoilers primarily create downforce, they can also help reduce drag under certain conditions (Nath et al, 2021).Interestingly, the positioning of spoilers or rear wings can significantly impact their effectiveness. Research has shown that an optimal automobile downforce-to-drag ratio is achieved when the rear wing is placed at 39% of the height between the upper surface of the automobile trunk and the automobile roof (Buljac et al, 2016). Additionally, the use of Gurney Flaps on front wings has been found to increase downforce by about 24% with only a limited increase in drag force (Basso et al, 2021).

Figure 1 - Racing car spoiler

Thus, it is essential to produce suitable spoilers for racing cars using an appropriate 3D printing machine. Accordingly, the selection of 3D printers is based on the criteria listed in Table 2.

Criteria like energy consumption and software compatibility were excluded to focus on key factors like PV, MPS, and temperature that directly impact spoiler manufacturing. Energy use has minimal effect on quality, and most printers support standard software with little impact on results. Among the considered criteria, four criteria are beneficial (higher is better), and the remaining four are non-beneficial (lower is better) in nature. PV (beneficial) is an essential factor to consider when selecting a 3D printer, and it's crucial for several reasons like size of object, efficiency, design flexibility, reduced assembly, cost effectiveness and scale of production. MPS is critical and beneficial in 3D printing selection due to its impact on time efficiency, productivity, cost savings, competitive

advantage, workflow optimization, and the balance between speed and print quality.

Table 2 - Criteria for 3D printer selection

Sl. No.	Criteria	Reference
1	Print volume (cu. mm) (PV)	Prabhu et al. (2020)
2	Max Print Speed (mm/sec) (MPS)	Prabhu et al. (2020), Ansari & Kamil (2021)
3	Layer Thickness (µm) (LT)	AlRumaih & Gad (2024)
4	No. of Extruders (NE)	Prabhu et al. (2020)
5	Machine Cost ($) (C)	Prabhu et al. (2020)
6	Manufacturer Filament Price ($/kg) (MFP)	Prabhu et al. (2020), Shaharuzaman et al. (2024)
7	Max Extruder Temperature (°C) (MET)	Ansari & Kamil (2021)
8	Max Bed Temperature (°C) (MBT)	Choi et al. (2016), Shaharuzaman et al. (2024)

Evaluating print speed alongside other factors such as PV, print resolution, material compatibility, and software capabilities can help to select a 3D printer that aligns with the needs and priorities. LT (non-beneficial) plays a crucial role in determining the resolution, surface finish, accuracy, strength, print speed, material compatibility, and support structure requirements of 3D-printed objects. Evaluating the ideal LT for any specific applications and balancing it with other factors such as MPS and material properties can help to achieve optimal results. NE in a 3D printer is decisive for multi-material printing, color variation, support material deposition, efficiency, productivity, tool changing capabilities, material mixing, flexibility, versatility, and achieving complex details in prints. Assessing the specific printing needs, material requirements, and desired functionalities can help to determine whether a printer with multiple extruders is suitable for the applications. C is a non-beneficial criterion in 3D printing selection due to its implications on initial investment, budget allocation, rate of interest (RoI), total cost of ownership, technology features, scalability, market competition, and overall cost-effectiveness. Balancing machine cost with performance, reliability, support, and long-term value is essential to make informed decisions and achieve desired outcomes in additive manufacturing applications. MFP is significant and non-beneficial in 3D printing selection as it influences cost management,

budget constraints, material variety, print quality, reliability, long-term savings, and access to technical support. Evaluating MFP alongside other factors such as filament properties, compatibility, and manufacturer reputation can help users make informed decisions when selecting filaments for 3D printing applications. MET is vital in 3D printing selection because it directly influences material compatibility, print quality, layer adhesion, filament flow, printing speed, material properties, and multi-material printing capabilities. Ensuring that a 3D printer extruder can reach and maintain the necessary temperatures for the chosen filaments is key to successful and reliable 3D printing operations. MBT in 3D printing selection for spoiler production is significant because it directly impacts adhesion, warping prevention, print quality, material compatibility, ease of print removal, and the versatility of materials that can be used in spoilers manufacturing. Ensuring that the heated bed of the 3D printer is set to the appropriate temperature for the chosen material is essential for achieving successful and high-quality prints. Table 3 presents the decision matrix developed for selecting 3D printer suitable for manufacturing spoilers for racing cars. The data of 16 printers with respect to the criteria is collected from literature and various websites (Prabhu et al, 2020; https://support.makerbot.com/s/article/1667337895715, https://www.3dwasp.com/en/delta-printer-delta-wasp-2040, https://www.treatstock.com/machines/item/342-up-plus-2)

Results and discussion

Application of Entropy - CRADIS method

Stage I: The Entropy Method (for criteria weighting)

At this stage, The Entropy method is employed to calculate the weights of the criteria used for selecting 3D printer for manufacturing racing car spoilers. First, the decision matrix is normalized using equations (1) and (2) for beneficial and non-beneficial criteria, respectively. The resulting normalized matrix is presented in Table 4. Subsequently, entropy values for each criterion are calculated using equation (3). Finally, the criteria weights shown in Table 5 are derived using equation (4). Based on Table 5, C2 and C3 emerge as the most significant criteria, while C8 is identified as the least significant.

Stage II: The CRADIS Method (for ranking alternatives)

In this stage, the CRADIS method is applied to determine the ranking of the alternatives. Equations (5), (6), and (7) yield the weighted normalized matrix with ideal and anti-ideal solutions. The lowest values across all criteria are represented by the anti-ideal solution (Tai), which

also includes the highest values. The anti-ideal solution (Tai) is in opposition to the ideal solution (Ti), as shown in Table 6.

Table 3 - Decision matrix for 3D printer selection for racing car spoiler

3D printer	PV	MPS	LT	NE	C	MFP	MET	MBT
Ultimaker 2 (A1)	230 x 225 x 205	300	20	1	2750	49.95	260	120
Zortrax (A2)	200 x 200 x 185	100	90	1	1990	59.00	380	110
Printrbot simple (A3)	150 x 150 x 150	80	100	1	999	28.00	220	80
Lulzbot Taz 6 (A4)	280 x 280 x 250	200	50	2	2500	65.00	240	110
Wanhao duplicator 4 (A5)	225 x 145 x 150	50	100	1	829	24.00	260	85
XYZ Da Vinci 1.0 (A6)	200 x 200 x 200	150	100	1	379	46.65	215	90
Airwolf 3D AW3D HD2X (A7)	280 x 200 x 300	150	60	1	3994	48.00	315	120
Afinia H+1 (A8)	255 x 205 x 225	200	150	1	1599	70.00	250	100
Ditto Pro (A9)	370 x 390 x 436	120	50	1	1899	45.00	280	80
Flashforge Creator X (A10)	225 x 145 x 150	100	100	2	2999	25.99	320	110
Felix 3.0 (A11)	255 × 205 × 235	150	50	1	1799	41.37	195	95
Makerbot Replicator Original (A12)	225 x 145 x 150	175	200	1	2000	33.00	230	100
Mbot Grid 2+ (A13)	235 x 210 x 180	120	100	2	1099	32.00	260	110
Delta non-turbo WASP 2040 (A14)	200 × 200 × 400	300	50	1	2999	24.00	350	100
Artifex duo 2 (A15)	156 × 310 × 223	150	50	2	1901	26.30	235	90
UP Plus 2 (A16)	140 x 140 x 135	30	150	1	850	55.00	260	100

The first and third values (0.169 and 1.000) in Table 4 have been calculated using equations (1) and (2) for the beneficial and non-beneficial criteria, respectively, as follows:

$$n_{11} = \frac{230 * 225 * 205}{370 * 390 * 436} = 0.169$$

$$n_{13} = \frac{20}{20} = 1$$

Table 4 - Normalized decision matrix for 3D printer selection of spoiler

3D printer	PV	MPS	LT	NE	C	MFP	MET	MBT
A1	0.169	1.000	1.000	0.500	0.138	0.480	0.684	0.667
A2	0.118	0.333	0.222	0.500	0.190	0.407	1.000	0.727
A3	0.054	0.267	0.200	0.500	0.379	0.857	0.579	1.000
A4	0.312	0.667	0.400	1.000	0.152	0.369	0.632	0.727
A5	0.078	0.167	0.200	0.500	0.457	1.000	0.684	0.941
A6	0.127	0.500	0.200	0.500	1.000	0.514	0.566	0.889
A7	0.267	0.500	0.333	0.500	0.095	0.500	0.829	0.667
A8	0.187	0.667	0.133	0.500	0.237	0.343	0.658	0.800
A9	1.000	0.400	0.400	0.500	0.200	0.533	0.737	1.000
A10	0.078	0.333	0.200	1.000	0.126	0.923	0.842	0.727
A11	0.195	0.500	0.400	0.500	0.211	0.580	0.513	0.842
A12	0.078	0.583	0.100	0.500	0.190	0.727	0.605	0.800
A13	0.141	0.400	0.200	1.000	0.345	0.750	0.684	0.727
A14	0.254	1.000	0.400	0.500	0.126	1.000	0.921	0.727
A15	0.171	0.500	0.400	1.000	0.199	0.913	0.618	0.889
A16	0.042	0.100	0.133	0.500	0.446	0.436	0.684	0.800

The weight of criterion PV (0.130), as presented in Table 5, is calculated using equations (3) and (4) as follows:

$$E_1 = (-3.976) * (-0.361) = 1.434$$

$$W_1 = \frac{1 - 1.434}{-3.331} = 0.130$$

Table 5 - Weights of 3D printer selection criteria for spoiler

Criteria	PV	MPS	LT	NE	C	MFP	MET	MBT
Weight	0.130	0.197	0.231	0.150	0.135	0.036	0.110	0.011

The weighted normalized value of 0.022 for the alternative A1 under the first criterion PV, is calculated using equation (5). Subsequently, maximum (T_i) and minimum (T_{ai}) values are determined using equations (6) and (7), respectively, as shown in Table 6.

$V_{11} = 0.169 * 0.130 = 0.022$

Ti = 0.130, Tai = 0.005

Equations (8) and (9) are then used to determine the deviation from T_i and T_{ai}, as shown in Tables 7 and 8.

Table 6 - Weighted normalized decision matrix with T_i and T_{ai} values

3D printer	PV	MPS	LT	NE	C	MFP	MET	MBT
T_i	0.130	0.200	0.230	0.150	0.140	0.040	0.110	0.010
A1	0.022	0.200	0.230	0.075	0.019	0.019	0.075	0.007
A2	0.015	0.067	0.051	0.075	0.027	0.016	0.110	0.007
A3	0.007	0.053	0.046	0.075	0.053	0.034	0.064	0.010
A4	0.040	0.133	0.092	0.150	0.021	0.015	0.069	0.007
A5	0.010	0.033	0.046	0.075	0.064	0.040	0.075	0.009
A6	0.017	0.100	0.046	0.075	0.140	0.021	0.062	0.009
A7	0.035	0.100	0.077	0.075	0.013	0.020	0.091	0.007
A8	0.024	0.133	0.031	0.075	0.033	0.014	0.072	0.008
A9	0.130	0.080	0.092	0.075	0.028	0.021	0.081	0.010
A10	0.010	0.067	0.046	0.150	0.018	0.037	0.093	0.007
A11	0.025	0.100	0.092	0.075	0.029	0.023	0.056	0.008
A12	0.010	0.117	0.023	0.075	0.027	0.029	0.067	0.008
A13	0.018	0.080	0.046	0.150	0.048	0.030	0.075	0.007
A14	0.033	0.200	0.092	0.075	0.018	0.040	0.101	0.007
A15	0.022	0.100	0.092	0.150	0.028	0.037	0.068	0.009
A16	0.005	0.020	0.031	0.075	0.062	0.017	0.075	0.008
T_{ai}	0.005	0.020	0.023	0.075	0.013	0.014	0.056	0.007

The deviation value of 0.108 for alternative A1 with respect to Ti in Table 7 has been calculated as follows:

$d_{11}^{+} = 0.130 - 0.022 = 0.108$

In the next step, the grade of deviation for each alternative from T_i and T_{ai} values is determined using equations (10) and (11). Then, equations (12) and (13) are applied to calculate the utility function for each alternative based on the deviation from the optimal solutions. The final step in ranking the alternatives involves using equation (14) to compute the average deviation from the degree of utility. The results are shown in Table 9.

Table 7 - Deviation from T_i values

3D printer	PV	MPS	LT	NE	C	MFP	MET	MBT
A1	0.108	0.000	0.000	0.075	0.121	0.021	0.035	0.004
A2	0.115	0.133	0.179	0.075	0.113	0.024	0.000	0.003
A3	0.123	0.147	0.184	0.075	0.087	0.006	0.046	0.000
A4	0.090	0.067	0.138	0.000	0.119	0.025	0.041	0.003
A5	0.120	0.167	0.184	0.075	0.076	0.000	0.035	0.001
A6	0.113	0.100	0.184	0.075	0.000	0.019	0.048	0.001

3D printer	PV	MPS	LT	NE	C	MFP	MET	MBT
A7	0.095	0.100	0.153	0.075	0.127	0.020	0.019	0.004
A8	0.106	0.067	0.199	0.075	0.107	0.026	0.038	0.002
A9	0.000	0.120	0.138	0.075	0.112	0.019	0.029	0.000
A10	0.120	0.133	0.184	0.000	0.122	0.003	0.017	0.003
A11	0.105	0.100	0.138	0.075	0.111	0.017	0.054	0.002
A12	0.120	0.083	0.207	0.075	0.113	0.011	0.043	0.002
A13	0.112	0.120	0.184	0.000	0.092	0.010	0.035	0.003
A14	0.097	0.000	0.138	0.075	0.122	0.000	0.009	0.003
A15	0.108	0.100	0.138	0.000	0.112	0.003	0.042	0.001
A16	0.125	0.180	0.199	0.075	0.078	0.023	0.035	0.002

The first deviation value 0.017 from Tai in the Table 8 has been calculated using equation (9) as follows:

$$d_{11}^{-} = 0.022 - 0.005 = 0.017$$

Table 8 - Deviation from T_{ai} values

3D printer	PV	MPS	LT	NE	C	MFP	MET	MBT
A1	0.017	0.180	0.207	0.000	0.006	0.006	0.019	0.000
A2	0.010	0.047	0.028	0.000	0.013	0.003	0.054	0.001
A3	0.002	0.033	0.023	0.000	0.040	0.021	0.007	0.003
A4	0.035	0.113	0.069	0.075	0.008	0.001	0.013	0.001
A5	0.005	0.013	0.023	0.000	0.051	0.026	0.019	0.003
A6	0.011	0.080	0.023	0.000	0.127	0.007	0.006	0.002
A7	0.029	0.080	0.054	0.000	0.000	0.006	0.035	0.000
A8	0.019	0.113	0.008	0.000	0.020	0.000	0.016	0.001
A9	0.125	0.060	0.069	0.000	0.015	0.008	0.025	0.004
A10	0.005	0.047	0.023	0.075	0.004	0.023	0.036	0.001
A11	0.020	0.080	0.069	0.000	0.016	0.009	0.000	0.002
A12	0.005	0.097	0.000	0.000	0.013	0.015	0.010	0.001
A13	0.013	0.060	0.023	0.075	0.035	0.016	0.019	0.001
A14	0.028	0.180	0.069	0.000	0.004	0.026	0.045	0.001
A15	0.017	0.080	0.069	0.075	0.015	0.023	0.012	0.002
A16	0.000	0.000	0.008	0.000	0.049	0.004	0.019	0.001

Deviation scores of alternative A1 with respect to T_i and T_{ai} (0.363 and 0.434 respectively), as shown in Table 9, are calculated using equations (10) and (11) as follows:

$$S_1^{+} = 0.108 + 0.000 + 0.000 + 0.075 + 0.121 + 0.021 + 0.035 + 0.004 = 0.363$$

$$S_1^- = 0.017 + 0.180 + 0.207 + 0.000 + 0.006 + 0.006 + 0.019 + 0.000 = 0.434$$

The utility functions (K_i^+ and K_i^-) of alternative A1 from the optimal deviation in Table 9 are 1.000 and 1.000, which has been calculated using equations (12) and (13) as follows:

S_1^+ = Optimal Value for K_i^+ = Minimum value in $S_i^+ = 0.363$

S_1^- = Optimal Value for K_i^- = Maximum value in $S_i^- = 0.434$

$$K_1^+ = \frac{0.363}{0.363} = 1.000$$

$$K_1^- = \frac{0.434}{0.434} = 1.000$$

The average deviation (Q_i) value of 1.000 for alternative A1 has been calculated using equation (14) as follows:

$$Q_1 = \frac{1.000 + 1.000}{2} = 1.000$$

The first rank is assigned based on the highest average deviation value. Among all the alternatives, Alternative 1 has the highest average deviation value of 1.000; therefore, it is ranked first.

Table 9 - Results of CRADIS method

3D printer	S_i^+	S_i^-	K_i^+	K_i^-	Q_i	Rank
A1	0.363	0.434	1.000	1.000	1.000	1
A2	0.642	0.155	0.565	0.357	0.461	12
A3	0.668	0.129	0.543	0.297	0.420	15
A4	0.482	0.315	0.753	0.726	0.740	3
A5	0.657	0.139	0.552	0.322	0.437	14
A6	0.541	0.256	0.671	0.589	0.630	6
A7	0.593	0.204	0.612	0.470	0.541	9
A8	0.620	0.177	0.586	0.408	0.497	11
A9	0.493	0.304	0.736	0.701	0.719	4
A10	0.583	0.214	0.622	0.493	0.558	8
A11	0.600	0.196	0.604	0.453	0.529	10
A12	0.655	0.141	0.554	0.326	0.440	13
A13	0.555	0.242	0.654	0.557	0.605	7
A14	0.444	0.353	0.817	0.813	0.815	2
A15	0.505	0.292	0.719	0.673	0.696	5
A16	0.716	0.081	0.507	0.186	0.346	16

Performance comparison and sensitivity analysis

Computation of ranking stability based on different MCDM method comparisons

A comparative performance study between this integrated method and the other six widely used MCDM methods like EDAS, COmbinative Distance-based Assessment (CODAS), MABAC, TOPSIS, PROMETHEE, and MARCOS is presented in order to determine the ranking of the considered 3D printers for racing car spoilers and to elucidate reliability of CRADIS method. These methods are selected due to their several benefits, broad range of applications and ability to effectively rank alternatives in MCDM environment. One of the recently developed MCDM methods is EDAS. According to the selected beneficial or non-benefit criteria, the distances in both the positive and negative directions are calculated using the average solution individually in this method (Ghorabaee et al, 2015). CODAS is considered an effective approach for evaluating alternatives. It employs l1- and l2-norm indifference spaces for criteria to assess the desirability of alternatives. The evaluation score is determined based on these spaces using a combination of Euclidean and Taxicab distances. Alternatives are ranked according to the evaluation results (Ghorabaee et al, 2016). The MABAC method is superior to many other conventional MCDM methods in a number of ways. No matter how many alternatives and criteria there are, mathematical formulas always remain the same. The core principle of the MABAC method is to evaluate the distance of each alternative's criteria function from the border approximation area (Pamucar & Cirovic, 2015). Both qualitative and quantitative criteria can be used with this method. According to Chang et al. (2010), TOPSIS is a significant distance-based method that ranks the alternatives according to their proximity to the ideal solution and their distance from the anti-ideal solution. Through the determination of the two distance measurements, this tool is useful and practical for the evaluation and selection of several reciprocally conflicting alternatives. PROMETHEE is an MCDM method used to rank alternatives based on multiple criteria or attributes and has been widely applied in various fields like business, engineering, environmental management, and public policy. The MARCOS method has the potential for subjectivity in assigning criteria weights and scores, reliance on accurate and reliable data for scoring alternatives, and the assumption of linear aggregation of criteria. The best alternatives are identified by the decision makers with the aid of the compromise solution.

Table 10 - Ranking stability analysis based on comparisons of various MCDM methods

3D printer	Rank						
	CRADIS	MABAC	MARCOS	CODAS	EDAS	TOPSIS	PROMETHEE
A1	1	2	1	1	1	2	3
A2	12	10	15	8	10	10	11
A3	15	13	13	14	14	11	14
A4	3	4	5	4	3	4	2
A5	14	12	8	16	13	12	13
A6	6	9	7	15	8	7	10
A7	9	11	11	9	9	8	8
A8	11	14	14	2	12	13	9
A9	4	5	9	6	4	1	5
A10	8	7	3	3	11	14	12
A11	10	8	10	13	6	6	6
A12	13	15	12	5	15	16	15
A13	7	6	6	7	7	9	7
A14	2	1	2	11	2	3	1
A15	5	3	4	10	5	5	4
A16	16	16	16	12	16	15	16

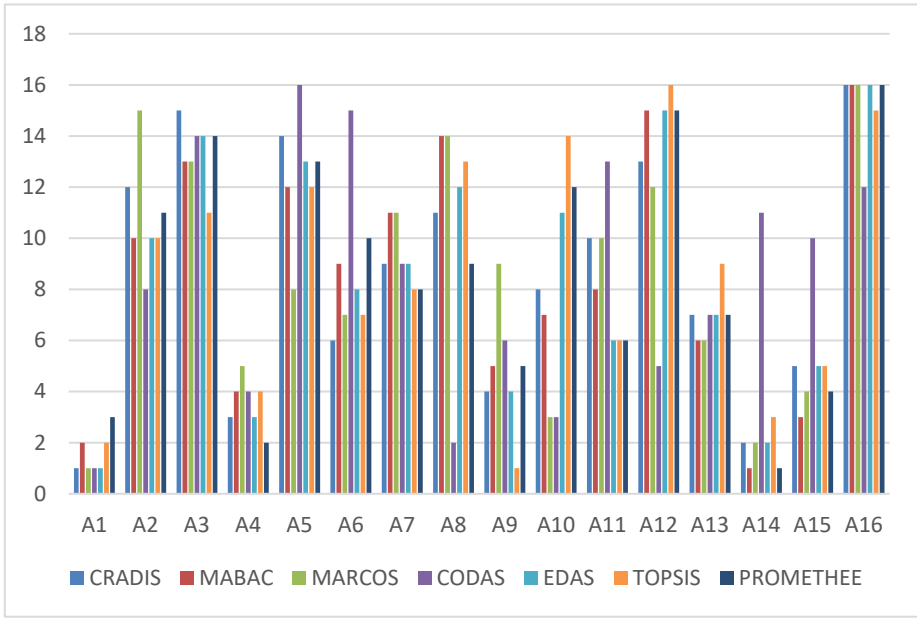

Figure 2 - Rankings of alternative 3D printers by different MCDM methods

Figure 2 illustrates the degree of similarity in the rankings obtained through the CRADIS method compared with the results from other MCDM methods. Table 10 presents the rankings derived from CRADIS and other MCDM methods. The results suggest that Ultimaker 2 (A1), Delta non-turbo WASP 2040 (A14), and Lulzbot Taz 6 (A4) are among the top alternatives for producing spoilers, whereas UP Plus 2 (A16) ranks lowest for this application.

Spearman rank correlation coefficient

Spearman's rank correlation coefficient is a non-parametric statistical measure used to assess the strength and direction of the relationship between two ranked variables. Unlike Pearson's correlation, which measures linear relationships, Spearman's correlation evaluates monotonic relationships, meaning that as one variable increases the other either consistently increases or decreases. It is calculated using the ranks of the data rather than the actual values, making it suitable for ordinal data or cases where the assumptions of normality and linearity are not met. The coefficient ranges from −1 (perfect negative correlation) to +1 (perfect positive correlation), with 0 indicating no correlation. It is widely used in fields such as psychology, economics, and social sciences to analyze relationships where data may not follow a normal distribution. Calculating the Spearman rank correlation coefficient allows for a comparison of the outcomes from various MCDM methods. An exceptional correlation between the rankings is indicated by a Spearman correlation coefficient value that is closer to 0.8 or higher. The Spearman correlation coefficient values between the various MCDM methods are displayed in Table 11. Table 11 demonstrates how well the ranking produced by CRADIS matches the ranking produced by the other MCDM methods. In the CODAS, all the values are less than 0.8, so this method exhibits an inappropriate correlation. The weaker correlation observed for the CODAS method can be attributed to its distinct evaluation mechanism. The CODAS method ranks alternatives based on their Euclidean and Taxicab distances from a negative-ideal solution, emphasizing how much worse an alternative is compared to the least desirable option. This contrasts with other methods that focus on closeness to an ideal solution or use aggregated scores. As a result, CODAS tends to penalize alternatives differently, especially when the performance values are marginal or closely clustered. Its sensitivity to distance-based dominance leads to rankings that can deviate significantly from those generated by methods using preference functions, normalization-based scoring, or utility-based evaluation.

Table 11 - Spearman's coefficient of the rankings obtained using different MCDM tools for 3D printing machine for spoiler

Method	CRADIS	MABAC	MARCOS	CODAS	EDAS	TOPSIS	PROMETHEE
CRADIS	1.0000	0.9235	0.8235	0.4000	0.9412	0.8412	0.9000
MABAC	0.9235	1.0000	0.8618	0.24412	0.9412	0.8441	0.8912
MARCOS	0.8235	0.8618	1.0000	0.2235	0.7353	0.5794	0.6735
CODAS	0.4000	0.24412	0.2235	1.0000	0.2618	0.0677	0.2882
EDAS	0.9412	0.9412	0.7353	0.2618	1.0000	0.9412	0.9647
TOPSIS	0.8412	0.8441	0.5794	0.0677	0.9412	1.0000	0.8941
PROMETHEE	0.9000	0.8912	0.6735	0.2882	0.9647	0.8941	1.0000

Conclusion

Selecting an appropriate 3D printer for producing spoilers for racing vehicle applications is one of the most difficult tasks because of the increasing complexity and cutting-edge features and capabilities that component designers and manufacturers are constantly adding to their creations. This study explores ways to help solve decision-making problems and offers information on a number of significant factors that should be taken into account for the best assessment and selection of 3D printing machines. In the current problem, the entropy-CRADIS method has been applied, and the ranking orders have been summarized. The strategy began with entropy and acquired weightage by maintaining cost reduction and surface finish as the primary objectives. When these weights are added to CRADIS, a ranking was produced, and the Delta non-turbo Ultimaker 2 (A1) came out on top. This method for choosing the best alternatives is very straightforward to understand and use. This strategy can also be applied to other decision-making scenarios with an infinite number of criteria and choices. With the aid of several MCDM methods, including EDAS, CODAS, MABAC, TOPSIS, PROMETHEE, and MARCOS, it is eventually determined that the best 3D printers for producing racing car spoilers are the Ultimaker 2 (A1), Delta non-turbo WASP 2040 (A14) and Lulzbot Taz 6 (A4). The Ultimaker 2 outperforms other 3D printers by offering a well-balanced combination of performance, material capability, and cost-effectiveness across key criteria. It provides a generous print volume suitable for most applications, along with a high maximum print speed that enhances productivity. Its ability to print with a fine layer thickness ensures high-resolution outputs, while a single extruder simplifies maintenance without compromising functionality. The printer is also competitively priced and uses moderately priced

manufacturer filament, contributing to lower operating costs. Additionally, its maximum extruder temperature and bed temperature are sufficient for printing a wide range of materials, making it both versatile and efficient. This well-rounded performance across both technical and economic parameters positions the Ultimaker 2 as a leading choice in desktop 3D printing. The findings indicate that UP Plus 2 (A16) cannot be used for the above-mentioned purposes. The final results of Spearman's ranking coefficient demonstrated a strong association between each of the several MCDM methods. Future study can include testing the methodology with dynamic or context-sensitive criteria weights that reflect changing priorities, such as balancing cost and quality at different production stages or varying based on material type, manufacturing scale, or environmental constraints. Applying this MCDM approach to other automotive components like air intakes, diffusers, or interior trim parts can validate its versatility and adaptability to different performance requirements, such as airflow optimization or surface finish. However, this study is limited by its reliance on manufacturer-provided data and the use of static criteria weights, which may not fully capture real-world variability and evolving priorities. Addressing these limitations in future work will enhance the robustness and applicability of the approach. Incorporating real-world printing trials with top-ranked printers will further refine the model and ensure alignment with actual manufacturing conditions, supporting broader adoption in automotive design and prototyping.

References

AlRumaih, H. S., & Gad, M. M. 2024. The Effect of 3D Printing Layer Thickness and Post-Polymerization Time on the Flexural Strength and Hardness of Denture Base Resins. *Prosthesis*, 6(4), pp.970-978. Available at: https://doi.org/10.3390/prosthesis6040070

Ansari, A. A & Kamil, M. 2021. Effect of print speed and extrusion temperature on properties of 3D printed PLA using fused deposition modeling process. *Materials Today: Proceedings,* 45(6), pp.5462-5468. Available at: https://doi.org/10.1016/j.matpr.2021.02.137

Basso, M., Cravero, C., & Marsano, D. 2021. Aerodynamic Effect of the Gurney Flap on the Front Wing of a F1 Car and Flow Interactions with Car Components. *Energies,* 14(8), 2059. Available at: https://doi.org/10.3390/en14082059

Berman, B., 2012. 3-D printing: The new industrial revolution. *Business horizons*, 55(2), pp.155-162. Available at: https://doi.org/10.1016/j.bushor.2011.11.003

Buljac, A., Džijan, I., Kozmar, H., Korade, I., & Krizmanić, S. 2016. Automobile aerodynamics influenced by airfoil-shaped rear wing. *International Journal of Automotive Technology*, 17(3), pp.377–385. Available at: https://doi.org/10.1007/s12239-016-0039-4

Chakraborty, S., Chatterjee, P., & Das, P. P. (2023). Multi-Criteria Decision-Making Methods in Manufacturing Environments: Models and Applications*. New York: Apple Academic Press.* Avaible at: https://doi.org/10.1201/9781003377030-16

Chang, C. H., Lin, J. J., Lin, J. H., & Chiang, M. C., 2010. Domestic open-end equity mutual fund performance evaluation using extended TOPSIS method with different distance approaches. *Expert systems with applications*, *37*(6), pp.4642-4649. Available at: https://doi.org/10.3846/btp.2017.012

Chatterjee, S., & Chakraborty, S., 2023. A multi-criteria decision-making approach for 3D printer nozzle material selection. *Reports in Mechanical Engineering*, 4(1), pp.62-79. Available at: https://doi.org/10.31181/rme040121042023c

Choi, Y., Kim, C., Jeong, H. & Youn, J. (2016). Influence of Bed Temperature on Heat Shrinkage Shape Error in FDM Additive Manufacturing of the ABS-Engineering Plastic. *World Journal of Engineering and Technology*, 4, pp. 186-192. Available at: https://doi.org/10.4236/wjet.2016.43D022.

Eftekhari, H., Al-Obaidi, A. S. M., Eftekhari, S & Ijost, I., 2023. Effect of a Spoiler on the Aerodynamic Performance of a Race Car on Track Using Two Different Turbulence Models. *Journal of Design for Sustainable and Environment*, 5 (2), pp. 28-37. Available at: https://doi.org/10.17509/ijost. v5i1.22701

Ford, S., & Despeisse, M., 2016. Additive manufacturing and sustainability: An exploratory study of the advantages and challenges. *Journal of Cleaner Production*, 137, pp.1573-1587. Available at: https://doi.org/10.1016/j.jclepro.2016.04.150

Genç, E., Keleş, M. K., & Özdağoğlu, A. 2024. A hybrid MCDM model for personnel selection based on a novel Gray AHP, Gray MOORA and Gray MAUT methods in terms of business management: An application in the tourism sector. *Journal of Decision Analytics and Intelligent Computing*, 4(1), 263–284. Available at: https://doi.org/10.31181/jdaic10024122024g

Ghorabaee, K, M., Zavadskas, E. K., Olfat, L., & Turskis, Z., 2015. Multi-criteria inventory classification using a new method of evaluation based on distance from average solution (EDAS). *Informatica*, *26*(3), pp.435-451. Available at: https://doi.org/10.15388/Informatica.2015.57

Ghorabaee, K, M., Zavadskas, E. K., Turskis, Z., & Antuchevičienė, J., 2016. A new combinative distance-based assessment (CODAS) method for multi-criteria decision-making. Available at: https://etalpykla.vilniustech.lt/handle/123456789/116529

Gibson, I., Rosen, D., & Stucker, B., 2015. Additive manufacturing technologies: 3D printing, rapid prototyping, and direct digital manufacturing. *Springer.* Available at: https://doi.org/10.1007/978-1-4419-1120-9

Guo, N., & Leu, M. C., 2013. Additive manufacturing: Technology, applications and research needs. *Frontiers of Mechanical Engineering*, 8(3), pp.215-243. Available at: https://doi.org/10.1007/s11465-013-0248-8

Huang, S. H., Liu, P., Mokasdar, A., & Hou, L., 2013. Additive manufacturing and its societal impact: A literature review. *International Journal of Advanced Manufacturing Technology*, 67(5-8), pp.1191-1203. Available at: https://doi.org/10.1007/s00170-012-4558-5

Jia, Y., He, H., Geng, Y., Huang, B., & Peng, X., 2017. High through-plane thermal conductivity of polymer based product with vertical alignment of graphite flakes achieved via 3D printing. *Composites Science and Technology*, 145, pp.55-61. Available at: https://doi.org/10.1016/j.compscitech.2017.03.035

Kapetaniou, C., Rieple, A., Pilkington, A., Frandsen, T., & Pisano, P., 2018. Building the layers of a new manufacturing taxonomy: How 3D printing is creating a new landscape of production eco-systems and competitive dynamics. *Technological Forecasting and Social Change*, *128*, pp.22-35. Available at: https://doi.org/10.1016/j.techfore.2017.10.011

Komatina, N. 2025. A Novel BWM-RADAR Approach for Multi-Attribute Selection of Equipment in the Automotive Industry. Spectrum of Mechanical Engineering and Operational Research, 2(1), pp.104-120. Available at: https://doi.org/10.31181/smeor21202531

Kousar, S., Ansar, A., Kausar, N., & Freen, G. 2025. Multi-Criteria Decision-Making for Smog Mitigation: A Comprehensive Analysis of Health, Economic, and Ecological Impacts. Spectrum of Decision Making and Applications, 2(1), pp.53-67. Available at: https://doi.org/10.31181/sdmap2120258

Kumar, R., & Pamucar, D. 2025. A Comprehensive and Systematic Review of Multi-Criteria Decision-Making (MCDM) Methods to Solve Decision-Making Problems: Two Decades from 2004 to 2024. Spectrum of Decision Making and Applications, 2(1), pp.178-197. Available at: https://doi.org/10.31181/sdmap21202524

Katz, J. (2006). Aerodynamics of race cars. Annual Review of Fluid Mechanics, 38, 27-63.

Khamhong, P., Yingviwatanapong, C., & Ransikarbum, K., 2019. Fuzzy analytic hierarchy process (AHP)-based criteria analysis for 3D printer selection in additive manufacturing. In *2019 Research, Invention, and Innovation Congress (RI2C),* (pp.1-5), IEEE. Available at: https://doi.org/10.1109/RI2C48728.2019.8999950

Lai, J., & Chang, Y., 2021. Technology assessment of 3D printing using a two-stage MCDM: case studies on molding industry. *International Journal of Innovation Management*, *9*(1), pp. 53-60. Available at: https://doi.org/10.1007/s00170-012-4558-5

Mardani, A., Jusoh, A., Nor, K., Khalifah, Z., & Zakwan, N., 2015. Multiple criteria decision-making techniques and their applications – A review of the literature from 2000 to 2014. *Economic Research-Ekonomska Istraživanja*, 28(1), pp.516-571. Available at: https://doi.org/10.1080/1331677X.2015.1075139

Matias, E., & Rao, B., 2015. 3D printing: On its historical evolution and the implications for business*. In 2015 Portland International Conference on Management of Engineering and Technology (PICMET)*, pp. 551-558. IEEE. Available at: https://doi.org/10.1109/PICMET.2015.7273052

Moarefi, A., Sweis, R. J., Hoseini-Amiri, S. M., & AlBalkhy, W. A., 2018. Shannon entropy weighting technique as a practical weighting decision-making tool in project management. *International Journal of Management Concepts and Philosophy*, 11(4), pp.377-392. Available at: https://doi.org/10.1504/IJMCP.2018.096054

Nagarajan, D., Gobinath, V. M., & Broumi, S., 2023. Multicriteria Decision Making on 3D printers for economic manufacturing using Neutrosophic environment. *Neutrosophic Sets and Systems*, 57(1), pp.3. Available at: https://digitalrepository.unm.edu/nss_journal/vol57/iss1/3

Nath, D. S., Pujari, P. C., Jain, A., & Rastogi, V. (2021). Drag reduction by application of aerodynamic devices in a race car. Advances in Aerodynamics, 3(1). Available at: https://doi.org/10.1186/s42774-020-00054-7

Pamučar, D., & Ćirović, G., 2015. The selection of transport and handling resources in logistics centers using Multi-Attributive Border Approximation Area Comparison (MABAC). *Expert systems with applications*, 42(6), pp.3016-3028. Available at: https://doi.org/10.1016/j.eswa.2014.11.057

Paul, D., Agarwal, P., Mondal, G., & Banerjee, D., 2015. A comparative analysis of different hybrid MCDM techniques considering a case of selection of 3D printers. *Management Science Letters*, 5, pp.695-708. Available at: https://doi.org/10.5267/j.msl.2015.5.003

Prabhu, S. R., Ilangkumaran, M., & Mohanraj, T., 2020. 3D Printing of automobile spoilers using MCDM techniques. *Materials Testing*, 62(11), pp.1121-1125. Available at : https://doi.org/10.3139/120.111592

Puška, A., Stević, Ž. & Pamučar, D., 2022. Evaluation and selection of healthcare waste incinerators using extended sustainability criteria and multi-criteria analysis methods. *Environment, Development and Sustainability*, 24, pp. 11195-11225. Available at : https://doi.org/10.1007/s10668-021-01902-2

Radovanovic, M., Petrovski, A., Cirkin, E., Behlić, A., Jokic, Z., Chemezov, D., Hashimov, E. G., Bouraima, M. B., & Jana, C. 2024. Application of the new hybrid model LMAW-G-EDAS multi-criteria decision-making when choosing an assault rifle for the needs of the army. *Journal of Decision Analytics and Intelligent Computing*, 4(1), pp.16–31. Available at: https://doi.org/10.31181/jdaic10021012024r

Raigar, J., Sharma, V. S., Srivastava, S., Chand, R., & Singh, J. 2020. A decision support system for the selection of an additive manufacturing process using a new hybrid MCDM technique. *Sādhanā,* 45, pp. 1-14. Available at: https://doi.org/10.1007/s12046-020-01338-w

Raja, S., & Rajan, A. J., 2022. A decision-making model for selection of the suitable FDM machine using fuzzy TOPSIS. *Mathematical Problems in Engineering*, *2022*(1), pp.7653292. Available at: https://doi.org/10.1155/2022/7653292

Rayna, T., & Striukova, L., 2016. From rapid prototyping to home fabrication: How 3D printing is changing business model innovation. *Technological forecasting and social change*, *102*, pp.214-224. Available at: https://doi.org/10.1016/j.techfore.2015.07.023

Sahoo, S. K., Choudhury, B. B., Dhal, P. R., & Hanspal, M. S. 2025. A Comprehensive Review of Multi-criteria Decision-making (MCDM) Toward Sustainable Renewable Energy Development. *Spectrum of Operational Research*, 2(1), pp.268-284. Available at: https://doi.org/10.31181/sor21202527

Sandström, C. G., 2016. The non-disruptive emergence of an ecosystem for 3D Printing - Insights from the hearing aid industry's transition 1989 - 2008. *Technological Forecasting and Social Change*, *102*, pp.160-168. Available at: https://doi.org/10.1016/j.techfore.2015.09.006

Sellamuthu, P., Kalita, K., Kumar, A., Chohan, J. S., Rathee, S., & Sharma, Y. K. (2024, December). A hybrid Merec-Mabac approach for 3D printer nozzle material selection. In *AIP Conference Proceedings.* 3217(1).

Shannon, C. E., 1948. A mathematical theory of communication. *The Bell System Technical Journal*, 27(3), pp. 379-423. Available at: https://doi.org/10.1002/j.1538-7305.1948.tb01338.x

Shaharuzaman, M. A., Sayed Idros, S. M. A., Taha, M. M., Mansor, M. R., Jumaidin, R., & Senan, H. (2024). Conceptual Design and Materials Selection of the FDM Composites for Passenger Vehicle's Spoiler. *Pertanika Journal of Science & Technology*, *32*. pp.21-36. Available at: https://doi.org/10.47836/pjst.32.S2.02

Tesic, D., & Marinkovic, D. 2023. Application of fermatean fuzzy weight operators and MCDM model DIBR-DIBR II-NWBM-BM for efficiency-based selection of a complex combat system. Journal of Decision Analytics and Intelligent Computing, 3(1), pp.243–256. Available at: https://doi.org/10.31181/10002122023t

Vinodh, S., & Shinde, P., 2018. Parametric optimization of 3D printing process using MCDM method*. In Precision Product-Process Design and Optimization: Select Papers from AIMTDR 2016*, pp. 141-159. Available at: https://doi.org/10.1007/978-981-10-8767-7_6

Wang, W., Wang, Y., Fan, S., Han, X., Wu, Q., & Pamucar, D., 2022. A complex spherical fuzzy CRADIS method based Fine-Kinney framework for occupational risk evaluation in natural gas pipeline construction. *Journal of Petroleum Science and Engineering*, 220, 111246. https://doi.org/10.1016/j.petrol.2022.111246

Wang, Y. C., Chen, T., & Lin, Y. C., 2023. 3D Printer Selection for Aircraft Component Manufacturing Using a Nonlinear FGM and Dependency-Considered Fuzzy VIKOR Approach. *Aerospace,* 10(7), pp. 591. Available at: https://doi.org/10.3390/aerospace10070591

Wang, Y., Zhong, R. Y., & Xu, X., 2018. A decision support system for additive manufacturing process selection using a hybrid multiple criteria decision-making method. *Rapid Prototyping Journal*, 24(9), pp. 1544-1553. Available at: https://doi.org/10.1108/RPJ-01-2018-0002

West, J., & Kuk, G., 2016. The complementarity of openness: How MakerBot leveraged Thingiverse in 3D printing. *Technological Forecasting and Social Change*, 102, pp.169-181. Available at: https://doi.org/10.1016/j.techfore.2015.07.025

Więckowski, J., & Sałabun, W. 2025. Comparative Sensitivity Analysis in Composite Material Selection: Evaluating OAT and COMSAM Methods in Multi-criteria Decision-making. Spectrum of Mechanical Engineering and Operational Research, 2(1), pp.1-12. Available at: https://doi.org/10.31181/smeor21202524

Wohlers, T., Gornet, T., Mostow, N., Campbell, I., Diegel, O., Kowen, J., & Peels, J., 2016. History of additive manufacturing. Available at: http://dx.doi.org/10.2139/ssrn.4474824

Yalçın, G. C., Kara, K., & Özyürek, H. 2025. Evaluating Financial Performance of Companies in the Borsa Istanbul Sustainability Index Using the CRITIC-MABAC Method. Spectrum of Operational Research, 2(1), pp.323-346. Available at: https://doi.org/10.31181/sor21202530

Yeh, C. C., & Chen, Y. F., 2018. Critical success factors for adoption of 3D printing. *Technological Forecasting and Social Change*, 132, pp. 209-216. Available at: https://doi.org/10.1016/j.techfore.2018.02.003

Yildirim, B., & Ayyildiz, E. (2025). Selecting the most suitable 3D printing technology for custom manufacturing using fuzzy decision-making methodology. *International Journal on Interactive Design and Manufacturing.* Available at : https://doi.org/10.1007/s12008-025-02258-x

Yushuo, C., & Ling, D. 2024. A Framework for Assessment of Logistics Enterprises' Safety Standardization Performance Based on Prospect Theory. *Journal of Operations Intelligence*, 2(1), pp.153-166. Available at: https://doi.org/10.31181/jopi21202418

Zavadskas, E. K., Turskis, Z., & Kildienė, S., 2014. State of art surveys of overviews on MCDM/MADM methods. *Technological and Economic Development of Economy*, 20(1), pp.165-179. Available at: https://doi.org/10.3846/20294913.2014.892037

Zeleny, M. (Ed.)., 2012. Multiple criteria decision-making Kyoto 1975 (Vol. 123). *Springer Science & Business Media*, 123. Available at: https://doi.org/10.1007/978-3-642-45486-8

Zhang, S., & Esangbedo, M. O., 2025. Urban Scenic Spot Activity Center Investment: Strategic Construction Company Selection Using the Grey System-II Thinking Compromise Ranking of Alternatives from Distance to Ideal Solution Multi-Criteria Decision-Making Method. *Systems*, 13(1), 67. Available at: https://doi.org/10.3390/systems13010067

Zhang, X., Toet, W., & Zerihan, J., 2006. Ground effect aerodynamics of race cars. *Applied Mechanics Reviews*, 59(1), pp.33-49. Available at: https://doi.org/10.1115/1.2110263

Sellamuthu, P., Kalita, K., Kumar, A., Chohan, J. S., Rathee, S., & Sharma, Y. K. (2024, December). A hybrid Merec-Mabac approach for 3D printer nozzle material selection. In *AIP Conference Proceedings.* 3217(1). Available at: https://doi.org/10.1063/5.0234604

https://support.makerbot.com/s/article/1667337895715 Date of accession: 15th december 2024
https://www.3dwasp.com/en/delta-printer-delta-wasp-2040/ Date of accession: 15th december 2024
https://www.treatstock.com/machines/item/342-up-plus-2 Date of accession: 16th december 2024

Izbor 3D štampača za spojlere trkačkih automobila korišćenjem modela ,,Entropy – CRADIS"

Rajeev Ranjan[a], *Sonu* Rajak[a], *Prasenjit* Chatterjee[b], **autor za prepisku**
[a] Department of Mechanical Engineering, National institute of Technology, Patna, India
[b] Department of Mechanical Engineering, MCKV Institute of Engineering, Howrah, West Bengal, India

OBLAST: mašinstvo
KATEGORIJA (TIP) ČLANKA: originalni naučni rad

*Sažetak***:**

Uvod/cilj: Cilj ovog istraživanja je da identifikuje najprikladniji 3D štampač za proizvodnju spojlera za trkačke automobile.

Metode: Šesnaest različitih 3D štampača je evaluirano na osnovu osam kriterijuma izbora, uključujući zapreminu štampe, maksimalnu brzinu štampe, debljinu sloja, broj ekstrudera, cenu mašine, cenu filamenta kod proizvođača, maksimalnu temperaturu ekstrudera i maksimalnu temperaturu radne površine. Težine kriterijuma su određene korišćenjem metode Entropy, dok je metoda kompromisnog rangiranja alternativa prema udaljenosti od idealnog rešenja (eng. CRADIS) primenjena za rangiranje mašina i pronalaženje najbolje opcije za proizvodnju spojlera. Za validaciju rezultata sprovedena je analiza osetljivosti korišćenjem različitih metoda.

Rezultati: Ultimaker 2 je identifikovan kao najprikladniji 3D štampač, sledi Delta Non-Turbo WASP 2040, dok UP Plus 2 zauzima najnižu poziciju.

Zaključak: Korišćenjem metoda Entropy i CRADIS, Ultimaker 2 je identifikovan kao 3D štampač sa najboljim performansama. Sledi Delta Non-Turbo WASP 2040, dok je UP Plus 2 rangiran kao najmanje pogodan. Različite višekriterijumske metode odlučivanja (MCDM) su primenjene za poređenje performansi i analizu osetljivosti, dok je Spirmanov koeficijent korelacije rangova korišćen za procenu korelacije između različitih metoda odlučivanja.

Ključne reči: aditivna proizvodnja, 3D štampanje, višekriterijumsko odlučivanje, Entropy, CRADIS, analiza osetljivosti.

Paper received on: 16 April 2025.
Manuscript corrections submitted on: 29 May 2025.
Paper accepted for publishing on: 9 June 2025.

© 2026 The Authors. Published by Vojnotehnički glasnik / Military Technical Courier (www.vtg.mod.gov.rs).This article is an open access article distributed under the terms and conditions of the Creative (http://creativecommons.org/licenses/by/4.0/rs/).

Comprehensive study of the effect of a structural parameter of hydraulic buffer on the firing stability of grenade launchers

Dung V. Nguyen[a], *Bien* V. Vo[b], *Phu* M. Nguyen[c], *Hung* M. Dao[d]

[a] Le Quy Don Technical University, Faculty of Special Equipments, Hanoi City, Socialist Republic of Vietnam,
e-mail: nguyenvandung.cl@gmail.com,
ORCID iD: https://orcid.org/0000-0003-3460-5238

[b] Le Quy Don Technical University, Faculty of Special Equipments, Hanoi City, Socialist Republic of Vietnam,
e-mail: vovanbien@lqdtu.edu.vn, **corresponding author**,
ORCID iD: https://orcid.org/0000-0002-1364-2884

[c] Department of Weapons and Ammunition, University of Defence, Brno, Czech Republic,
e-mail: minhphu.nguyen@unob.cz,
ORCID iD: https://orcid.org/0009-0000-8599-1445

[d] Tran Dai Nghia University,
Ho Chi Minh City, Socialist Republic of Vietnam,
e-mail: daomanhhung.vhp@gmail.com,
ORCID iD: https://orcid.org/0009-0007-8807-1864

https://doi.org/10.5937/vojtehg74-58331

FIELD: mathematics, mechanical engineering
ARTICLE TYPE: original scientific paper

Abstract:

Introduction/purpose: The article's main goal is to present a novel method for evaluating the stability of automatic weapons mounted on tripods when firing in series.

Methods: The mathematical model is established based on the theory of many-body mechanics. The Lagrange II equation is used to establish the system of differential equations of motion of mechanical system. The mathematical model considers the influence of the ground elasticity and the impact of the gunner through elastic-damping connections. Dynamic simulations were performed on the AGS-17 grenade launcher. The calculated results were then compared with the experimental results to verify the proposed model.

Results: The comparison results show an unexpected confidence level between the theoretical model and experimental results. The errors in muzzle velocity and firing rate are 2.52% and 6.18%, respectively. Based

on the theoretical basis of the mathematical model, the influence of some structural parameters of the hydraulic buffer on the firing stability of the automatic grenade launcher was investigated. The research results provide a reliable theoretical basis to improve, design, and manufacture hydraulic buffers for grenade launchers in particular and automatic guns in general.

Conclusion: The research results presented in this paper ensure high accuracy and reliability. This paper provides a reliable scientific document for the optimal design of the overall structure of the weapon system.

Keywords: grenade launcher, firing stability, automatic weapon, automatic firing systems, hydraulic buffer.

Introduction

In the current development trend of military science, the development of weapons is a matter of concern for many countries. In addition to procuring modern weapons, numerous governments are always interested in designing, manufacturing, and improving existing weaponry. This is to improve the combat strength of the Army and ensure its autonomy in defending the country. To master this problem, an in-depth study of the nature of shooting phenomena is necessary. Furthermore, examining the firing stability of the gun under different combat conditions provides a more accurate understanding of the cause of firing errors. From there, specific design, manufacturing, and production solutions are recommended to improve the weapon's shooting efficiency.

To evaluate the firing efficiency of a weapon, one of the important parameters is firing accuracy. Many factors affect the accuracy of shooting, among which the stability of the shot plays the most important role. The more stable the gun, the higher the firing efficiency of the weapon. As a result, numerous studies have been published on the shooting stability of weapons. Notable studies that have presented the stability of the weapon's shot can be found in the literature (Balla et al, 2015; Doan et al, 2023). A common limitation in previous studies is the lack of attention to the simultaneous operation of the automatic firing system and the movement of the entire weapon system. As a result, the interaction between the automatic firing system and the overall weapon system has not been thoroughly investigated (Ich, 2017; Macko et al, 2021). An automatic fire system is a system whose kinetic characteristics directly affect the stability of the entire weapon system. Furthermore, this system is also a constituent element of automatic weapons. Some studies on the firing stability of automatic guns on tripods have not yet addressed the effect of the gunner's impact (Sy et al, 2019), or have only mentioned the gunner's effect on the weapon system as a passive elastomer or a

constant load (Lu et al, 2019). Several studies have addressed the influence of the elastic background on the weapon system as an elastic element with viscous drag (Bien et al, 2021; Doan et al, 2023). These studies have focused on studying the firing stability of automatic weapons in different directions and have achieved certain results.

Modern grenade launchers often operate using the free bolt principle. A key drawback of automatic weapons utilizing this mechanism is the significant mass of the bolt, which generates a substantial impact force when it strikes the rear and front of the gun housing. This leads to several adverse effects during rapid firing, such as reduced firing stability, potential damage to components, and a shorter weapon lifespan. To mitigate these issues, a hydraulic buffer is employed to slow the bolt's movement in both directions. This mechanism helps reduce the impact force between the bolt and the gun housing, thereby enhancing the gun's overall firing stability.

However, after a period of using this weapon, some failures mainly appear in the hydraulic buffer mechanism. Some adverse effects occur during firing, such as decreased shooting accuracy, and increased dispersion of bullets when firing in series. Some serious effects also damage the gun, such as: leaking hydraulic oil, flattening the push-in spring, not ejecting the bullet, the bolt not closing completely, and the shell being deformed, etc. Therefore, it is necessary to study the effects of some structural parameters of the hydraulic buffer mechanism on the firing stability of automatic guns when firing in series. This research not only helps to overcome the above failure phenomena but also gives recommendations for the exploitation and use process as well as the manufacture of suitable replacement hydraulic buffer mechanisms. The previous publications of the research groups have solved the dynamics problem of the automatic firing system of automatic guns operating according to the principle of free reverse bolts (Bien et al, 2021) and the dynamics of grenade launchers mounted on the tripod when firing (Bien et al, 2021).

In this study, the authors build a mathematical model to determine the firing stability parameters of automatic weapons mounted on tripods. This mathematical model is established using the theory of many-body mechanics based on Lagrange II equations. The research content focuses on establishing mathematical models, using numerical methods to solve problems, and evaluating the mathematical models using experimental measurement results. The AGS-17 grenade launcher (Figure 1) was used to calculate the theory and experimentally verify the mathematical model. In addition, the study also evaluates the influence of some structural parameters of the hydraulic buffer mechanism on the stability of the

weapon system. The results obtained from this study can be used to optimize the structure of the weapon system.

Figure 1 – Overview of the AGS-17 grenade launcher

Problem formulation

Overview of the hydraulic buffer mechanism in automatic grenade launchers

Due to the large mass of the automatic grenade launcher, the contact between the bolt and the gun box in the rear and front positions is particularly large. When the rate of fire is not too high, using a hydraulic buffer mechanism is a reasonable solution. Figure 2 shows the structure of the hydraulic buffer mechanism of the AGS-17 grenade launcher.

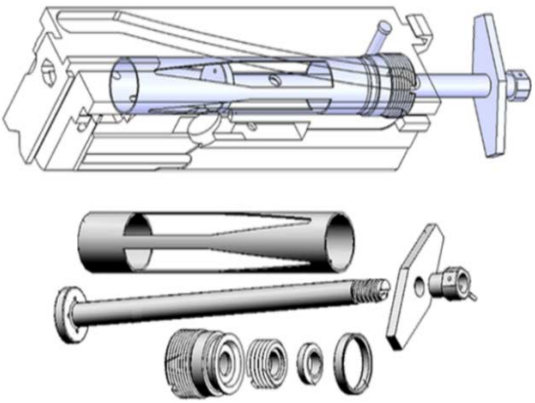

Figure 2 – Hydraulic buffer mechanism

The hydraulic buffer mechanism must meet the following requirements:

- Working reliably, braking smoothly, reducing collisions in both directions;
- Simple structure, ensuring convenience for fabrication and exploitation;
- Ensuring that key operational parameters, such as braking force, recoil length, recoil speed, and return speed, remain within allowable limits while still providing sufficient energy for the automatic firing system to function stably.

**. Seting up the computational model*

Based on the structural characteristics of the hydraulic buffer mechanism used on the AGS-17 grenade launcher, the principle model for determining the hydraulic braking force is presented in Figure 3.

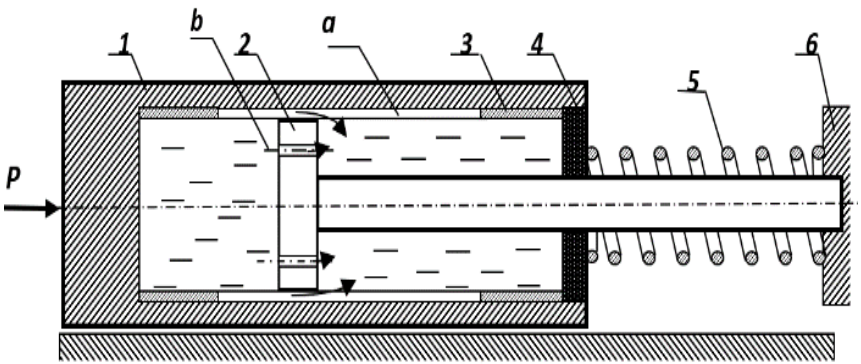

Figure 3 – Working principle model of hydraulic buffer mechanism
1. Bolt; 2. Piston; 3. Regulating tube; Sealing Parts; 5. Return spring; 6. Gun body; a - Oil drain; b - Oil drain hole

In order to determine the hydraulic braking force, the following assumptions are made:

- The oil used in the hydraulic buffer is an ideal incompressible fluid, and the oil flow is steady and continuous.
- The energy loss of the flowing oil due to friction is considered proportional to the kinetic energy of the flowing oil.
- A correction factor is used for flow constriction when oil flows through the cross-section a_x.

The hydraulic braking force is generated by fluid flow between chambers through different gaps. The hydraulic braking force is a function of the variables a_x (oil flow gap area) and V_{kn}^2 (bolt displacement velocity):

$$F_{tl} = f_{(a_x)} V_{kn}^2 \quad (1)$$

*. Determining the hydraulic braking force

Because the slope of the oil flow gap of the hydraulic damper on the AGS-17 grenade launcher varies with the travel length (see Figure 3 and Figure 4), the hydraulic braking force also varies accordingly.

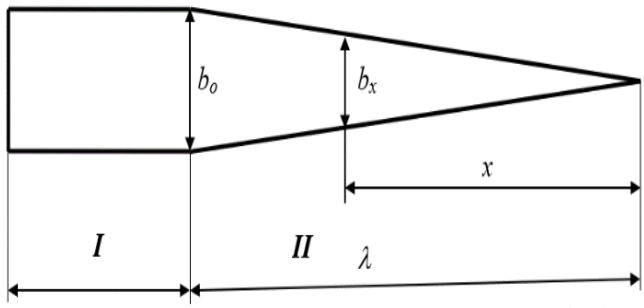

Figure 4 – Oil flow groove diagram

According to the documents (Bien et al, 2021), the hydraulic braking force is determined as follows:

- On section I: The section where the oil flow cross-section is constant.

$$F_{tl} = \frac{k\gamma}{2g} \cdot \frac{A_t^3}{\left(a_0 + a_1\right)^2} V_{kn}^2 \quad (2)$$

- On section II: Section with variable oil flow cross-section.

$$F_{tl} = \frac{k\gamma}{2g} \cdot \frac{A_t^3}{\left(a_x + a_1\right)^2} V_{kn}^2 \quad (3)$$

where k – main flow drag coefficient, γ – specific gravity of the liquid, a_0 – the area of the oil groove on section I, a_1 – cross-sectional area of oil flow hole, V_{kn} – reverse part velocity, A_t – cross-sectional area of the piston; $a_x = a_0 \frac{x}{\lambda}$ – oil flow area at position x on segment II.

The calculated results of the hydraulic braking force of the AGS-17 grenade launcher are shown in Figure 5.

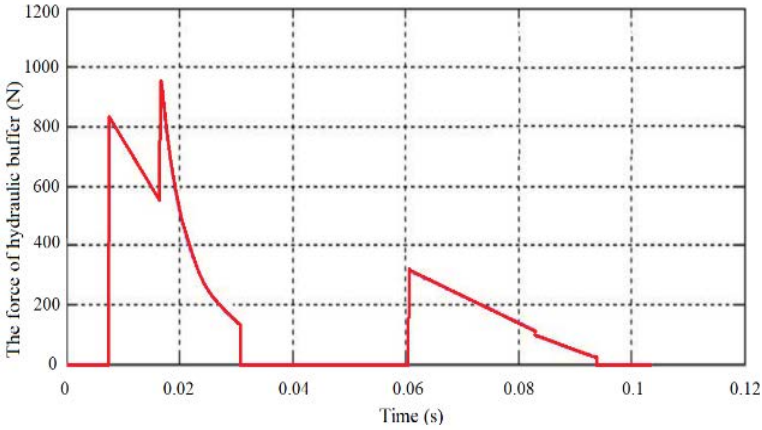

Figure 5 – The braking force of the hydraulic buffer

Model of AGS-17 grenade launcher on a tripod

The problem of oscillation of the AGS-17 grenade launcher on a tripod firing on an elastic foundation has been detailed by Bien et al. (2021). Accordingly, the dynamic model consisting of 3 solids with 9 degrees of freedom (DOFs) is presented in Figure 6, and the mechanical structure of the weapon system is shown in Figure 7.

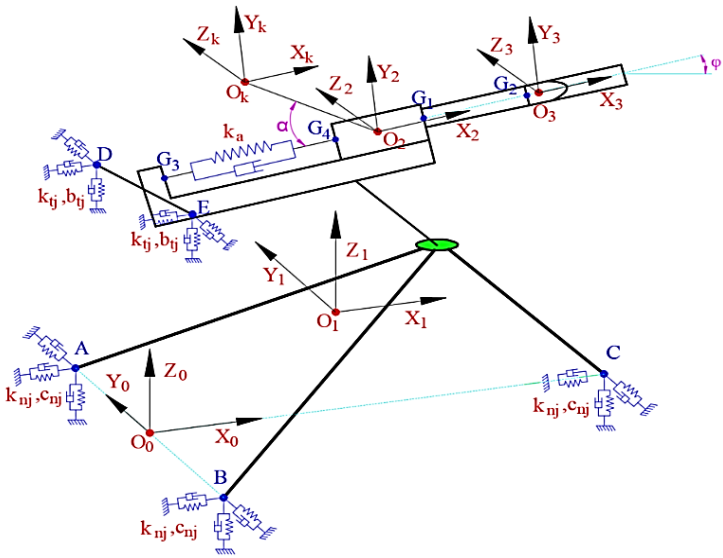

Figure 6 – Automatic gun model mounted on the tripod (Bien et al, 2021)

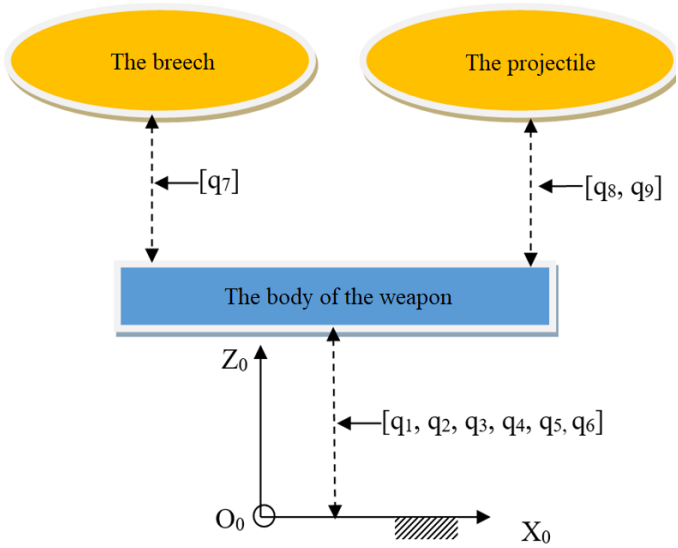

Figure 7 – Diagram of weapon structure

To investigate the dynamics of the system, we assign the system and each object in the system a Cartesian coordinate system so that the description of the configuration of the mechanical system is most effective (see Figure 6):

- Fixed coordinate system (earth coordinate system) O_0: The origin is located at the point between the hind legs in the initial position. The X_0 and Z_0 axes belong to the firing plane (the vertical plane containing the barrel axis) and the x_0 axis is parallel to the horizontal plane, the Z_0 axis is perpendicular to the horizontal plane, and the Y_0 axis is perpendicular to the $X_0O_0Z_0$ plane.

- Moving coordinate system O_1: attached to object 1, the origin O_1 coincides with the center of mass of object 1, and the X_1 axis is parallel to the barrel axis, the Z_1 axis is perpendicular to the horizontal plane, Y_1 axis is perpendicular to the $X_1O_1Z_1$ plane.

- Moving coordinate system O_2: attached to object 2, the origin O_2 coincides with the center of gravity of object 2. The X_2 axis is parallel to the X_1 axis, the Z_2 axis is parallel to the Z_1 axis, and the Y_2 axis is parallel to the Y_1 axis.

- Moving coordinate system O3: attached to object 3, the origin O3 coincides with the center of gravity of object 3. The X3 axis is parallel to the X1 axis, the Z3 axis is parallel to the Z1 axis, and the Y3 axis is parallel to the Y1 axis.

- Moving coordinate system Ok: the origin coincides with the center of gravity of the body k. The Xk axis is parallel to the relative motion of the body k in the O1 coordinate system, and the Yk and Zk axes are parallel to the corresponding axes of the O1 coordinate system.

As shown in Figure 6 and Figure 7, the mechanical system is considered to be a chain configuration, containing 3 solids with 9 DOFs. Object 1 is the gun body (including the gun box, gun rack, range mechanism, direction mechanism, ammunition box, and the compacted mass of the gunner) with mass m_1. Body 1 has 6 DOFs: 3 rotations around the 3 axes X_0, Y_0, and Z_0 and 3 translational displacements along the X_0, Y_0, and Z_0 axes. Object 2 is a bolt of mass m_2. Body 2 has a translational displacement relative to body 1 along the X_1 axis. Object 3 is a bullet of mass m_3. Body 3 has 2 DOFs: translational displacement and rotational motion relative to body 1 along the X_1 axis. In addition, in this study, the working mechanisms of the automatic firing system (object *k*) are also taken into account (see Figure 6). These links move in directional grooves on body 1 and have a motion connection with body 2. The motion characteristics of the working links are taken into account when using the transmission linkage equations between the working link and the base link (object 2) of the automatic firing system.

Based on the analysis above, the mechanical system is set up with 10 generalized coordinates as follows $[q_j]=[q_1, q_2, q_3, q_4, q_5, q_6, q_7, q_8, q_9, q_k]$, where: q_1 - translational motion of body 1 along the X_0-axis; q_2 - translational motion of body 1 along the Y_0-axis; q_3 - translational motion of body 1 along the Z_0-axis; q_4 - rotation about the X_0-axis of object 1; q_5 - rotation about the Y_0-axis of object 1; q_6 - rotation about the Z_0-axis of object 1; q_7 - translational motion of body 1 along the X_1-axis; q_8 - translational motion of body 1 along the Y_1-axis; q_9 - rotation about the X_1-axis of object 3; q_k - translation or rotation about the X_k-axis of object *k*. The investigated mechanical system has 9 DOFs and 10 generalized coordinates, in which the independent generalized coordinates are from q_1 to q_9. The remaining coordinates, q_k, depend on the generalized coordinates.

According to the document (Bien et al, 2021), the system of differential equations describing the motion of the mechanical system in space is established based on the Lagrange II equation, equation (4), (Ahmed, 2013).

$$\frac{d}{dt}\left(\frac{\partial T}{d\left(\frac{dq_j}{dt}\right)}\right)-\frac{\partial T}{dq_j}=Q_j \quad \left(j=1\div 10\right) \tag{4}$$

where, T – total kinetic energy of the whole system; q_j – generalized coordinate j-th; Q_j – generalized force corresponding to the generalized coordinate q_j.

The establishment of a system of equations determining the kinetic and potential energy of the mechanical system as well as the generalized forces is detailed in (Bien et al, 2021). The system of differential equations describing the vibrations of the mechanical system is expressed by formula (5).

$$EQS=\left\{eq_1,eq_2,eq_3,...,eq_8,eq_9\right\} \tag{5}$$

The determination of the forces acting on the mechanical system has been detailed in (Bien et al, 2021). Input parameters are determined based on design documents, and some parameters such as the center of gravity and moment of inertia of the objects are determined using Inventor software (see Figure 8). Some other parameters are measured directly on the gun. The system of equations (5) is solved numerically by the Matlab programming software presented in the document (Bien et al, 2021).

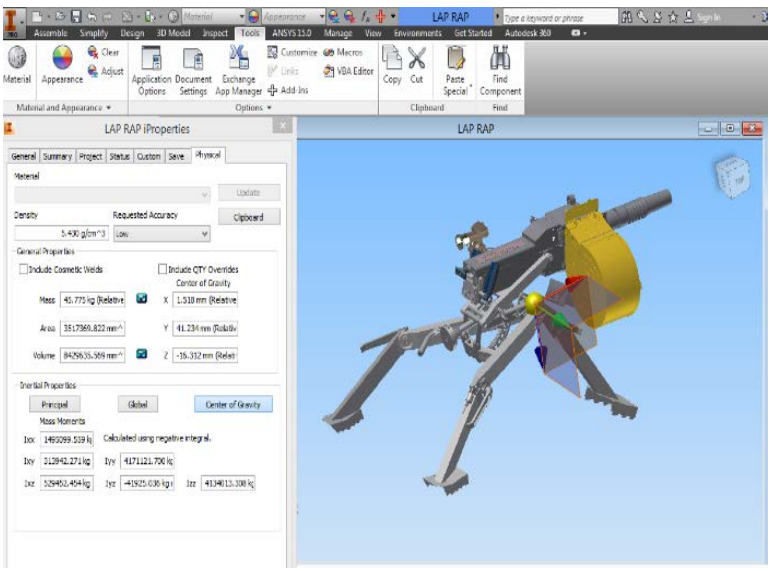

Figure 8 – Determining input parameters using Inventor software

Verification test

To verify the vibration model of the AGS-17 grenade launcher on a tripod when firing, the authors developed a plan and conducted a test with the selected parameters as follows: the bouncing angle of the gun's barrel in the vertical plane; the bouncing angle of the gun's barrel in the horizontal plane and the gun's backward movement. The structural diagram of the measuring system, as well as the equipment used in the experiment, have been detailed in Bien et al. (2021). The structural diagram of the experimental measurement system and the experimental deployment is shown in Figure 9. Some experimental images are shown in Figure 10 and Figure 11.

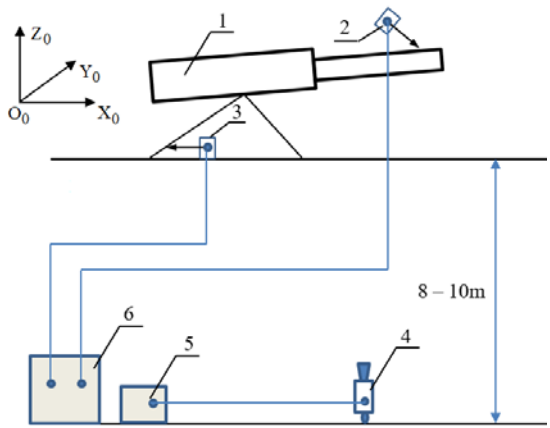

Figure 9 – Experimental diagram: 1. Gun; 2,3. Displacement measuring device; 4. High-speed camera; 5. Computer; 6. DEWETRON 3000 device.

Figure 10 – Experimental layout

Figure 11 – Ammunition used in the test

The results of the test are the displacement of the barrel in the vertical plane, displacement of the barrel in the horizontal plane, and the gun's backward movement. The experimental bounce angle of the gun is calculated using the following formula:

$$\alpha_y = arctg\frac{z_n}{l};\quad \alpha_z = arctg\frac{y_n}{l} \tag{6}$$

where: z_n, y_n - displacement of the barrel tip relative to the initial position; l - length from barrel tip to armrest.

The steps for conducting the experiment and processing the results have been detailed in previous publications of the research team (Bien et al, 2021).

Results and discussion

Verifying the mathematical model

To obtain results with high accuracy, the system of equations (5) is solved simultaneously with the system of differential equations for the interior ballistics of the AGS-17 grenade launcher (system of equations (7)). Numerical methods were used to solve the problem. Matlab software was used as a tool to help the author solve this problem. The algorithm diagram for solving the system of oscillation equations of the AGS-17 grenade launcher is shown in Figure 12.

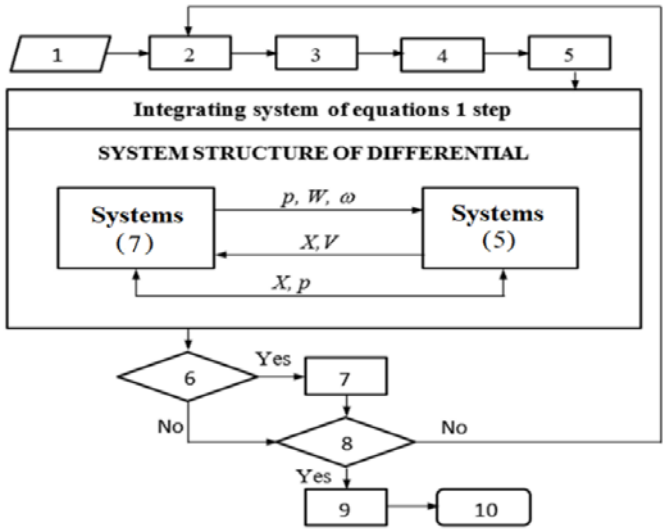

Figure 12 – Problem solving diagram

Symbols in Figure 12: 1 – enter initial parameters; 2 – determine the forces acting on the base link (bolt); 3 – determine the value of the resistance force; 4 - determine the gear ratios ki and transmission efficiency ηi; 5 – determine the coefficients ξi; 6 – check whether there is a collision; 7 – calculate the base link velocity after the collision; 8 – condition analysis to finish the calculation; 9 – record results; 10 – end.

$$\begin{cases} \dfrac{dv}{dt} = \xi_1\xi_3 \dfrac{p.S}{\varphi.m}, \\ \dfrac{\mathrm{dl}}{\mathrm{dt}} = \xi_1\xi_3.v\ , \\ \dfrac{\mathrm{dz}}{\mathrm{dt}} = \xi_2 \dfrac{p}{I_k}\ , \\ \dfrac{\mathrm{d}\omega_c}{dt} = \xi_2\chi.\omega_t\left(1+2\lambda z\right)\dfrac{p}{I_k} - \left(1-\xi_3\right)G\ , \\ \dfrac{dw}{dt} = \xi_2\dfrac{1-\alpha\delta}{\delta}\chi.\omega_t\left(1+2\lambda z\right)\dfrac{p}{I_k} + \xi_3 Sv + S\dfrac{dx}{dt}\xi_x\ , \\ \dfrac{dp}{dt} = \dfrac{1}{w}\left\{\xi_2\dfrac{p\chi.\omega_t}{I_k} f\left(1+2\lambda z\right) - kp\dfrac{dw}{dt} - K_{\mathrm{p}}\left(1-\xi_3\right)G\ - K_{\mathrm{t}}p\right\}. \end{cases} \quad (7)$$

where v – bullet's velocity; p – combustion gas pressure in the barrel; S – cross-sectional area of the barrel; φ – coefficient of secondary works

account; α – covolume; δ – specific gravity of the propellant; f – powder force; k – adiabatic exponent; w – volume of space after the bottom of the bullet; w_0 – initial volume of the combustion chamber; m – mass of the bullet; ω_t – weight of the propellant; ω_c – weight of combustible gas; I_k – pressure impulse of the combustible gas; χ, λ – geometrical properties of the propellant; z – relative burning thickness of the propellant; x – displacement of the bolt; K_t – heat loss function; l – bullet displacement in the barrel; K_p – combustible gas flow function; G – air flow through the barrel mouth; ξ_1, ξ_2, ξ_3, ξ_x - the correction coefficients are determined according to Table 1.

Table 1 - Values of correction coefficients in the system of equations (7)

ξ	ξ1		ξ2		ξ3		ξx	
Value	1	0	1	0	1	0	1	0
Condition	p>po	p<po	z<1	z≥1	l<ld	l≥ld	x≠0	x=0

where p_o – shot start pressure; l_d - length of the barrel with a spiral groove.

Solving the system of differential equations according to the block diagram in Figure 12 using Matlab programming software, some typical results are presented in Figures 13-18: The pressure of the combustion gas in the barrel and the velocity of the bullet are shown in Figure 13; the velocity and displacement of the bolt with respect to time are shown in Figure 14; The barrel's bounce angle in the vertical plane when firing bursts of three rounds is shown in Figure 15; The barrel's bounce angle in the horizontal plane when firing bursts of three rounds is shown in Figure 16; The barrel's bounce angle in the vertical plane when firing bursts of five rounds is shown in Figure 17; The barrel's bounce angle in the horizontal plane when firing bursts of five rounds is shown in Figure 18.

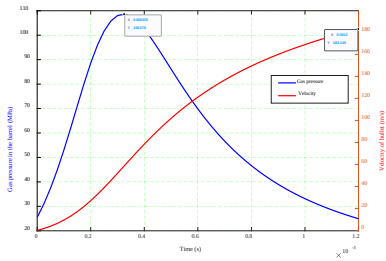

Figure 13 – Combustion gas pressure and bullet velocity in the barrel

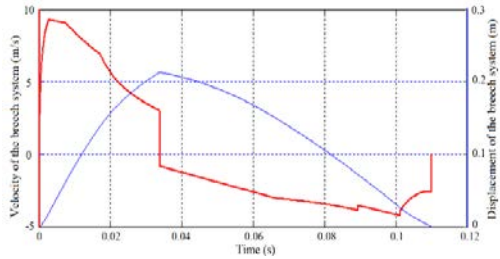

Figure 14 – Velocity and displacement of the bolt with time

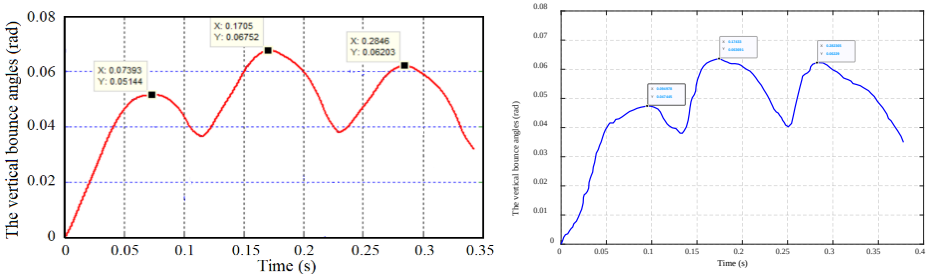

a. Theoretical results *b. Experimental results*

Figure 15 – The barrel's bounce angle in the vertical plane when firing bursts of three rounds

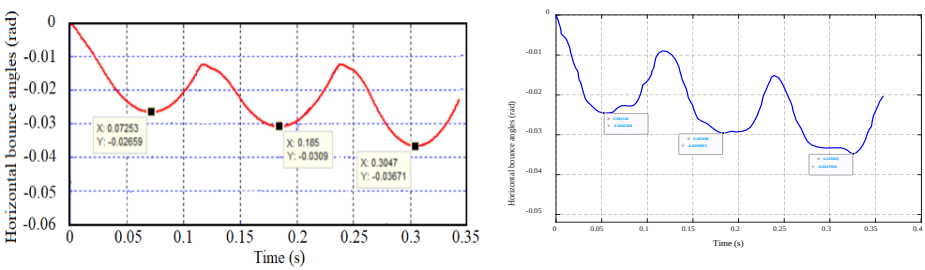

a. Theoretical results *b. Experimental results*

Figure 16 – The barrel's bounce angle in the horizontal plane when firing bursts of three rounds

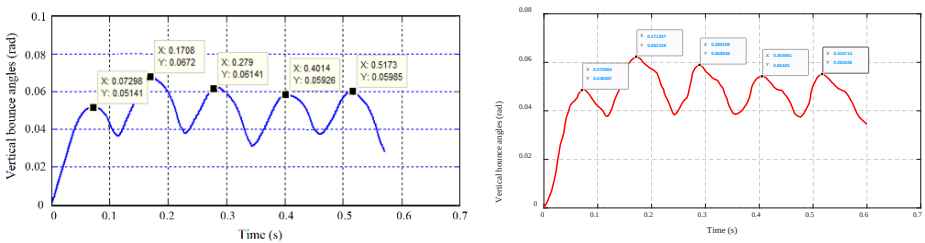

a. Theoretical results *b. Experimental results*

Figure 17 – The barrel's bounce angle in the vertical plane when firing bursts of five rounds

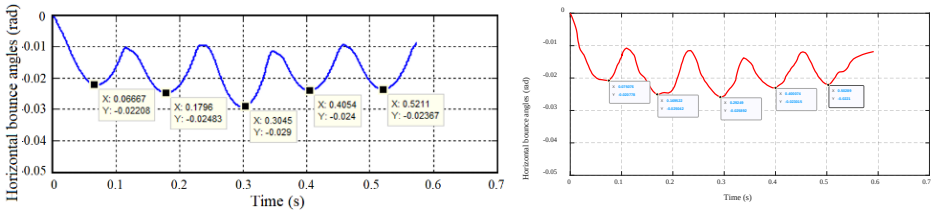

a. Theoretical results *b. Experimental results*

Figure 18 – The barrel's bounce angle in the horizontal plane when firing bursts of five rounds

The obtained results can be interpreted as follows:

- Solving the interior ballistic problem gives quite reliable results, with the maximum combustion gas pressure in the barrel being 108.576 MPa (Figure 13), while the published measurement results are 112.58 MPa (Bien et al, 2021), and the error is 3.566%. The maximum velocity of the bullet is 183.149 m/s (Figure 13), whereas the published measurement results are 187.88 m/s (Bien et al, 2021), and the error is 2.52%.

- The cycle of a firing is 0.1092 s (Figure 14), the corresponding theoretical rate of fire is 549 rds/min, the published rate of fire is 517 rds/min (Bien et al, 2021), and the error is 6.18%.

- The comparison between the theoretical calculation results and the experimental measurement results shows that (Figures: 15-18): the mathematical model and solution method are consistent and reliable. The error is within the allowable limit (less than 10%). This dynamic model can be used in the further study of the AGS-17 grenade launcher.

Investigating the effect of the oil type used in the hydraulic buffer

The buffer force has a great influence on the operation of the automatic firing system as well as the vibration of the gun when firing in series. According to formulas (2) and (3), this force depends on many factors such as the type of oil used in the hydraulic buffer mechanism, the velocity of movement of the barrel, the cross-section of the oil flow, etc. Within the framework of the article, the authors focus on investigating the effects of changing the oil types used in the hydraulic buffer and changing the oil flow cross-section on the stability of the grenade launcher when firing in series.

During the use of the AGS-17 grenade launcher, the amount of oil in the buffer mechanism will be consumed and degraded. Oil changes and

additions should be carried out regularly. However, if only a specific type of oil can be used, it will cause significant difficulties during operation and use, especially in combat conditions. For this reason, the article investigates the influence of some oils used for the buffer mechanism on the stability of the gun when firing. These oils are commonly used in weapons. The basic characteristics of the oils used in this study are presented in Table 2.

Table 2 – Properties of some hydraulic oils

Characteristic	Oil Steol-M	Oil AY	Petroleum
Specific weight (γ)	1.09 ÷ 1.1 (kG/dm3)	0.89 ÷ 0.9 (kG/dm3)	0.78 ÷ 0.83 (kG/dm3)
Evaporation temperature (td)	> 57oC	> 45oC	-
The boiling temperature at atmospheric pressure (tk)	89 ÷ 92oC	350oC	300oC
Viscosity:			
0oC	0.279	1.65	-
20oC	0.109	0.4	-
40oC	-	-	0.1 ÷ 0.9
50oC	0.37	0.106	-

Solve the system of differential equations for the oscillations of the AGS-17 grenade launcher according to the algorithm diagram shown in Figure 12, while changing the type of oil used in the hydraulics buffer; other parameters remain unchanged. Some typical results are given as follows, Figures 19 - 22.

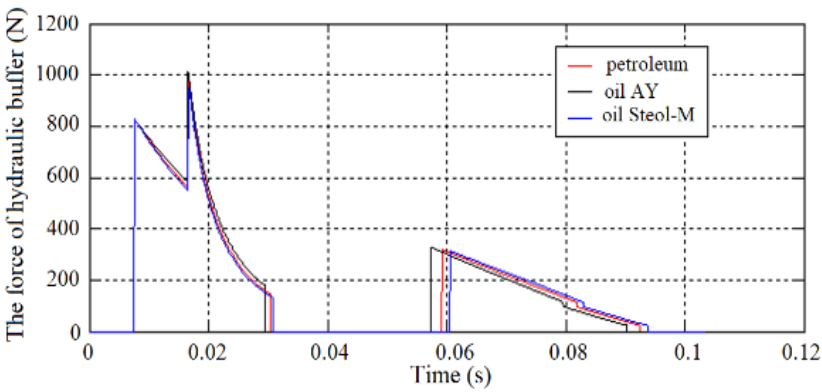

Figure 19 – Force of hydraulic buffer

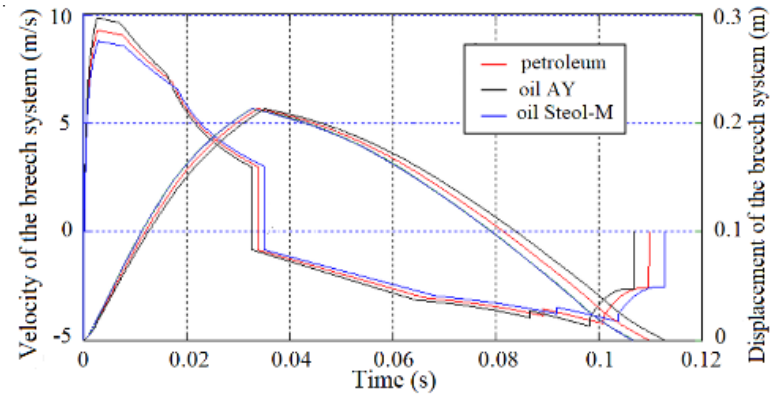

Figure 20 – Velocity and displacement of the bolt

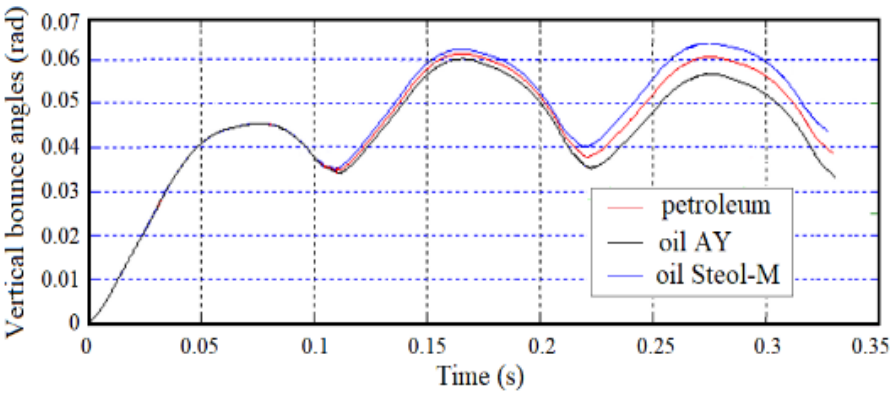

Figure 21 – The barrel's bounce angle in the vertical plane when firing bursts of three rounds

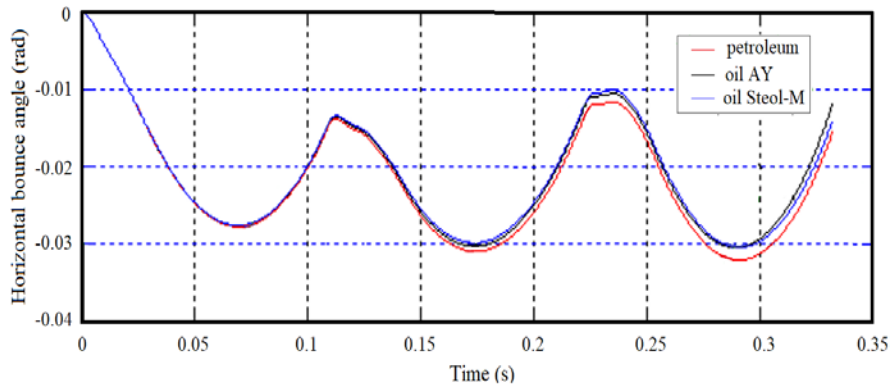

Figure 22 – The barrel's bounce angle in the horizontal plane when firing bursts of three rounds

The obtained results can be commented on as follows:

The hydraulic braking force, displacement, and velocity of the bolt chang when the oil type used in the hydraulic buffer is changed (Figures 19-20). However, the survey results show that the variation of the bounce angle in the vertical plane (Figure 21) and the bounce angle in the horizontal plane (Figure 22) of the barrel is relatively small. This is explained by the fact that these oils have similar properties and can be substituted for each other during operation and use. This facilitates the repair and use of the gun.

Influence of the oil flow cross-section in the hydraulic buffer mechanism

According to the design characteristics of the AGS-17 automatic grenade launcher, the oil flow area in the hydraulic buffer includes the oil hole area on the piston, the oil flow area on the piston pipe, and the gap between the piston and the piston pipe (Figure 3).

Changes in the oil flow area of the hydraulic buffer may be due to manufacturing tolerances and wear over time. This can change the hydraulic braking force compared to the original design, causing instability in the gun. Investigating the influence of this factor on the stability of the gun helps designers determine the allowable tolerance range during manufacturing as well as repair. The system of differential equations describing the gun's oscillation is solved according to the diagram in Figure 12, while keeping other parameters unchanged and varying the cross-sectional area of oil flow. The results are obtained as shown in Figures 23-25.

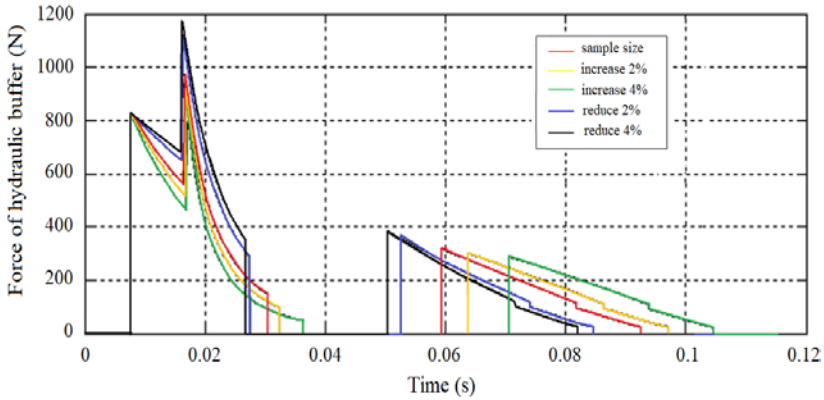

Figure 23 – Hydraulic braking force with different oil flow area

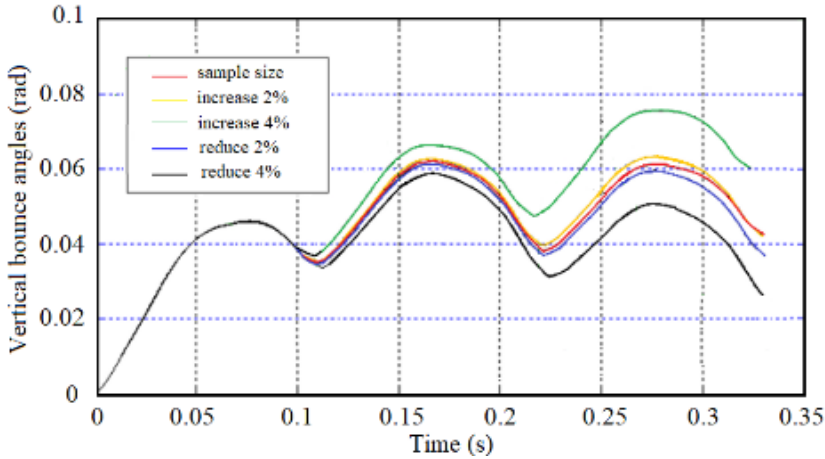

Figure 24 – The barrel's bounce angle in the vertical plane

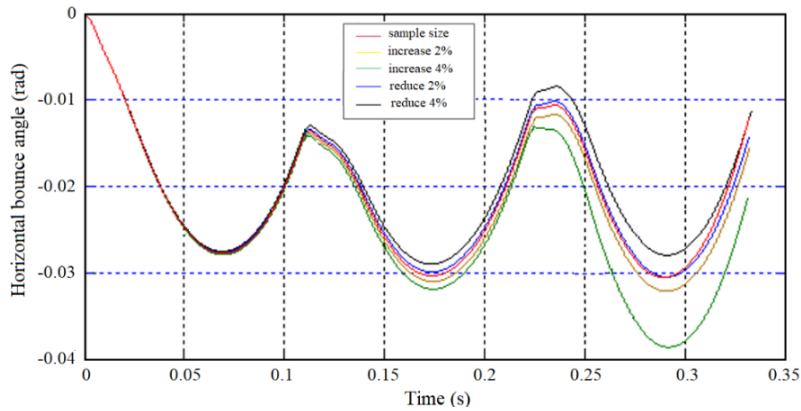

Figure 25 – The barrel's bounce angle in the horizontal plane

The obtained results can be commented on as follows:

The hydraulic braking force changes significantly when changing the oil flow area in the hydraulic buffer mechanism (Figure 23). This change causes instability in the gun. The vibration of the system is inversely proportional to this change in cross-section (Figures 24-25). According to the survey results, to ensure that the vertical bounce angle and the horizontal bounce angle do not exceed the allowable limit, the increase or decrease in the oil flow cross-section must not exceed 2% (0.07 rad for vertical bounce angle and 0.05 rad for horizontal bounce angle) from the 2nd shot onwards when the system oscillates. This limit is determined by testing the standard Russian gun model and the results of solving the

stability problem of the system according to the model presented in documents (Bien et al, 2021). This will be a reliable theoretical basis for the designer to refer to during the design of hydraulic buffer mechanisms, giving the allowable tolerance range when manufacturing products.

Conclusion

The content of this study presents a method for setting up a dynamic model of small automatic weapons mounted on tripods when firing in series. The mathematical model is established based on the theory of many-body mechanics and the Lagrange II equations. In this dynamic model, the influence of the elastic ground and the impact of the gunner are taken into account through elastic-damping connections. The AGS-17 grenade launcher was selected for dynamic simulation and validation of the mathematical model. Based on the obtained results, some main conclusions can be summarized as follows:

- The content of the research has perfected the dynamics model of an automatic weapon mounted on a tripod when firing in space. The results of weapon system dynamics analysis can be performed at locations with different background characteristics.

- A detailed diagram for solving the system of oscillation differential equations of the weapon system on a tripod is established. This diagram can be used as a reference source for researchers when assessing the firing stability of automatic weapons on racks.

- The research content has also provided a measurement method with modern high-precision equipment to evaluate the firing stability of the weapon system.

- The analytical results ensure high accuracy and reliability. This is a reliable scientific document for the optimal design of the overall structure of the weapon system.

References

Balla, J., Krist, Z., and Ich, L. 2015. Experimental study of turret-mounted automatic weapon vibrations. *International Journal of Mechanics*, 9(1).

Balla, J. 2011. Dynamics of Mounted Automatic Cannon on Track Vehicle. *International Journal of Mathematical Models and Methods in Applied Sciences*, 5(3), 423-422.

Ich, L. 2017. Oscillation of the particles of the gun carriage of the automatic weapon, (Ph.D. Thesis), Brno: *University of Defence*.

Balla, J., Havlicek, M., Jedlicka, L., Krist, Z., and Racek, F. 2011. Firing stability of mounted small arms, *International Journal of Mathematical Models and Methods in Applied Sciences*, 5(3), 412-422.

Dung, N, T., Dung, N, V., Phuc, T, V., and Linh, D, D. 2017. Biomechanical Analysis of the Shooter-Weapon System Oscillation, *2017 International Conference on Military Technologies* (ICMT), Czech Republic. Available at: https://ieeexplore.ieee.org/document/7988729.

Bien, V, V., Phuc, T, V., and Macko, M. 2021. Effect of Some Structural Parameters on Firing Stability of Shooter-weapon System. *Advances in Military Technology*, 16(2), 235-251. Available at: https://doi.org/10.3849/aimt.01487.

Macko, M., Bien, V, V., Quang, M, A. 2021. Dynamics of Short Recoil-operated Weapon, *Problems of Mechatronics. Armament, Aviation, Safety Engineering*, 12(3), 9-26. Available at: https://promechjournal.pl/article/152432/en

Bien, V, V., Hieu, T, T., Macko, M., Dung, N, V., Phon, N, D. and Tien, V, D. 2021. Effect of Some Structural Parameters on the Firing Stability of the PKMS Machine Gun when Firing with Complicated Boundary Conditions, 2021 *International Conference on Military Technologies* (ICMT), 1-6. Available at: https://ieeexplore.ieee.org/document/9502820

Lu, Y., Zhou, K., He, L., Li, J., & Huang, X. 2019. Research on the floating performance of a novel large caliber machine gun based on the floating principle with complicated boundary conditions. *Defence Technology*. 15(4), 607-614.

Bien, V, V., Konecny, P., and Phon, N, D. 2021. Effect of Shot Duration on the Firing Accuracy when Burst Fire of Unguided Rockets, 2021 *International Conference on Military Technologies* (ICMT), 1-6. Available at: https://ieeexplore.ieee.org/document/9502812

Tien, V., Macko, M., Prochazka, S. and Bien, V, V. 2022. Mathematical Model of a Gas-Operated Machine Gun. Advances in Military Technology, 17(1), 63-77. Available at: https://aimt.cz/index.php/aimt/article/view/1449

Popelinsky, L. 2000. Design of automatic weapons – calculation of functional diagram of automatic weapon. Brno: *Military Academy Brno*.

Balla, J., Mach, R. 2007. Kinematics and dynamics of Gatling weapons (Periodical style). *Advances in Military Technology*, 2(2), 121-133.

Fiser, M., Popelinsky, L. 2007. Small Arms, Brno: *University of Defence*.

Sy, N, T., Beer, S., Bien, V, V., Phon, N, D., and Phu, N, M. 2019. Oscillation of the Anti-tank Missile System Fagot Fired on the Elastic Ground, 2019 *International Conference on Military Technologies* (ICMT), 1-5. Available at: https://ieeexplore.ieee.org/document/8870069

Doan, D, V., Bien, V, V., Quang, M, A., and Phu, N, M. 2023. A Study on Multi-Body Modeling and Vibration Analysis for Twin-Barrel Gun While Firing on Elastic Ground. *Applied Engineering Letters*, 8(1), 36-43. Available at: https://doi.org/10.18485/aeletters.2023.8.1.5

Bien et all. 2021. Effect of some structural parameters on the operation of automatic system with simple blowback breech. *2021 International Conference on Military Technologies* (ICMT), 1-6. Available at: https://ieeexplore.ieee.org/document/9502757.

Bien et all. 2021. Firing stability of automatic grenade launcher mounted on tripod. *2021 International Conference on Military Technologies* (ICMT), 1-8. Available at: https://ieeexplore.ieee.org/document/9502836 .

A.S. Ahmed. 2013. Dynamics of multibody systems 4th ed. Chicago: *University of Illinois*.

Kari, A., Jovanović, D., Jerković, D., and Hristov, N. 2016. Stress analysis of integrated 12.7 mm machine gun mount. *Scientific Technical Review*, 66(4), 47-51.

Chuong, P, H. 2022. Dynamics of automatic firing gun. *Military Technical Academy*, Hanoi, Vietnam.

Dao, H, M. 2016. Study on the dynamics of the AGS-17 30mm grenade launcher and the effect of some structural factors on gun stability when fired (Ph.D. Thesis), *Military Technical Academy*, Hanoi, Vietnam.

Chaturvedi, E. 2019. Investigating T finned Barrels for Machine Guns: Enhancement in Heat Dissipation and Flexural Rigidity along with Weight Reduction. *Advances in Military Technology*, 14(1), 59-69. Available at: https://aimt.cz/index.php/aimt/article/view/1254

Liu, Q., Zhou, K., Shen, C., and He, L. 2021. Effect of an Internal Impact Balance Mechanism on the Perceptible Recoil of Machine Gun. *In E3S web of conferences 231*, 03001. Available at: https://doi.org/10.1051/e3sconf/202123103001

Hai, N, T., Phu, N, M. 2019. Vibration of launcher on multiple launch rocket system BM-21 with the change of rocket's mass center when fired. *Journal of Science and Technique*, 14(3).

Sveobuhvatna studija uticaja strukturnog parametra hidrauličnog amortizera na stabilnost gađanja bacača granata

Dung V. Nguyen[a], *Bien* V. Vo[a], **autor za prepisku**, *Phu* M. Nguyen[b], *Hung* M. Dao[c]

[a] Le Quy Don Technical University, Faculty of Special Equipments, Hanoi City, Socialist Republic of Vietnam

[b] Department of Weapons and Ammunition, University of Defence, Brno, Czech Republic

[c] Tran Dai Nghia University, Ho Chi Minh City, Socialist Republic of Vietnam

OBLAST: matematika, mašinstvo
KATEGORIJA (TIP) ČLANKA: originalni naučni rad

Sažetak:

Uvod/cilj: Glavni cilj rada je predstavljanje nove metode za procenu stabilnosti automatskog naoružanja montiranog na tronožac tokom rafalne paljbe.

Metode: Matematički model je uspostavljen na osnovu teorije mehanike sistema sa više tela. Lagranževa jednačina druge vrste korišćena je za formiranje sistema diferencijalnih jednačina kretanja mehaničkog sistema. Matematički model uzima u obzir uticaj elastičnosti podloge i uticaj

nišandžije putem elastično-prigušnih veza. Dinamičke simulacije sprovedene su na bacaču granata AGS-17. Dobijeni rezultati proračuna su upoređeni sa eksperimentalnim rezultatima radi verifikacije predloženog modela.

Rezultati: Rezultati poređenja pokazuju neočekivano visok nivo podudaranja između teorijskog modela i eksperimentalnih rezultata. Greške u početnoj brzini projektila i brzini paljbe iznose 2,52%, odnosno 6,18%. Na osnovu teorijske osnove matematičkog modela, ispitan je uticaj pojedinih strukturnih parametara hidrauličnog amortizera na stabilnost gađanja automatskog bacača granata. Rezultati istraživanja predstavljaju pouzdanu teorijsku osnovu za unapređenje, projektovanje i proizvodnju hidrauličnih amortizera za bacače granata, kao i za automatsko naoružanje uopšte.

Zaključak: Rezultati istraživanja prikazani u ovom radu pružaju visoku tačnost i pouzdanost. Rad predstavlja pouzdan naučni dokument za optimalno projektovanje strukture sistema naoružanja.

Ključne reči: bacač granata, stabilnost gađanja, automatsko naoružanje, sistemi automatske paljbe, hidraulični amortizer.

Paper received on: 19 April 2025.
Manuscript corrections submitted on: 3 October 2025.
Paper accepted for publishing on: 9 February 2026.

© 2026 The Authors. Published by Vojnotehnički glasnik / Military Technical Courier (www.vtg.mod.gov.rs). This article is an open access article distributed under the terms and conditions of the Creative Commons Attribution license (http://creativsecommons.org/licenses/by/4.0/rs/).

Contribution to the damage analysis of pipeline cracking under high pressure

Amina Ismahene Fezazi[a], *Belaïd* Mechab[b], *Mokadem* Salem[c], *Boualem* Serier[d]

University of Sidi Bel Abbes, Faculty of Technology, Mechanical Engineering Department, mechanical physics of materials laboratory, Sidi Bel Abbes 22000, Algeria

[a] e-mail: ismahene.fezazi@gmail.com, **corresponding author,**
ORCID iD: https://orcid.org/0009-0002-6738-3774

[b] e-mail: bmechab@yahoo.fr,
ORCID iD: https://orcid.org/0009-0000-7483-5527

[c] e-mail: moka_salem@yahoo.fr,
ORCID iD: https://orcid.org/0000-0001-7558-714X

[d] e-mail: serielem@yahoo.fr,
ORCID iD: https://orcid.org/0000-0002-1460-9322

https://doi.org/10.5937/vojtehg74-58675

FIELD: mechanical engineering, materials
ARTICLE TYPE: original scientific paper

Abstract:

Introduction/purpose: This study aims to contribute to the prediction of pipeline damage caused by cracking in hydrocarbon-transport pipelines, subjected to high internal pressures, in response to the growing demand in industrialised countries.

Methods: To achieve this objective and analyse crack propagation in terms of Stress Intensity Factor (SIF) evaluation, the Finite Element Method (FEM) was employed. The study considers the effects of the transported medium's internal pressure on the one hand, and external stresses caused by natural phenomena such as earthquakes, landslides, and others, on the other. These external stresses are represented by tensile and compressive forces. Particular attention was given to the propagation of three types of cracks: circumferential, longitudinal, and mixed-mode cracks.

Results: The affected tubular structure zone is highly susceptible to mode I cracking. In contrast to the two initial types of cracking defects, an oriented crack at an angle of π/4 with respect to the pipeline's longitudinal axis develops nearly equally in modes I and II. Its growth kinetics are closely linked to its size, internal pressure, and the intensity of external forces.

Tensile forces promote the opening of circumferential cracks, the closure of longitudinal cracks, and mixed-mode (I and II) propagation of oriented cracks. Conversely, compressive forces favour the closure of

circumferential and oriented cracks while encouraging the opening of longitudinal cracks.

Conclusion: The study reveals that, under identical loading conditions, longitudinally initiated cracks pose the greatest danger in terms of mode I crack growth. The risk of pipeline rupture is particularly high along the pipeline, and it increases significantly with higher internal pressure.

Key words: Pipeline, pressure, external forces, Finite Element Method (FEM), crack, Stress Intensity Factor.

Introduction

Pipelines are structures designed exclusively for the transport of hydrocarbons. For instance, liquid petroleum and gases are often conveyed over long distances via pipelines. The mixture of oil and natural gas extracted from a well must be transported as a two-phase flow through pipelines to processing facilities, where the oil can be separated from the gas. Predicting rupture and ensuring the reliability of these structures in various practical applications is crucial, given their economic and safety implications (De Barros et al, 2020; Nikhil et al, 2021; Barsoum & Yurindatama, 2020; Zheng et al, 2021).

Pipeline cracking presents a serious threat to the integrity, safety, and longevity of hydrocarbon and fluid transport systems (Mechab et al., 2011; 2014). It may result from material fatigue, stress corrosion cracking, or fluctuations in mechanical and environmental conditions, often leading to failures ranging from minor leaks to catastrophic ruptures (Qin & Cheng, 2021; Ma et al, 2024). To mitigate these risks, implementing robust preventative strategies is essential. These include regular inspections, the use of corrosion-resistant materials, the application of protective coatings, and the integration of advanced monitoring technologies. Such measures not only help detect early signs of degradation but also enhance the reliability and service life of pipeline infrastructure.

Numerous authors have studied the fracture behaviour of pipelines through numerical simulations, aiming to assess their mechanical integrity while considering different crack configurations (Fezazi et al, 2020; Mechab et al, 2018; Mechab et al, 2020; Metehri et al, 2024; Salem et al, 2019; Wu et al, 2022; Zhou et al, 2025; Zhou et al, 2020; Chattopadhyay et al, 2014; Weltevreden et al, 2021).

The parameters related to the ductile fracture mechanics of cracked pipelines under high internal pressure are critical for evaluating the integrity of damaged structures (Muthanna et al, 2021). Rahman (1995) analysed the behaviour of short cracks initiated in pipelines subjected to

internal pressure and bending loads, where one key observation was that for through-thickness cracks, the effect of internal pressure was significant for structures made from high work-hardening materials, but negligible for materials with the opposite behaviour.

In this work, the Finite Element Method (FEM) was employed to analyse the propagation of cracks initiated in pipelines under high internal pressure. This behaviour was assessed in terms of variations in the Stress Intensity Factor. The crack propagation criterion was evaluated based on crack size, location, and the pressure of the transported medium. To this end, the computational software Abaqus 6.14 was used. This software suite provides powerful engineering simulation capabilities based on the finite element method.

Developed models and results

To achieve this objective, a three-dimensional model was developed. This model consists of a tubular structure (pipeline) with a length of 5000 mm, an external diameter of 1000 mm, and a wall thickness of 30 mm, containing a crack of size "a". The structure is subjected to internal pressures. For this purpose, three models were developed (Figure 1), differing only in the nature of the crack defect: a model containing: a circumferential crack (Figure 1a), a longitudinal crack (Figure 1b), and a mixed crack, i.e., oriented at 45° (Figure 1c). To simulate extreme conditions, an elastic approach was adopted for this study. The growth of these cracks was analysed in terms of the variation of the Stress Intensity Factor in opening mode (the most critical mode) and shear mode.

In order to optimize the transport of hydrocarbons through pipelines and meet the ever-increasing demand for this type of energy, it is necessary to significantly increase the pressure of the transported medium (oil or gas). To withstand such pressures and meet this growing demand, it is essential to increase the flow rate, and consequently the pressure, of the transported medium. However, such pressures pose a risk of pipeline rupture. To minimize this risk, it is preferable to use pipelines with larger dimensions (both diameter and wall thickness).

The pipeline used in this analysis is made of SA312TP304 steel, defined by its characteristics (Table 1) and dimensions, characterised by the R/t ratio (where R is the radius and t is the wall thickness).

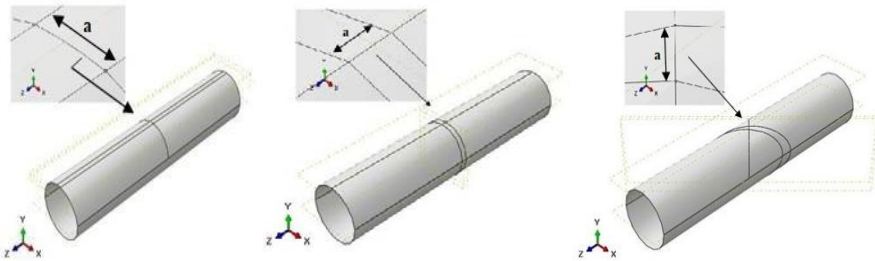

a) b) c)

Figure 1 - Pipeline containing a crack: (a) circumferential, (b) longitudinal, (c) mixed (45° orientation)

Table 1 – Mechanical properties of SA312TP304 steel (Kim et al, 2002)

Material	Young's modulus E (MPa)	Poisson's Ratio v	Tensile strength σu (MPa)	Tensile yield stress σy (MPa)	α	n
SA312TP304	204330	0.3	550.5	268.91	7.33	3.52

Pressure–crack interaction

The interaction between internal pressure and the presence of cracks is a key parameter in determining the survival of these tubular structures (gas and oil pipelines). This interaction enables the analysis of the ultimate pressure in order to minimise the risk of pipeline rupture and prevent disasters associated with such damage. The boundary conditions imposed on the cracked pipelines are illustrated in Figure 2.

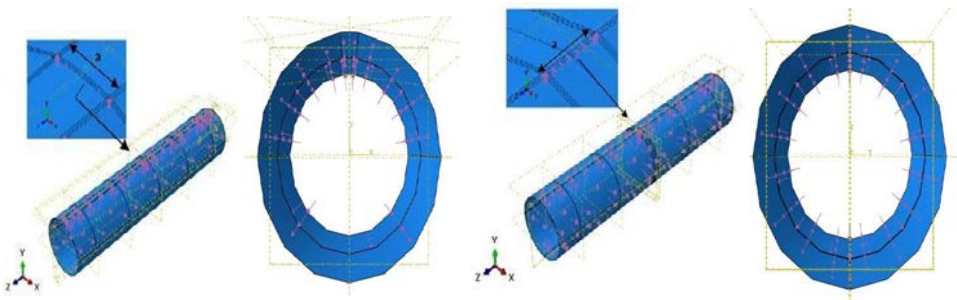

a) Circumferential crack b) Longitudinal crack

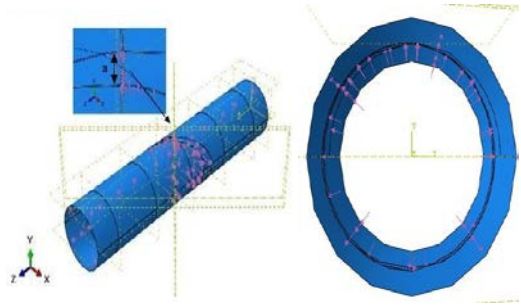

c) *Mixed crack*

Figure 2 - Boundary conditions applied to the cracked pipeline under internal pressure

Finite element modelling requires a full meshing of the structure using linear S4 elements with four nodes, with a total of 55168 elements (Figure 3). For reasons of reliability and reproducibility of the results, the mesh was particularly refined in the vicinity of the crack front (Figure 3).

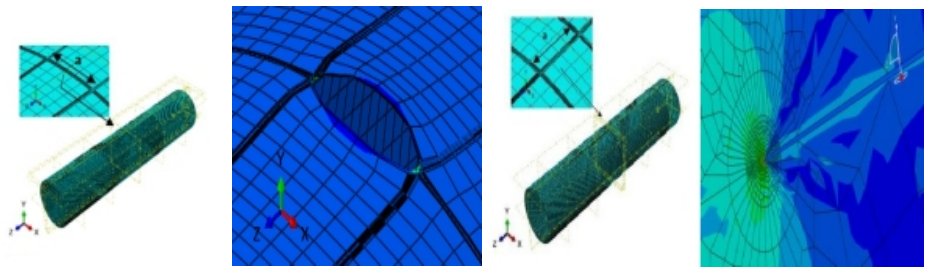

a) Circumferential crack *b) Longitudinal crack*

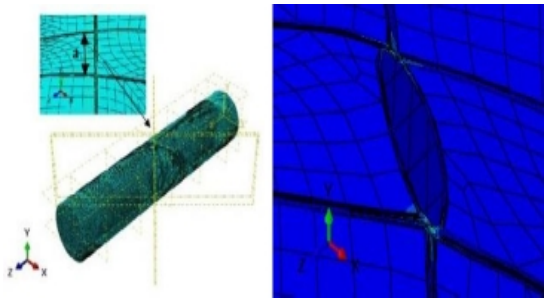

c) *Mixed crack*

Figure 3 - Mesh of the analysed structure

Pressure–circumferential crack interaction

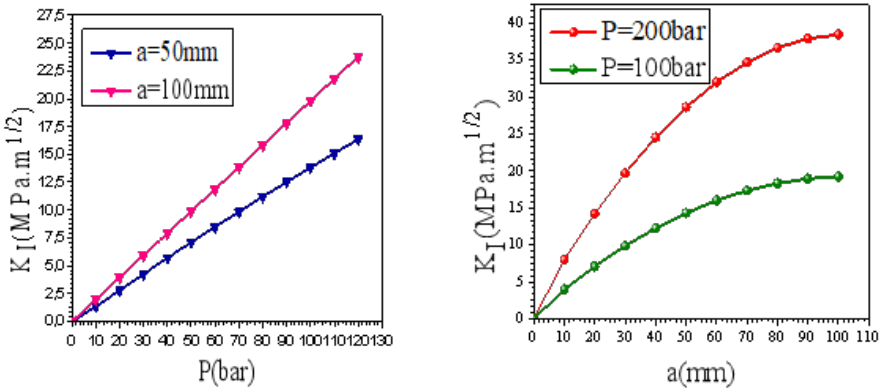

a) *b)*

Figure 4 - Effect of Pressure and Circumferential Crack Size on its Propagation Kinetics in Mode I

This interaction is illustrated in Figure 4. Analysis of this figure clearly shows that a circumferential crack becomes increasingly unstable as the internal pressure rises (Figure 4a). This behaviour is even more pronounced when the cracks are longer (Figure 4b). The instability is characterised here in terms of the evolution of the Stress Intensity Factor in Mode I. It is important to note that the difference between the fracture criterion for short cracks and that for long crack fronts becomes increasingly significant as the internal pressure within the pipeline increases (Figure 4).

Pressure–longitudinal crack interaction

The cracked pipeline is subjected to pressures exerted by the transported medium, which increases the risk of instability of the initiated longitudinal crack, as shown in Figure 5. This risk is characterised here by an intensification of the Stress Intensity Factor in Mode I. These figures show that the propagation kinetics of such a crack increase significantly with higher internal pressures (Figure 5a). This behaviour becomes even more pronounced as the crack length grows (Figure 5b).

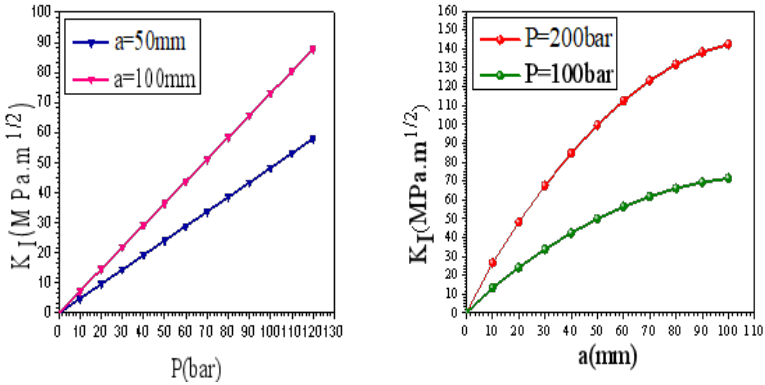

a) *b)*

Figure 5 - Effect of Pressure and Longitudinal Crack Size on its Propagation Kinetics in Mode I

Pressure–crack interaction for a crack oriented at 45°

The results obtained are illustrated in Figures 6 and 7. These figures show that an oriented crack propagates almost equally, under the effect of internal pressure, in mixed Modes I and II. The propagation kinetics increase significantly with crack length, regardless of the mode of growth. The instability of cracks in Modes I and II becomes more likely as internal pressures rise (Figure 6). Thus, pipelines subjected to high internal pressures are particularly prone to cracking damage (Figure 7). Longer cracks exhibit a higher propagation rate in both opening (Mode I) and shear (Mode II) modes. This propagation behavior is distributed almost equally between Mode I and Mode II. The Stress Intensity Factor in Mode I is consistent, in terms of magnitude, with that observed in Mode II.

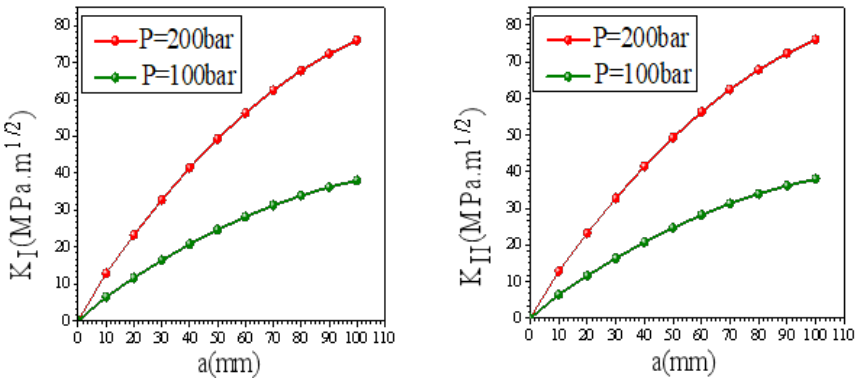

a) *b)*

Figure 6 - Behaviour of a Crack of Size "a" Oriented at 45° in Modes I and II

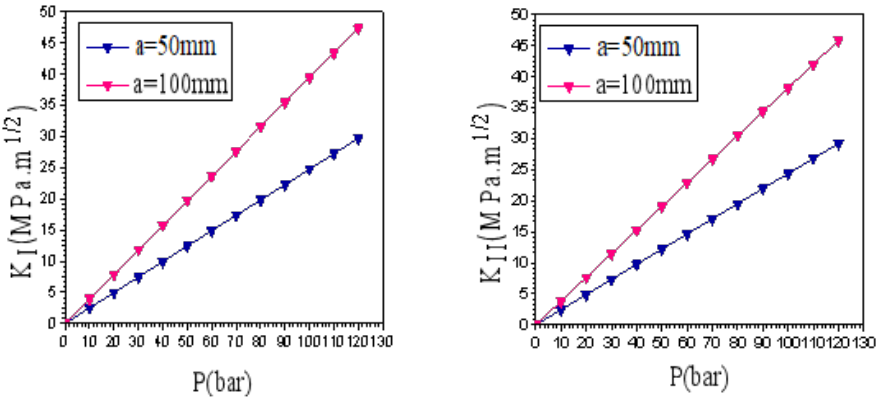

a) *b)*

Figure 7- Effect of Internal Pressure on the Mode I and Mode II Behaviour of a Crack Oriented at 45°

Interaction between external forces and cracks

These types of forces, whether tensile or compressive, generally represent the effects resulting from natural disasters such as earthquakes, landslides, or other phenomena. To simulate such loadings, longitudinal displacements "U" were imposed on the pipeline.

Interaction between external forces and circumferential cracks

The imposed tensile displacements (U > 0) (Figure 8) increase the risk of instability in the opening mode of an initiated circumferential crack. These displacements generate stresses that act as crack-opening forces. Positive values of the Stress Intensity Factor (SIF) are characteristic of such crack opening (Figure 9). In the case of long crack fronts, the fracture resistance of the pipeline can be exceeded for any imposed displacement greater than 3.5 mm. In such cases, sudden crack propagation becomes inevitable. It should be noted, however, that even in the absence of internal pressure from the transported medium, this type of loading alone may be fatal to the tubular structure, leading to catastrophic rupture. Conversely, an imposed compressive displacement (U < 0) applied to the pipeline enhances the mechanical behavior of the cracked zone through a crack-closing mechanism (Figure 10). The compressive stresses generated by this type of displacement act as stabilizing (closing) forces on the crack.

Negative values of the Stress Intensity Factor are indicative of this crack closure behavior (Figure 11). It is important to note that, compared to internal pressure, and under our simulation conditions, the effect of external loadings is much more significant in terms of the evolution of the Stress Intensity Factor in opening mode. This clearly demonstrates that natural disasters can cause pipeline rupture through the initiation and propagation of circumferential cracks.

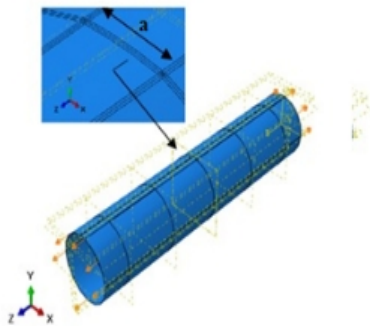

Figure 8 - Boundary conditions for a pipeline with a circumferential crack subjected to tensile forces (U > 0)

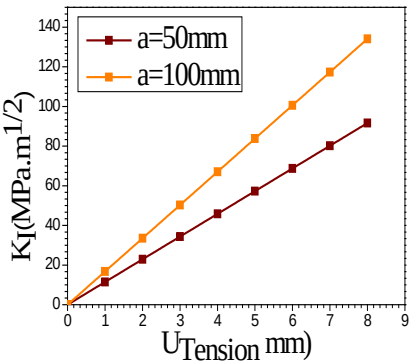

Figure 9 - Effect of Imposed Displacement U on Mode I Propagation of a Crack (U > 0, Tension)

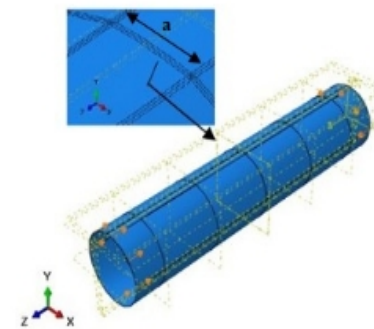

Figure 10 - Boundary conditions for a pipeline with a circumferential crack subjected to compressive forces (U < 0)

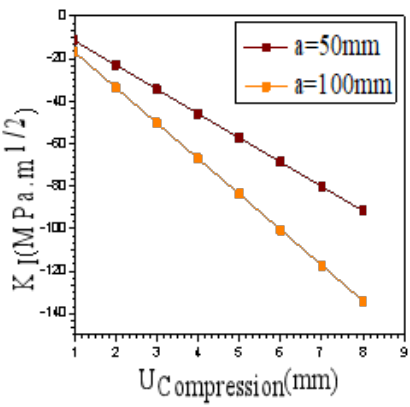

Figure 11 - Effect of Imposed Displacement U on Mode I Propagation of a Crack (U < 0, Compression)

Interaction between external forces and longitudinal cracks

Interaction between external forces and cracks

These types of forces, whether tensile or compressive, generally represent the effects resulting from natural disasters such as earthquakes, landslides, or other phenomena. To simulate such loadings, longitudinal displacements "U" were imposed on the pipeline.

Interaction between external forces and circumferential cracks

The imposed tensile displacements (U > 0) (Figure 8) increase the risk of instability in the opening mode of an initiated circumferential crack. These displacements generate stresses that act as crack-opening forces. Positive values of the Stress Intensity Factor (SIF) are characteristic of such crack opening (Figure 9). In the case of long crack fronts, the fracture resistance of the pipeline can be exceeded for any imposed displacement greater than 3.5 mm. In such cases, sudden crack propagation becomes inevitable. It should be noted, however, that even in the absence of internal pressure from the transported medium, this type of loading alone may be fatal to the tubular structure, leading to catastrophic rupture. Conversely, an imposed compressive displacement (U < 0) applied to the pipeline enhances the mechanical behavior of the cracked zone through a crack-closing mechanism (Figure 10). The compressive stresses generated by this type of displacement act as stabilizing (closing) forces on the crack. Negative values of the Stress Intensity Factor are indicative of this crack closure behavior (Figure 11). It is important to note that, compared to internal pressure, and under our simulation conditions, the effect of external loadings is much more significant in terms of the evolution of the Stress Intensity Factor in opening mode. This clearly demonstrates that natural disasters can cause pipeline rupture through the initiation and propagation of circumferential cracks.

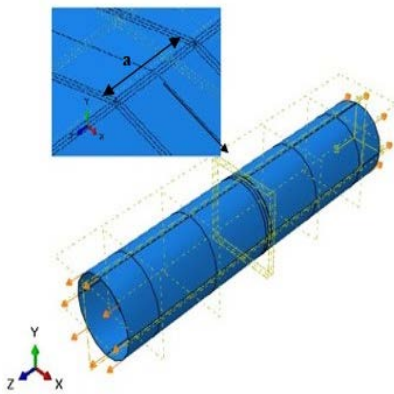

Figure 12 - Boundary conditions for a pipeline with a longitudinal crack subjected to tensile forces (U > 0)

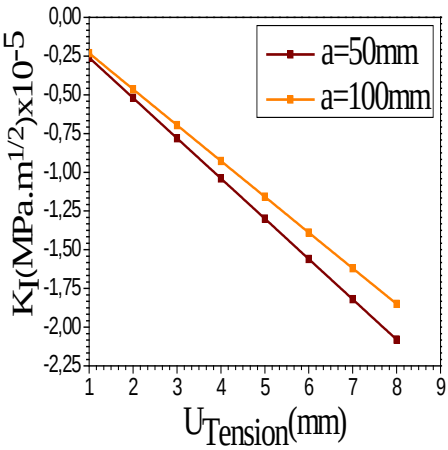

Figure 13 - Effect of Imposed Displacement U on Mode I Propagation of a Crack (U > 0, Tension)

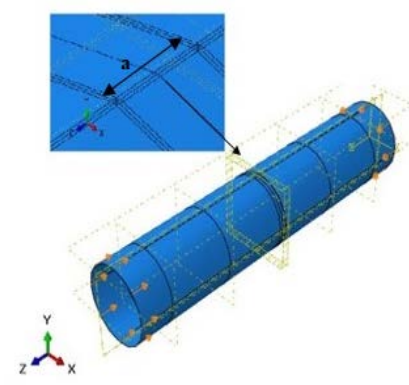

Figure 14 - Boundary conditions for a pipeline with a longitudinal crack subjected to compressive forces

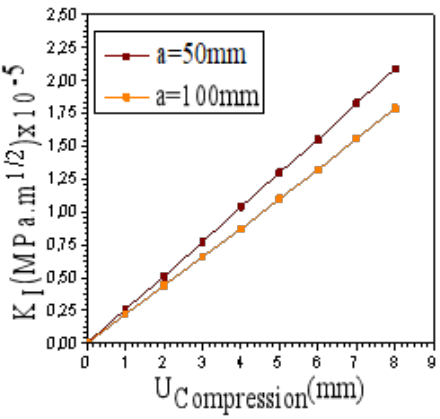

Figure 15 - Effect of Imposed Displacement U on Mode I Propagation of a Crack (U < 0, Compression*)*

Interaction between external forces and a crack oriented at 45°

The same simulation conditions as those used previously were retained for this part of the study. The model analysed in this case differs from the previous one only by the orientation of the crack (Figure 16). The same types of loadings - imposed tensile displacements (U > 0) (Figure 16) and compressive displacements (U < 0) (Figure 17) - were separately applied to the cracked pipeline. It should be recalled that these forces simulate external loadings acting on the cracked pipeline.

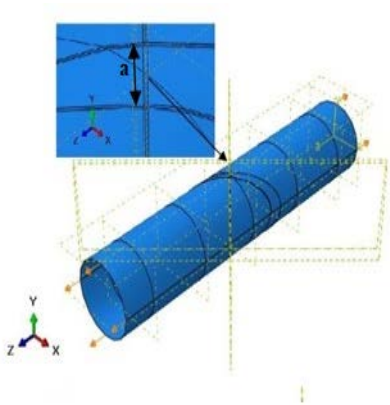

Figure 16 - Boundary conditions for a pipeline containing a crack oriented at 45° subjected to tensile forces (U > 0)

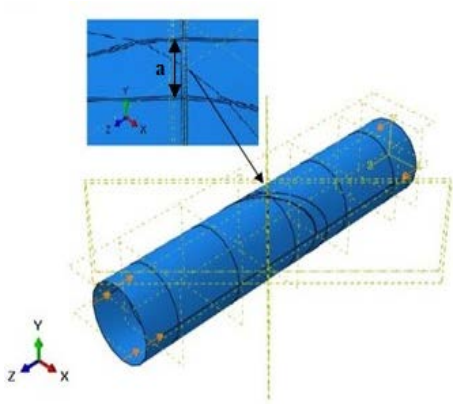

Figure 17 - Boundary conditions for a pipeline containing a crack oriented at 45° subjected to compressive forces (U < 0)

The results of this analysis, illustrated in Figure 18, confirm that a mixed crack, i.e., a crack oriented at 45° and subjected to tensile loading, propagates in a mixed mode, with both opening (Mode I) and shearing (Mode II) of the crack lips. The propagation kinetics in these two modes are comparable in terms of the values of the Stress Intensity Factors KI and KII. Regardless of the failure mode, longer cracks subjected to large displacement amplitudes exhibit significant instability. Combined with the operational loading of the pipeline (internal pressure) (Figure 6 and 7), these external forces may lead to sudden crack propagation. This risk becomes particularly likely for long cracks subjected to both high internal pressures and intense tensile displacements.

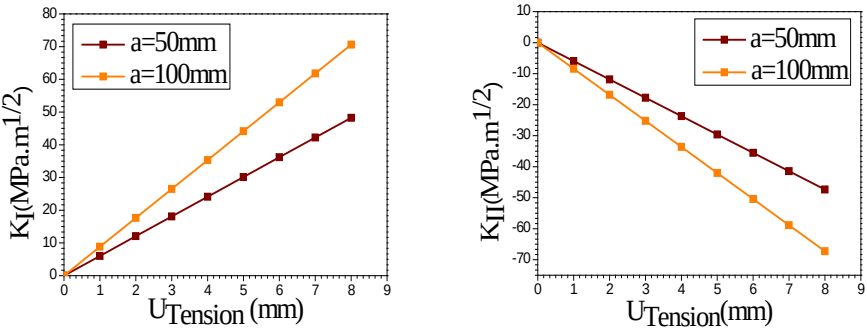

Figure 18 - Effect of Imposed Displacement U on the Propagation Kinetics in Modes I and II of a Crack Oriented at 45° (U > 0, Tension)

A different mode of crack propagation is observed when the pipeline is subjected to imposed compressive displacements (U < 0) (Figure 19). This figure clearly shows that a crack defect subjected to compression propagates through shearing of the crack lips (pure Mode II). The propagation kinetics, in terms of the value of the Stress Intensity Factor in Mode II, increase significantly with larger imposed displacements. This behaviour is even more pronounced for larger crack sizes. In opening mode (Mode I), this type of compressive loading (U < 0) leads to crack stabilisation through a closing phenomenon. Thus, this loading acts as a crack-closing force, which is reflected by negative values of the Stress Intensity Factor, as illustrated in Figure 19. The superposition of such external loading with the operational loading of the pipeline (Figure 6 and 7) leads to the propagation of the oriented crack in mixed Modes I and II. Under our simulation conditions, for large imposed displacements (U < 0), high internal pressures, and long cracks, the crack tends to propagate preferentially through shearing of the crack lips (pure Mode II).

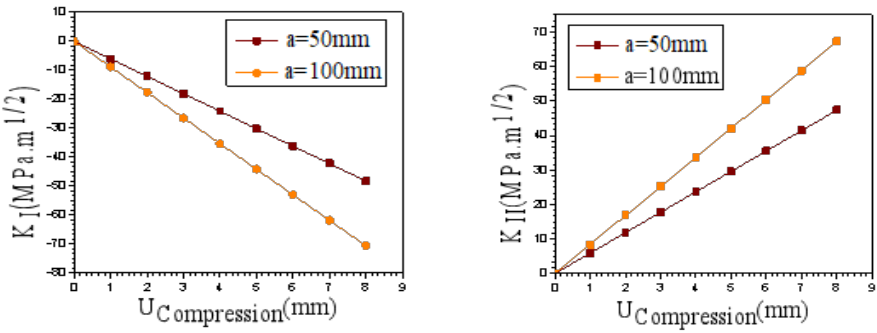

Figure 19 - Effect of Imposed Displacement U on the Propagation Kinetics in Modes I and II of a Crack Oriented at 45° (U > 0, compression)

Conclusion

The results obtained in this study have shown the following:

Under identical simulation conditions, longitudinal cracks initiated in a pipeline under high internal pressure are significantly more unstable in opening mode (Mode I) compared to circumferential and 45°-oriented cracks. Oriented cracks preferentially propagate, under the effect of internal pressure, in mixed Modes I and II. The risk of rupture is much higher in the case of longitudinal cracks; that is, pipeline bursting occurs exclusively along its longitudinal axis. This zone of the pipeline is therefore particularly pre-exposed to sudden damage.

External loadings in the form of imposed tensile displacements (U > 0) promote opening-mode propagation of circumferential cracks, closure of longitudinal cracks, and mixed-mode (Modes I and II) growth of oriented cracks. Conversely, imposed compressive displacements (U < 0) produce opposite behaviour: closure of circumferential cracks, opening of longitudinal cracks, and shearing-mode (Mode II) growth of oriented cracks.

The superposition of operational loads with external loadings significantly increases the crack propagation kinetics, regardless of the crack type (longitudinal, circumferential, or mixed), particularly in the case of long cracks.

References

De Barros, S., Budhe, S. & Banea, M. D. 2020. Prediction of the burst pressure for defective pipelines using different semi-empirical models. *Frattura ed Integrità Strutturale/Fracture and Structural Integrity*, 14(52), pp.137-147. Available at: https://doi.org/10.3221/IGF-ESIS.52.12

Nikhil, R., Krishnan, S. A., Sasikala, G. et al. 2021. Study on fracture transferability from compact type specimen to pipe for 316LN stainless steel. *International Journal of Pressure Vessels and Piping*, 192, pp. 104437. Available at: https://doi.org/10.1016/j.ijpvp.2021.104437

Barsoum, I.& Yurindatama, D. T. 2020. Collapse analysis of a large plastic pipe using cohesive zone modelling technique. *International Journal of Pressure Vessels and Piping*, 187, pp. 104155. Available at: https://doi.org/10.1016/j.ijpvp.2020.104155

Zheng. Q, Abdelmoety. A. K., LI, Y. et al. 2021. Reliability analysis of intact and defected pipes for internal pressure related limit states specified in CSA Z622: 19. *International Journal of Pressure Vessels and Piping*, 192(4), pp. 104411. Available at: 10.1016/j.ijpvp.2021.104411

Fezazi, A.I., Mechab, B., Salem, M. & Serier, B. 2021. Numerical prediction of the ductile damage for axial cracks in pipe under internal pressure. *Frattura ed Integrità Strutturale*, 15(58), pp.231-241. Available at: https://doi.org/10.3221/IGF ESIS.58.17.

Qin G, Cheng F Y. 2021. A review on defect assessment of pipelines: Principles, numerical solutions, and applications. International Journal of Pressure Vessels and Piping, 191, pp. 104329. Available at: https://doi.org/10.1016/j.ijpvp.2021.104329

Ma Y., Li B., Fang H., Du X., Wang, N., Zang, Q., Zhai, K., Di, D., 2024. Mechanical behavior and parameter sensitivity analysis of water supply steel pipes under complex service load combinations. Structures, 67(12), pp. 106956. Available at: https://doi.org/10.1016/j.istruc.2024.106956

Mechab, B., Chioukh, N., Mechab, Bo. & Serier, B. 2018. Probabilistic Fracture Mechanics for Analysis of Longitudinal Cracks in Pipes under Internal Pressure. *Journal of Failure Analysis and Prevention*, 18, pp.1643-1651. Available at: https://doi.org/10.1007/S11668-018-0564-8.

Mechab, B., Salem, M., Medjahdi, M. & Serier, B. 2020. Probabilistic Elastic plastic Fracture Mechanics Analysis of Propagation of Cracks in Pipes under Internal Pressure. *Frattura ed Integrità Strutturale,*14(54), pp.202-210. Available at: https://doi.org/10.3221/IGF-ESIS.54.15 .

Mechab, B., Serier, B., Bachir Bouiadjra, B.A., Kaddouri, K. & Feaugas, X. 2011. Linear and non-linear analyses for semi-elliptical surface cracks in pipes under bending. *International Journal of Pressure Vessels and Piping*, 88(1), pp.57-63. Available at: https://doi.org/10.1016/J.Ijpvp.2010.11.001.

Mechab, B., Serier, B., Kaddouri, K., Bachir Bouiadjra, B.A. 2014. Probabilistic elastic plastic analysis of cracked pipes subjected to internal pressure loads. *Nuclear Engineering and Design*, 275, pp.281-286. Available at: https://doi.org/10.1016/j.nucengdes.2014.05.008.

Metehri, A., Mechab,B., Bachir Bouiadjra, B. 2024. A new investigation used to predict the burst pressure in straight corroded pipes under internal pressure. *MILITARY TECHNICAL COURIER*, 72(4), pp.1747-1771. Available at: https://doi.org/10.5937/vojtehg72-50357.

Salem, M., Mechab, B., Berrahou, M., Bachir Bouiadjra, B.A. & Serier, B. 2019. Failure Analyses of Propagation of Cracks Repaired Pipe Under Internal Pressure. *Journal of Failure Analysis and Prevention,* 19(2), pp.212-218. Available at: https://doi.org/10.1007/s11668-019-00592-3.

Wu H, Zhao H, Li X, Feng X , Chen Y. 2022. Experimental and numerical studies on collapse of subsea pipelines with interacting corrosion defects. Ocean Engineering, 260, pp.112066. Available at: https://doi.org/10.1016/j.oceaneng.2022.112066

Zhou L, Gong S, Yuan L, Wang X, Wang Z. 2025. Evaluation on collapse behaviour of thick-walled pipes with corrosion defect under combined external pressure, axial tension and bending moment. Structures, 75, pp.108593. Available at: https://doi.org/10.1016/j.istruc.2025.108593

Zhou, R., Fang, W.P., Wu, J.S. 2020. A risk assessment model of a sewer pipeline in an underground utility tunnel based on a Bayesian network. Tunn. Undergr. Space Technol, 103(3), pp.103473. Available at: https://doi.org/10.1016/j.tust.2020.103473

Chattopadhyay, J., Dutta, B. K. & Vaze, K. K. 2014. Development of new correlations for improved integrity assessment of pipes and pipe bends. *Nuclear Engineering and Design*, 269, pp.108-115. Available at: https://doi.org/10.1016/j.nucengdes.2013.08.015

Weltevreden, M., Hadley, I., and Coules, H. 2021. Probabilistic treatment of pipe girth weld residual stress in fracture assessment. *International Journal of Pressure Vessels and Piping,* 192(3), pp. 104397. Available at: 10.1016/j.ijpvp.2021.104397

Muthanna, B.G.N., Bouledroua, Omar., Meriem-Benziane, M. et al. 2021. Assessment of corroded API 5L X52 pipe elbow using a modified failure assessment diagram. *International Journal of Pressure Vessels and Piping,* 190, pp. 104291. Available at: https://doi.org/10.1016/j.ijpvp.2020.104291

Rahman, S. 1995. A stochastic model for elastic-plastic fracture analysis of circumferential through-wall-cracked pipes subject to bending. *Engineering Fracture Mechanics*, 52(2), pp. 265-288. Available at: https://doi.org/10.1016/0013-7944(95)00018-Q

Kim, Y.J., Kim, J. S, LEE, Y. Z et al. 2002. Non-linear fracture mechanics analyses of part circumferential surface cracked pipes. *International Journal of Fracture,* 116, pp.347-375. Available at: https://doi.org/10.1023/A:1020779611803

Prilog analizi oštećenja cevovoda usled pucanja pod visokim pritiskom

Amina Ismahene Fezazi, **autor za prepisku**, *Belaïd* Mechab, *Mokadem* Salem, *Boualem* Serier
University of Sidi Bel Abbes, Faculty of Technology, Mechanical Engineering Department, mechanical physics of materials laboratory, Sidi Bel Abbes 22000, Algeria

OBLAST: mašinsko inženjerstvo, materijali
KATEGORIJA (TIP) ČLANKA: originalni naučni rad

Sažetak:

Uvod/cilj: Ovaj rad ima za cilj da doprinese predviđanju oštećenja usled pucanja u cevovodima za transport ugljovodonika koji su izloženi visokim unutrašnjim pritiscima, a kao odgovor na rastuću potražnju u industrijalizovanim zemljama.

Metode: Da bi se postigao ovaj cilj i analiziralo širenje pukotina u smislu određivanja faktora intenziteta napona (eng. SIF), primenjena je metoda konačnih elemenata (eng. FEM). Studija razmatra uticaj unutrašnjeg pritiska transportovanog fluida, kao i spoljašnjih naprezanja izazvanih prirodnim pojavama kao što su zemljotresi, klizišta i druge pojave. Ova

spoljašnja naprezanja predstavljena su zateznim i pritisnim silama. Posebna pažnja posvećena je širenju tri tipa pukotina: obodne, uzdužne i pukotine u mešovitom režimu.

Rezultati: Zahvaćena zona cevaste strukture veoma je podložna pucanju u režimu I. Za razliku od dva početna tipa defekta pucanja, orijentisana pukotina pod uglom π/4 u odnosu na uzdužnu osu cevovoda razvija se gotovo podjednako u režimima I i II. Kinetika njenog rasta usko je povezana sa njenom veličinom, unutrašnjim pritiskom i intenzitetom spoljašnjih sila. Zatezne sile podstiču otvaranje obodnih pukotina, zatvaranje uzdužnih pukotina i širenje orijentisanih pukotina u mešovitom režimu (I i II). Nasuprot tome, pritisne sile pogoduju zatvaranju obodnih i orijentisanih pukotina, dok istovremeno podstiču otvaranje uzdužnih pukotina.

Zaključak: Studija pokazuje da, pod identičnim uslovima opterećenja, uzdužno inicirane pukotine predstavljaju najveću opasnost u pogledu rasta pukotine u režimu I. Rizik od pucanja cevovoda naročito je izražen duž cevovoda i značajno se povećava sa porastom unutrašnjeg pritiska.

Ključne reči: cevovod, pritisak, spoljašnje sile, metoda konačnih elemenata (FEM), pukotina, faktor intenziteta napona.

Paper received on: 6 May 2025.
Manuscript corrections submitted on: 24 June 2025.
Paper accepted for publishing on: 26 June 2025.

© 2026 The Authors. Published by Vojnotehnički glasnik / Military Technical Courier (www.vtg.mod.gov.rs). This article is an open access article distributed under the terms and conditions of the Creative Commons Attribution license (http://creativsecommons.org/licenses/by/4.0/rs/).

Application of the FMECA method for identifying failures in wind turbine systems

Branislava Radišić[a], *Ljiljana* Radovanović[b], *Borivoj* Novaković[c], *Jasmina* Pekez[d], *Slavica* Prvulović[e], *Eleonora* Desnica[f]

University of Novi Sad, Technical Faculty "Mihajlo Pupin", Zrenjanin, Republic of Serbia

[a] e-mail: branislava.radisic@uns.ac.rs, **corresponding author**, ORCID iD: https://orcid.org/0009-0007-3664-2012

[b] e-mail: ljiljana.radovanovic@uns.ac.rs, ORCID iD: https://orcid.org/0000-0002-5234-4820

[c] e-mail: borivoj.novakovic@uns.ac.rs, ORCID iD: https://orcid.org/0000-0003-2816-3584

[d] e-mail: jasmina.pekez@uns.ac.rs, ORCID iD: https://orcid.org/0000-0003-0454-5326

[e] e-mail: slavica.prvulovic@uns.ac.rs, ORCID iD: https://orcid.org/0000-0001-6353-7145

[f] e-mail: eleonora.desnica@uns.ac.rs, ORCID iD: https://orcid.org/0000-0002-4724-5764

https://doi.org/10.5937/vojtehg74-58801

FIELD: mechanical engineering
ARTICLE TYPE: research paper

Abstract:

This paper presents the potential causes of component failures in wind turbine systems that affect their reliable and efficient operation. Component failures in wind turbines can lead to complete system failure, resulting in downtime, reduced reliability, and increased costs. To fully utilize wind energy, minimizing the risk of component failures is essential. By applying the FMECA method (Failure Mode Effects and Criticality Analysis – FMECA), critical components of wind turbine systems have been identified, providing the opportunity to prioritize problem-solving. The results emphasize the importance of maintenance and design optimization to reduce the risk of failures and maximize the utilization of wind energy.

Introduction/purpose: The reliability of wind turbine systems plays a crucial role in ensuring *a* stable and efficient electricity supply from renewable sou-

ACKNOWLEDGMENT: The research was supported through the project "Creating laboratory conditions for research, development, and education in the field of the use of solar resources in the Internet of things", at the Technical Faculty "Mihajlo Pupin" Zrenjanin, financed by the Provincial Secretariat for Higher Education and Scientific Research, Republic of Serbia, Autonomous Province of Vojvodina, project number 003101190 2024 09418 003 000 000 001.

rces. The failure of any component can lead to system downtime, reduced reliability, and increased operational costs. In this context, it is essential to identify and analyze potential failures in order to improve overall system reliability. *The aim of this paper is to analyze the reliability of a wind turbine system using the FMECA method. The focus is on identifying the most critical components and understanding the causes and consequences of their failures, thereby contributing to the improvement of system design, maintenance, and operation.*

Methods: This paper applies the FMECA (Failure Modes, Effects and Criticality Analysis) method, which enables a detailed assessment of potential system failures, their causes and effects, and the identification of the most critical system points based on quantitative parameters. The methodology includes the following steps: identification of key components of the wind turbine, including the rotor, gearbox, generator, control system, and other subsystems; definition of possible failure modes for each component, with corresponding mechanisms that may lead to failure (e.g., wear, overheating, mechanical damage, etc.); evaluation of the consequences of failures, both on the specific component and on the overall operation of the wind turbine; quantitative risk assessment through the assignment of values for: the probability of potential failure occurrence (R_1), the severity of the potential failure (R_2), and the probability of detecting the failure and preventing its manifestation (R_3); calculation of the criticality level (R) using the expression: $R = R_1 \cdot R_2 \cdot R_3$*; ranking of components based on R values to identify those that pose the greatest threat to system reliability and require prioritized monitoring or optimization.*

Results: The results of the FMECA analysis indicate that the most critical components of the wind turbine system are: gearbox – the highest criticality level (R value), as gearbox failure can lead to complete system shutdown and costly repairs; generator – high severity of failure and moderate likelihood of failure detection; wind turbine control system – although failures are less frequent, the consequences can be severe due to the loss of control over the turbine. Based on the analysis, components have been classified according to maintenance and monitoring priorities to enable timely detection of potential failures and prevent major breakdowns.

Conclusion: The FMECA method *is* an effective tool for identifying and ranking potentially critical components of wind turbine systems. The results indicate that the gearbox, generator, and control system are the most sensitive points in the system. Their preventive maintenance, along with the implementation of condition monitoring systems and design improvements,

can significantly enhance reliability and reduce operational costs. *The analysis can serve as a foundation for improving maintenance strategies and increasing wind farms operational efficiency.*

Key words: wind energy, wind turbines systems, component failures, FMECA method, reliability, preventive maintenance.

Introduction

The advantages of using renewable natural resources, and especially wind energy, are considerable. In addition to being unlimited and renewable, wind potential also represents a clean source of energy. During wind exploitation, there is no air pollution, no smog, and no production of gases that cause acid rain or greenhouse gas emissions.

Also, wind energy is one of the cheapest sources of energy. In order to fully utilize the potential of wind energy, it is important to understand the devices through which it is converted into mechanical work, namely wind turbine systems. A wind turbine system is a complex electromechanical system that converts wind energy into electrical energy. It consists of various subsystems and components such as: tower – a load-bearing structure in the form of a column, made of steel/concrete; wind turbine – includes the rotor and blades driven by the wind; mechanical shaft – accelerates the gearbox through rotation; gearbox – serves to increase the rotor's rotation rate from a low value to a speed sufficient to drive the generator; generator – converts mechanical energy into electrical energy; yaw system – tracks the wind direction; control and power electronics system – regulates the generator's rotational speed and controls the output voltage; hydraulic and cooling system; connection to an energy storage system or the power grid.

The greatest problem during the operation of a wind turbine system is component failure, which can lead to the failure of the entire system, resulting in system downtime, reduced reliability, and increased costs. For ranking system components according to their level of criticality, the Failure Mode, Effects and Criticality Analysis (FMECA) method is highly significant.

Wind potential and wind turbine system

"Wind represents the large-scale movement of air" (Jovanović & Baroš, 2023). Wind is the horizontal flow of air masses caused by differences in temperature, i.e. differences in air pressure. It is considered that wind is a consequence of solar radiation, since it heats the planet Earth unevenly, which leads to variations in air pressure. After

hydropower, wind energy is the most economical renewable energy source (Adamović et al, 2013). Wind turbine systems are a type of power plant that use wind energy. They consist of a supporting structure, i.e. a tower, a wind turbine, a generator, a component that regulates the generator's rotational speed and the output voltage of the wind generator, and a system for energy storage or a connection to the electrical grid. The main condition for installing a wind generator is wind speed, which depends on terrain characteristics, surrounding objects, and their heights. The wind should blow at an average speed of 6 m/s, for 2800 hours per year (a year has 8760 hours), in order for a certain location to be considered suitable for wind farm construction (Jovanović & Baroš, 2023). The working principle of a wind generator is as follows: the wind drives the wind turbine, which is located at the top of the supporting structure and usually consists of three blades. The turbine is connected to an electric generator, which converts mechanical energy into electrical energy. The mechanical assembly forms the link between the turbine and the generator, and it consists of: a low-speed shaft, a gearbox (speed multiplier), a brake, and a high-speed shaft (Hrnjak & Katić, 2021). "The heavier the air, the more energy is obtained at the wind turbine" (Adamović et al, 2014). The density of air is 1.225 [kg/m^3] at a standard atmospheric pressure of 1013 [mbar] and a temperature of 15 [°C]. During winter, more energy will be produced at the same wind speed than in summer, because cold air is denser than warm air. A proper choice of technology greatly influences reliability. "The failure rate increases with larger turbines, but downtime duration decreases with increased turbine size" (Adamović et al, 2014). It is important to highlight the role of maintenance, which ensures higher availability without excessive cost increase.

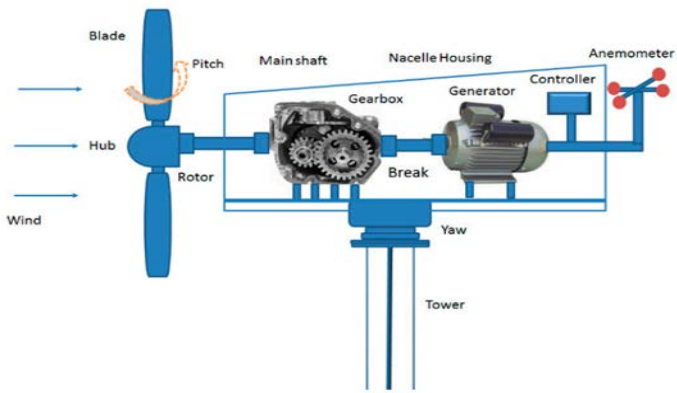

Figure 1 – Wind Turbine System (Gao & Liu, 2021)

Equipment reliability can be improved through preventive maintenance measures, as timely repairs prevent the wear of certain components. Figure 1 shows the wind turbine system.

The reliability of a wind turbine system is defined as the probability that the system will perform a specific function without failure under given conditions for a defined period of time.

Every production system must ensure two things, namely:

- reliability of operation, which enables uninterrupted process flow,
- safety of human life and health, as well as the preservation of material and natural resources.

The term failure refers to a condition in which the quality of the system is compromised (Adamović & Radovanović, 2008). The production of energy largely depends on the reliability of the wind turbine system. By understanding failures and minimizing them, high reliability can be achieved. Through maintenance planning, more efficient maintenance is ensured, and the possibility of reducing failures increases. In order to select the most effective maintenance strategy, it is necessary to identify the most critical components of the wind turbine system, which are prone to failure. It is also essential to consider reliability improvement and the reduction of maintenance costs.

Reliability analysis of a wind turbine system is based on a systematic approach to its subsystems, since the overall reliability directly depends on the reliability of the subsystems (Botsaris et al, 2012).

Wind energy is one of the dominant renewable energy sources worldwide. However, wind turbine systems are often prone to failure, and Hossain et al. (2018) argue that the harsh environmental conditions in which wind turbines are deployed are the main cause of such failures. The authors emphasize that implementing reliable condition monitoring is essential.

Graph 1 presents the types of failures that occur in a wind turbine system.

For generators, the causes leading to failure include:

- open/short circuit,
- insulation damage,
- imbalance,
- broken rotor bar,
- bent shaft,
- bearing failure,
- air gap eccentricity,

- magnet failures,
- rotor mass imbalance.

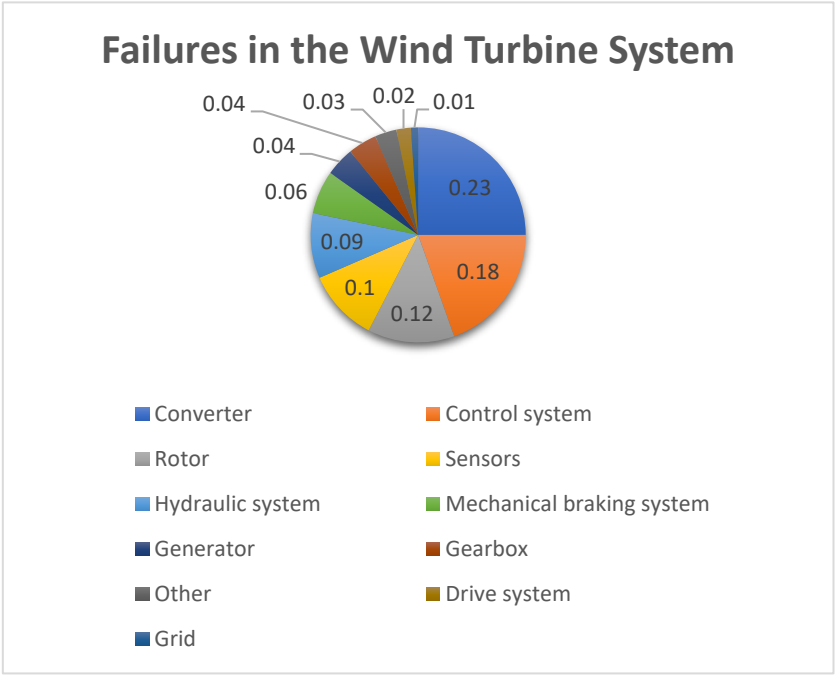

Graph 1 - Types of failures in the wind turbine system (Hossain et al, 2018)

Gearbox failures account for about 35% of total wind turbine failures, and the most common include:

- gear tooth abrasion,
- tooth cracking,
- tooth breakage,
- surface fatigue.

These faults can lead to significant temperature increases.

Tower failures are mainly caused by:

- structural corrosion,
- structural cracks,
- structural damage.

Tower failures are triggered by improper installation, overloading, poor quality control, as well as by extreme weather conditions such as lightning, fire, and earthquakes (Hossain et al, 2018).

An increasing number of countries aim to produce the highest share of their electricity from wind energy. It is evident that as wind turbines

develop, both their dimensions and weight increase. Figure 2 shows the trend in the increase of rotor diameter and wind turbine power.

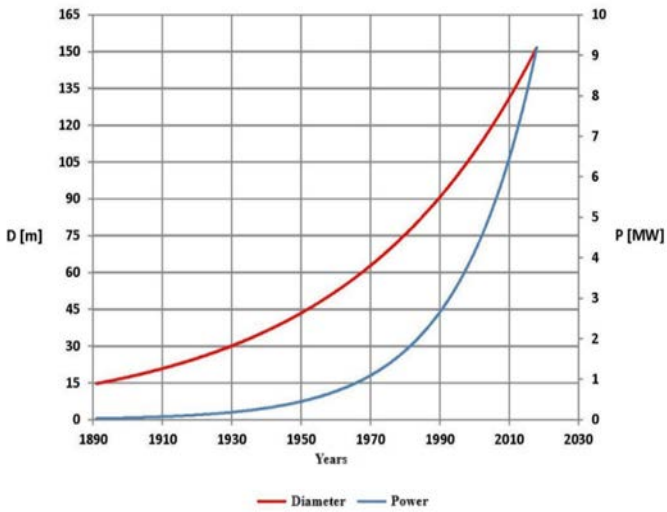

Figure 2 - Trend in the increase of rotor diameter and wind turbine power (Hossain et al, 2018)

Failure mode, effects and criticality analysis (FMECA)

For the initial selection of critical system components, which were entered into the working sheet of the FMECA method, the following subsystems were selected: tower, generator, yaw system, and gearbox. The reason for choosing these parts of the wind turbine system is that they represent general events in the FTA (Fault Tree Analysis) which can directly lead to the failure of the entire wind turbine system (Novaković et al, 2023). The FTA analysis of the wind turbine system was addressed in the paper “Evaluating wind turbine power plant reliability through fault tree analysis,” Novaković B., 2023, Applied Engineering Letters, 8(4), pp. 175–182. Therefore, it can be freely stated that this research is a continuation of the aforementioned study.

Pal Kour et al. (2019) report that industries have acknowledged the importance of wind turbine system reliability. Reliability analysis can reduce the number of hazardous events by lowering the failure rate. There are various methods for performing reliability analysis of wind turbine systems, among which are Fault Tree Analysis (FTA) and Failure Mode and Effect Analysis (FMEA). These two are analytical techniques that can

be applied to analyze the reliability of a system and its related features (Pal Kour et al, 2019).

For a detailed and more objective analysis of the wind turbine system, FMEA and FTA methods are suitable. FTA is based on deductive logic that assumes failures and their likelihood of occurrence, while FMEA investigates the behavior of system components during failure. FMEA involves the evaluation of indicators such as severity, occurrence, and detection. FMEA identifies failure modes and the effects (consequences) they leave on the system or other components (Tazi et al, 2017).

FMEA is used to identify and prevent problems, focusing primarily on preventing issues and improving safety. The Risk Priority Number (RPN) is used to assess the risk of a specific failure. This number is the product of occurrence, severity, and detection ratings. The main reason for conducting FMEA is to prevent the possibility that a new system or process may fail to meet proposed requirements under certain conditions and within defined purposes and boundaries. Additionally, the purpose of the method is to eliminate failures and improve the system. When used during the design phase, the goal is to prevent future failures. When used during operation, the aim is system control and monitoring. Key advantages of using FMEA include: cost reduction, shortened time from design to commissioning, improved quality, increased reliability, and enhanced safety (Dev Sharma & Srivastava, 2018).

The Failure Mode and Effect Analysis (FMEA) method is one of the best analyses for assessing reliability during the design phase. FMEA is a specific but subjective analysis used to identify potential causes and failure modes and to evaluate their consequences. The main goal is to detect and identify failures, then mitigate and reduce their risk. Therefore, it can be concluded that this analysis increases system reliability, quality, and safety (Tavner et al, 2010).

FMEA is an inductive method based on analyzing failures and their impact on the system, with the aim of acting preventively to avoid them. It anticipates risks, reduces them, or eliminates them. Its ease of application is one of its greatest advantages. A drawback of FMEA is that it focuses more on individual failure states than on their combinations. FTA compensates for this limitation (Arabian-Hoseynabadi et al, 2010).

However, for this research, the FMECA method, an extended version of FMEA, is of interest. FMECA includes risk ranking related to failure modes, allowing prioritization of solutions (Catelani et al, 2020). Each failure may have several causes, which must be documented in the FMECA report. Furthermore, the consequences of each failure for the system must be recorded. Failure effects are classified as local and global.

Local effects refer to the impact of the failure on the observed subsystem, while global effects represent higher-level consequences.

Therefore, the Failure Mode, Effects and Criticality Analysis (FMECA) is a logical extension of the FMEA method, encompassing both failure mode analysis and criticality assessment. Criticality analysis is the process of evaluating the degree of component criticality relative to the system. Criticality refers to the severity of failure consequences. Quantifying criticality and the probability of failure helps in making decisions about corrective actions and their priorities, as well as in determining clear boundaries between acceptable and unacceptable risk. Each observed failure effect is classified by its criticality in terms of the entire system's functionality. Table 1 provides an overview of criticality categories for each failure effect, according to the failure effects criticality scale (Gardijan, 2001).

Criticality analysis is performed using a method known locally as the critical elements method. The level of failure criticality in this method can be determined using criticality factors:

- Factor R_1 – the probability of occurrence of a potential failure, determined according to Table 2,
- Factor R_2 – significance of potential failure, determined according to Table 3,
- Factor R_3 – probability of detecting a failure and preventing its manifestation, determined according to Table 4.

Criticality Level R, which is determined according to Table 5, is obtained as the product of these three factors:

$$R=R_1 \cdot R_2 \cdot R_3 \quad (1)$$

Table 1 - Categories of Failure Effect Criticality (Gardijan, 2001)

Failure Effect	Criticality Category (Criticality Level)
Insignificant loss of function	I
Partial loss of function	II
Loss of function after a certain period	II
Severe damage	III
Immediate function interruption with safety risk	IV

Table 2 - Probability of Occurrence of Potential Failure (Gardijan, 2001)

Evaluation Criterion R_1		
Probability of Occurrence	$\boldsymbol{R_1}$	Possible Failure Rate
Very Low	1	0
Low	2-3	1/20000-1/10000
Measurable	4-6	1/2000-1/1000-1/1200
High	7-8	1/100-1/20
Very High	9-10	1/10-1/2

Table 3 - Significance of Potential Failure (Gardijan, 2001)

Evaluation Criterion R_2	
Significance	$\boldsymbol{R_2}$
Negligible	1
Low	2-3
Moderate	4-6
High	7-8
Critical	9-10

Table 4 - Probability of failure detection (Gardijan, 2001)

Evaluation Criterion $\boldsymbol{R_3}$	
Probability of failure detection	$\boldsymbol{R_3}$
High	1
Measurable	2-5
Low	6-8
Very Low	9
Unlikely	10

Table 5 - Criticality Level (Gardijan, 2001)

Evaluation Criterion R	
Criticality Level	R
Low	<50
Medium	50-100
High	100-200
Critical	>200

The numerical values of factors R1, R2, and R3 are determined by comparing the established condition with the corresponding criterion for selecting parameter values, always considering the worst-case scenario. The values of all three factors range from 1 to 10, with each value having a specific meaning, as shown in the tables.

By multiplying all three factors, the criticality level is obtained, which represents the degree of system criticality. Criticality is low if $R \leq 50$, and "critical" if $R > 200$. When the criticality is "critical," i.e., $R > 200$, certain corrective actions need to be defined to improve the condition or bring the system status back within acceptable limits.

The critical components of the wind turbine system identified are:

- Tower,
- Generator,
- Yaw system,
- Gearbox.

In the FMECA worksheet, tabularly presented in Figure 3, an overview of the failure modes, causes, and effects in the wind turbine system is provided. After this activity, a criticality analysis is conducted. The quantification of criticality and failure probability is carried out to assist in making decisions about corrective actions and their priorities, as well as in determining a clear boundary between acceptable and unacceptable risk.

Component	Function	Failure Type	R1	Failure Consequence		R2	Failure Cause	Failure Detection	R3	Criticality Level (Condition Rating) R	Corrective Actions	Remarks
				Local	Final							
1	2	3	4	5	6	7	8	9	10	11	12	13
Tower	Steel/Concrete Support	Structural Failure	3	Tower Failure	IV	7	Corrosion of Structure	Visual	1	21 (Low)	Anti-corrosive coatings	
Generator	Conversion of Mechanical Energy to Electrical	Rotor and Stator Failure	6	Generator Failure	III	9	Broken Bars	Visual	1	54 (Medium)	Bar Replacement	
		Bearing Failure	4	Generator Failure	III	8	Abnormal Vibrations	Vibroacoustic Method	5	160 (High)	Bearing Replacement	
Yaw System	Wind Direction Tracking	Yaw Motor Failure	1	Yaw System Failure	Loss of Function After Some Time	5	Wear	Mechanical Repair	9	45 (Low)	Yaw Motor Replacement	
		Meteorological Unit Failure	7	Yaw System Failure	Loss of Function After Some Time	4	Blade Damage	Visual	6	168 (High)	Meteorological Unit Replacement	
Gearbox	Acceleration of Rotor Speed from Low to the Speed Sufficient to Start the Generator	Poor Lubrication	9	Gearbox Failure	III	5	Presence of Contaminants in Oil	Spectrometric Analysis / Ferrography / Viscosity Measurement	4	180 (High)	Oil Replacement and Control	
		Poor Equipment	7	Gearbox Failure	III	7	Abnormal Vibrations	Vibroacoustic Method	3	147 (High)	Gearbox Replacement	

Figure 3 - FMECA Worksheet for Selected Components of the Wind Turbine System

Conclusion

The aim of the research presented in this paper is to identify potential causes of failures in the wind turbine system components, which affect reliable and efficient operation, and to determine which component of the wind turbine system is most critical in terms of failure occurrence.

For these four subsystems, the criticality level was determined using the FMECA method, and it was concluded that the most critical part of the wind turbine system is the gearbox, with the failure cause being the presence of contaminants in the oil and a criticality level of 180, which represents a high criticality level.

It was concluded that component failures can lead to the failure of the entire wind turbine system, causing its downtime, which in turn reduces

reliability and increases maintenance costs. The FMECA method highlights the critical components of the system and provides an efficient method for system analysis. It also allows for the prioritization of problem-solving actions.

There are certain preventive measures and maintenance practices that can significantly impact the lifespan of the wind turbine system:

- Regular maintenance – inspection of all mechanical and electrical components, replacement of consumables, and monitoring of software systems,
- Real-time monitoring – modern monitoring systems that can detect and report irregularities or faults before they lead to more serious problems,
- High-quality staff training – personnel must be well-trained and familiar with all aspects of operation and maintenance.

With regular maintenance and proper monitoring, failures in wind turbines can be minimized.

References

Adamović Ž., Radovanović Lj., 2008. Pouzdanost mašina, Univerzitet u Novom Sadu, Tehnički fakultet „Mihajlo Pupin“, Zrenjanin, Srbija, (in Serbian).

Adamović Ž., Ilić B., Vulović M., Vulović S., Meza S., Jurić S., 2013. Obnovljivi izvori energije, Srpski akademski centar, Novi Sad, Srbija, (in Serbian).

Adamović Ž., Ilić B., Vulović S., Stanković N., Vulović M., 2014. Tehnikčka dijagnostika elektana i toplana – Pouzdano održavanje termoelektrana, hidroelektrana, solarnih elektrana, vetroelektrana i toplana, Društvo za tehničku dijagnostiku – Adam institut, Smederevo, Srbija, (in Serbian), ISBN 978-86-83701-33-9.

Arabian-Hoseynabadi H., Oraee H., Tavner P.J., 2010. Failure Modes and Effects Analysis (FMEA) for wind turbines, International Journal of Electrical Power & Energy Systems, 32(7), pp.817-824. https://doi.org/10.1016/j.ijepes.2010.01.019

Botsaris P. N., Konstantinidis E. I., Pitsa D., 2012. Systemic Assessment and Analysis od Factors Affect the Reliability of a Wind Turbine, Journal of Applied Engineering Science, 10(2), pp.85-92. https://doi.org/10.5937/jaes10-2130

Catelani M., Ciani L., Galar D., Patrizi G., 2020. Risk Assessment of a Wind Turbine: A New FMECA-Based Tool With RPN Threshold Estimation, IEEE Access, 8, pp.20181-20190. https://ieeexplore.ieee.org/document/8966244 DOI: 10.1109/ACCESS.2020.2968812

Dev Sharma K., Srivastava S., 2018. Failure Mode and Effect Analysis (FMEA) Implementation: A Literature Review, Journal of Advance Research in Aeronautics and Space Science, 5(1&2), pp.1-17. ISSN: 2454-8669.

Gao Z., Liu X., 2021. An Overview on Fault Diagnosis, Prognosis and Resilient Control for Wind Turbine Systems, Processes, 9(2), 300. https://doi.org/10.3390/pr9020300

Gardijan P., 2001. Mogućnosti realizacije metoda analize otkaza za mašinsko sredstvo, Vojnotehnički glasnik/Military Technical Courier, 49(4-5), pp.412-423.

Hossain M. L., Abu-Siada A., Muyeen S. M., 2018. Methods for Advanced Wind Turbine Condition Monitoring and Early Diagnosis: A Literature Review, Energies, 11(5), 1309. https://doi.org/10.3390/en11051309

Hrnjak M., Katić V., 2021. Glavne karakteristike i komponente vetroelektrane u Jugoistočnom Banatu, In: Zbornik radova Fakulteta Tehničkih nauka, 36(09), pp.1525-1528, (in Serbian) https://doi.org/10.24867/14BE15Hrnjak

Jovanović O., Baroš Z., 2023. Perspektiva korišćenja energije vetra u Srbiji, Ecologica, 30(109), pp.35-42. https://doi.org/10.18485/ecologica.2023.30.109.6

Novaković B., Radovanović Lj., Vidaković D., Đorđević L., Radišić B., 2023. Evaluating wind turbine power plant reliability through fault tree analysis, Applied Engineeting Letters, 8(4), pp.175-182. https://doi.org/10.18485/aeletters.2023.8.4.5

Pal Kour K., Talwar L., Singh Bhangu N., 2019. Wind Turbine Reliability Analysis in case of Wind Generator, International Journal of Innovative Research in Science Engineering and Technology (IJIRSET), 8(9), pp.9371-9378. ISSN(Online): 2319-8753

Tazi N., Châtelet E., Bouzidi Y., 2017. Using a Hybrid Cost-FMEA Analysis for Wind Turbine Reliability Analysis, Energies, 10(3), 276. https://doi.org/10.3390/en10030276

Tavner P. J., Higgins A., Arabian H., Long H., Feng Y., 2010. Using an FMEA method to compare prospective wind turbine design reliabilities, In: European Wind Energy Conference (EWEC 2010), 1, pp.2501-2538. ISBN: 978-1-61782-310-7.

Primena FMECA metode za identifikaciju otkaza u vetroturbinskim sistemima

Branislava Radišić, **autor za prepisku**, *Ljiljana* Radovanović, *Borivoj* Novaković, *Jasmina* Pekez, *Slavica* Prvulović, *Eleonora* Desnica
Univerzitet u Novom Sadu, Tehnički fakultet „Mihajlo Pupin”, Zrenjanin, Republika Srbija

OBLAST: mašinstvo
KATEGORIJA (TIP) ČLANKA: naučni rad

Sažetak:

U ovom radu prikazani su potencijalni uzroci otkaza komponenti vetroturbinskog sistema koji utiču na pouzdan i efikasan rad iste. Otkazi komponenti u vetroturbinama mogu dovesti do potpunog otkaza sistema, što rezultira zastojima, smanjenom pouzdanošću i povećanim troškovima.

Zarad maksimalnog iskorišćenja potencijala energije vetra, bitno je potencijalne otkaze svesti na minimun. Primenom FMECA metode (Failure mode Effects and Criticallity Analysis) utvrđene su kritične komponente vetroturbinskog sistema, čime se pruža mogućnost da se odrede prioriteti za rešavanje problema. Rezultati naglašavaju važnost održavanja i optimizacije dizajna radi smanjenja rizika od otkaza i maksimizacije iskorišćenja energije vetra.

Uvod/cilj: Pouzdanost vetroturbinskih sistema igra ključnu ulogu u obezbeđivanju stabilnog i efikasnog snabdevanja električnom energijom iz obnovljivih izvora. Otkaz bilo koje komponente može izazvati zastoj sistema, smanjiti njegovu pouzdanost i povećati troškove eksploatacije. U tom kontekstu, važno je prepoznati i analizirati potencijalne kvarove kako bi se poboljšala celokupna pouzdanost sistema. Cilj ovog rada je analiza pouzdanosti vetroturbinskog sistema primenom FMECA metode. Fokus je na identifikaciji najkritičnijih komponenti i razumevanju uzroka i posledica njihovih otkaza, kako bi se doprinelo unapređenju projektovanja, održavanja i rada sistema.

Metode: U ovom radu primenjena je metoda FMECA (Failure Modes, Effects, and Criticality Analysis), koja omogućava detaljnu procenu potencijalnih otkaza sistema, njihovih uzroka i posledica, kao i identifikaciju najkritičnijih tačaka sistema na osnovu kvantitativnih parametara. Metodologija obuhvata sledeće korake: identifikaciju ključnih komponenti vetroturbine, uključujući rotor, menjač, generator, sistem za upravljanje i druge podsisteme; definisanje mogućih načina otkaza za svaku komponentu, uz navođenje mehanizama koji mogu dovesti do kvara (habanje, pregrevanje, mehaničko oštećenje itd.); procenu posledica otkaza, kako na samu komponentu, tako i na celokupan rad vetroturbine; numeričku procenu rizika kroz dodeljivanje vrednosti za: verovatnoću pojave potencijalnog otkaza (R1), značaj potencijalnog otkaza (R2) i verovatnoću otkrivanja otkaza i sprečavanje njegovog ispoljavanja (R3); izračunavanje nivoa kritičnosti (R) korišćenjem izraza $R = R_1 \cdot R_2 \cdot R_3$*; rangiranje komponenti prema R vrednostima, radi identifikacije onih koje najviše ugrožavaju pouzdanost sistema i zahtevaju prioritetno praćenje ili optimizaciju.*

Rezultati: Rezultati FMECA analize pokazali su da su najkritičnije komponente vetroturbinskog sistema: menjač – najviši nivo kritičnosti (R vrednost), jer otkaz menjača može dovesti do potpunog zastoja sistema i iziskuje skupe popravke; generator – visoka ozbiljnost otkaza i srednji nivo mogućnosti otkrivanja problema; sistem za upravljanje vetroturbinom – iako su otkazi ređi, posledice mogu biti ozbiljne zbog gubitka kontrole nad turbinom. Na osnovu analize, komponente su svrstane u prioritete održavanja i praćenja, s ciljem pravovremene detekcije potencijalnih kvarova i prevencije havarija.

Zaključak: FMECA metoda se pokazala kao efikasno sredstvo za identifikaciju i rangiranje potencijalno kritičnih komponenti vetroturbinskog sistema. Rezultati ukazuju na to da menjač, generator i sistem za upravljanje predstavljaju najosetljivije tačke sistema. Njihovo preventivno održavanje, uz uvođenje sistema za praćenje stanja i unapređenje dizajna, može značajno povećati pouzdanost i smanjiti operativne troškove. Ova analiza može poslužiti kao osnova za unapređenje strategija održavanja i povećanje efikasnosti rada vetroparkova.

Ključne reči: energija vetra, vetroturbinski sistem, otkazi komponenti, FMECA metoda, pouzdanost, preventivno održavanje.

Paper received on: 12 May 2025.
Manuscript corrections submitted on: 20 June 2025.
Paper accepted for publishing on: 1 February 2026.

© 2026 The Authors. Published by Vojnotehnički glasnik / Military Technical Courier (www.vtg.mod.gov.rs). This article is an open access article distributed under the terms and conditions of the Creative Commons Attribution license (http://creativsecommons.org/licenses/by/4.0/rs/).

Battlesight zero in context of counter UAV engagement

Ivan Pemčák

University of Defence, Weapons and ammunition department, Brno, Czechia,

e-mail: ivan.pemcak@unob.cz,

ORCID iD: https://orcid.org/0009-0000-2224-4792

https://doi.org/10.5937/vojtehg74-59713

FIELD: military science, weapon construction
ARTICLE TYPE: original scientific paper

Abstract:

Introduction/purpose: This paper explores the optimal zeroing distance for an assault rifle on the modern battlefield. Traditionally, armies have used sight settings that align the projectile's trajectory with the line of sight at distances of 25 m and 300 m. This configuration is well suited for assault rifles chambered in 7 mm to 8 mm calibers when fired from the prone position at an approaching figure target. However, with the increasing use of smaller-caliber ammunition (5 mm to 6 mm) and evolving battlefield threats, including drones, it is necessary to reassess this traditional approach. This study investigates the optimal first zeroing distance when engaging both drone-type targets and standard NATO Type E figure targets. All tests and configurations were conducted using the BREN 2 assault rifle used by the Czech Army.

Methods: This study uses probability-of-hit simulation methods. The parameters of the BREN 2 weapon under investigation were experimentally verified.

Results: The probability of hitting a point target depends significantly on the setting of the sight zeroing distance. The greater the deviation of the projectile trajectory from the line of sight, the lower the probability of hitting the target without distance adjustment.

Conclusion: The findings suggest that for engaging small, irregular targets such as UAVs, zeroing distances between 50 m and 100 m are more effective, without compromising combat effectiveness against standard figure targets.

Key words: hit probability, collimator sight, zeroing, point blank range, BREN 2.

ACKNOWLEDGMENT: This work was created at the Department of Weapons and Ammunition, Faculty of Military Technologies, University of Defence. It was financed from the specific research project SV24-201.

Introduction

The probability of hitting a target is one of the basic prerequisites for successful engagement by fire. Hit probability has been a concern of most armies in the past, whether for training plans, ammunition consumption norms, or tactical and logistical requirements. When firing a small arm, the critical factors affecting the probability of hitting a target are the dispersion characteristics of the weapon-shooter-ammunition system and knowledge of the range of fire. Historically, small arms (rifles, assault rifles, machine guns, and rarely pistols) were equipped with adjustable mechanical sights (Faust, 2021). Mechanical sights allowed the shooter to adjust the firing distance so that the bullet's mean flight path passed through the target. In practice, this meant that the shooter either estimated the distance and adjusted it on the gun before firing or fired with the setting he had been trained to and adjusted the aiming point. Some types of military weapons were equipped with so-called battle sight settings. The battle sight is used for a immediate firing at close targets, regardless of the distance. Rifles used in both WW I and WW II allowed for adjustments to extreme shooting distances, where the target was usually no longer visible. Lessons learned from WW II combat led to the development of a new type of assault weapon called the assault rifle. It was found that the firing range only exceptionally exceeded 300 m, and that most combat use took place at distances of less than 200 m (Hitchman, 1952). The use of full-size rifle ammunition at these distances was a waste of the potential of this ammunition, which also excessively burdens the shooter. Furthermore, the weight of ammunition limits the volume of ammunition carried. An assault rifle is defined as a select-fire long weapon with a detachable magazine using a reduced rifle cartridge. The effective aimed range of assault rifles is declared to be 300-400 m. Mechanical sights could usually be set up to 900 m. Assault rifles made extensive use of the battle sight or universal sight setting, which utilized a ballistic principle known as the point-blank range. The point-blank range is the distance over which the bullet's flight path does not overshoot the target. In practice, this means that a target of a given size can be shot without changing the sight setting, and at this distance the bullet's flight path will pass through at least part of the target.

The point-blank range was usually related to the specific target. In the case of the AK-47, it was the height of the human figure, and the point-blank range was considered to be 300 m (Chivers, 2010). With the transition to the micro-caliber ammunition used in modern assault rifles, the trend of using point-blank range has become even more pronounced. The modern 5.56x45 NATO or 5.45x39 ammunition has a significantly

flatter trajectory at the start of the flight path than the 6-8 mm caliber ammunition used previously. A further contributing factor was the introduction of collimator sights, which generally cannot be easily and effectively reset to the desired range. Thus, they are usually set to the distance of the point-blank range (Blish, 2008).

Most infantry shooters conduct their fire in a "point-and-shoot" style of fire. This approach works well for firing at figure targets or at known targets at known ranges, where the shooter already knows from experience how to transfer fire (training shooting at a known range) (UNOB, 2024). On the modern battlefield, small unmanned aerial vehicles (UAVs) are appearing on a mass scale. In combat operations, it is sometimes necessary to shoot at these targets as well. It is therefore appropriate to revise the infantry weapons requirements so that they are able to engage these 'point targets'. The simplest cost-effective of an established assault rifle for firing at these types of targets is to change the weapon's rectification.

Zeroing of assault rifle

Rectification is an essential step in preparing a weapon for firing. The terms rectification and zeroing are very often used synonymously in shooting terminology. In fact, rectification is the broader term, as it is the general process of bringing the barrel bore axis to a defined position relative to a reference position (optical line of sight, level, gyrocompass etc.). Zeroing is a more specific term applied to direct-fire weapons, where the reference position is the optical line of sight. When zeroing small arms, the final step in the zeroing process is to verify the correctness of the zeroing by firing. The firing of the weapon is performed at a precisely known distance, usually at a rectification target. Firing during zeroing of the weapon is conducted from the most stable firing position e.g., the prone position with support or from a shooting bench (U.S. Army, 1981; USMC, 2001). Schematically, the flight path of the projectile is shown in Figure 1.

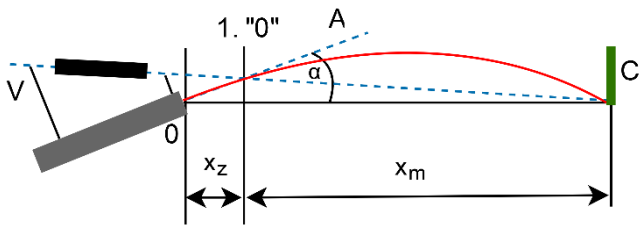

Figure 1 - Zeroing distance

It is clear from the figure that the bullet's flight path intersects the optical line of sight at two points (planes). For practical reasons, the so-called first zeroing plane (1.”0”) is most often used. In the figure, the first zeroing plane is shown at a distance x_z, which corresponds to the point-blank range for a human-sized target C up to distance x_m. This means that target C will be hit at any distance up to x_m when aiming at its lower edge.

The most common zeroing distances are 25, 50 and 100 m (Cooper, 2020; HogoNext, 2024). The 25 m range is often used for military applications and close combat situations. It is reported that the second zeroing distance is approximately at 250 m with this setting. This dogma is so firmly established in some militaries that it carries over to other types of weapons to which this rule does not fully apply. This traditionalism is one of the reasons for the implementation of this work (AČR, 2010).

The 50 m zeroing range is commonly regarded as a compromise for short and medium range shooting. The 100 m distance is used for sport shooting at a fixed, known target distance, or for competitive tactical shooting, where standard sized targets at known distances are used (Wohn, 2019; Clecker, 2020; Cooper, 2020).

One of the critical inputs determining the position of the first zeroing plane, apart from the actual ballistics of the projectile, is the position of the optical sight relative to the axis of the barrel bore. In modern assault rifles, the optical line of sight is determined by means of a collimator sight. This sight is either integrated into the weapon or, more usually, attached to the mounting interface on the weapon chassis above the barrel. The distance between the axis of the barrel bore and the line of sight is called parallax. This paper examines the Bren 2 assault rifle, which uses an Aimpoint collimator sight with a parallax of 8 cm (Česká zbrojovka, 2025).

Dispersion of fire

To calculate or model the probability of hitting a target, it is necessary to obtain information about the dispersion characteristics of a specific weapon system. For the BREN 2 assault rifle chambered in 5.56×45 mm NATO with SS109 ammunition, the dispersion data used in this work were obtained experimentally at the Department of Arms and Ammunition, University of Defence. The measurements were carried out during the international experimental shooting event Hard-Kill 2024 and can be considered indicative values.

Table 1 - Dispersion of Bren 2 rifle at 100m distance

Standing – free hand	Prone – with rest
σ_x =0.096 m σ_y =0.103 m	σ_x =0.026 m σ_y =0.030 m

The characteristics used correspond to the dispersion of very good shooters. The obtained dispersion characteristics are listed in meters for a distance of 100 m. That is, at a distance of 100 m, the standard deviation σ_x is 0.096 m. The same applies to other standard deviations. By comparing the obtained dispersion characteristics with the known dispersions of weapons for which firing tables are available, it can be concluded that up to a distance of 400 m the dispersion characteristics can be linearized. Furthermore, from a comparison of the tabulated dispersion characteristics of the AK-74 rifle and the experimentally obtained dispersion characteristics of the BREN 2 rifle, it can be concluded that these characteristics are comparable (USSR, 1977). For the purposes of this work, no additional individual shooter or weapon error was considered. As a result, the obtained hit probabilities are very high compared to real-world experiences. During the Hard-Kill 2024 experimental shooting tests, shooters achieved hits on the drone silhouette with only 14% of their shots when firing from a standing position at a distance of 100 m. Simulated firing under the same conditions yielded a hit probability of 19% (UNOB, 2024).

Hit probability simulation

Two types of targets were chosen for the hit probability analysis. The first target is the standard NATO type E target widely used for practice shooting in many armed forces (U.S. Army, 2016). The second one is a self-designed "drone silhouette" target designed for use in previous publications (Pemčák et al., 2022).

The type E target represents a forward-facing running figure. This type of target is often used in scenarios with multiple figures appearing and representing attacking infantry. The “drone silhouette” target was developed for training purposes in anti-drone defense. The body of the drone is deliberately designed with low contrast against a white background, with a contrast of k=0.3. The probability of hitting a drone propeller has been examined in previous articles (Pemčák et al., 2023). When the rotor area is hit, the probability of striking the propeller is estimated to be approximately 0.15. Furthermore, a single hit to a propeller blade has a conditional probability of disabling the aircraft of only about

0.3. For this reason, the rotor areas shown on the target are not used to determine the probability of a drone hit.

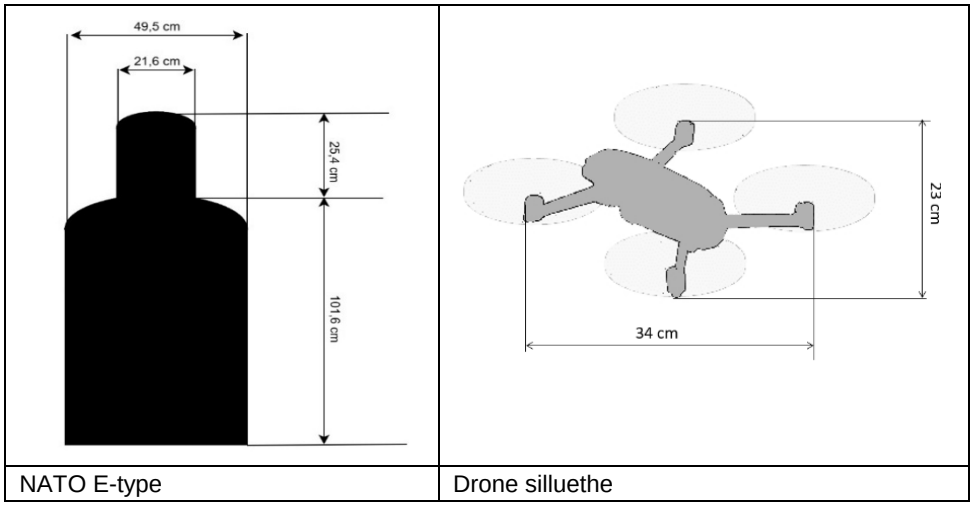

NATO E-type	Drone silluethe

Figure 2 - Examined targets

The hit probability was determined using a stochastic simulation based on Monte Carlo principles. Shot dispersion was modeled using normally distributed random values, generated by a pseudorandom number generator based on the Mersenne Twister algorithm. The dispersion of shots is modeled as a two-dimensional normal distribution centered on the aim point. The standard deviation of the distribution, which reflects the accuracy of the weapon system, is based on empirical dispersion values listed in Table 1. The simulation was conducted over a range of distances from 0 to 400 m, with a step of 1 m. At each distance, 10,000 independent trials (shots) were simulated toward the target under investigation. This sample size ensures sufficient statistical reliability of the results. The simulation follows a binomial distribution, where only two outcomes are possible — hit or miss. For such binary events (e.g., success/failure), an approximate normal confidence interval can be applied when the number of trials is sufficiently large. The number of experiments is based on the classical interval estimation theory for the proportion in the Bernoulli distribution and relies on the central limit theorem (Gross, 2019). The number of experiments is then given by the relation:

$$n = \frac{z^2 \cdot p(1-p)}{\varepsilon^2} \quad (1)$$

z is quantile of normal distribution (for 95%, z = 1.96)

ε is the desired maximum estimation error (half the width of the confidence interval)

p is probability of success of experiment

Calculating for 95% confidence of the estimate with a maximum error of ε=1% we get:

$$n = \frac{1.96^2 \cdot 0.5 \cdot 0.5}{0.01^2} \approx 9604$$

The realized number of experiments (shots) in each step, n = 10,000, exceeds the minimum required sample size of 9,604 trials to achieve a 95% confidence level with a maximum margin of error of 1%. For the generation of hit probability the experimentally obtained dispersion characteristics of the Bren 2 assault rifle are used. Simulated shots are generated in accordance with a normal distribution, with the mean value positioned point of aim. For the E-type target, the point of aim was placed at the center mass of the torso (the upper third of the target height). The point of aim for the drone target was at the geometric center of the target.

Two firing positions are considered in this paper. The first is the standing firing position without weapon support. The second firing position is the prone position with support. These are two very different yet widely used positions. The standing position is a tactical posture used by the shooter during brief halts in combat. It is one of the least stable positions but it allows for rapid movement and transfer of fire. On the other hand, the prone position with support is the most stable shooting position and is used for precision fire, for example, in defensive positions.

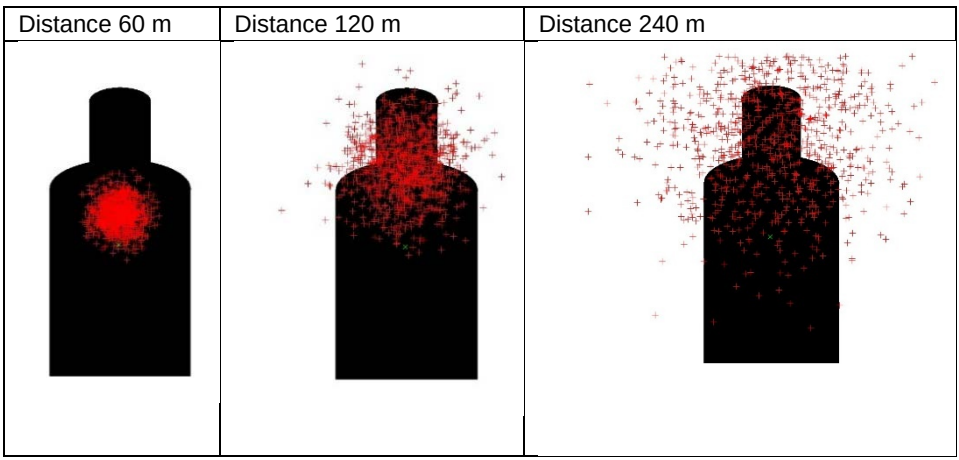

Figure 3 - Difference in size and position of hit pattern

Firing at a single target at distances from 0 to 400 m was simulated using the described model. For illustration, Figure 3 shows simulations of firing at NATO type E target at three different distances, with the first zeroing distance set at 20 m.

The effect of increasing distance is clearly visible in the figure. A shift in the center of the hit pattern is observed, assuming constant aiming at the center of the target. There is also an increase in the dispersion pattern as the distance increases. Each simulation configuration (target, range, target type) was generated for different sight zeroing ranges. The zeroing distances (first zeroing range) were set in the range of 20 to 50 m with 5 m increments, with an additional setting at 100 m.

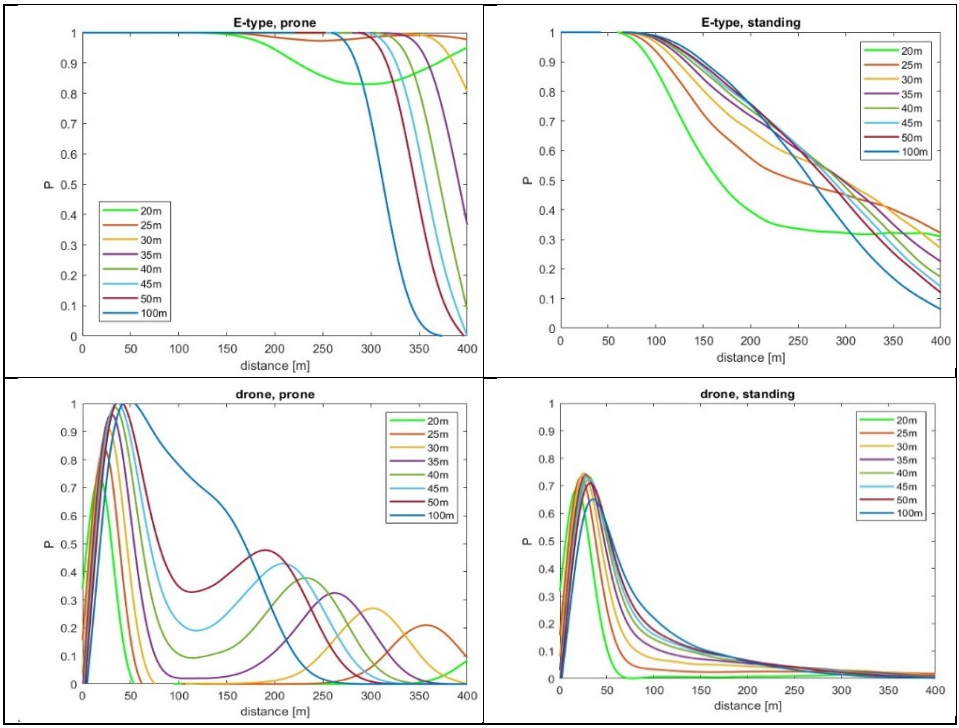

Figure 4 - Hit probabilities

It is usually assumed that the probability of hitting a target decreases with increasing distance and consequently with increasing dispersion. The graphs showing the probability of hitting a target when shooting from the standing position are consistent with this assumption. However, graphs of the probability of hitting a target when shooting from the prone position

(i.e., precision aiming) show an uncharacteristic decrease and subsequent increase in hit probability for some settings of first zeroing distance settings. This phenomenon is caused by the elevation and depression of the projectile's flight path compared to the optical line of sight, when on the downward portion of the trajectory, sufficiently small projectile dispersion is maintained. Furthermore, it can be observed that when shooting at a drone, the probability curve starts at zero and then sharply increases to its maximum value. This effect is caused by the parallax of the optical sight and the axis of the barrel bore, where the parallax exceeds the distance of the aiming point from the edge of the target.

The magnitude of the elevation (or decrease) of the projectile's flight path compared to the optical line of sight is shown in Figure 5 for each considered sight setting.

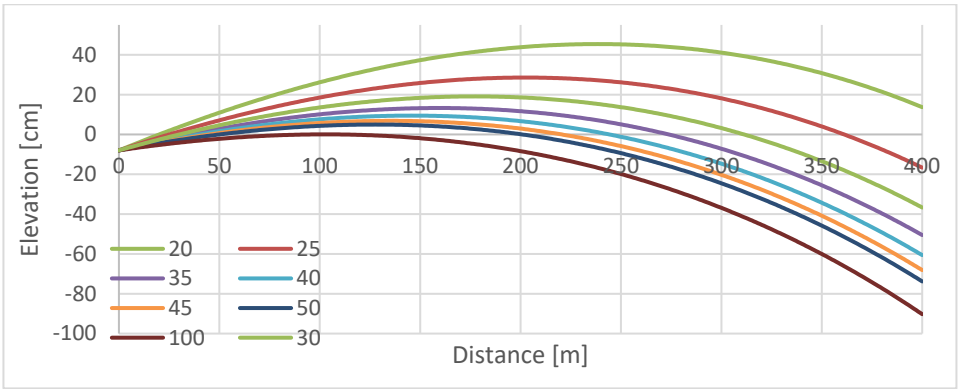

Figure 5 - Bullet flight path

Bullet trajectories were calculated using a freely available ballistic software tool that implements a standard external ballistic model based on Newtonian mechanics. The model accounts for aerodynamic drag using the G1 drag function. The equations of motion were solved numerically based on specified initial conditions, including muzzle velocity, ballistic coefficient, and environmental parameters. The weapon and ammunition parameters used in the analysis are listed below.

Cartridge:	5,56 x 45 NATO
Projectile weight:	4 g / 62 grs
Projectile type:	SS109
Ballistic coefficient G1	0,35
Initial projectile velocity	855 m/s

Parallax of optical sight 8 cm

The parameters of a normal atmosphere (200 m AMSL, 20°C, 0 m/s wind) have been used.

These parameters correspond to the BREN 2 assault rifle with an Aimpoint collimator and standard full-metal jacketed ammunition used by NATO forces. The mean bullet trajectory, and especially the elevation above the optical sight, were experimentally verified for 25 m and 50 m settings at the outdoor firing range of the Weapons and Munitions Department of the University of Defence (Čermák, 2025).

Optimalization

The process of evaluating the effectiveness of a shooting is generally assessed against one type of target. For assault rifles, the running-figure target is very frequently used, although individual armies may have slightly different shapes and target designations. For example, the U.S. Army refers to this target as Type E or L-7, while in the Czech Army this type of target is referred to as target No. 8. These targets are used because of their shape similarity to the expected target on the battlefield. In addition, the target's shape similarity to the expected enemy silhouette helps soldiers to train the muscle memory of shooting and suppresses the moral block of shooting at another person (Marshall, 2011). In assessing the suitability of a sight for universal use, hit probabilities for each sight setting will be compared across all examined targets. Therefore, the effectiveness of fire against both the drone-sized target and the type-E target will be studied at the same time. The expected maximal ranges and shooting conditions are given in Table 2. To evaluate shooting efficiency, a dimensionless unit is used, which can be referred to as the cumulative hit probability over a given range of distances. This unit is defined as:

$$C_i = \int_{d_{max}}^{0} P_i(x)dx \quad (2)$$

Where C is cumulative probability of i-th setting of collimator sight with probability function Pi over distance from 0 to d_{max}, and where d_{max} is the maximum distance of simulated firing described in Table 2.

The cumulative probability represents the area under the function of the hit probability versus distance. For the examined targets, the value of the cumulative probability is calculated over only limited ranges, rather than over the entire interval under study. The ranges over which the C is calculated are depicted in Table 2. The drone-type target is considered to be engaged at ranges of up to 100 m from the standing position and up to 150 m when firing from the prone position. Firing from the prone position (or from a supported position) can be expected most often during police

operations. It is unlikely that a soldier conducting combat operations would be able to detect and identify a drone-sized target at such distances, but this cannot be ruled out. Firing at a forward-running figure (E-type target) at a distance of 300 m (300 yards is also cited in the literature) is considered a basic shooting task. As already mentioned, this task is based on the lessons learned from WW II and the Vietnam War. On today's battlefields, this type of firing task may not be as common as it was in the past. Therefore, the long-established rules of weapon rectification in military use require re-evaluation. At the same time, it should be emphasized that at the time when 300 m was established as the optimal second firing plane, collimator sights were not yet massively employed. Thus, it was not possible to effectively "over-aim" over the target to compensate for the drop in the bullet trajectory at longer ranges. It was only possible to lower the aiming point on closer targets. When a collimator sight is applied to an assault rifle, the target is not obscured even when over-aiming. When firing at a figure target from the prone position, the sight setting does not affect the probability of a hit up to a distance of 250 m. Exceptions are sight settings with the first zeroing distance set to 20 m and 25 m, where the hit probability already decreases at these distances. For standing firing, the distance over which shooting results are not affected by the sight setting is up to 50 m.

Table 2 - Maximal distances of engagement

Target	Shooting position	dmax
Dron	Standing	100
	Prone with rest	150
Type-E	Standing	300
	Prone with rest	400

For the purpose of comparing the results, the measured C values were normalized. The normalized values of the cumulative probability C_n are calculated according to Eq:

$$C_n = \frac{C_i}{C_{max}} \tag{3}$$

Where C_i are the individual cumulative probabilities for a given shooting position and a given target and C_{max} is the highest value in the set of cumulative probabilities for a given shooting position and a given target.

Table 3 shows the zeroing distances that achieve the highest normalized cumulative hit probability for the examined firing positions and targets. Values 0.95 - 1 are marked in green and represent the ideal zeroing distance from the examined options for a given combination of

dispersion and target shape. The table illustrates one of the reasons why most Western armies adopted in the past the 1st zeroing plane at 25 m or 30 m. Most military trials and weapons testing are conducted from the prone position at known distances. In this position (for a given dispersion of fire), the sight setting for the first firing plane at 25 m or 30 m shows the best results. However, the other tasks examined show significantly better results at longer ranges of the 1st zeroing plane. The nature of contemporary conflicts must be taken into account, as it can be expected that shooting at shorter ranges will be more frequent (especially in urban combat) than in past conflicts. At the same time, it can be assumed that when engaging targets at longer ranges, the shooter will have sufficient time to transfer the point of aim to the targets. With this assumption in mind, the calculation of the cumulative probability of firing from the prone position at a figure target has been modified so that if the target is at a distance greater than 200 m, the shooter will not aim at the center mass of the body but at the upper part of the figure (the head). The graph of the hit probability with this condition and for firing from the prone position at a figure target is shown in Figure 6.

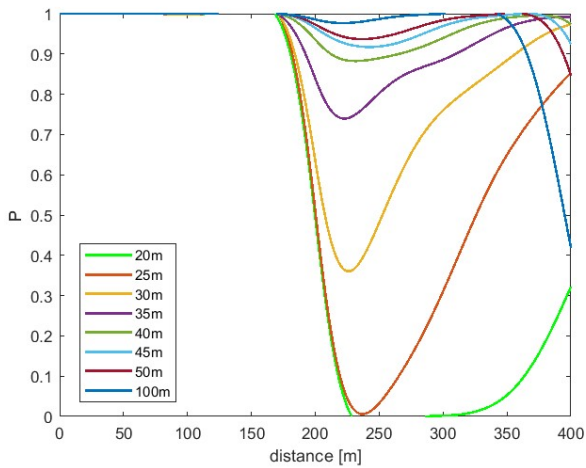

Figure 6 - Hit probability (prone, E-type) with aim point shift at 200 m

A significant drop in the hit probability can be observed for settings with a short 1st zeroing distance after the point of aim has been shifted at 200 m. Obviously, for these sight settings it is more advantageous not to transfer the aiming point. After incorporating the newly obtained cumulative probability into Table 3, a significant shift can be observed. The

results indicate that the higher distances of the 1-shot plane are more advantageous.

The following criteria were chosen to evaluate the suitability of each setting for engaging different targets and different maximum distances. The cumulative probabilities for each shooting target and position are summed, where one sum includes firing from the prone position without aimpoint transfer, denoted as Σ^1. The sum including aimpoint transfer at 200 m is denoted as Σ^2. The sight setting with the highest sum of cumulative probabilities is considered the most suitable for all examined positions. The most suitable universal firing distance appears to be 100 m, regardless of whether the aiming point is transferred.

Table 3 - Normalized cumulative probabilities

		Normalized cumulative probability Cn							
Target	1st zeroing distance	20	25	30	35	40	45	50	100
Dron	Standing	0,59	0,73	0,85	0,93	0,97	1	1	0,98
	Prone with rest	0,20	0,26	0,32	0,40	0,51	0,63	0,74	1
Type-E	Standing	0,77	0,90	0,96	0.99	1	1	1	0,98
	Prone with rest 1	0,94	1	1	0,97	0,93	0,90	0,87	0,79
	Prone with rest 2 (point of aim shifted at 200m)	0,52	0,69	0,86	0,95	0,99	1	1	0,98
	Σ1	2,5	2,89	3,13	3,29	3,41	3,53	3,61	3,75
	Σ2	2,08	2,58	2,99	3,27	3,47	3,63	3,74	3,94

Discussion

Initially, it was expected that the established rectification distance of 30 m would be at least partially confirmed, with a possibility that a 50 m zeroing distance might also prove promising. However, the results indicate that the optimal distance lies between 50 m and 100 m. For this reason, it seems appropriate to investigate the suitability of the use of shooting distances between 50 m and 100 m that were not previously considered.
As expected, there is less elevation of the projectile's path above the optical intent at distances of up to 100 m, with the disadvantage of a more pronounced projectile drop at longer distances.

The bullet trajectories are significantly more similar to each other than those corresponding to shorter zeroing distances. With this setup, probability curves were again generated for first zeroing distances from 50

m to 100 m in 10 m incerements. Next, integral evaluation and normalization were performed to obtain the cumulative probability over the examined distance, as in the previous case. The normalization was performed only among the 6 newly generated cumulative probabilities; therefore, these results are not comparable with the previously processed experiment. From the graphs, it can be observed that, as expected, the probability curves of the hits are not significantly different from each other.

Table 4 - Bullet flight path

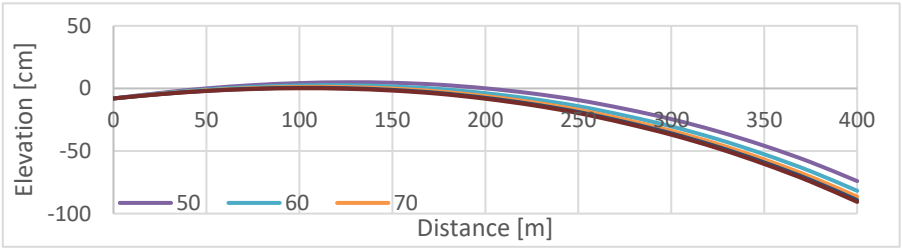

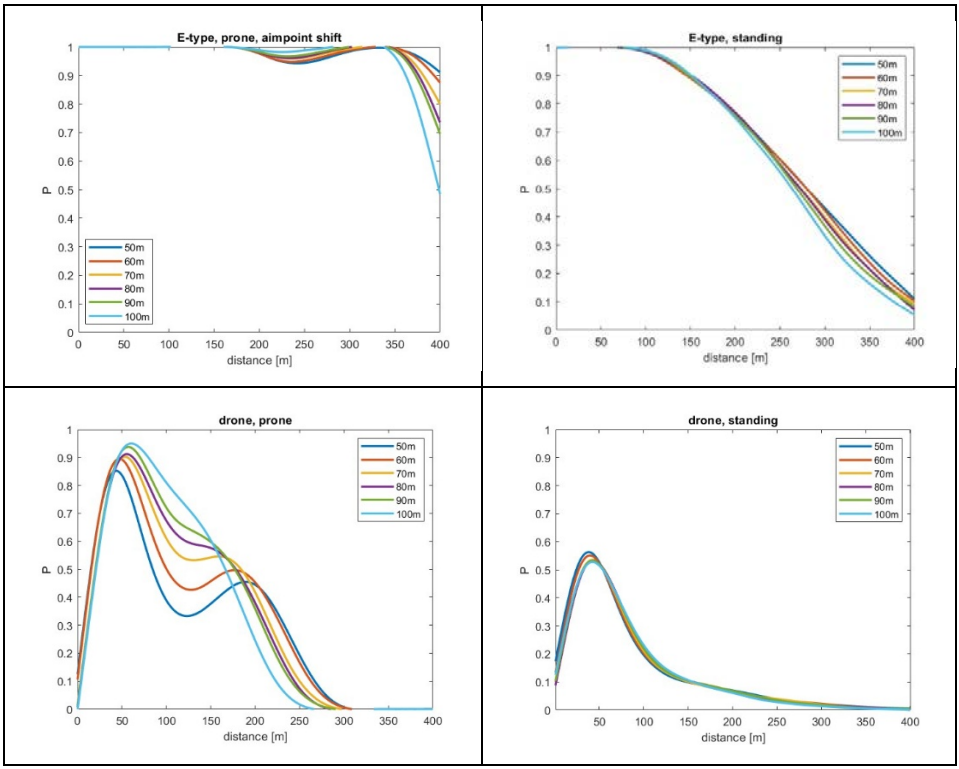

Figure 7 - Hit probabilities

Only when shooting at a small target (drone) with relatively high accuracy do the differences between the curves become more pronounced. It can be observed that the curve for 100 m shows the highest probability of all at a distance of approximately 100 - 150 m, but it is the lowest in the 150 - 200 m section.

Using the same procedure as for the analysis of the previous shot distances, the cumulative probabilities for the settings under study were calculated. The maximum firing distances are consistent with the previous example and are listed in Table 2. The cumulative probability sums are denoted as Σ^1 without the use of the aim point shift, and Σ^2 with the aim point shift for the prone position at a distance of 200 m. The results are presented in Table 5.

Table 5 - Normalized cumulative probabilities

		Normalized cumulative probability Cn					
Target	First zeroing distance	50	60	70	80	90	100
Dron	Standing	1	0,98	0,96	0,96	0,96	0,98
	Prone with rest	0,73	0,79	0,87	0,91	0,93	1
Type-E	Standing	1	1	0,99	0,98	0,98	0,96
	Prone with rest 1	1	0,99	0,96	0.95	0,94	0,9
	Prone with rest 2 (point of aim transitioned at 200m)	1	1	1	1	1	0,98
	Σ1	3,73	3,76	3,78	3,8	3,81	3,84
	Σ2	3,73	3,77	3,82	3,85	3,87	3,92

In this case, the best values of the individual cumulative probabilities for a given shooting task are not highlighted as was done in the previous table due to their similarity. The cumulative totals are again shown for both the variants without and with transfer of the aim point. The values are indicated using a color scale, with green representing the most appropriate setting. It is important to note that the settings do not differ significantly from one another.

Conclusion

This paper discusses sight settings for an assault rifle with respect to ammunition properties and contemporary tactical use. The work demonstrates methods for determining the optimal distance of the first firing plane with regard to small drone-type targets. The results indicate that the previously preferred 30 m (sometimes 30 yards) firing distance is

only advantageous when firing from the prone position at distances of up to 300 m. For shooting at a figure target from the standing position, it is more advantageous to use a 100 m zeroing distance. The same applies when engaging small drone-type targets. In this case, it is more advantageous to use a 50m first zeroing distance for the considered firing distances of up to 100 m or 150 m.

For this reason, the optimal settings for an optimal solution to all tested shooting tasks within the settings range of 50 m to 100 m were further investigated. The analysis showed only minor differences between the settings. However, it was also confirmed that the 100 m shooting distance is the most effective. Among the assessed shooting tasks, the shooting of the drone target from the prone position with support was also included, which was the only task that exhibited a lower success rate at the first plane setting of 50 m. When this shooting task is excluded, the best rectification distance is 50 m.

Setting the fisrt zeroing plane to 100 m or 50 m significantly increases shooting effectiveness on the contemporary battlefield compared to the previously used ranges of 25 m to 30 m. Furthermore, when firing from a stable shooting position (prone), it is advantageous to transfer the aiming point when engaging a figure target at a distance greater than 200 m. In conclusion, it must be emphasized that without sufficient marksmanship training, high-quality shooting results cannot be expected. At the same time, the best sight setup is the one with which the shooter regularly trains and which is adapted to the expected combat mission.

References

Blish, F., 2008. *Battlesight zero (BZO): Who has it right?*

Clecker, R. M., 2019. *Long range shooting handbook: A beginner's guide to precision rifle shooting*. North Shadow Press. ISBN 978-0999417300.

Cooper, J., 2020. *The Art of the Rifle* [e-book]. Pennsauken, NJ: BookBaby. ISBN 978-1098332082.

Čermák, J., 2025. *Shooting accuracy of the mechanical sqad.* Master thesis. Brno: Univerzita obrany.

Česká zbrojovka, 2025. CZ BREN 2 5.56×45 NATO (8"). [Online] Available at: https://www.czub.cz/en/firearms-and-products-product/cz-bren-2-556-8 [Accessed: 26 5 2025].

Faust, F., 2021. Mosin-Nagant M1891: *Facts and circumstance in the history and development of the Mosin-Nagant rifle*. Rushden: Middle Coast Publishing. ISBN 978-0934523493.

Gross, B., Harris, J. & Riehl, E. 2019*. Fat chance: Probability from 0 to 1.* Cambridge: Cambridge University Press. ISBN 978-1108728188*.*

Hitchman, N. A., 1952. *Operational requirements for infantry hand weapons (ORO-T-160)*. Chevy Chase, Operations Research Office.

HogoNext, 2024. *How to Zero a Rifle.* [Online] Available at: https://hogonext.com/how-to-zero-a-rifle [Accessed: 4 16 2025].

Chivers, C.J. 2010. *The gun: The AK-47 and the evolution of war.* New York: Simon & Schuster. ISBN 978-0743270762.

Marshall, S., 2011. *Men Against Fire: The Problem of Battle Command.* Washington, D.C: Literary Licensing, LLC. ISBN 978-1258143541

Military rule book AČR, 2010. *Vševojsk-4-2: Combat operations of the mechanized platoon.* Prague, Czech Republic:Ministry of Defence of the Czech Republic (in Czech)

Pemčák, I., Skala, J. & Bača, J. 2022. Suitability of using different types of shotgun shells in defence against low-slow-small UAV. *Science & Military,* 17(2), pp.5–10. Available at: https://doi.org/10.52651/sam.a.2022.2.5-10.

Pemčák, I., Skala, J., Nováčková, K. & Krejčí, J. 2023. Probability of hitting the drone propeller by projectile. *In: 2023 9th International Conference on Military Technologies (ICMT 2023) – Proceedings.* Brno: University of Defence. Available at: https://doi.org/10.1109/ICMT58149.2023.10171307.

U. S. Army, 1981. *Field manual 22-9: Rifle marksmanship, M16A1 rifle.* Washington D.C.: Department of Army.

U. S. Army, 2016. *TC 3-22.9: Rifle and Carbine*. Washington, D.C.: Headquarters: Department of the Army.

University of Defence (UNOB), 2024. Results of experimental shooting HARD KILL 2024: Effects against Class I UAS using small-caliber firearms. Brno: University of Defence. MO 298063/2025-2994

United States Marine Corps (USMC), 2001. *Marine Corps reference publication (MCRP) 3-01A: Rifle marksmanship.* Washington D.C.: Headqarters USMC.

USSR Ministry of Defense, 1977. *Firing tables for ground targets using small arms of caliber 5.45 and 7.62.* Moscow: Military Publishing House of the Ministry of Defense of the USSR.

Wohn, H., 2019. *IPSC the basics: From the beginning to the first match.* Nordestedt: Books on Demand. ISBN 978-3750520431.

Bojni nišan nula u kontekstu dejstva na bespilotne letelice

Ivan Pemčák
University of Defence, Weapons and ammunition department, Brno, Czechia

OBLAST: vojne nauke, konstrukcija naoružanja
KATEGORIJA (TIP) CLANKA: originalni naučni rad

Sažetak:

Uvod/cilj: Ovaj rad razmatra optimalnu daljinu upucavanja automatske puške na savremenom bojištu. Tradicionalno, oružane snage koriste nišanska podešavanja koja usklađuju putanju projektila sa linijom

nišanjenja na razdaljinama od 25 m i 300 m. Ovakva konfiguracija je pogodna za automatske puške kalibra od 7 mm do 8 mm pri dejstvu iz ležećeg stava na cilj oblika figure u prilasku. Međutim, sa sve većom upotrebom municije manjeg kalibra (5 mm do 6 mm) i razvojem pretnji na bojištu, potrebno je preispitati ovaj tradicionalni pristup. U radu se ispituje optimalna početna razdaljina upucavanja pri dejstvu kako na cljeve tipa dron tako i na standardne NATO figuralne ciljeve tipa E. Sva ispitivanja i podešavanja sprovedena su upotrebom automatske puške BREN 2 koja se koristi u Oružanim snagama Češke Republike.

Metode: U radu su primenjene metode simulacije verovatnoće pogotka. Podešavanja ispitivanog naoružanja BREN 2 su ekperimentalno verifikovana.

Rezultati: Verovatnoća pogotka tačkastog cilja u značajnoj meri zavisi od podešavanja daljine upucavanja nišana. Što je veće odstupanje putanje projektila od linije nišanjenja, manja je verovatnoća pogađanja cilja bez korekcije razdaljine.

Zaključak: Rezultati istraživanja ukazuju da su pri dejstvu na male i nepravilne ciljeve kao što su bespilotne letelice daljine upucavanja između 50 m i 100 m efikasnije, pri čemu se ne narušava borbena efikasnost protiv standardnih ciljeva u obliku figure.

Ključne reči: verovatnoća pogotka, kolimatorski nišan, upucavanje, daljina direktnog hica, BREN 2.

Paper received on: 24 June 2025.
Manuscript corrections submitted on: 18 July 2025.
Paper accepted for publishing on: 8 September 2025.

© 2026 The Authors. Published by Vojnotehnički glasnik / Military Technical Courier (www.vtg.mod.gov.rs).This article is an open access article distributed under the terms and conditions of the Creative Commons Attribution license (http://creativecommons.org/licenses/by/4.0/rs/)

Finite element-based optimization of composite wrap repair for welded pipelines with surface cracks: influence of geometry, adhesive properties, and internal pressure on mode I fracture behavior

Nedir Hachemi[a], *Noureddine* Mahmoudi[b], *Foudil* Khelil[c], *Abed* Bouadi[d],*Youcef* Moulai Arbi[e]

[a] University of Mustapha Stambouli, Laboratory of Quantum Physics of Matter and Mathematical Modeling (LPQ3M), Mascara, People's Democratic Republic of Algeria,

e-mail: nedirhachemidz@gmail.com, **corresponding author**,

ORCID ID: https://orcid.org/0009-0008-2211-0776

[b] University of Saida Dr. Moulay Tahar, Faculty of Technology, Department of Civil Engineering and Hydraulics, Saida, People's Democratic Republic of Algeria,

e-mail: mahmoudi.noureddine@yahoo.fr,

ORCID ID: https://orcid.org/0000-0002-9740-0857

[c] University of Mustapha Stambouli, Laboratory of Quantum Physics of Matter and Mathematical Modeling (LPQ3M), Mascara, People's Democratic Republic of Algeria,

e-mail: khelilfoudil@yahoo.com,

ORCID ID: https://orcid.org/0000-0002-1671-0766

[d] University of Mustapha Stambouli, Mascara, People's Democratic Republic of Algeria,

e-mail: bouadi.abed@gmail.com,

ORCID ID: https://orcid.org/0000-0003-2378-0292

[e] University of Mustapha Stambouli, Laboratory of Quantum Physics of Matter and Mathematical Modeling (LPQ3M), Mascara, People's Democratic Republic of Algeria,

e-mail: youcef.moulaiarbi@univ-mascara.dz,

ORCID ID: https://orcid.org/0000-0002-6534-8820

https://doi.org/10.5937/vojtehg74-59078

FIELD: mechanical engineering, materials
ARTICLE TYPE: original scientific paper

Abstract:

Introduction/purpose: The structural integrity of pressurized pipelines is often threatened by surface cracks, especially in welded regions. This study evaluates the effectiveness of composite wrap reinforcement in repairing longitudinal semi-elliptical cracks in welded steel pipelines subjected to

internal pressure. Although environmental effects such as temperature, moisture, and chemical exposure were not modeled, they are acknowledged as key factors influencing the long-term durability of composite repairs.

Methods: A three-dimensional finite element model was developed for a welded pipeline (outer diameter = 1016 mm, thickness = 12.8 mm) containing an external semi-elliptical crack (2c = 10.24 mm, a = 2.56 mm). The Virtual Crack Closure Technique (VCCT) was applied to compute Mode I Stress Intensity Factors (SIFs) under internal pressures of 2–12 MPa. A parametric study assessed the influence of patch length (100–400 mm), thickness (6–12 mm), and circumferential coverage angle (30°–360°), as well as adhesive shear modulus, thickness, and debonding effects.

Results: Increasing patch length, thickness, and coverage angle reduced SIFs, improving crack-tip stress attenuation. A higher adhesive shear modulus enhanced interfacial load transfer, while excessive adhesive thickness impaired efficiency. Localized adhesive debonding significantly increased SIFs under pressure, highlighting the sensitivity of repair performance to bonding quality.

Conclusions: This study provides design insights for optimizing composite reinforcement in welded pipeline repairs. Although a rectangular patch was analyzed, future work should investigate alternative geometries to mitigate edge stress concentrations and incorporate fatigue and environmental effects to better predict long-term service performance.

Key words: pipeline weld repair, composite wrap reinforcement, stress intensity factor (SIF), crack propagation, finite element eethod (FEM).

Introduction

Pipelines are a critical component of modern infrastructure, providing a safe, efficient, and cost-effective means of transporting liquids, gases, and solids over long distances (Klass et al., 2014). They are widely used across various sectors such as oil and gas, water supply, chemical processing, and power generation, ensuring continuous flow and reducing dependence on traditional transportation methods like trucking and railways (Baghban et al., 2022). Pipelines are typically categorized based on their function: those transporting crude oil and refined petroleum products, natural gas distribution lines, water and wastewater conveyance systems, as well as industrial pipelines used for the transfer of chemicals and slurry mixtures (Sontti et al., 2023). Their significance lies in their ability to support economic growth, reduce transportation costs, minimize environmental impacts, and ensure the safe handling of hazardous materials (Qu et al., 2022). Stainless steel pipelines are particularly valued for their corrosion resistance, mechanical strength, and long-term

durability, making them ideal for applications requiring high-performance materials (Berkache, 2021).

However, welding defects such as cracks remain a major challenge in pipeline construction and maintenance, posing threats to structural integrity and operational safety (León-Henao et al., 2024). Understanding the causes, types, and prevention methods of weld cracking is therefore crucial to ensuring the long-term reliability of these industrial systems (Guo et al., 2024; Pengchao, 2025).

Welding is a critical process in pipeline fabrication, but it can introduce various defects that compromise system integrity (Chen et al., 2022). Weld cracks may result from excessive heat input, insufficient cooling, or residual stresses, potentially leading to failure under pressure (Guo et al., 2024). Porosity, caused by trapped gas, weakens the weld bead structure (Feng et al., 2016). Incomplete fusion and lack of penetration - typically due to insufficient heat or poor technique - lead to weak joints that are prone to failure (Lai et al., 2022). Slag inclusions and contamination from impurities also compromise weld strength. Additionally, distortion and warping from uneven heat distribution can disrupt pipeline alignment and structural integrity. Addressing these defects through stringent procedures, robust quality control, and advanced repair methods is essential to maintaining pipeline reliability (Mandal et al., 2024; Cui et al., 2024; Djendara et al., 2025; Al Shabibi, 2024).

Pipeline repair offers numerous advantages, ensuring longevity, efficiency, and safety while minimizing service interruptions (Mohammadi et al., 2021; Zhou et al., 2021) It is also cost-effective, as repairs are significantly less expensive than full pipeline replacements (Patrick, 2004; Chan et al., 2015). Modern repair technologies - such as composite wraps and mechanical clamps - enable operational continuity with minimal downtime (Feng et al., 2016; Ma et al., 2021). Repairs also help protect the environment by preventing leaks that could contaminate soil and water resources. These interventions enhance structural integrity and reduce the risk of catastrophic failures (Mandal et al., 2024; Cui et al., 2024). Recent technologies, including epoxy-based composite reinforcements, offer improved crack resistance and significantly extend pipeline service life (Mohammadi et al., 2021; Saeedi et al., 2024). Implementing effective repair strategies thus optimizes resource use, ensures regulatory compliance, and reinforces the sustainability of critical infrastructure (Patrick, 2004).

In real-world applications, pipeline repair performance may also be affected by environmental factors such as temperature fluctuations, moisture ingress, and chemical exposure, which can alter the mechanical

properties of composite materials and weaken adhesive bonding over time (Banea et al., 2009; Ngabonziza et al., 2010). Although not addressed in the present study, these effects are critical to consider when evaluating the long-term durability of repair systems.

Several experimental studies have explored the repair of cracked pipelines using composite materials, combining both experimental and numerical approaches. Zarrinzadeh et al. (2017) investigated fatigue crack growth in aluminum tubes repaired with glass/epoxy patches using both testing and XFEM modeling. Li et al. (2020) conducted tests on externally cracked API 5L X65 pipes reinforced with various composite systems, revealing that the number of layers had a greater impact on performance than bond length. Lim et al. (2019) performed full-scale burst tests on repaired pipelines, demonstrating a 23% increase in burst pressure. Abduljabbar et al. (2022) studied pipelines repaired with carbon-fiber-reinforced polymers under internal pressure, finding lower burst pressures than standard predictions. Shafaee et al. (2023) evaluated the strength of pipes repaired with glass-fiber patches under pressure, highlighting the influence of layer count and fiber orientation. These findings confirm the effectiveness of composite repair systems as modern and economical alternatives to conventional methods.

Numerical studies have also been conducted to evaluate the performance of composite repairs. Chen et al. (2022) used finite element modeling to study the mechanical behavior of pipelines repaired with CFRP, showing that thicker layers and higher-stiffness interface materials enhance performance. Dumetriscu et al. (2021) compared different composite patch design methods based on defect orientation and width. Cao et al. (2022) applied the GTN model to simulate fracture behavior in circumferential welded joints, identifying the heat-affected zone (HAZ) as a common crack initiation site. Lim et al. (2019) also demonstrated a 23% increase in burst pressure through simulations, emphasizing the importance of material properties. These studies underscore the critical role of numerical modeling in optimizing composite repair designs.

While many studies assume a perfect bond between the composite wrap and the pipeline surface, real-world repairs often suffer from adhesive imperfections due to improper surface preparation, aging, or operational fatigue. These imperfections, particularly debonding zones, can significantly degrade the effectiveness of the reinforcement by limiting stress transfer across the interface. The presence of even small debonded regions can lead to localized stress concentrations and reduce the energy absorption capability of the bonded joint, thus increasing the risk of crack propagation or premature failure. Therefore, the consideration of adhesive

debonding as a parametric factor in numerical models is crucial to more accurately reflect the actual performance and durability of composite repair systems under realistic service conditions (Benkheira et al., 2022; Banea et al., 2009).

Building upon the earlier work by Majdoub et al. (2018), which investigated the effectiveness of composite wrap repair for longitudinal surface cracks in pressurized pipelines using finite element analysis, the present study aims to extend this analysis to welded pipeline regions. Specifically, it addresses the additional complexities introduced by weld zones, such as heterogeneous mechanical properties and stress concentrations.

The objective of this work is to propose and evaluate a composite wrapping technique for reinforcing cracked pipeline welds. A finite element analysis was conducted to assess the behavior of cracks located in the weld metal (WM) after repair, focusing on calculating stress intensity factors under elastic conditions. The influence of the composite wrap's geometric properties on reducing crack tip stress intensity was also examined. This study specifically focuses on how varying the composite reinforcement geometry affects the mechanical response of cracks located in the weld zone, providing novel insights into the optimization of repair strategies for welded pipeline systems.

Model description and mechanical properties

A pipeline model featuring a circumferential welded joint was developed, with a diameter of D = 1016 mm, a wall thickness of t = 12.8 mm, and an overall length of L = 40 m. The weld geometry is illustrated in Figure 1. Although the presence of residual weld reinforcement typically increases the local wall thickness, thereby enhancing the load, bearing capacity of the weld region (Chen et al., 2016; Guo et al., 2019; Mohammed et al., 2025) this effect was neglected in the present study to maintain a conservative approach in the numerical analysis.

An external longitudinal semi-elliptical surface crack was introduced in the weld zone, with a total surface length of 2c = 10.24 mm and a crack depth of a = 2.56 mm. To repair the damaged area, a composite overwrap system consisting of unidirectional glass fibers embedded in an epoxy matrix was applied. The fibers were aligned in the axial direction (0° orientation) and wrapped circumferentially around the pipeline at the weld location.

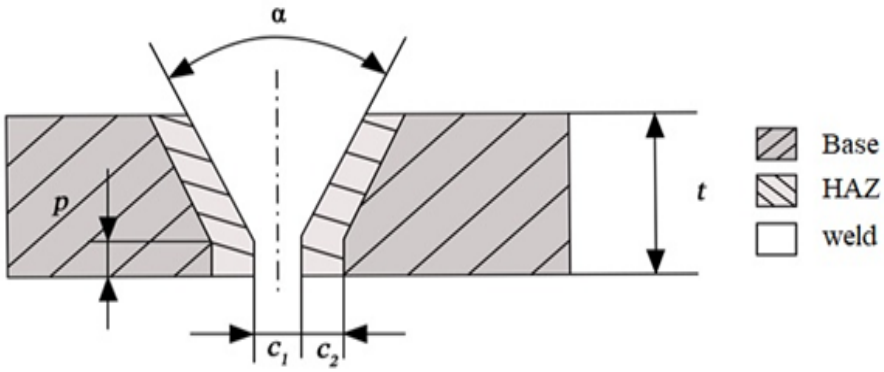

Figure 1 - Schematic representation of the circumferential welded joint geometry

Tables 1 and 2 provide a summary of the geometric dimensions and mechanical properties associated with the various regions of the model, including the base metal (BM), weld metal (WM), heat-affected zone (HAZ), composite overwrap, and adhesive interface.

Table 1 - Geometric properties of the pipeline and repair components

L (mm)	D (mm)	T (mm)	c_1 (mm)	c_2 (mm)	p (mm)	α°
4000	1016	12.8	2	2	2	55

To realistically simulate the repair system, a debonded region was introduced at the interface between the composite wrap and the adhesive layer. This debonded zone was modeled as an unbonded surface segment of 10 mm length, centered axially along the composite patch.

Table 2 - Material properties and mechanical characteristics of the base metal (BM), weld bead (WB), heat-affected zone (HAZ), composite wrap (Glass/Epoxy), and adhesive (Medjdoub et al., 2018; Chang et al., 2023; Fan et al., 2024)

Property	Materials					Description
	BM	WB	HAZ	Glass/Epoxy	Adhesive	
E_1	200000	200000	200000	160000	2400	Young's modulus in X direction (MPa)
E_2				25400		Young's modulus in Y direction (MPa)
E_3				25400		Young's modulus in Z direction (MPa)
ν_{12}	0.3	0.3	0.3	0.21	0.3	Poisson's Ratio in X-Y plan
ν_{13}				0.21		Poisson's Ratio in X-Z plan
ν_{23}				0.15		Poisson's Ratio in Y-Z plan
G_{12}				7200		Shear modulus in X-Y plan (MPa)
G_{13}				5500		Shear modulus in X-Z plan (MPa)
G_{23}				5500		Shear modulus in Y-Z plan (MPa)
G_a	1120	1900	2250	3500	[1200-1900-2250-3500-4200]	Shear modulus of adhesive (MPa)
σ_0	555.0	610.5	499.5			Yield stress (MPa)

Numerical modeling

The mechanical behavior of a pressurized pipeline featuring a surface-breaking crack and repaired with a composite overwrap was investigated through finite element analysis using Abaqus 2017. The model was discretized employing three-dimensional, 8-node linear brick elements with reduced integration (C3D8R), which offer an optimal compromise between computational accuracy and efficiency (Chen et al., 2021; Meniconi et al., 2002).

A structured global mesh was generated to accurately represent the geometry of the pipe and the repair system. Local mesh refinement was introduced in critical regions-most notably at the crack front and interfacial zones-where steep stress gradients are expected. The crack front was meshed with small, regular elements to resolve the stress singularity and allow accurate computation of fracture parameters, such as mode I stress intensity factors (Hirose et al., 2013). This resolution is essential for evaluating the crack-driving forces under loading conditions representative of service environments.

The composite wrap and adhesive layer, which are both relatively thin and mechanically dissimilar to the steel substrate, were modeled with finely layered elements to prevent artificial stiffness mismatches and ensure reliable simulation of stress transfer through the bonded interfaces. This is particularly important for capturing the interaction between the repair system and the host structure, as it governs the effectiveness of the load redistribution mechanism and the durability of the repair (Aabid et al., 2025; Thankur et al., 2024).

In order to assess the influence of interfacial imperfections on the repair efficiency, a debonded region was introduced at the interface between the composite wrap and the adhesive layer. This region was modeled as an unbonded surface of 10 mm in axial length, centered at the middle of the composite patch.

A frictionless contact interaction was defined in this zone to prevent artificial stress transfer, simulating a loss of adhesion due to manufacturing defects, surface contamination, or in-service degradation. The rest of the interface remained perfectly bonded using a tie constraint.

This approach enables a more realistic evaluation of the stress redistribution capacity of the repair system, particularly under thermal and mechanical loading. The introduction of such local debonding defects provides critical insight into the limits of adhesive performance and the need for strict quality control during repair application.

The final mesh consisted of 197,182 elements. Mesh quality, convergence behavior, and stability were rigorously assessed to validate the nonlinear solution, with special attention given to the crack tip and the material interfaces. All boundary conditions, material definitions, and contact interactions were thoroughly verified to preserve physical realism in the simulation (Madenci et al., 2020).

Figure 1 presents the overall finite element mesh, highlighting the region around the surface crack where mesh refinement was applied. Figure 2 focuses on the composite repair zone, showing detailed meshing of the overwrap and adhesive interface, which are critical to the accurate representation of interfacial stress transmission.

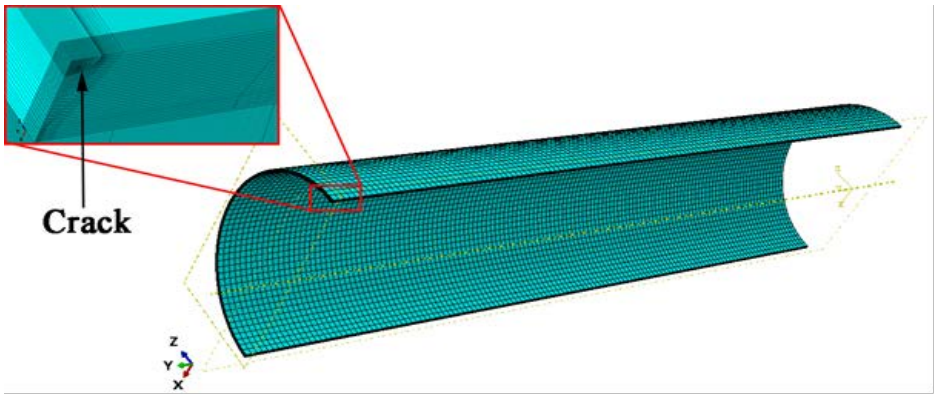

Figure 2 - Global view of the finite element mesh of the cracked pipeline, with a zoom on the surface crack region. Local mesh refinement enables accurate capture of stress singularities at the crack front

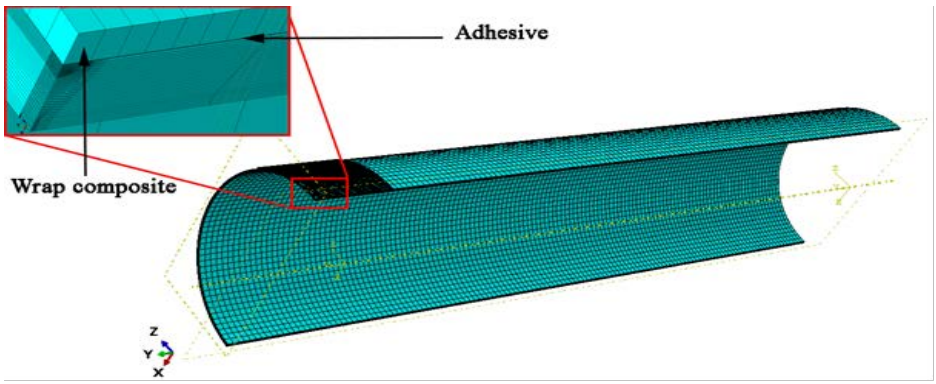

Figure 3 - Mesh representation of the repair zone, including the composite overwrap and adhesive layer. Refined meshing in these areas ensures accurate stress transfer between materials with differing stiffnesses

Boundary conditions

Leveraging the geometric and loading symmetries inherent to the repaired pipeline, the computational model was simplified to a quarter-cylinder segment (representing half the length and half the circumference), thereby significantly reducing computational demands while preserving the accuracy of stress predictions. The internal surface of the pipe was subjected to pressures ranging from 2 to 12 MPa, applied in 2 MPa increments, as depicted in Figure 4. These pressure levels correspond to standard operational and overpressure scenarios typical of oil and gas transmission pipelines (Chen et al., 2021). The internal pressure generates hoop and axial stresses within the pipe wall, which interact with both the crack and the bonded composite repair, thereby affecting local stress concentrations and the potential for damage progression.

Symmetry boundary conditions were imposed to replicate the full geometry: along the longitudinal symmetry plane, displacements and rotations were restricted $U_Y = \theta_X = \theta_Z = 0$; on the circumferential symmetry plane, the constraints $UZ = \theta_X = \theta_Y = 0$ were applied, as shown in Figure 5. These conditions effectively eliminate rigid body motion while maintaining mechanical equilibrium.

The contact interactions between the steel pipe, adhesive layer, and composite wrap were defined using surface-to-surface contact pairs in Abaqus/Standard. A hard contact formulation was applied in the normal direction to prevent penetration, while a frictionless model was assumed in the tangential direction to simulate ideal bonding. This approach captures the stress transfer mechanism between the host pipe and the repair system under internal pressure, which is essential for accurate damage assessment (Lim et al., 2019; Medjdoub et al., 2018).

In the finite element model, boundary conditions were applied to replicate the operational environment of the pipeline under internal pressure and symmetry constraints.

To accurately capture the effect of adhesive debonding, a localized debonded zone at the composite-adhesive interface was modeled using surface-to-surface contact interactions with frictionless behavior. This contact allowed separation without shear transfer, representing the loss of adhesion in that region.

The rest of the composite wrap interface was constrained with tie conditions to simulate perfect bonding. These boundary and contact conditions ensured realistic simulation of load transfer and stress redistribution in the presence of bonding imperfections (Zarrinzadeh et al., 2017).

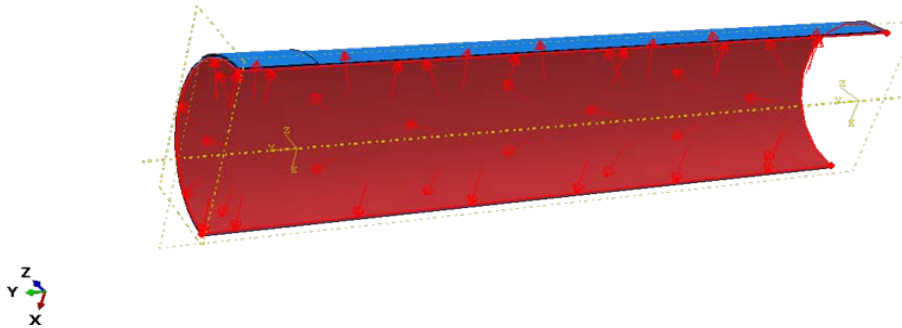

Figure 4 - Application of internal pressure on the internal surface of the quarter-cylinder pipe model

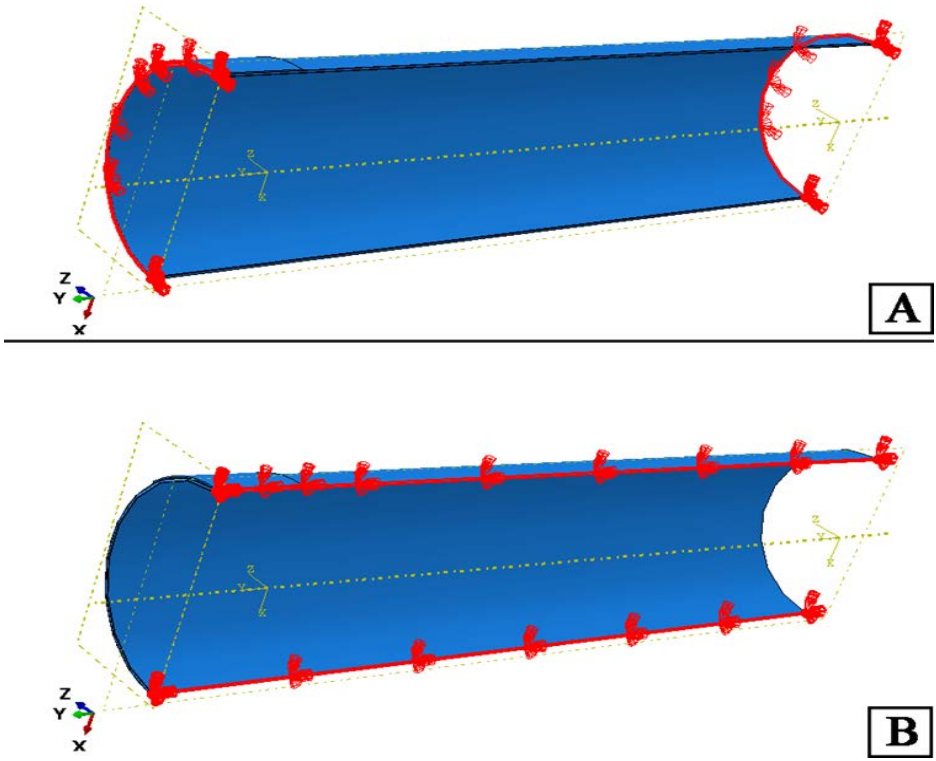

Figure 5 - Boundary conditions applied to the repaired pipeline model – (A) Longitudinal symmetry plane (UY = θX = θZ = 0); (B) Circumferential symmetry plane (UZ = θX = θY = 0)

Results and discussion

The stress intensity factors (SIFs) at the crack front were determined using the Virtual Crack Closure Technique (VCCT). This approach, based on the energy balance principle originally proposed by Irwin (Irwin, 2007), facilitates the calculation of energy release rates corresponding to various fracture modes. Specifically, for Mode I loading, the energy release rate G_i is related to the stress intensity factor K_i and the elastic modulus E through the following relationship (Leski, 2007):

$$G_i = \frac{k_i^2}{E} \tag{1}$$

VCCT is particularly effective for linear elastic materials and supports various material behaviors, including isotropic, orthotropic, and anisotropic elasticity (Kruger, 2004; Hartquist, 2025). Physically, this technique assumes that the energy required to close a crack is equivalent to the energy released during its propagation, making it well-suited for evaluating fracture toughness in composite materials.

The precision of the VCCT is highly contingent upon the quality of the finite element mesh. To reduce numerical errors and enhance solution reliability, it is advisable to employ elements of uniform size both ahead of and behind the crack tip (Leski, 2007; Durmus et al., 2025). Mesh refinement near the crack front is crucial, as stress gradients are highest in this region. Therefore, a mesh convergence study was conducted to balance accuracy with computational efficiency. As demonstrated in recent studies (Guessab et al., 2025; Stapley, 2025; Karmakov et al., 2020), convergence testing is essential to ensure that the computed SIFs are not sensitive to further refinement.

This study examined two configurations. The first focused on assessing the effects of geometric parameters - namely, the length, thickness, and wrap coverage angle of a composite patch- applied to a longitudinal semi-elliptical surface crack. These variables play a crucial role in the load transfer process and stress distribution around the crack tip, thereby impacting the effectiveness of the patch in impeding crack propagation.

In the second configuration, we examined the influence of the adhesive layer's shear modulus and thickness on the variation of the SIF. Adhesive properties directly affect the stress transfer between the composite patch and the substrate, and hence the effectiveness of the repair. A stiffer adhesive can improve load transfer but may induce higher

peel stresses, whereas a more compliant adhesive distributes stresses more evenly (Goland et al., 1944; Aderdiran et al., 2025; Kumar et al., 2025).

For comparison purposes, an unrepaired pipe configuration was also analyzed and presented as a baseline reference. This approach enables quantification of the repair's effectiveness in reducing the SIF and improving the structural integrity of the damaged component.

Effect of composite patch length on mode i stress intensity factor in repaired cracked pipes under internal pressure

Figure 6 depicts the relationship between the Mode I Stress Intensity Factor (KI) and internal pressure for various composite patch lengths Lp ranging from 100 mm to 400 mm. The purpose of this analysis is to assess how patch length influences the mechanical behavior of a cracked pipeline reinforced with a composite overwrap. To isolate this variable, other geometric parameters were kept constant, including a patch thickness of tp = 6 mm, an adhesive layer thickness of ta = 0.1 mm, and a full circumferential wrap angle of θ = 360°, representing complete encirclement of the pipe circumference.

The selection of these values is based on both mechanical and practical considerations. The patch thickness was chosen to ensure adequate stiffness without introducing excessive structural weight, while the thin adhesive layer configuration promotes efficient shear transfer and minimizes stress concentrations. A 360° wrap provides uniform load distribution and reinforcement symmetry around the pipe's circumference, which reduces local imbalances induced by internal pressure. These simulation conditions are representative of real-world repair scenarios used in industry.

Numerical analysis reveals that increasing the patch length leads to a progressive reduction in the KI values. This trend is attributed to the enlarged bonded area between the composite patch and the metallic substrate, which enhances load transfer through the adhesive layer. A longer patch enables more effective redistribution of stress around the crack, thereby lowering the stress concentration at its tip. This behavior aligns with recent findings demonstrating that increasing patch length improves the system's capacity to divert mechanical loads away from the damaged zone (Abdulla et al., 2024; Ali et al., 2013).

As expected, increasing the internal pressure results in higher KI values due to the intensification of hoop stresses induced by service

loading. However, this rise is mitigated by the presence of the composite patch, especially when longer patches are employed. The composite reinforcement functions as a mechanical shield that limits the amplification of local stresses at the crack front. This stress-mitigating effect becomes more pronounced as the reinforced area is extended. Previous studies have shown that this load-sharing mechanism is more effective when the bonded surface is optimized (Karmakov et al., 2020; Tian et al., 2025; Yu et al., 2021).

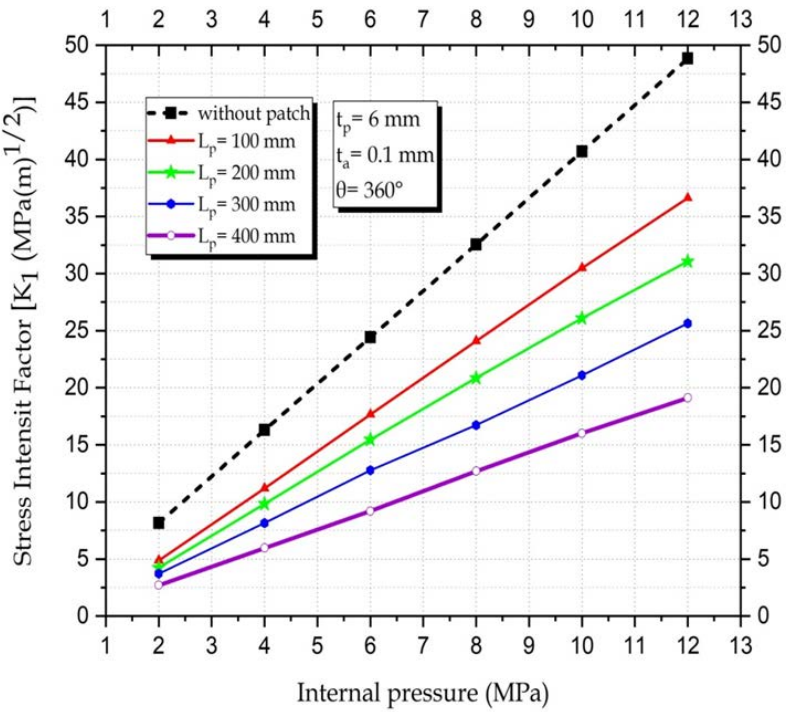

Figure 6 - Variation of SIF with Internal Pressure for Various Wrap Lengths

The observed decrease in SIF with increasing patch length aligns with experimental findings by (Lim et al., 2019), who conducted full-scale burst pressure tests on repaired steel pipelines. Their results showed a 23% improvement in burst pressure when using longer composite wraps, confirming that an increased bonded surface enhances stress redistribution around the crack. These outcomes corroborate our

simulation, where longer patches resulted in lower KI values under internal pressure.

Effect of composite wrap recovery angle on stress intensity factor

Figure 7 illustrates the changes in the stress intensity factor (SIF) at the crack front as a function of internal pressure for composite wrap thicknesses varying between 6 mm and 12 mm. All simulations were performed with a fixed wrap length of Lp = 400 mm, adhesive thickness of ta = 0.1 mm, and full circumferential coverage (θ = 360°).

The results reveal a strong inverse correlation between wrap thickness and SIF values. In the unpatched configuration, the SIF increases nearly linearly with internal pressure, reaching up to 48 MPa.m1/2 at 12 MPa. In contrast, specimens reinforced with composite wraps exhibit significantly lower SIFs. Notably, a 12 mm wrap results in a reduction exceeding 60% compared to the unreinforced case under identical pressure conditions.

This behavior can be explained by the enhanced stiffness and stress redistribution provided by thicker composite layers. The bonded wrap mitigates the concentration of mechanical energy at the crack tip, thereby reducing the local driving force for crack propagation. These findings are consistent with the literature, where increased wrap thickness has been shown to lower fracture parameters in repaired pressure pipelines (Savani, 2022; Liu et al., 2017; Said et al., 2025).

Moreover, even though the adhesive layer is thin, it plays a key role in transferring loads between the steel substrate and the composite material. A well-bonded interface ensures effective mechanical synergy, which becomes more pronounced as the wrap thickness increases (Zhou et al., 2021; Aabid et al., 2025).

Although few studies have isolated the wrap recovery angle, the trends observed here are in line with the work of (Zarrinzadeh et al., 2017), who noted improved fatigue performance when using optimized patch dimensions and orientation. Their results suggest that increasing the effective engagement angle improves crack containment, supporting our findings that wider wrap angles reduce SIF values more effectively under pressure.

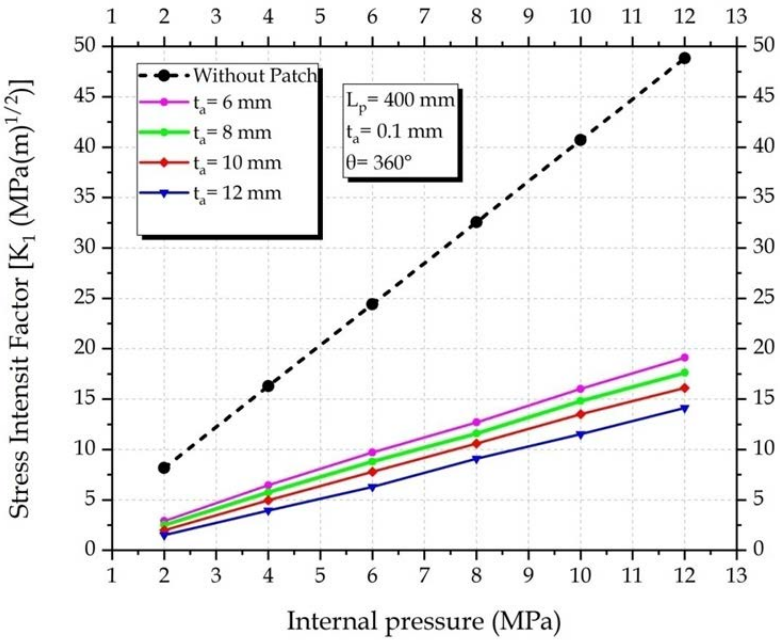

Figure 7 - Variation of SIF with Internal Pressure for Different Wrap Thicknesses

Influence of the composite wrap coverage angle on the stress intensity factor

Figure 8 illustrates the effect of the composite wrap coverage angle on the variation of the stress intensity factor (SIF) at the crack front, under different levels of internal pressure. The simulations were performed using a wrap length of Lp = 400 mm, a composite thickness of tp = 12 mm, and an adhesive thickness of ta = 0.1 mm. The wrap coverage angle θ\theta was varied from 30° to 360°.

The results clearly show that increasing the wrap angle leads to a reduction in the SIF for a given internal pressure. This reduction becomes especially significant beyond 180°, reaching its lowest value at full 360° coverage, where the crack is entirely encased by the composite material. This behavior can be attributed to the enhanced redistribution of mechanical stresses around the crack zone offered by a more extensive coverage.

The composite wrap acts as a mechanical barrier, absorbing a portion of the internal loads and limiting localized deformation near the defect. The broader the wrap coverage, the more effectively it redistributes these

stresses, reducing the concentration at the crack tip. Recent studies have confirmed this trend, highlighting that full wrap coverage (θ = 360°) significantly improves the durability and safety of pressure pipelines (Srilakshmi, 2014; Davaripour et al., 2022; Mousa et al., 2023).

Therefore, the selection of the wrap angle plays a critical role in the design of an effective repair. While partial coverage can enhance performance, full circumferential wrapping ensures optimal stress mitigation and crack containment.

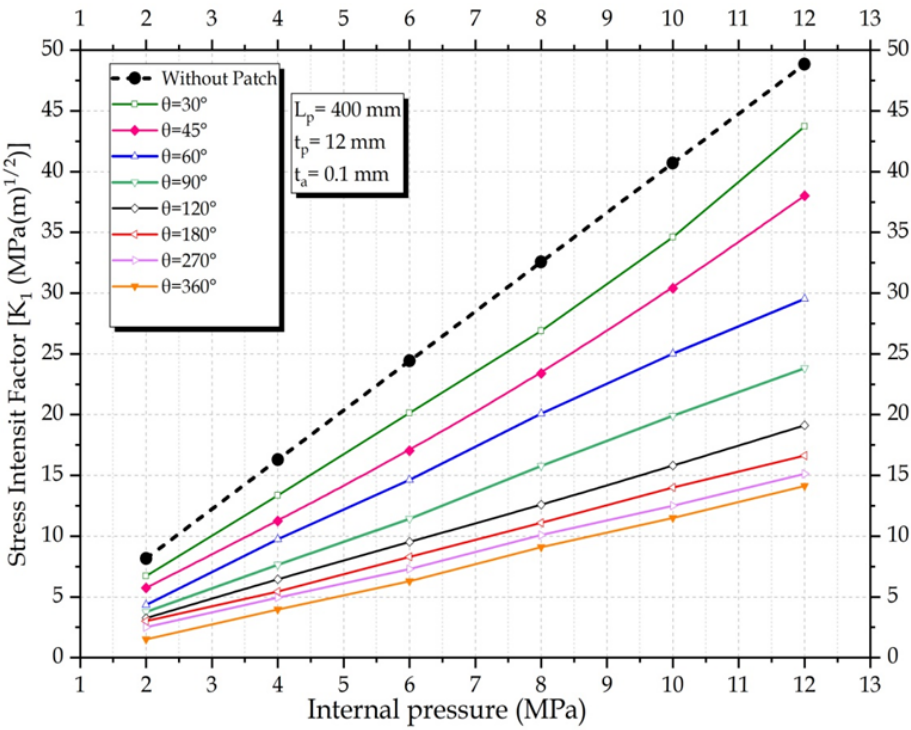

Figure 8 - Variation of SIF with Internal Pressure for Different Wrap Coverage Angles

Effect of adhesive shear modulus on repair performance

We analyzed how adhesive shear modulus and thickness affect the efficiency of composite repairs. Figure 9 displays changes in the Mode I stress intensity factor (SIF, KI) under varying internal pressures. Simulations were performed for adhesive shear moduli ranging from 1120 MPa to 4200 MPa. The adhesive layer thickness remained constant at 0.1 mm. The overwrap was 400 mm long and 12 mm thick. A full 360° wrap was applied to provide complete circumferential reinforcement.

It is observed that an increase in the adhesive shear modulus leads to a progressive reduction in the KI value at the crack front. This behavior can be explained by the fact that a stiffer adhesive (with higher shear modulus) facilitates a more efficient load transfer and promotes a more uniform stress distribution across the bonded joint. This redistribution decreases the stress concentration at the crack tip, thereby reducing the likelihood of crack propagation (Abdull et al., 2024; Alexander, 2007) .

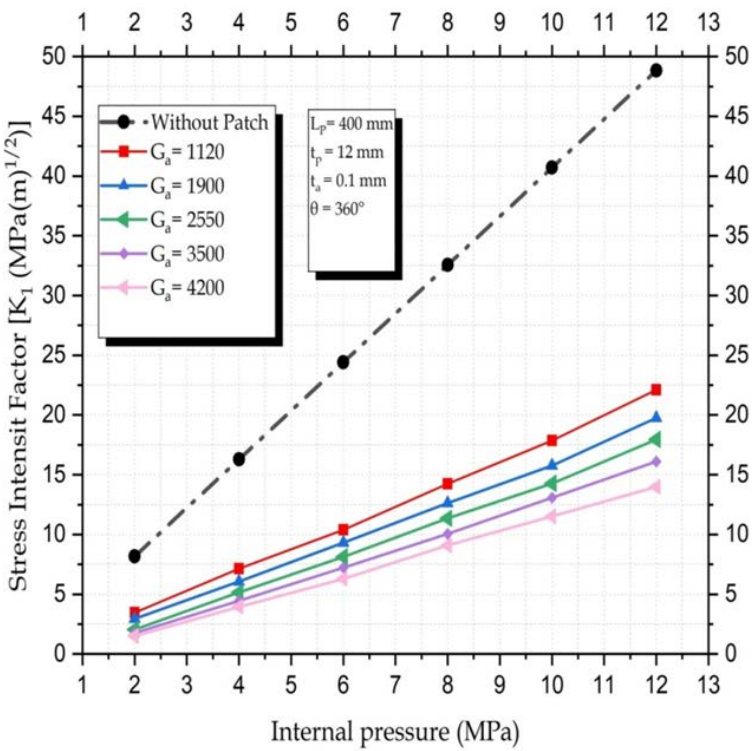

Figure 9 - Variation of Stress Intensity Factor (SIF) with Internal Pressure for Various Adhesive Shear Moduli

This mechanism is consistent with established findings in the mechanics of bonded materials, where increased joint stiffness minimizes local deformation and improves the load-sharing capability between the composite patch and the metallic substrate (Banea et al., 2009; Wei et al., 2024). At elevated internal pressures, this effect becomes more pronounced due to the amplification of circumferential (hoop) stresses,

making the adhesive interface stiffness even more critical to repair durability (Deng et al., 2017).

In summary, this analysis demonstrates that optimizing the adhesive shear modulus is a key factor in enhancing the performance of composite repairs, especially in environments subjected to high internal pressures. Recent studies emphasize that for a repair to be both durable and reliable, the selection of the adhesive should not be based solely on strength, but must also consider stiffness, toughness, and substrate compatibility (Mohammadi et al., 2021).

Experimental results from (Shafaee et al., 2023) showed that increasing fiber coverage (layer count and orientation) in glass/epoxy patches significantly improved the load-bearing capacity of repaired pipelines. Their findings validate our numerical conclusion that full circumferential coverage (360°) yields the lowest SIF values by fully encasing the defect zone and promoting uniform stress redistribution.

Influence of adhesive thickness on the stress intensity factor

Figure 10 presents the influence of the adhesive thickness ta on the Mode I Stress Intensity Factor (KI), under a configuration where the adhesive shear modulus is fixed at Ga = 4200 MPa, with a composite wrap length of Lp = 400 mm, wrap thickness tp = 12 mm, and a full wrap angle of θ = 360° ensuring complete confinement of the pipe.

The numerical results clearly demonstrate that increasing the adhesive thickness leads to a significant rise in KI at the crack front. In other words, the thicker the adhesive layer, the less effective the repair becomes in reducing the stress concentration. This behavior is directly related to the overall stiffness of the bonded joint: a thinner adhesive layer allows for more efficient load transfer to the composite wrap, enhancing stress confinement around the crack (Shafaee et al., 2023).

In contrast, a thicker adhesive layer becomes more deformable, which introduces a local damping effect that reduces load transfer. This excessive deformation may result in internal stress accumulation within the adhesive, increasing the risk of debonding or adhesive failure (Benkheira et al., 2022; Banea et al., 2022). Consequently, a thicker layer diminishes the patch's ability to contain the stresses effectively, leading to an increased KI with higher internal pressures.

These results highlight the need for an optimal balance: while a minimum adhesive thickness is required to ensure proper wetting and surface adhesion, excessive thickness can be detrimental to the mechanical performance of the repair. Recent studies generally

recommend keeping the adhesive thickness below 0.2 - 0.3 mm for repairs subjected to high internal pressures (Soutis et al., 1997).

The negative impact of increased adhesive thickness on repair efficiency matches the observations by Benkheira et al. (2022) and Jawwad et al. (2024), who experimentally showed that thicker adhesive layers increase local compliance and reduce stress transfer efficiency. They also reported a higher risk of debonding and crack growth in specimens with excessive adhesive thickness, which is in line with our numerical results showing elevated SIF values for thicker adhesive interfaces.

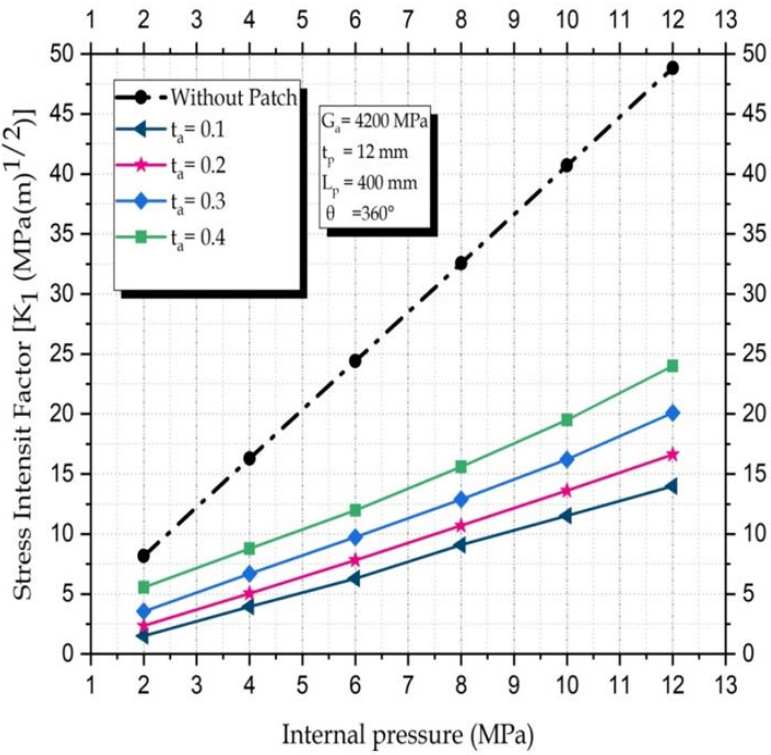

Figure 10 - SIF vs. internal pressure for different thickness of adhesive

Impact of adhesive debonding on stress intensity factor in composite-patched pipelines

The graph in Figure 11 illustrates the variation of the Mode I Stress Intensity Factor (SIF) as a function of internal pressure for three different conditions: an unrepaired cracked pipeline, a pipeline repaired with a perfectly bonded composite wrap, and a pipeline repaired with a composite wrap exhibiting a localized adhesive debonding defect. The SIF quantifies the intensity of the stress field near the crack tip and is directly related to the likelihood of crack propagation and eventual failure. The unrepaired pipeline exhibits the highest SIF values, increasing linearly with internal pressure, indicating a high risk of crack growth under operational loading. The application of a composite wrap significantly reduces the SIF by providing a mechanical reinforcement that redistributes and lowers the stress concentration at the crack tip. However, the presence of adhesive debonding compromises this load transfer mechanism. The debonded interface acts as a localized stress concentrator, disrupting the shear load path between the composite and the pipe substrate, thereby increasing the SIF compared to the ideal bonded case. This effect intensifies with increasing pressure, highlighting the susceptibility of the repair to failure when adhesive integrity is lost.

These findings underscore the critical importance of ensuring strong adhesive bonds during repair application and monitoring their condition during service to prevent premature failure. Similar conclusions have been reached in recent experimental and numerical studies demonstrating that even small debonding defects can significantly degrade repair performance (Lai et al., 2022; Benkheira et al., 2022).

Our simulation results indicating increased SIF due to adhesive debonding are strongly supported by the work of Zarrinzadeh et al. (2023), who experimentally studied composite-patched aluminum pipes and found that even small debonding zones significantly compromised fatigue performance. Benkheira et al. (2022) and Deng et al. (2025) also confirmed through tests that interfacial defects cause stress concentration and reduced load transfer, validating the critical role of bond integrity in ensuring repair efficiency.

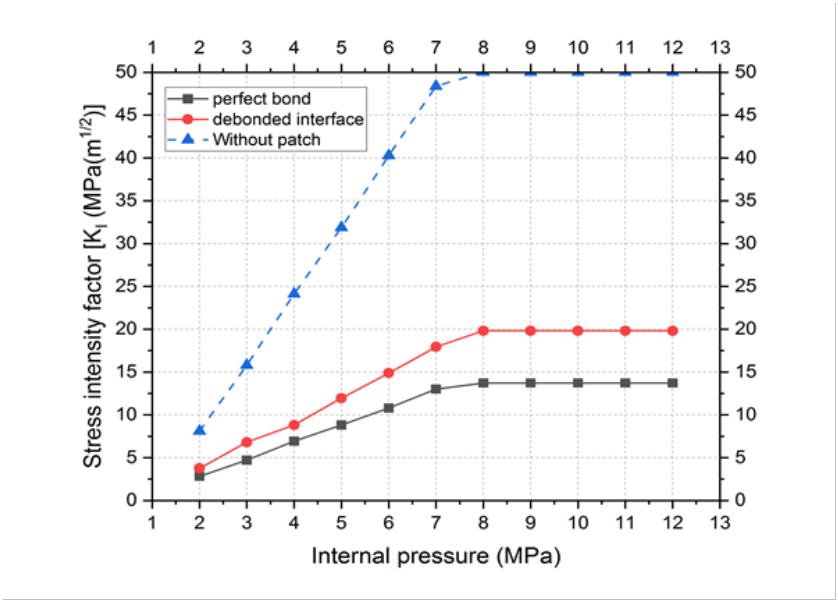

Figure 11 - Impact of Adhesive Debonding on Stress Intensity Factor

Conclusion

This study has provided a comprehensive numerical evaluation of composite wrap reinforcements applied to pipelines containing longitudinal semi-elliptical surface cracks in welded regions. Using advanced finite element modeling and the Virtual Crack Closure Technique (VCCT), the influence of key geometric and interfacial parameters on the Mode I Stress Intensity Factor (SIF) was systematically investigated.

The results confirm that increasing the composite wrap length and thickness significantly enhances the repair's ability to redistribute stresses and attenuate crack tip driving forces. A full wrap angle of 360° was found to be particularly effective, as it ensures complete circumferential confinement, resulting in the greatest reduction of the SIF under internal pressure. In addition to geometric parameters, the adhesive layer's mechanical properties were shown to play a pivotal role in repair performance. A higher adhesive shear modulus facilitates improved load transfer across the interface, while excessive adhesive thickness reduces structural stiffness, leading to elevated SIF values. These findings underscore the importance of simultaneously optimizing both the stiffness and thickness of the adhesive layer to ensure effective stress transfer and prevent failure modes such as debonding.

The simulation results further demonstrate that localized adhesive debonding significantly compromises the stress redistribution capability of the composite repair system. The loss of bonding integrity increases the SIF and raises the risk of premature crack propagation. These findings highlight the critical need for strict quality control during repair application and suggest that in-service inspections should prioritize early detection of bonding defects. Future studies should incorporate detailed Finite Element Analyses of interfacial stress and traction distributions to provide deeper insights into local load transfer mechanisms and better characterize failure initiation zones.

Moreover, although this study employed a rectangular patch geometry consistent with industrial practice, it is recognized that alternative patch profiles-such as tapered or elliptical shapes-may offer improved stress distribution by mitigating edge stress concentrations. Investigating these geometries could enhance repair robustness and reduce failure risk, particularly at patch boundaries where high local stresses typically arise.

In real-world operating conditions, the long-term behavior of composite repairs may also be influenced by environmental factors, including thermal cycling, moisture ingress, and chemical exposure. These effects can degrade adhesive and composite material properties over time, thereby reducing repair effectiveness. Future research should therefore address environmental degradation within the modeling framework to improve durability predictions and expand applicability.

Finally, while this investigation focuses on static loading conditions, fatigue crack growth remains a primary concern in pressurized pipelines. Incorporating fatigue analysis into future simulations would enable evaluation of the long-term performance of composite-reinforced weld zones under cyclic pressure variations. This extension would provide essential insights into the service life of repaired structures and strengthen the practical relevance of the proposed repair approach.

References

Aabid, A., Bin Rosli, M. and Hrairi, M . 2025 . Enhancing repair of cracked plate using fiber-reinforced composite patch: Experimental and simulation analysis, *Forces in Mechanics*, 18, p. 100302. Available at: https://doi.org/10.1016/j.finmec.2024.100302

Abduljabbar, A., Khazal, H. and Hassan, A.K.F. 2022 .Experimental study on repair of cracked pipe under internal pressure , *Periodicals of Engineering and*

Natural Sciences (PEN), 10(6), pp. 67–76. Available at: http://dx.doi.org/10.21533/pen.v10i6.3369

Abdulla, M., Hrairi M., Aabid, A. and Abdullah, N. 2024 .Influence of adhesive curing temperature and geometrical parameters on composite patch repair of cracked structures , *Journal of Advanced Research in Fluid Mechanics and Thermal Sciences,* 119(1), pp. 1–12. Available at: https://doi.org/10.37934/arfmts.119.1.112

Adediran, I., Fritz, J. and Truster, T. 2025. Comparative analysis of different adhesive model representations in single lap joints using finite element analysis, *Applied Sciences*, 15(5). Available at: https://doi.org/10.3390/app15052661

Al Shabibi, A., Aal Thani, I., Al Jahwari, F. and Goher, K. 2024. Failure analysis using finite element method of defective pipelines reinforced with composite repair system, *Petroleum Science and Technology*, pp. 1–19. Available at: https://doi.org/10.1080/10916466.2024.2384524

Alexander, C. 2007. Guidelines for repairing damaged pipelines using composite materials in *Nnational Aassociation of Ccorrosion Eengineering. NACE.* Availabel at: https://www.chrisalexander.com/wp-content/uploads/2020/05/8-5.pdf

Ali Ghaffari, M. and Hosseini-Toudeshky, H. 2013. Fatigue crack propagation analysis of repaired pipes with composite patch under cyclic pressure , *Journal of Pressure Vessel Technology*, 135(3), p. 031402. Available at: https://doi.org/10.1115/1.4023568

Ali, A.J., Toor, Z.S,. Shifa, M. and Manzoor, O. 2024. Root cause analysis of glass fiber-reinforced polymer composite pipe failed in marine environment*, Journal of Failure Analysis and Prevention*, 24(3), pp. 1351–1364. Available at: https://doi.org/10.1007/s11668-024-01926-6

Baghban, A. and Yousefikhoshbakht, M. 2022. A mathematical model for planning oil products distribution via pipeline, arXiv preprint arXiv:2203.15295. Available at: https://doi.org/10.48550/arXiv.2203.15295

Banea, M.D. and da Silva, L.F. 2009. Adhesively bonded joints in composite materials: an overview , Proceedings of the Institution of Mechanical Engineers, Part L*: Journal of Materials: Design and Applications*, 223(1), pp. 1–18. Available at: https://doi.org/10.1243/14644207JMDA219

Benkheira, A., Belhouari, M. and Gong, X.L. 2022 . Experimental and numerical study of the effect of debonding defect in composite patch repairs on composite plate , *Journal of Failure Analysis and Prevention*, 22(4), pp. 1669–1692. Available at: https://doi.org/10.1007/s11668-022-01455-0

Berkache, A., Lee, J. and Choe, E. 2021 . Evaluation of cracks on the welding of austenitic stainless steel using experimental and numerical techniques , *Applied Sciences*, 11(5), p. 2182. Available at: https://doi.org/10.3390/app11052182

Cao, Y., Chang, Q. and Zhen, Y. 2022. Numerical simulation of fracture behavior for the pipeline with girth weld under axial load, *Engineering Failure Analysis,* 136, p. 106221. Available at: https://doi.org/10.1016/j.engfailanal.2022.106221

Chan, P.H., Tshai, K,Y., Johnson, M. and Li, S.2015. Finite element analysis (FEA) modelling of fiber-reinforced polymer (FRP) repair in offshore risers , in Rehabilitation of Pipelines Using Fiber-reinforced Polymer (FRP) *Composites. Elsevier*, pp. 177–210. Available at: https://doi.org/10.1016/B978-0-85709-684-5.00009-6

Chang, Q., Cao, Y., Zhen, Y. and Fagen, L. 2023. Study on the effect of loading conditions on the fracture behavior of pipeline with girth weld , *International Journal of Pressure Vessels and Piping*, 203, p. 104940. Available at: https://doi.org/10.1016/j.ijpvp.2023.104940

Chen, J., Wang, H., Salemi, M. and Balagruru, P.N . 2021. Finite element analysis of composite repair for damaged steel pipeline , *Coatings,* 11(3), p. 301. Available at: https://doi.org/10.3390/coatings11030301

Chen, Y., Xie, Y., Wang, W. and Li, J. 2022. Failure analysis of weld cracking of gas gathering pipeline in dewatering station , *Journal of Engineering and Applied Science,* 69(1), p. 94. Available at: https://doi.org/10.1186/s44147-022-00131-2

Chen, Y., Feng, R. and Ruan, X. 2016 . Behaviour of steel-concrete-steel SHS X-joints under axial compression*, Journal of Constructional Steel Research*, 122, pp. 469–487. Available at: https://doi.org/10.1016/j.jcsr.2016.04.006

Cui, C., Bortot, P., Ortolani, M. and Martinez-Paneda, E. 2024. Computational predictions of hydrogen-assisted fatigue crack growth , *International Journal of Hydrogen Energy*, 72, pp. 315–325. Available at: https://doi.org/10.1016/j.ijhydene.2024.05.264

Davaripour, F., Roy, K. and Maghoul, P. 2022 .Application of CFRP wrap for reinforcing undamaged thin-walled pipe bends under thermal expansion loads*, Journal of Pipeline Systems Engineering and Practice*, 13(4), p. 04022040. Available at: https://doi.org/10.1061/(ASCE)PS.1949-1204.0000677

Deng, J., Zhou, G., Bordas, S., Xiang, C. and Cai, D. 2017. Numerical evaluation of buckling behaviour induced by compression on patch-repaired composites, *Composite Structures*, 168, pp. 582–596. Available at: https://doi.org/10.1016/j.compstruct.2016.12.071

Deng, J., Huang, W. and Cheng, X. 2025. Tensile properties of scarf-repaired composite laminates with bonding defects, *Applied Composite Materials,* 32(2), pp. 575–597. Available at: https://doi.org/10.1007/s10443-024-10286-1

Djendara, A.A., Khiari, M.A., Benzaama, A., and Bencherif, M. 2025. Study of heat-induced and residual stress patterns in stainless steel pipe welds, *Studies in Science of Science*, 43(2), pp. 219–234. Available at: https://doi.org/10.5281/zenodo.14967753

Dumitrescu, A., Minescu, M. Dinita, A, and Lambrescu, I.2021. Corrosion repair of pipelines using modern composite materials systems: A numerical performance evaluation*, Energies,* 14(3), p. 615. Available at: https://doi.org/10.3390/en14030615

Durmus, H., Kaman, M.O., Yanen, C. and Mustafa, A. 2025. Fracture behavior of cracked composite plates repaired with a patch under various loading

conditions , *Sādhanā,* 50(1), p. 15. Available at: https://doi.org/10.1007/s12046-025-02678-1

Fan, Y., Shuai, Y., Shuai, J., Zhang, T., Zhang, Y., Shi, L. and Shan, K. 2024. The effect of pipeline root weld microstructure on crack growth behaviour , *Engineering Failure Analysis*, 161, p. 108265. Available at: https://doi.org/10.1016/j.engfailanal.2024.108265

Feng, Q., Li, R., Nie, B., Liu, S., Zhao, L. and Zhang, H. 2016 . Literature review: Theory and application of in-line inspection technologies for oil and gas pipeline girth weld defection, *Sensors,* 17(1), p. 50. Available at: https://doi.org/10.3390/s17010050

Goland, M. and Reissner, E. 1944. The stresses in cemented joints . *Journal of Applied Mechanics*, 11(1), pp.A17–A27. Available at: https://doi.org/10.1115/1.4009336

Guessab, A., Slamene, A., Hamza, B. and Mokhtari, M. 2025. Localized heat treatment and XFEM-based investigation of damage mechanisms in reinforced notched plates under uniaxial tensile stress, *Mechanics of Advanced Materials and Structures,* 32(5), pp. 826–840. Available at: https://doi.org/10.1080/15376494.2024.2356073

Guo, L., Wang, J., Wu, S. and Zhong, L. 2019. Experimental investigation and analytical modelling of blind bolted flush or extended end plate connections to circular CFDST columns, *Engineering Structures*, 192, pp. 233–253. Available at: https://doi.org/10.1016/j.engstruct.2019.04.053

Guo, L., Wang, L., Wang, L., Wu, M., Pan, T., Xiao, H., Qiao, N. and Li, X. 2024. Failure analysis of fillet weld crack in linepipe , *Materials Technology*, 39(1), p. 2366745. Available at: https://doi.org/10.1080/10667857.2024.2366745

Hartquist, C., Wang, S., Cui, Q., Matsuki, W., Deng, B. and Zhao, X. 2025. Scaling law for intrinsic fracture energy of diverse stretchable networks', *Physical Review X,* 15(1), p. 011002. Available at: https://doi.org/10.1103/PhysRevX.15.011002

Hirose, Y., Matsuda, H., Matsubara, G., Masaki, H., Yoshida, K. and Inamura, F. 2013. Numerical analysis of splice-type crack arrester with a filler under mode-I type loading , *Composite Structures*, 100, pp. 127–134. Available at: https://doi.org/10.1016/j.compstruct.2012.12.045

Irwin, G.R. 1957. Analysis of stresses and strains near the end of a crack traversing a plate. *Journal of Applied Mechanics*, 24(3), pp.361–364.Available at: https://doi.org/10.1115/1.4011547

Karmakov, S., Cepero-Mejías, F. and Curiel-Sosa, J. 2020. Numerical analysis of the delamination in CFRP laminates: VCCT and XFEM assessment, *Composites Part C: Open Access*, 2, p. 100014. Available at: https://doi.org/10.1016/j.jcomc.2020.100014

Klass, A.B. and Meinhardt, D. 2014. Transporting oil and gas: US infrastructure challenges, *Iowa Law Review*, 100, p. 947. Available at: https://ssrn.com/abstract=2410977

Krueger, R. 2004. Virtual crack closure technique: History, approach, and applications', *Applied Mechanics Reviews*, 57(2), pp. 109–143. Available at: https://doi.org/10.1115/1.1595677

Kumar, V. and Singh, A. 2025. Investigation of mode I fatigue crack growth in CFRP-aluminium adhesive joints: Effects of loading protocols, fiber bridging, and similitude parameters, *Engineering Fracture Mechanics*, 319, p. 111010. Available at: https://doi.org/10.1016/j.engfracmech.2025.111010

Lai, H., Fan, D. and Liu, K. 2022. The effect of welding defects on the long-term performance of HDPE pipes, *Polymers,* 14(19), p. 3936. Available at: https://doi.org/10.3390/polym14193936

León-Henao, H., et al. 2024. Failure analysis of a welded 316L stainless-steel stack with premature damage due to stress-corrosion cracking , *Journal of Failure Analysis and Prevention,* 24(6), pp. 2683–2699. Available at: https://doi.org/10.1007/s11668-024-01990-y

Leski, A. 2007. Implementation of the virtual crack closure technique in engineering FE calculations , *Finite Elements in Analysis and Design*, 43(3), pp. 261–268. Available at: https://doi.org/10.1016/j.finel.2006.10.004

Li, Z., Jiang, X., Hopman, H., Zhu, L. and Liu, Z. 2020. External surface cracked offshore steel pipes reinforced with composite repair system subjected to cyclic bending: An experimental investigation, *Theoretical and Applied Fracture Mechanics,* 109, p. 102703. Available at: https://doi.org/10.1016/j.tafmec.2020.102703

Lim, K.S., Azraai, S., Yahaya, N., Noor, N.M., Zardasti, L. and Kim, J.H. 2019. Behaviour of steel pipelines with composite repairs analysed using experimental and numerical approaches, *Thin-Walled Structures*, 139, pp. 321–333. Available at: https://doi.org/10.1016/j.tws.2019.03.023

Liu, J., Qin, M., Zhao, Q., Chen, L., Liu, P. and Gao, J. 2017. Fatigue performances of the cracked aluminum-alloy pipe repaired with a shaped CFRP patch, *Thin-Walled Structures*, 111, pp. 155–164. Available at: https://doi.org/10.1016/j.tws.2016.11.008

Ma, Q., Tian, G., Zeng, Y., Li, R., Song, H., Wang, Z., Gao, B. and Zeng, K. 2021. Pipeline in-line inspection method, instrumentation and data management, *Sensors,* 21(11), p. 3862. Available at: https://doi.org/10.3390/s21113862

Madenci, E., Özkılıç, Y.O. and Gemi, L. 2020. Experimental and theoretical investigation on flexure performance of pultruded GFRP composite beams with damage analyses , *Composite Structures,* 242, p. 112162. Available at: https://doi.org/10.1016/j.compstruct.2020.112162

Mandal, T.K., Parker, J., Gagliano, M. and Martinez-Paneda, E. 2024. Computational predictions of weld structural integrity in hydrogen transport pipelines, *International Journal of Hydrogen Energy.* Available at: https://doi.org/10.1016/j.ijhydene.2024.01.258

Medjdoub, S.M., Bouiadjra, B.B. and Abdelkader, M. 2018. Effect of the geometrical parameters on the efficiency of bonded composite wrap for repairing cracked pipes, *Strength, Fracture and Complexity*, 11(4), pp. 309–317. Available at: https://doi.org/10.3233/SFC-180232

Meniconi, L.C., Freire, J.L., Vieira, R.D, and Diniz, J.L. 2002. Stress analysis of pipelines with composite repairs, *in International Pipeline Conference*. Available at: https://doi.org/10.1115/IPC2002-27372

Mohammadi, S., Yousefi, M. and Khazaei, M. 2021. A review on composite patch repairs and the most important parameters affecting its efficiency and durability, *Journal of Reinforced Plastics and Composites*, 40(1–2), pp. 3–15. Available at: https://doi.org/10.1177/0731684420941602

Mohammed, B., Noureddine, M. and Youcef, M.A. 2025. Numerical optimization by the PFEMCT-SIF method of the crack propagation of a linear elastic material, *Vojnotehnički glasnik*, 73(1), pp. 136–161. Available at: https://doi.org/10.5937/vojtehg73-52739

Mousa, S., et al. 2023. The efficiency of advanced polymeric composite sleeves in the rehabilitation of cracked pipelines under combined loadings , *Journal of Materials Research and Technology*, 25, pp. 6395–6406. Available at: https://doi.org/10.1016/j.jmrt.2023.07.078

Nasiri, S. and Khosravani, M.R. 2023. Failure and fracture in polyethylene pipes: Overview, prediction methods, and challenges*, Engineering Failure Analysis,* 152, p. 107496. Available at: https://doi.org/10.1016/j.engfailanal.2023.107496

Ngabonziza, Y., Ergun, H., Kuznetsova, R., LI, J., Liaw, B., Delal, F. & Chang, J. 2010. An experimental study of self-diagnosis of interlaminar damage in carbon-fiber composites. *Journal of Intelligent Material Systems and Structures,* 21**,** 233-242.available at: https://doi.org/10.1177/1045389X09347019

Patrick, A.J. 2004 . Composites—case studies of pipeline repair applications, *Pigging Products and Services Association*, 12. Available at: https://ppsa-online.com/papers/2004-London-8-Patrick.pdf

Pengchao, C. 2025. Advancements and future outlook of safety monitoring, inspection and assessment technologies for oil and gas pipeline networks , *Journal of Pipeline Science and Engineering Journal of Pipeline Science and Engineering*. Available at: https://doi.org/10.1016/j.jpse.2025.100267

Qu, H.J., Tao, F., Gu, N., Montoya, T., Taylor, J.M., Schaller, R.F., Schindelholz, E. and Wharry, J.P. 2022 .Crystallographic effects on transgranular chloride-induced stress corrosion crack propagation of arc welded austenitic stainless steel , *npj Materials Degradation*, 6(1), p. 43. Available at: https://doi.org/10.1038/s41529-022-00252-2

Saeedi, A., Motavalli, M. and Shahverdi, M. 2024. Recent advancements in the applications of fiber-reinforced polymer structures in *railway industry—A review, Polymer Composites,* 45(1), pp. 77–97. Available at: https://doi.org/10.1002/pc.27817

Said, J.M., Abdul Rahman, N.L., Jumahat, A., Zahib, Z.M. and Iman Mahadzir, M.Z. 2025. Hydrostatic pressure analysis of yarn composites patch for PVC pipes, *Journal of Mechanical Engineering,* 22(1). Available at: https://doi.org/10.24191/jmeche.v22i1.2921

Savari, A. 2022. Failure analysis of composite repaired pipes subjected to internal pressure , *Journal of Reinforced Plastics and Composites,* 41(19–20), pp. 745–764. Available at: https://doi.org/10.1177/07316844211070545

Shafaee Fallah, A., Sadeghian, M. and Golmakani, M.E. 2023 .Experimental and numerical study on the strength of repaired steel pipes with composite patches under internal pressure , *Mechanics of Advanced Composite Structures,* 10(2), pp. 437–448. Available at: https://doi.org/10.22075/macs.2023.29108.1459

Sontti, S.G. and Zhang, X. 2023. Numerical insights from a population balance model into the distribution of bitumen residues in industrial horizontal pipes during the hydrotransport of oil sands tailings , *Industrial & Engineering Chemistry Research,* 63(1), pp. 691–705. Available at: https://doi.org/10.1021/acs.iecr.3c03140

Soutis, C. and Hu, F. 1997. Design and performance of bonded patch repairs of composite structure , *Proceedings of the Institution of Mechanical Engineers, Part G: Journal of Aerospace Engineering*, 211(4), pp. 263–271. Available at: https://doi.org/10.1243/0954410971532668

Srilakshmi, R. 2014. Experimental and numerical investigation of adhesively bonded composite patch repair of an inclined center cracked aluminium panel under static and fatigue load . *Department of Mechanical and Aerospace Engineering.* Available at: https://raiith.krc.iith.ac.in/handle/123456789/54450

Stapley, G. 2025. Desiccation shrinkage and cracking modelling of expansive soil using XFEM . *Queensland University of Technology.* Available at: https://doi.org/10.5204/thesis.eprints.255411

Thakur, H.K. and Prasad, G. 2024 .Mode 1, Mode II, and mixed Mode I/II fracture behavior of laminated structures , in *Fracture Behavior of Nanocomposites and Reinforced Laminate Structures. Springer,* pp. 123–155. Available at: https://doi.org/10.1007/978-3-031-68694-8_6

Tian, D., Gong, Y., Li, Z., Zou, L., Zhang, J., Zhao, L. and Hu, N. 2025. A new analytical method for determining J-integral–crack opening displacement curve of DCB specimen with large scale fiber bridging, *Engineering Fracture Mechanics,* 321, p. 111121. Available at: https://doi.org/10.1016/j.engfracmech.2025.111121

Wei, Y., Jin, X., Luo, Q., Li, Q. and Sun, G. 2024. Adhesively bonded joints—a review on design, manufacturing, experiments, modeling and challenges, *Composites Part B: Engineering,* 276, p. 111225. Available at: https://doi.org/10.1016/j.compositesb.2024.111225

Yu, Z., Zhang, J., Shen, J, and Chen, H. 2021. Simulation of crack propagation behavior of nuclear graphite by using XFEM, VCCT and CZM methods , *Nuclear Materials and Energy,* 29, p. 101063. Available at: https://doi.org/10.1016/j.nme.2021.101063

Zarrinzadeh, H., Kabir, M. and Deylami, A. 2017. Crack growth and debonding analysis of an aluminum pipe repaired by composite patch under fatigue loading, *Thin-Walled Structures,* 112, pp. 140–148. Available at: https://doi.org/10.1016/j.tws.2016.12.023

Zarrinzadeh, H., Kabir, M. and Deylami, A. 2017. Experimental and numerical fatigue crack growth of an aluminium pipe repaired by composite patch, *Engineering Structures,* 133, pp. 24–32. Available at: https://doi.org/10.1016/j.engstruct.2016.12.011

Zhou, W., Ji, X.L., Yang, S., Liu, J. and Ma, L.H. 2021. Review on the performance improvements and non-destructive testing of patches repaired composites, *Composite Structures,* 263, p. 113659. Available at: https://doi.org/10.1016/j.compstruct.2021.113659

Optimizacija popravke zavarenih cevovoda sa površinskim pukotinama pomoću kompozitnog omota zasnovana na metodi konačnih elemenata: uticaj geometrije, svojstava adheziva i unutrašnjeg pritiska na ponašanje pukotine u modu I

Nedir Hachemi[a], **autor za prepisku**, *Noureddine* Mahmoudi[b], *Foudil* Khelil[a], *Abed* Bouadi[c], *Youcef* Moulai Arbi[a]

[a] University of Mustapha Stambouli, Laboratory of Quantum Physics of Matter and Mathematical Modeling (LPQ3M), Mascara, People's Democratic Republic of Algeria

[b] University of Saida Dr. Moulay Tahar, Faculty of Technology, Department of Civil Engineering and Hydraulics, Saida, People's Democratic Republic of Algeria

[c] University of Mustapha Stambouli, Mascara, People's Democratic Republic of Algeria

OBLAST: mašinstvo, materijali
KATEGORIJA (TIP) ČLANKA: originalni naučni rad

*Sažetak***:**

Uvod/cilj: Strukturni integritet cevovoda pod pritiskom često je ugrožen pojavom površinskih pukotina, naročito u zavarenim zonama. Ovaj rad ispituje efikasnost ojačanja kompozitnim omotom pri sanaciji dužinskih polueliptičnih pukotina u zavarenim čeličnim cevovodima izloženim unutrašnjem pritisku. Iako uticaji okoline poput temperature, vlage i hemijskog dejstva nisu modelovani, isti su prepoznati kao ključni faktori koji utiču na dugoročnu izdržljivost kompozitnih popravki.

Metode: Razvijen je trodimenzionalni model konačnih elemenata za zavareni cevovod (spoljašnji prečnik = 1016 mm, debljina = 12,8 mm) sa spoljašnjom polueliptičnom pukotinom (2c = 10,24 mm, a = 2,56 mm). Tehnika virtuelnog zatvaranja pukotine primenjena je za proračun faktora intenziteta napona u modu I pod dejstvom unutrašnjih pritisaka u opsegu od 2 do 12 MPa. Parametarskom analizom ispitan je uticaj dužine omota (100–400 mm), njegove debljine (6–12 mm) i obuhvatnog ugla oko cevi (30°–360°), kao i modula smicanja adheziva, njegove debljine i efekata odlepljivanja.

Rezultati: Povećanje dužine, debljine i obuhvatnog ugla omota dovelo je do smanjenja faktora intenziteta napona, čime je poboljšano ublažavanje

oterećenja u vrhu pukotine. Veći modul smicanja adheziva poboljšao je prenos opterećenja na interfejsu, dok je prevelika debljina adhezivnog sloja smanjila efikasnost popravke. Lokalizovano odlepljivanje adheziva značajno je povećalo faktore intenziteta napona pod pritiskom, ukazujući na veliku osetljivost učinka popravke na kvalitet vezivanja lepka.

Zaključak: Rad pruža smernice za projektovanje i optimizaciju kompozitnih ojačanja pri sanaciji zavarenih cevovoda. Iako je u radu analiziran pravougaoni omot, buduća istraživanja bi trebalo da obuhvate alternativne geometrijske oblike u cilju smanjenja koncentracije opterećenja na ivicama, kao i da uzmu u obzir uticaje okoline i zamora materijala radi pouzdanije dugoročne procene.

Ključne reči: popravka cevovoda zavarivanjem, ojačanje kompozitnim omotom, faktor intenziteta napona (FIN), širenje pukotine, metoda konačnih elemenata (MKE).

Paper received on: 27 May 2025.
Manuscript corrections submitted on: 17 August 2025.
Paper accepted for publishing on: 8 September 2025.

© 2026 The Authors. Published by Vojnotehnički glasnik / Military Technical Courier (www.vtg.mod.gov.rs).This article is an open access article distributed under the terms and conditions of the Creative Commons Attribution license (http://creativecommons.org/licenses/by/4.0/rs/

Organic geochemical assessment of black shales: case study of Oued Soura, Tamtret region, Algeria

Abdelghani Kadou[a], *Boudjema* Rebhi[b]

[a] University Tahri Mohammed,
Laboratory of Chemistry and Environmental Science, Béchar, Algeria;
e-mail: kadouabdelghani@gmail.com,
ORCID iD: https://orcid.org/0009-0004-8053-4455

[b] University Tahri Mohammed,
Laboratory of Chemistry and Environmental Science, Béchar, Algeria;
e-mail: rebhibouj@gmail.com,
ORCID iD: https://orcid.org/0009-0002-6793-1603

https://doi.org/10.5937/vojtehg74-59070

FIELD: organic geochemistry, petroleum geology, sedimentology, geochemical characterization, unconventional hydrocarbon exploration, shale gas and oil, thermal maturity analysis, source rock evaluation, energy resources, stratigraphy
ARTICLE TYPE: original scientific paper

Abstract:

Introduction/purpose: Black shales are increasingly recognized as significant unconventional hydrocarbon sources due to their organic richness and potential for oil and gas generation. However, their complex geochemical nature, especially in underexplored regions such as Tamtert in southwestern Algeria, poses challenges to accurate evaluation. This study aims to assess the hydrocarbon potential of black shales from the Djebel-Zereg area using advanced organic geochemical methods.

Methods: Five black shale samples were collected from Djebel-Zereg, Tamtert region. Total Organic Carbon (TOC) content was determined, and Rock-Eval 6 pyrolysis and elemental analysis were conducted. Parameters measured included TOC, S1, S2, Tmax, Hydrogen Index (HI), Oxygen Index (OI), and vitrinite reflectance (Ro), providing data on organic matter type, thermal maturity, and hydrocarbon generative capacity.

Results: TOC values ranged from 0.51 to 2 wt.% with an average of 1.33 wt.%, indicating acceptable to very good source rock quality. S2 values ranged from 0.45 to 4 mg HC/g rock, and the average Production Index (PI) was 2.23. HI values (51–233 mg HC/g TOC), along with OI and Tmax, indicated the presence of type II and III kerogen, suggesting

ACKNOWLEDGMENT: The authors would like to extend their sincere gratitude to Eng. Boualem Ikhlef for his invaluable support and assistance in conducting the analyses, which greatly contributed to the success of this study.

potential for both oil and gas generation. Tmax values (435–465°C, average 447°C) and vitrinite reflectance (0.68%–1.19%) confirmed thermal maturity. A positive correlation between TOC and S1 values supported the presence of indigenous hydrocarbons.

Conclusion: The integrated geochemical approach confirms that the Djebel-Zereg black shales are thermally mature, organic-rich rocks with promising oil shale potential. These findings support further exploration and development of unconventional hydrocarbon resources in the Tamtert region.

Keywords: Black shale, Djebel-Zereg, elemental analysis, hydrocarbon potential, organic matter, Rock-Eval pyrolysis, source rock evaluation, total organic carbon.

Introduction

The growing demand for energy has made unconventional hydrocarbon resources, particularly black shale, a key focus of exploration efforts (Feng et al., 2024; Qin et al., 2022). These formations, rich in organic matter have the potential to generate significant amounts of oil and gas through thermal and biological processes (Zhao et al., 2022). However, assessing the hydrocarbon potential of black shale requires accurate and effective geochemical methods to evaluate organic richness, thermal maturity, and generative capacity (Carvajal-Ortiz & Gentzis, 2015; Liu et al., 2022). Traditional methods for evaluating black shale typically involve geochemical tools such as kerogen analysis, bitumen extraction, and Ro measurement. These methods have been used for decades to estimate the organic content and thermal maturity of shales (Hackley & Cardott, 2016). However, they often fall short in providing a complete picture of the shale's potential, particularly in terms of spatial heterogeneity and the complexity of organic matter composition. For instance, bitumen extraction may not fully account for the variation in organic matter types within a shale formation, while vitrinite reflectance primarily estimates maturity but does not provide in-depth insights into the generation capacity of the shale (Hackley et al., 2021).

In this context, we intend to review some recent related work in an attempt to more clearly identify research gaps, thereby setting the stage to highlight and justify the contributions of this study. Furthermore, by situating our analysis within both the specific geographical distinctions of Tamtert and the broader methodological landscape, we aim to demonstrate how this work not only addresses unresolved challenges but also offers a novel

perspective that enhances the current body of knowledge. This dual emphasis on regional specificity and methodological innovation reinforces the relevance and necessity of our approach. For instance, in (Akintola, 2023), authors proposed a systematic evaluation of unconventional shale gas reservoirs in Permian Bini River Formation of Gongola Sub-basin, Northern Benue Trough, Northeastern Nigeria, focusing on shale lithologies as the primary material of interest. They employed a combination of petrographic, mineralogical (X-ray diffraction), and geomechanical (i.e., uniaxial compressive strength and Schmidt rebound hardness tests) methods to characterize the shale's mineral composition, textural features, and mechanical properties. The study's main advantages lie in its detailed site-specific analysis, which provides foundational insights into the mechanical suitability and frackability of the shales for unconventional resource development, particularly in a relatively underexplored region. However, the study's limitations arise from its exclusion of more comprehensive geochemical assessments that would provide a fuller understanding of the shale's hydrocarbon generation potential, thermal history, and elemental distribution, parameters that are critical for more robust reservoir characterization and resource estimation. The authors in (Chabalala et al., 2023), evaluated the thermal maturity of black shale samples from the Karoo Basin in South Africa using traditional petrographic techniques and Raman spectroscopy. The materials studied include shale samples from Ripon, Whitehill, Collingham, and Prince Albert Formations of the Karoo Supergroup, as well as comparative samples from the Berea Sandstone project in the USA. The methods employed were organic petrology, including Ro and maceral analysis, programmed pyrolysis, and Raman spectroscopy. A key advantage of this study is its integration of Raman parameters with vitrinite reflectance to offer a more detailed understanding of molecular transformations in overmature shales, thereby enhancing thermal maturity assessments. However, the study's limitation lies in its lack of broader geochemical profiling techniques that could provide a more holistic view of the shale's hydrocarbon generative capacity, organic content variability, and elemental composition, which are factors essential for comprehensive resource evaluation. In (Zhang et al., 2024), authors investigated the geochemical properties and gas-bearing characteristics of lower Cambrian black shales, specifically from the Niutitang, Wunitang, and Liuchapo Formations, in Western Hunan Province, China. Utilizing core samples from the

XAD1 exploratory well, they employed a combination of geochemical techniques including TOC analysis, Rock-Eval pyrolysis, bitumen reflectance, Soxhlet extraction, and GC-MS, complemented by Grand Canonical Monte Carlo (GCMC) molecular dynamics simulations to model methane adsorption under varying geological conditions. A key strength of the study is its integration of burial history reconstruction with advanced adsorption simulations, which allowed for a dynamic understanding of how tectonic events and changes in temperature and pressure influenced shale gas enrichment and loss over geological time. However, the work is limited by its relatively narrow analytical focus, as it omits a broader set of geochemical tools that could offer more comprehensive insights into the shale's organic richness, maturity evolution, and elemental composition, factors that are critical for a fuller evaluation of shale gas potential. In (Gao et al., 2024), the authors developed a comprehensive analysis of the geochemical characteristics and shale oil occurrence in Qingshankou Formation, Gulong Sag, Songliao Basin, focusing on mature to high-maturity shale resources. The materials discussed include shale samples from Qingshankou Formation, analyzed for TOC, Rock-Eval pyrolysis parameters, Ro, kerogen elemental composition, chloroform asphalt A, and Gas Chromatography (GC) to evaluate organic matter abundance, type, and maturity. The methods employed involve Rock-Eval pyrolysis, TOC determination, Ro measurements, kerogen carbon isotope analysis, and biomarker studies to assess shale oil occurrence and sweet spot evaluation. The advantages of this study lie in its systematic approach to correcting light-hydrocarbon loss and heavy hydrocarbons, providing a more accurate representation of in-situ retained hydrocarbons, and establishing geochemical criteria for sweet spot identification. However, limitations include the reliance on specific analytical techniques that may not fully capture the heterogeneity of organic matter or the broader geochemical context, potentially overlooking variations in thermal maturity and elemental composition that could further refine the evaluation of shale oil potential. In (Shi et al., 2024), the authors investigated the sedimentary paleoenvironment and organic matter enrichment mechanisms in Ying 4 Member of southern Shuangcheng area, Songliao Basin, focusing on black laminated and massive mudstone samples. The materials discussed include source rocks characterized by TOC content, kerogen types, and trace elements such as Sr, Cu, Ba, V, Ni, and P, which were used to infer paleoclimate, paleosalinity, redox conditions, and pale-

oproductivity. The methods employed encompassed organic carbon content measurement, kerogen microscopic examination, Rock-Eval pyrolysis, Ro analysis, and major/trace element geochemistry to reconstruct the sedimentary environment and identify controlling factors of organic matter enrichment. The advantages of this study lie in its integrated approach, combining multiple geochemical proxies to establish a productivity model for organic matter enrichment, highlighting the role of warm, humid paleoclimate and volcanic activity in enhancing lake productivity. However, limitations include the reliance on specific elemental ratios and localized sampling, which may not fully capture the broader geochemical variability or the interplay of additional factors such as sedimentation rates or diagenetic alterations that could further refine the understanding of organic matter preservation and distribution.

Table 1 in this case summarizes the key aspects of each study, highlighting their materials, methods, advantages, and limitations while maintaining a focus on geochemical gaps.

Table 1 – Comparative analysis of shale reservoir studies: materials, analytical methods, strengths, and research gaps

Ref.	Year	Materials	Methods	Advantages	Limitations (Gaps)
(Akintola, 2023)	2022	Shale lithologies from Permian Bini River Formation, Gongola Sub-basin, Nigeria	Petrographic, mineralogical (XRD), geomechanical (uniaxial compressive strength, Schmidt rebound hardness)	Detailed site-specific analysis; foundational insights into mechanical suitability and frackability	Lacks comprehensive geochemical assessments (hydrocarbon potential, thermal history, elemental distribution)
(Chabalala et al., 2023)	2023	Black shale samples from Karoo Basin (Ripon, Whitehill, Collingham, Prince Albert Formations), Berea Sandstone (USA)	Organic petrology (vitrinite reflectance, maceral analysis), programmed pyrolysis, Raman spectroscopy	Integration of Raman with vitrinite reflectance for molecular-level thermal maturity assessment	Limited broader geochemical profiling (hydrocarbon generation, organic content variability, elemental composition)
(Zhang et al., 2024)	2024	Lower Cambrian black shales (Niutitang, Wunitang, Liuchapo Formations), XAD1 well, Western Hunan, China	TOC, Rock-Eval pyrolysis, bitumen reflectance, Soxhlet extraction, GC-MS, GCMC molecular dynamics simulations	Burial history + adsorption modeling for dynamic gas enrichment insights	Narrow analytical focus; lacks broader geochemical tools (organic richness, maturity evolution, elemental composition)
(Gao et al., 2024)	2024	Shale samples from Qingshankou Formation, Gulong Sag, Songliao Basin	Rock-Eval pyrolysis, TOC, vitrinite reflectance, kerogen isotopes, chloroform asphalt "A," biomarker studies	Corrects light-hydrocarbon loss; establishes sweet spot criteria	Overlooks broader geochemical context (thermal maturity, elemental composition heterogeneity)
(Shi et al., 2024)	2024	Black laminated/massive mudstone (Ying 4 Member), southern Shuangcheng area, Songliao Basin	TOC, kerogen microscopy, Rock-Eval, Ro, major/trace element geochemistry	Integrated proxies for productivity model; links paleoclimate/volcanism to enrichment	Relies on localized sampling/elemental ratios; misses sedimentation/diagenetic factors

To address these gaps, this work employs a refined geochemical toolkit, including TOC analysis, Rock-Eval pyrolysis, and elemental analysis, to deliver a more comprehensive and quantitative assessment of the black shale's hydrocarbon potential. These methods were selected because:

- TOC analysis provides direct measurement of organic richness, a metric often underreported in studies relying solely on Ro or petrography (Chabalala et al., 2023; Shi et al., 2024).
- Rock-Eval pyrolysis quantifies both hydrocarbon yield (S1, S2) and thermal maturity (T_{max}), addressing limitations in studies like (Gao et al., 2024) that lacked correction for light-hydrocarbon loss.
- Elemental analysis (e.g., Sr/Cu, V/Ni) deciphers paleoenvironmental controls on organic matter enrichment, a factor overlooked in localized studies (Shi et al., 2024).

This research targets the Djebel-Zereg region in southwestern Algeria, a previously unexplored basin within Wadi Saoura area (coordinates: X1 = 1° 49' 30", Y1 = 29° 54' 30"). As the first organic geochemical study in this region, it aims to:

- Assess energy production capacity by correlating TOC and Rock-Eval data with generative potential (cf. (Gao et al., 2024)).
- Delineate thermal maturity using pyrolysis and Ro, bridging gaps in overmature shale analyses (Chabalala et al., 2023).
- Evaluate paleoenvironmental influences (redox, productivity) via elemental ratios, expanding on models in (Shi et al., 2024).

Following such a methodological approach, the study attempts to fill regional knowledge gaps and also advances methodological rigor beyond prior works (Table 1), offering a template for understudied shale basins. The findings will directly inform sustainable hydrocarbon exploitation strategies in Algeria's Beni Abbas Basin.

The remainder of this paper is organized as follows: Section 2 outlines the materials and methods used, including the geological setting of the study area, the sampling process, and the geochemical analysis techniques applied, such as TOC, elemental analysis, and Rock-Eval pyrolysis. Section 3 presents the results and discussion, focusing on organic matter richness, quality, and thermal maturation, with insights into the hydrocarbon potential of the Djebel-Zereg black shale. Finally, Section 4 provides the conclusion, summarizing the findings and suggesting areas for further research.

Materials and methods

This section outlines the geological context of the study area and details the materials and analytical methods used to investigate the geochemical characteristics of the sampled black shales. The analyzed samples were collected from the upper Devonian 'Argiles de Marhouma' Formation, exposed in Djebel Zereg area near Tamtert in the Saoura Valley, southwestern Algeria. Understanding the stratigraphy and sedimentology of this formation is essential for interpreting the organic geochemistry and thermal maturity of its shales. This multidisciplinary approach combines field observations with laboratory analyses, including TOC, elemental composition, and Rock-Eval pyrolysis, to comprehensively characterize the depositional environment and hydrocarbon potential of the formation.

Geological setting

The Saoura Valley in southwestern Algeria extends from the Ouarourout region in the north to the Idhir area in the south. Bounded by the Hercynian Ougarta Mountains to the west and the expansive Great Western Erg to the east, the valley features well-exposed upper Devonian outcrops. Within this framework, the 'Argiles de Marhouma' Formation forms the principal unit of interest, lying stratigraphically below the 'Grès de Ouarourout' Formation. The Tamtert region, located centrally within the valley, provides excellent exposures of these formations, enabling detailed field observations and sampling, as shown in Figure 1 (Malti, 2012).

The 'Argiles de Marhouma' Formation has been subdivided into four lithologically and paleontologically distinct members, as depicted in the stratigraphic column of Figure 2 (adapted from (Malti, 2012)). These members reflect variable sedimentary environments and depositional dynamics over time. The lowermost member, cropping out exclusively in Gara Diba area, is composed of laminated limestones within a calcareous clay matrix. These fossiliferous limestones, which contain *Manticoceras* sp., mark the member as belonging to Frasnian I γ interval. Its restricted lateral distribution suggests localized depositional settings, potentially controlled by paleotopography or sediment supply limitations.

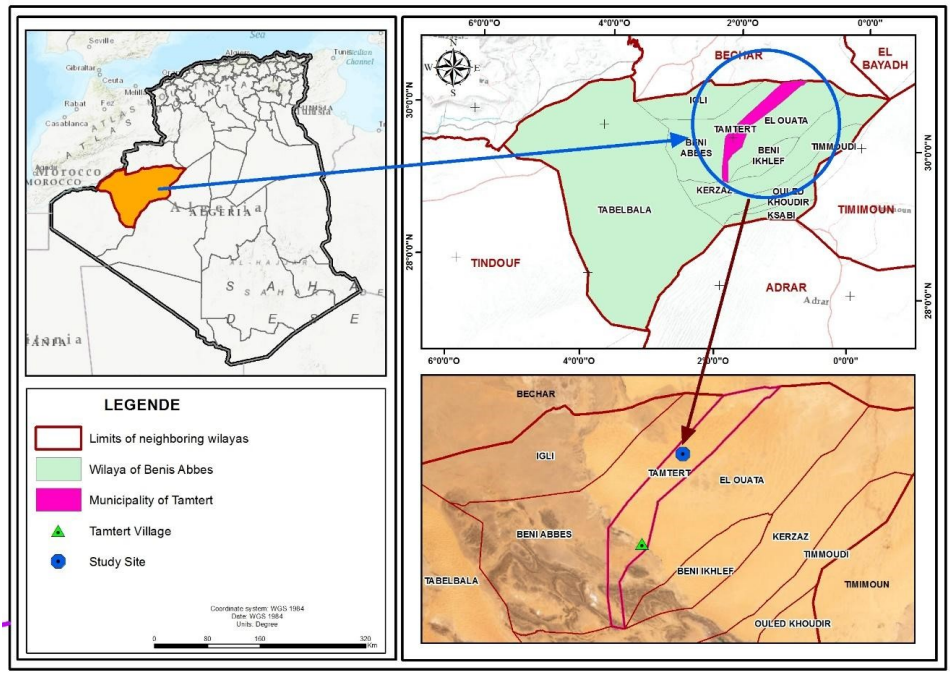

Figure 1 – Geographical location of the Tamtert region (Malti, 2012)

Above this lies a more heterogeneous unit composed predominantly of red clays with silty and calcareous intercalations. This member is subdivided into two segments. The first features thick, schistified red clays interbedded with thin flakes of silty sandstone, topped by a reddish micritic limestone. Beneath this lies a clay-rich interval punctuated by sporadic nodular limestone layers, including a prominent, weathered, nodular bed indicative of periodic carbonate deposition under oxidizing conditions. The second segment is composed primarily of clay enriched with hematitic 'griotte' limestone levels and capped by thin blue-gray limestone beds, the uppermost containing abundant fossil remains such as crinoid stems and bivalves. These lithological features point to changing sedimentation rates and intermittent oxygenation during deposition.

The third member is dominated by thick-bedded 'griotte' limestones alternating with greenish clays. Its base consists of slumped, dark clays with silty concretions, transitioning into distinctive limestone beds with spherical, ball-like structures similar to those of overlying Ouarourout Formation. The recurrence of these alternating lithologies, some with meter-scale thick-

ness, suggests periodic carbonate sedimentation, possibly influenced by sea-level fluctuations or regional climatic changes. The lithological diversity and slumping structures reflect a dynamic and unstable depositional setting.

The uppermost member, from which the samples for this study were taken, shows the greatest lithological variation. It consists of red and green clays with interspersed silty beds and discrete nodular levels of 'griotte' limestone. The lower portion includes red clays forming a trough-like structure interbedded with dark, organic-rich layers and small silty nodules. Higher up, the succession reaches a thickness of approximately 62 meters, comprising alternating greenish clays, silty terracotta horizons, and ferruginous nodular levels, likely recording redox fluctuations during deposition. The uppermost segment is a deeper clay-dominated trough with abundant greenish silts and scattered 'griotte' limestone nodules. These dark clays, rich in organic matter, were the target of geochemical sampling and analysis.

Together, the four members of the 'Argiles de Marhouma' Formation provide a record of shifting depositional environments in Saoura Basin during the late Devonian, capturing both marine incursions and periods of continental influence, as detailed in Figure 2.

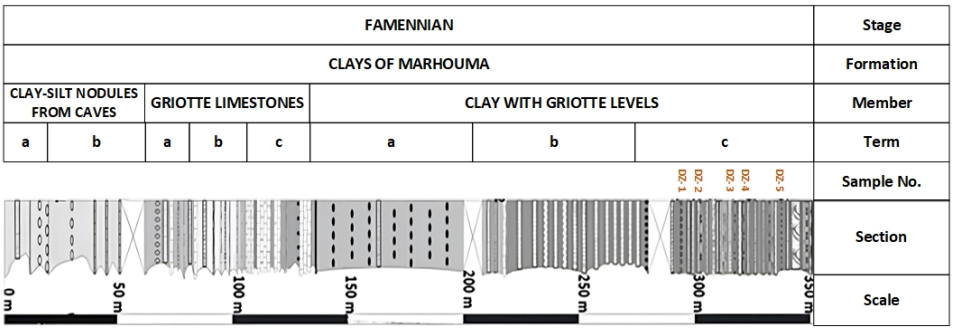

Figure 2 – Modified lithostratigraphic columnar section of 'Argiles de Marhouma' Formation in Saoura Valley (Tamtert-Zereg). Reproduced from (Malti, 2012)

Samples and methods

The methods used in this study are primarily geochemical techniques that provide insights into the organic content, hydrocarbon potential, and thermal maturity of shale samples. These methods rely on quantitative

measurements and data interpretation, involving both chemical and mathematical processes to extract meaningful geochemical information.

Elemental analysis

To better understand the geochemical characteristics and organic matter quality of the collected shale samples, elemental analysis was conducted as a foundational component of this study. This procedure enables a precise assessment of major elemental constituents, which is essential for interpreting the depositional environment and diagenetic evolution of organic-rich rocks.

Each shale sample was first ground to a fine powder (<80 μm) to ensure homogeneity and improve reaction efficiency during subsequent treatments. Bitumen extraction was then performed over a 60-hour period using a solvent mixture of 93% dichloromethane (DCM) and 7% methanol (MeOH). This step was critical for removing free hydrocarbons, thereby isolating the mineral matrix and kerogen-bound organic matter for more accurate elemental characterization. Following extraction, residual material was subjected to acid demineralization using 6N hydrochloric acid (HCl) and a 1:1 hydrofluoric acid (HF:HCl) mixture. This treatment dissolved carbonate and silicate phases, respectively, leaving behind the acid-insoluble organic fraction. Special care was taken during this step to minimize loss of organic material while ensuring complete removal of mineral content that could skew the elemental analysis.

Elemental composition was determined using a Thermo Finnigan EA1112 Flash Analyzer. Approximately 1 mg of the demineralized sample was encapsulated in a tin capsule and combusted in an oxygen-rich environment. The resulting gases (i.e., carbon dioxide (CO_2), water vapor (H_2O), nitrogen (N_2), and sulfur dioxide (SO_2)) were separated and quantified using a scatterometer detector system. The concentrations of carbon (C), hydrogen (H), nitrogen (N), and sulfur (S) were calculated from signal intensities, with calibration performed against certified reference standards to ensure analytical precision and accuracy.

Although the method is primarily chemical in nature, it incorporates quantitative analytical techniques to determine elemental concentrations. These values are fundamental in assessing the kerogen type, thermal maturity, and redox conditions of deposition, offering valuable insights into

both the paleoenvironment and hydrocarbon potential of the shale units studied.

Total organic carbon

In evaluating the hydrocarbon potential of sedimentary rocks, TOC content serves as a primary indicator of organic matter richness and preservation. As such, TOC analysis was carried out to complement elemental data and provide a more comprehensive understanding of organic geochemistry of the shale samples. Prior to TOC measurement, the finely powdered samples were subjected to acid treatment to eliminate any inorganic carbon (primarily carbonates) that could interfere with the analysis. This was achieved by using a diluted hydrochloric acid solution ($HCl:H_2O$ = 1:4), applied until effervescence ceased, indicating the complete removal of carbonate phases. The samples were then thoroughly rinsed with deionized water and dried to ensure accurate TOC determination without dilution or contamination.

The remaining material, containing only organic carbon, was analyzed using a LECO carbon analyzer that is a combustion-based system capable of high-precision carbon quantification. During the analysis, samples were oxidized at high temperatures in an oxygen-rich environment, and the evolved CO_2 was measured using an infrared detection system. The resulting signal was calibrated against known standards, ensuring the reliability and repeatability of the TOC values obtained. Although the overall procedure is relatively straightforward, TOC analysis is a critical quantitative technique in organic geochemistry. It reflects the abundance of preserved organic matter and provides input for the calculation of important indices, such as the HI and OI, when integrated with pyrolysis data. These parameters collectively inform interpretations of source rock quality, depositional conditions, and the potential for hydrocarbon generation.

Rock-Eval Pyrolysis

Rock-Eval pyrolysis is a well-established analytical technique used to evaluate the quantity, type, and thermal maturity of organic matter in sedimentary rocks. In this study, the method was employed to derive several geochemical parameters that are essential for classifying kerogen, assessing hydrocarbon-generating potential, and reconstructing depositional en-

vironments. Prior to analysis, the powdered and decarbonated samples were placed in a programmed pyrolysis chamber and gradually heated under an inert nitrogen atmosphere. This stepwise heating induces the thermal decomposition of organic constituents, allowing the quantification of various hydrocarbon fractions and associated gases.

The following primary outputs were obtained:

- S1: Represents the quantity of free hydrocarbons (in mg HC/g rock) that volatilize at low temperatures without cracking.
- S2: Measures hydrocarbons generated from the thermal breakdown of kerogen during progressive heating.
- Tmax: The temperature at which S2 peak occurs; used as a proxy for the thermal maturity of the organic matter.
- S3: Reflects the amount of CO_2 released during pyrolysis, related to oxygenated functional groups in the kerogen.

From these measurements, several critical geochemical indices were calculated:

- PI = S1 / (S1 + S2), indicating the extent of hydrocarbon generation.
- HI = (S2 / TOC) $\times$ 100, providing insight into the type and quality of organic matter.
- OI = (S3 / TOC) $\times$ 100, reflecting the relative oxygen content and depositional redox conditions.

These indices are instrumental in characterizing kerogen types (I, II, III, IV), assessing thermal evolution, and distinguishing between oil- and gas-prone source rocks. For instance, higher HI values typically indicate oil-generative potential, while OI can be used to infer the oxidative conditions under which the organic matter was deposited. The Rock-Eval procedure followed standard protocols as outlined in established methodologies (Espitalie et al., 1977; Peters & Cassa, 1994), ensuring consistency and comparability with previous studies. The analysis combines direct thermal measurements with mathematical interpretation, providing a multidimensional view of organic matter characteristics. The results, summarized in Table 2, form a cornerstone of the organic geochemical framework used in this study and serve as a basis for further interpretation of petroleum potential, thermal maturity trends, and paleoenvironmental reconstructions.

Table 2 – Results of TOC, Ro, and Pyrolysis data (Rock-Eval 6) analyses for Djebel-Zereg samples

Sample No	S1 (mg/g)	S2 (mg/g)	GP	S3 (mg/g)	TOC Wt.%	HI (mg/g)	OI (mg/g)	Tmax (°C)	R0	PI	C (wt%)	H (wt%)	H/C
1	0.57	0.62	1.19	0.56	0.51	125	114	455	1.03	0.68	20.12	0.59	0.35
2	0.05	0.45	0.50	0.02	0.92	51	22	445	0.85	0.10	35.52	2.04	0.68
3	0.20	3.48	3.68	0.10	1.50	233	8	436	0.68	0.05	55.25	5.06	1.21
4	0.76	4.00	4.76	0.16	2.00	192	8	440	0.76	0.15	54.12	2.68	0.59
5	0.20	1.05	1.05	0.39	0.75	140	52	464	1.19	0.16	49.27	2.81	0.68

Results and Discussion

This section presents and interprets the geochemical data obtained from elemental analysis, TOC measurements, and Rock-Eval pyrolysis to assess the hydrocarbon potential of Djebel-Zereg shale samples. The analysis focuses on key parameters such as organic matter richness, quality, and thermal maturity, each of which plays a critical role in determining the generative capacity of source rocks. The integration of these results allows for a comprehensive evaluation of the samples' suitability as petroleum source rocks and provides insights into the paleoenvironmental and diagenetic history of the organic matter. The discussion is structured into subsections to address each aspect in detail.

Organic Matter Richness

The richness of organic matter in black shale plays a critical role in assessing the hydrocarbon-generating potential of source rocks. For clastic shale source rocks to be effective, TOC value should exceed 0.5 weight percent. In this study, TOC values ranged from 0.51% to 2%, with an average of 1.33% (Table 2). This suggests that samples contain a substantial amount of organic matter capable of hydrocarbon generation. According to the classification system proposed by (Peters & Cassa, 1994; Landais, 1997), these TOC values range from fair to excellent, indicating the presence of a potentially viable source. However, reliance solely on TOC values to assess the generative capacity of source rocks can be misleading, as TOC measures both hydrocarbon-generative organic matter and inert organic matter, leading to an imprecise evaluation of rock potential (McCarthy et al., 2011).

To further evaluate the hydrocarbon potential, generative potential (GP), calculated as the sum of S1 (free hydrocarbons) and S2 (hydrocarbons generated from kerogen cracking), was assessed. GP values ranged from 0.50 to 4.76 mg/g (average 2.23 mg/g) (Table 2). According to (Tissot &

Welte, 1984), rocks with a GP of less than 2 mg/g are typically gas-prone or non-generative, whereas rocks with a GP between 2 and 6 mg/g exhibit moderate source rock potential, suggesting reasonable gas/oil generation. Samples with a GP greater than 6 mg/g are considered good source rocks. Based on these GP values and the HI versus TOC plot (Figure 3), samples 3 and 4 exhibit fair genetic potential with acceptable gas/oil presence, while the remaining samples are categorized as gas-producing rocks.

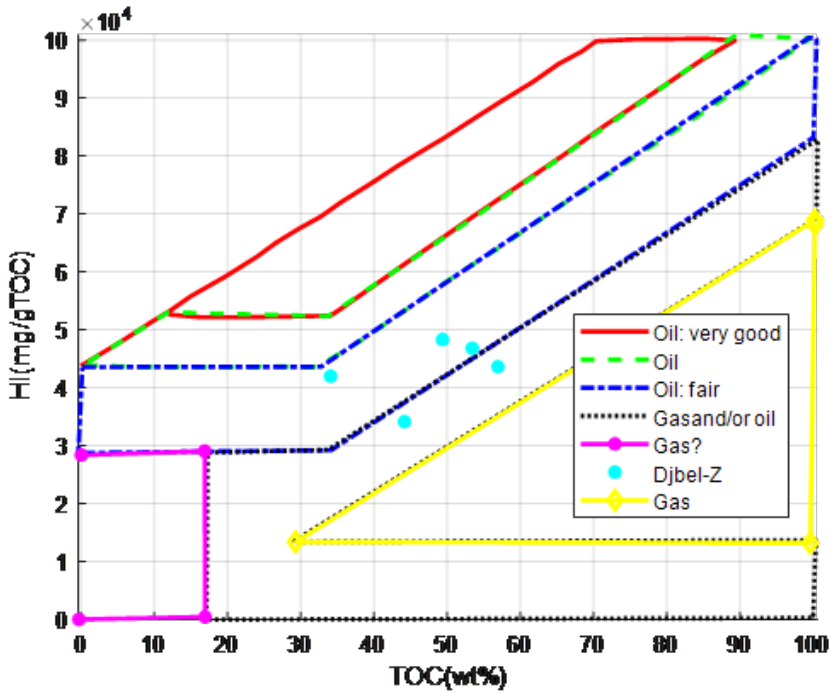

Figure 3 – Cross plot of HI versus TOC for Djebel-Zereg samples. Reproduced from (Sohail et al., 2024)

The migration index (S1/TOC) was calculated to distinguish migrating hydrocarbons from indigenous hydrocarbons. A high TOC with low S1 values suggests the presence of indigenous hydrocarbons (Landais, 1997). The S1 versus TOC plot (Figure 4) further confirms that the studied samples contain indigenous organic matter.

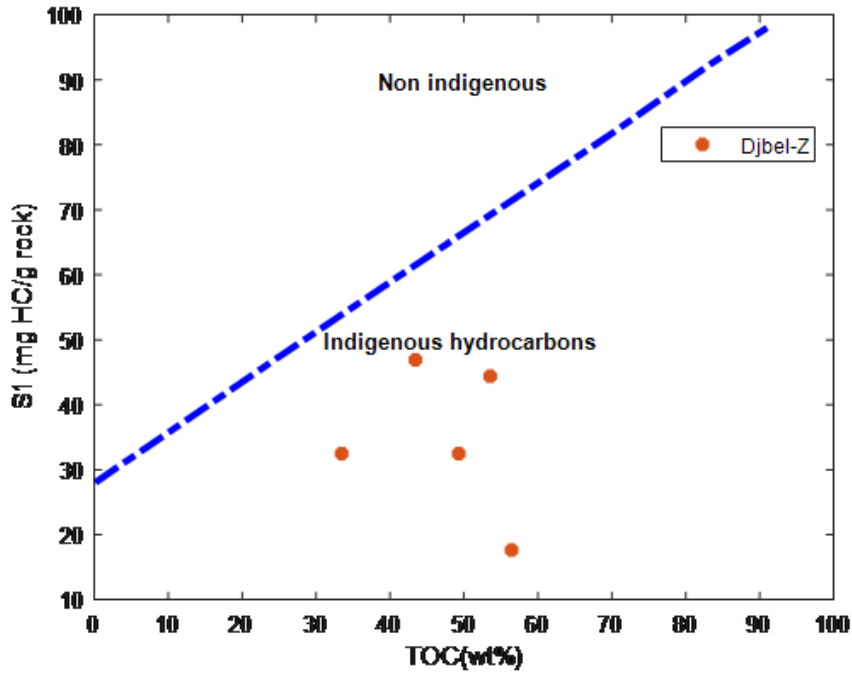

Figure 4 – Cross plot of S1 versus TOC for Djebel-Zereg samples. Reproduced from (Edress et al., 2022)

Organic Matter Quality

The hydrocarbon potential of source rocks depends on the richness of organic matter and on the type of organic materials present. The classification of organic matter is typically informed by HI and OI values. Organic materials with HI values below 150 mg/g correspond to type III organic matter, which is primarily gas-generative. HI values ranging from 150 to 300 mg/g suggest a mixture of type II and type III organic matter, indicating a significant gas generation capability with a minor oil component. HI values exceeding 300 mg/g indicate type II organic matter, which is particularly efficient in generating oil with lesser amounts of gas, while values exceeding 600 mg/g are typically associated with type I or II organic matter, both of which are potent oil producers (Waples, 1985).

In this study, HI values ranged from 50 to 233 mg/g, and OI values varied from 8 to 114 mg/g. These measurements suggest that the majority

of black shale samples are predominantly composed of type III and type II organic materials, indicating a preference for gas generation, with only trace amounts of oil. This finding is further supported by the HI vs. OI plot (Figure 5), which shows that the samples are predominantly composed of a mixture of type III and type II organic materials.

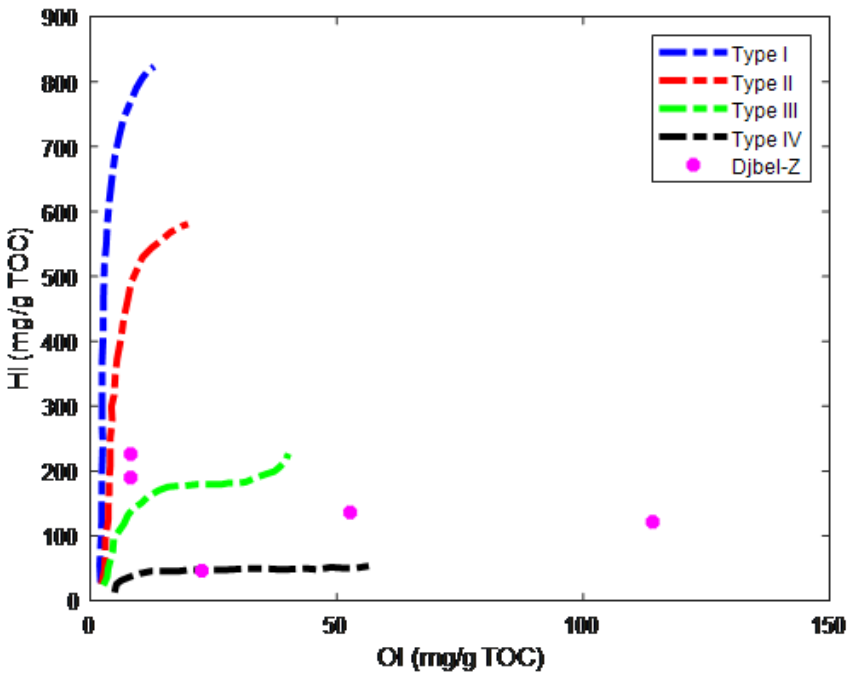

Figure 5 – Cross plot of HI versus OI for Djebel-Zereg samples. Reproduced from (Akinwumiju & Satterfield, 2024)

To refine the classification of organic materials present, H/C atomic ratio was also considered. The H/C ratio is a key factor in determining the quality of organic matter and, consequently, the hydrocarbon potential of source rocks. Organic matter is categorized into three types based on the H/C atomic ratio: type I and II organic matter with H/C ratios $\geq$1.5, type II organic matter with ratios between 1.2 and 1.5, and type III organic matter with ratios typically below 1.0. The H/C ratios in this study ranged from 0.35 to 1.21, with an average of 0.70, suggesting that the samples contain both

type III and type II organic materials. This further corroborates the potential for gas generation with minimal oil production.

3.3. Thermal Maturation Stage

Thermal maturity is an essential factor in evaluating the hydrocarbon potential of source rocks. It provides insight into the extent to which organic matter has been converted into hydrocarbons due to heat-driven processes (Peters & Cassa, 1994). The degree of thermal maturity can be evaluated using Tmax values obtained from Rock-Eval pyrolysis. In this study, Tmax values ranged from 436 to 464°C, with an average of 447°C, indicating that the organic matter in these samples has achieved early maturity. These values are typical for both oil and gas generation, as confirmed by the Tmax versus HI plot (Figure 6).

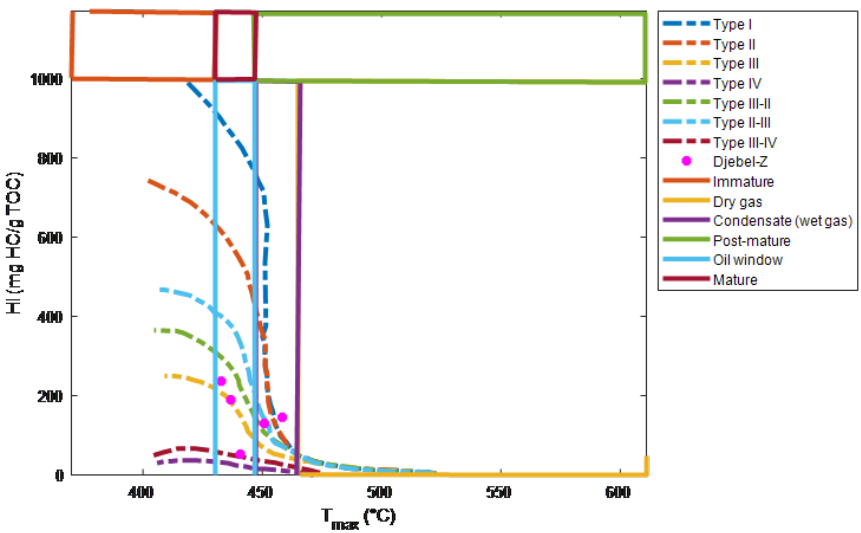

Figure 6 – Cross plot of (HI) versus (Tmax) for Djebel-Zereg samples. Reproduced from (Hong et al., 2021)

Vitrinite reflectance (Ro) is another key indicator of thermal maturity, particularly for organic matter types II and III. Ro is sensitive to the temperature and pressure conditions experienced by the organic material, making it a reliable gauge for assessing thermal maturity (**?**). The Tmax values from Rock-Eval pyrolysis were used to calculate Ro using the formula: Ro

= (0.018 × Tmax) - 7.16 (Dembicki, 2009). The Ro values for Djebel-Zereg samples ranged from 0.68 to 1.12, with an average of 0.90. These relatively high values indicate that the majority of the samples have reached the necessary maturity stage for hydrocarbon generation.

Conclusion

This research offers a comprehensive evaluation of the organic matter characteristics within Djebel-Zereg oil shale, providing valuable insights into its hydrocarbon generation potential. Based on a rigorous series of organic geochemical analyses, including Rock-Eval pyrolysis and elemental analysis, the study reveals several important findings. Djebel-Zereg black shale demonstrates an organic richness that ranges from acceptable to very good, with TOC contents between 0.51% and 2%, averaging 1.33%, and GP values ranging from 0.50 to 4.76 mg/g, with an average of 2.23 mg/g. These findings are consistent with established criteria for source rocks with significant hydrocarbon potential. Additionally, HI values, ranging from 51 to 233 mg/g, alongside OI and HI versus Tmax plots, confirm the presence of type II and III organic matter, indicating a strong potential for both gas and oil generation. Furthermore, the TOC and S1 values across all samples suggest that the hydrocarbons present in the Djebel-Zereg black shale are indigenous, free from external contamination or migration, which underscores the integrity of the source rock. The thermal maturity indicators, such as Tmax values (435–464 °C) and vitrinite reflectance (Ro) values (0.68%–1.19%), indicate that the shale has reached the necessary maturity for hydrocarbon production. These results position the Djebel-Zereg oil shale as a promising resource, characterized by its high TOC content, the presence of type II and III organic matter, and sufficient thermal maturity. While this study provides a solid initial assessment using a range of analytical techniques, further investigation is needed to broaden the sample set and include advanced methodologies such as gas chromatography, gas chromatography–mass spectrometry, carbon isotope analysis, and mineralogical studies through scanning electron microscopy, X-ray diffraction, and X-ray fluorescence. Such analyses will offer a deeper understanding of the geochemical and mineralogical properties of these black shales and their full potential as an unconventional energy resource.

References

Akintola, G.O. 2023. Geochemical evaluation of the carbonaceous shale associated with the Permian Mikambeni Formation of the Tuli Basin for potential gas generation, South Africa. *Open Geosciences*, 15(1), p. 20220549.

Akinwumiju, A.A. & Satterfield, D. 2024. Geochemical characterization and paleo-burial history modelling of unconventional resources: A case study from the Kimmeridge Clay Formation (KCF) in the UK North Sea. *Unconventional Resources*, 4, p. 100098.

Carvajal-Ortiz, H. & Gentzis, T. 2015. Critical considerations when assessing hydrocarbon plays using Rock-Eval pyrolysis and organic petrology data: Data quality revisited. *International Journal of Coal Geology*, 152, pp. 113–122. URL http://dx.doi.org/https://doi.org/10.1016/j.coal.2015.06.001. 31st Annual Meeting of TSOP

Chabalala, V., Wagner, N. & Malumbazo, N. 2023. Application of Organic Petrology and Raman Spectroscopy in Thermal Maturity Determination of the Karoo Basin (RSA) Shale Samples. *Minerals*, 13(9), p. 1199.

Dembicki, Harry, J. 2009. Three common source rock evaluation errors made by geologists during prospect or play appraisals. *AAPG Bulletin*, 93(3), pp. 341–356.

Edress, N.A.A., Fagelnour, M.S. & Hassan, M.H.M. 2022. Subsurface geology and geochemical evaluation of the Middle Jurassic-Lower Cretaceous organic-rich intervals, West Kalabsha area, Western Desert, Egypt. *Arabian Journal of Geosciences*, 15(16), p. 1401.

Espitalie, J., Laporte, J.L., Madec, M., Marquis, F., Leplat, P., Paulet, J. & Boutefeu, A. 1977. Rapid Method for Source Rock Characterization and for Evaluating their Petroleum Potential and their degree of evolution, pp. 1–19.

Feng, G., Wang, G., Xie, H., Hu, Y., Meng, T. & Li, G. 2024. A Review of Exploration and Development Technologies for Coal, Oil, and Natural Gas. *Energies*, 17(14), p. 3600.

Gao, B., Feng, Z., Luo, J., Shao, H., Bai, Y., Wang, J., Zhang, Y., Wang, Y. & Yan, M. 2024. Geochemical Characteristics of Mature to High-Maturity Shale Resources, Occurrence State of Shale Oil, and Sweet Spot Evaluation in the Qingshankou Formation, Gulong Sag, Songliao Basin. *Energies*, 17(12), p. 2877.

Hackley, P.C. & Cardott, B.J. 2016. Application of organic petrography in North American shale petroleum systems: A review. *International Journal of Coal Geology*, 163, pp. 8–51.

Hackley, P.C., Jubb, A.M., McAleer, R.J., Valentine, B.J. & Birdwell, J.E. 2021. A Review of Spatially Resolved Techniques and Applications of Organic Petrography in Shale Petroleum Systems. *International Journal of Coal Geology*, 241, p. 103745.

Hong, S.K., Choi, J., Shinn, Y.J., Lee, H.S. & Ardakani, O.H. 2021. Estimation of original TOC using molybdenum bulk concentration: A case study of the devonian muskwa shale in the western Canada sedimentary basin. *Marine and Petroleum Geology*, 128, p. 104991.

Petroleum Geochemistry and Geology, Second Edition, Edited by John M. Hunt. Book review.

Liu, B., Mastalerz, M. & Schieber, J. 2022. SEM Petrography of Dispersed Organic Matter in Black Shales: A Review. *Earth-Science Reviews*, 224, p. 103874.

Malti, F.Z. 2012. *Passage devonien-carbonifère dans l'Ougarta Sahara Occidental, Algérie (Biostratigraphie et paléoenvironnement)*. Ph.D. thesis, Université d'Oran2 Mohamed ben Ahmed. URL https://ds.univ-oran2.dz:8443/jspui/handle/123456789/2126. Doctorat Sciences de la Terre.

McCarthy, K., Rojas, K., Niemann, M., Palmowski, D., Peters, K. & Stankiewicz, A. 2011. Basic Petroleum Geochemistry for Source Rock Evaluation. *Oilfield Review*, 23, pp. 32–43.

Peters, K.E. & Cassa, M.R. 1994. Applied Source-Rock Geochemistry. In: L.B. Magoon & W.G. Dow (eds.) *The Petroleum System: From Source to Trap*. Tulsa: American Association of Petroleum Geologists, pp. 93–120.

Qin, X., Singh, H. & Cai, J. 2022. Sorption Characteristics in Coal and Shale: A Review for Enhanced Methane Recovery. *Capillarity*, 5(1), pp. 1–11.

Shi, L., Yu, X., Yuan, J., Xu, J., Yang, L., Sun, L., Li, G., Zhang, Y., Chen, D. & Li, G. 2024. Sedimentary Paleoenvironment and Organic Matter Enrichment of the Ying 4 Member in the Southern Shuangcheng Area, Songliao Basin. *Minerals*, 14(11), p. 1152.

Sohail, J., Mehmood, S., Jahandad, S., Ehsan, M., Abdelrahman, K., Ali, A., Qadri, S.M.T. & Fnais, M.S. 2024. Geochemical Evaluation of Paleocene Source Rocks in the Kohat Sub-Basin, Pakistan. *ACS Omega*, 9(12), pp. 14123–14141.

Tissot, B.P. & Welte, D.H. 1984. *Petroleum Formation and Occurrence*. Springer-Verlag. ISBN 978-3-642-87815-2. URL http://dx.doi.org/10.1007/978-3-642-87813-8.

Waples, D. 1985. Geochemistry in Petroleum Exploration. *International Human Resources Development Corporation*.

Zhang, K., Tang, X., Liu, X., Zhao, Z. & Li, M. 2024. Geochemical Properties and Gas-Bearing Analysis of Lower Cambrian Black Shale in Western Hunan Province. *Energies*, 17(7), p. 1743.

Zhao, Y., Gao, P., Zhou, Q., Xiao, X., Xing, Y. & Liu, W. 2022. A Review of the Heterogeneity of Organic-Matter-Hosted Pores in Shale Reservoirs. *Energies*, 15(23), p. 8805.

Organsko-geohemijska procena crnih škriljaca: Studija slučaja doline Saoura, region Tamtert, Alžir

Abdelghani Kadoua, **autor za prepisku**, *Boudjema* Rebhib

University Tahri Mohammed, Laboratory of Chemistry and Environmental Science,
Béchar, Algeria

OBLAST: hemijska tehnologija i materijali
KATEGORIJA (TIP) ČLANKA: originalni naučni rad

Sažetak:

Uvod/cilj: Crni škriljac se sve više prepoznaje kao značajni nekonvencionalni izvor ugljovodonika zbog svog bogatstva organskom materijom i potencijala za proizvodnju nafte i gasa. Međutim, njegova složena geohemijska priroda, posebno u nedovoljno istraženim regionima poput Tamerta u jugozapadnom Alžiru, predstavlja izazov za preciznu procenu. Cilj ovog istraživanja je procena potencijala crnih škriljaca iz oblasti Džebel-Zereg korišćenjem naprednih metoda organske geohemije.

Metode: Prikupljeno je pet uzoraka crnog škriljca iz Džebel-Zerega, region Tamert. Određen je sadržaj ukupnog organskog ugljenika (eng. TOC), a sprovedene su i Rock-Eval 6 piroliza i elementarna analiza. Mereni parametri uključivali su TOC, S1, S2, Tmax, Indeks vodonika (HI), Indeks kiseonika (OI) i refleksivnost vitrinita (Ro), što je omogućilo analizu tipa organske materije, termalne zrelosti i kapaciteta generisanja ugljovodonika.

Rezultati: Vrednosti sadržaja ukupnog organskog ugljenika kretale su se od 0,51 do 2 %, sa prosekom od 1,33 %, što ukazuje na prihvatljiv do vrlo dobar kvalitet matičnih stena. Vrednosti S2 kretale su se od 0,45 do 4 mg HC/g stene, a prosečni Indeks proizvodnje (PI) iznosio je 2,23. HI vrednosti (51–233 mg HC/g TOC), zajedno sa OI i Tmax, ukazuju na prisustvo kerogena tipa II i III, što sugeriše potencijal za proizvodnju i nafte i gasa. Vrednosti Tmax (435–465 °C, prosečno 447 °C) i refleksivnost vitrinita (0,68–1,19 %) potvrđuju termalnu zrelost. Pozitivna korelacija između TOC i S1 vrednosti podržava prisustvo endogenih ugljovodonika.

Zaključak: Integrisani geohemijski pristup potvrđuje da su crni škriljci iz Džebel-Zerega termalno zreli i bogati organskom materijom, sa obećavajućim potencijalom za proizvodnju naftnih škri-

ljaca. Ovi rezultati podržavaju dalja istraživanja i razvoj nekonvencionalnih izvora ugljovodonika u regionu Tamert.

Ključne reči: crni škriljac, Džebel-Zereg, elementarna analiza, potencijal ugljovodonika, organska materija, Rock-Eval piroliza, procena matičnih stena, ukupni organski ugljenik.

Paper received on: 27 May 2025.
Manuscript corrections submitted on: 16 June 2025.
Paper accepted for publishing on: 5 October 2025.

© 2026 The Authors. Published by Vojnotehnički glasnik / Military Technical Courier (http://vtg.mod.gov.rs). This article is an open access article distributed under the terms and conditions of the Creative Commons Attribution license (http://creativecommons.org/licenses/by/4.0/rs/).

Laser obscuration and infrared emission characteristics of red phosphorus and Mg-Al based smoke composition

Thang D. Pham[a], *Nhan* D. Phan[b], *Toan* T. Nguyen[c]

Le Quy Don Technical University, Faculty of Special Equipment

[a] Hanoi, Socialist Republic of Vietnam,
e-mail: thangpham@lqdtu.edu.vn,
ORCID iD: https://orcid.org/0000-0002-4377-8694

[b] e-mail: pdnhan912@yahoo.com,
ORCID iD: https://orcid.org/0000-0002-1947-2310

[c] e-mail: trungtoanktqs@mta.edu.vn, **corresponding author**,
ORCID iD: https://orcid.org/0000-0002-4753-9869

https://doi.org/10.5937/vojtehg74-58344

FIELD: pyrotechnic materials, chemical technologies
ARTICLE TYPE: original scientific paper

Abstract:

Introduction/purpose: The capability for laser attenuation and infrared (IR) radiation emission is one of the most essential characteristics determining the camouflage effectiveness of multispectral smoke screens on the battlefield. In this study, the effects of red phosphorus and Mg-Al content, the initial mass of the smoke composition, and the relative humidity on the obscuration characteristics of smoke cloud, including the degree of laser attenuation, the mass extinction coefficient, the Yield factor, and the Figure of Merit, were examined. Additionally, the IR emission properties of smoke screens based on RP/Mg-Al were also evaluated.

Methods: Laser radiation attenuation was evaluated by comparing the initial laser power to the power measured after passing through the smoke screen. A 1.064 μm, 11.0 mW continuous-wave laser was transmitted through the test chamber and measured with a power meter. The infrared properties of the smoke clouds were analyzed using an SR-5000N spectral radiometer within the 2.5 – 14.0 μm range.

Results: The results indicate that increasing the content of red phosphorus, sample masses, and relative humidity enhances the laser obscuration characteristics. Notably, for a 1 m^3 smoke chamber, the estimated optimal sample masses are 3.25 g and 2.30 g at 65% and 90% relative humidity, respectively. Furthermore, increasing Mg-Al content enhances IR emission in the β band (3-5 μm), while emission in the γ band (8-14 μm) decreased.

Conclusion: The laser obscuration characteristics of RP/Mg-Al-based smoke compositions can be effectively controlled by optimizing the RP/Mg-Al content and relative humidity levels. Moreover, the RP/Mg-Al-based

compositions demonstrate strong IR radiation characteristics, which are also influenced by the content of RP and Mg-Al. Future research should focus on evaluating the obscuration characteristics of RP/Mg-Al-based compositions in the near- and far-IR regions.

Keywords: multispectral smoke, obscuration performance, infrared radiation characteristics, red phosphorus, Mg-Al alloy.

Introduction

In modern warfare, laser technology is widely utilized in guidance systems, target acquisition, and rangefinding, while infrared (IR) technology enables surveillance, tracking, and thermal imaging (Lyubomir et al., 2021; Suliman & Kivrak, 2023). The rapid evolution of guided weapons and IR imaging devices has rendered traditional smoke screens, such as C_2Cl_6/C_6Cl_6 (HC smokes) and white phosphorus, ineffective in concealing combat vehicles on the battlefield (Harmata, 2018). Consequently, multispectral smoke screens are required to meet new demands, including effective attenuation of laser radiation and enhanced IR emission for jamming purposes (Koch, 2012). Red phosphorus (RP) smoke is effective at attenuating radiation in the laser (1.064 μm) and near-IR (0.7–1.4 μm) spectra, but it exhibits limited performance in the mid-IR (3–5 μm) and far-IR (8–14 μm) ranges. Incorporating high heat-generating fuels and fluorocarbon-based oxidizers into RP formulations enhances both laser attenuation and IR obscuration capabilities, providing effective countermeasures against laser-guided weapons and IR-based threat systems (Koch, 2008; Smit et al., 2009).

Previous studies have evaluated obscuration efficiency using parameters such as the degree of laser attenuation (A), the mass extinction coefficient (α_λ), the yield factor (Y_f), and the Figure of Merit (F_m), which are influenced by component ratios, initial mass (m_p), and relative humidity (RH). The role of H_3PO_4 droplets from RP oxidation in obscuring the 3-5 μm and 8-14 μm bands was highlighted (Suzuki, 2002). A 100% obscuration in the visible ranges and 76% in the 8-14 μm band was observed with the 80% RP and 20% KNO_3 mixture at 85% RH. Moreover, the α_λ values were 1.04 $m^2.g^{-1}$ (3-5 μm) and 0.85 $m^2.g^{-1}$ (8-14 μm) at 55% RH (Gautam et al., 2006). Effective attenuation of IR radiation at wavelengths of 0.82 μm, 3-5 μm, and 10.6 μm with high efficiency was achieved by the pyrotechnic charges composed of plasticized RP combined with epoxy resin. Specifically, the mixture of 55% RP, 12% Mg, 28% $NaNO_3$, and 5% resin achieved the α_λ value of 0.51 $m^2.g^{-1}$ (3-5 μm) and 0.36 $m^2.g^{-1}$ (10.6 μm) (Klusáček & Navrátil, 2004). Mg_4Al_3 alloy

powder was utilized as a high-energy fuel, achieving an α_λ of 1.44 $m^2 . g^{-1}$ at 1.064 μm (Cudziło & Trzcinski, 1999). Tests of 66 mm Buck MASKE RP smoke rounds on M1A1 Abrams and M88A2 Hercules vehicles were conducted, resulting in screening times of 60 s in the visible region and 30 s in IR bands (Smit et al., 2007).

Meanwhile, research on IR emission characteristics of RP-based smoke remains sparse. High IR emission in the 2-5 μm band was produced by a mixture of RP, Mg, and oxidizers (Teflon/KNO_3), with a 1.5 m thick smoke layer at 2 $g.m^{-3}$ (Cudziło, 2001). The addition of 20% RP to an Mg/PTFE/Viton mixture was observed to enhance the radiating area and intensity with minimal impact on radiation itself (Li et al., 2017). A composition of 59% RP, 21% Zr, 15% KNO_3, and 5% polyacrylate binder was found to exhibit greater spectral energy in the (8-14 μm) band than the (3-5 μm) band. The γ/β band ratio and spectral energy suggest that the combustion flame of the pyrolant cannot be characterized as a graybody (Koch, 2022). It is evident that studies on the obscuration and IR emission characteristics of RP-based smoke have shown notable results. However, the available research on the RP and Mg-Al-based multispectral smoke formulations remains limited.

This work investigates the obscuration behaviors and IR emission properties of RP/Mg-Al-based smoke screens. The effects of various factors, such as RP and Mg-Al content, sample mass, and relative humidity on the obscuration characteristics, including the degree of laser attenuation, the mass extinction coefficient, the Yield factor, and the Figure of Merit were examined under 1.064 μm laser radiation. Moreover, IR emission properties, such as spectral radiance and emission distribution, were measured with a spectroradiometer that covered the wavelength range of 2.5-14 μm.

Materials and methods

Materials

The raw materials employed in this study comprised Mg-Al alloy powder (50:50 wt.%), polytetrafluoroethylene (PTFE) powder, red phosphorus (RP) powder, and sodium nitrate ($NaNO_3$) powder, all sourced from Shanghai Macklin Biochemical Co., Ltd. The commercial grade Viton A rubber (vinylidene fluoride-hexafluoropropene copolymer, 66 wt.% fluorine content) was obtained from DuPont Company (Wilmington, DE, USA). Analytical grade acetone (CH_3COCH_3) was purchased from Xilong Co., Ltd. Technical specifications of the investigated materials are summarized in Table 1.

Table 1 - Several technical parameters of the materials

Materials	Molecular formula	Purity, %	Mean size, μm
Red phosphorus	P	≥ 99	40
Magnesium- Aluminum Alloy	Mg-Al	≥ 98	74
Teflon (PTFE)	$(C_2F_4)_n$	≥ 99	20
Sodium nitrate	$NaNO_3$	≥ 98	60
Manganese dioxide	MnO_2	≥ 98	10
Viton A	$C_{10}H_7F_{13}$	≥ 99	-
Acetone	C_3H_6O	≥ 99.5	-

Experiment and methods

Sample preparation

The mixture containing Mg-Al alloy, PTFE, $NaNO_3$, and MnO_2 powders (MAT mixture) was mixed through a 0.5 mm silk sieve. A binder solution was prepared by dissolving Viton A rubber in acetone at a 1:15 w/v ratio. After adding the MAT mixture and RP to the binder solution, the mixture was stirred at 600 rpm for 30 minutes to prepare the MATV-RP mixture. The obtained MATV-RP mixture was passed through a 1.25 mm mesh and was air-dried for 30 minutes. Final drying was carried out under at 55 °C for 5 hours. The preparation process and the components of MATV-RP mixture are expressed in Figure 1 and Table 2.

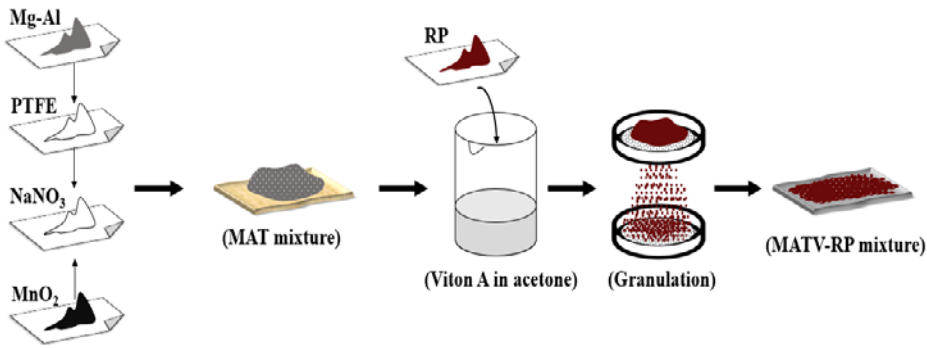

Figure 1 - The preparation process diagram of MATV-RP mixture

Table 2 - The components of MATV-RP mixture

Samples	Content (%)					
	RP	Mg-Al	PTFE	$NaNO_3$	MnO_2	Viton A
M1	40	35	10	6.5	0.5	8
M2	45	30	10	6.5	0.5	8
M3	50	25	10	6.5	0.5	8
M4	55	20	10	6.5	0.5	8
M5	60	15	10	6.5	0.5	8
M6	65	10	10	6.5	0.5	8

Experimental techniques

The experimental setup for measuring the obscuration characteristics of the smoke screen under 1.064 μm laser radiation is illustrated in Figure 2.

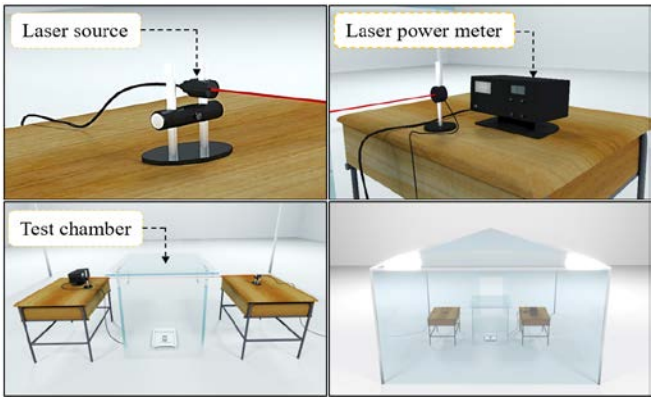

Figure 2 - Experimental setup for measuring the obscuration characteristics

The degree of laser radiation attenuation was determined by comparing the initial laser power (without obscuring) with the laser power measured after passing through the screening smoke. A 1.064 μm continuous-wave laser source with an output power of 11.0 mW was directed through the cubical test chamber and measured by a laser power meter. The total path length through the screening smoke was 600 mm. The transmittance T (i.e., the degree of transmission) was determined using the formula (Cudziło & Papliński, 1999):

$$T = \frac{I_{min}}{I_0} \tag{1}$$

where, I_0 and I_{min} are the initial laser intensity without smoke and the minimum laser intensity after passing through the screening smoke, respectively.

The degree of laser attenuation (A) can be calculated using the following formula (Koch, 2012):

$$A(\%) = (1 - T).100 \quad (2)$$

The mass extinction coefficient α_λ ($m^2.g^{-1}$) is derived from the Lambert-Beer law through the following expression (Kiteto & Mecha, 2024; Koch, 2012):

$$\alpha_\lambda = -\frac{\ln T}{C.L} \quad (3)$$

where C is the smoke concentration ($g.m^{-3}$); L is the thickness of the smoke screen (m).

The Yield factor Y_f of the smoke composition typically represents the ratio of the mass of the aerosol m_s to the initial mass of the smoke composition m_p. Essentially, it measures how efficiently the material contributes to producing the desired smoke effect. Mathematically, it could be expressed as (Koch, 2012):

$$Y_f = \frac{m_s}{m_p} \quad (4)$$

To comprehensively assess the camouflage capability of a smoke composition, the concept of the Figure of Merit (F_m) is commonly used, which is the product of the Yield factor and the mass extinction coefficient (Koch, 2012):

$$F_m = \alpha_\lambda.Y_f \quad (5)$$

The IR radiation characteristics of smoke clouds were measured by the spectral radiometer (SR-5000N, CI systems) with a working wavelength from 2.5-14.0 μm (Figure 3). 15 grams of the sample were burned using an electric primer in a cubic test chamber with a volume of 0.216 m^3.

The lenses of the radiometer were positioned facing the smoke cloud through a source window on the wall of the test chamber, and the distance between the lenses and the source window was approximately 5.0 m. The emission intensity was scanned every second within the 2.5-14.0 μm wavelength range and repeated. The IR emission intensity and radiance were determined using the built-in software.

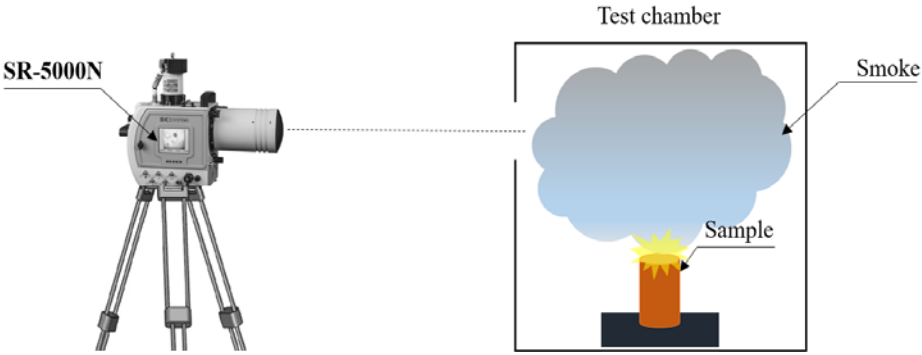

Figure 3 - Experimental setup for measuring the IR emission characteristics

The radiance distribution function for the wavelength range from λ_1 to λ_2 describes the radiance of an emissive surface within that specific range, represented as $L(\lambda_1\text{-}\lambda_2)$ (W.sr^{-1}.cm^{-2}) (Arecchi et al., 2007).

$$L_{(\lambda_1-\lambda_2)} = \int_{\lambda_1}^{\lambda_2} L_\lambda(\lambda).d\lambda \tag{6}$$

Results and discussion

Effect of RP content on the obscuration characteristics

The obscuration characteristics of M1-M6 samples at different relative humidity levels are presented in Table 3. It should be noted that the initial mass of the smoke composition m_p was fixed at 0.5 grams and the RP content was increased from 40-65%, as detailed in Table 2. The smoke concentration *C* was theoretically computed based on the free energy minimization method (Belov, 1998).

The results indicate that increasing RP content enhances the smoke concentration C and Yield factor Yf, resulting in higher mass extinction coefficient αλ and Figure of Merit Fm, while the transmittance T decreased significantly. When the mp is fixed, a higher RP content increases the actual mass of RP, resulting in enhanced smoke production and elevated concentrations of combustion products (P2, P4) (Toan et al., 2022). Notably, the obtained Yield factors (Yf = 1.59-2.22) are higher than those reported for Ti/poly-carbon monofluoride and Mg/poly-carbon monofluoride (Yf = 1.0-1.2), as well as RP/Mg/Teflon-based compositions (Yf = 0.8) (Cudziło & Trzcinski, 1999), reflecting the superior obscuration

capabilities of RP/Mg-Al-based smoke for enhanced protection against laser irradiation.

Table 3 - Effect of RP content on obscuration characteristics at 65% and 90% RH

Samples	Mass of RP (gram)	C, (g.m-3)	Yf	65% RH			90% RH		
				T, (%)	αλ, (m2.g-1)	Fm, (m2.g-1)	T, (%)	αλ, (m2.g-1)	Fm, (m2.g-1)
M1	0.20	3.68	1.59	22	0.69	1.09	12	0.96	1.53
M2	0.23	3.96	1.71	18	0.72	1.23	08	1.06	1.82
M3	0.25	4.26	1.84	15	0.74	1.37	06	1.10	2.03
M4	0.28	4.58	1.98	07	0.97	1.91	05	1.11	2.16
M5	0.30	4.87	2.10	06	0.98	2.03	04	1.13	2.32
M6	0.38	5.13	2.22	03	1.14	2.52	02	1.27	2.82

Furthermore, higher relative humidity enhances water absorption by H_3PO_4 droplets, leading to larger smoke particles that contribute to increased the mass extinction coefficient α_λ and Figure of Merit F_m (Milham et al., 1982). The obtained α_λ values are higher than those of RP/KNO_3 mixture in the spectral ranges of (3-5 µm) and (8-14 µm) (Gautam et al., 2006). Moreover, the F_m values obtained at 65% RH are comparable to those reported for mixtures containing RP, Mg_4Al_3, $Ba(NO_3)_2$, and Viton A (Toan et al., 2022). Overall, the combination of higher RP content and elevated RH substantially enhances both the mass extinction coefficient and Figure of Merit, thereby optimizing the camouflage performance of the smoke screen.

The degree of laser radiation attenuation A at different RP content and RH is presented in Figure 4 and Table 4.

The maximum A_{max} and average A_{avg} attenuation levels, as well as the screening time for maintaining over 85% laser radiation attenuation ($t_{A > 85\%}$), increased with higher RP content and relative humidity. Additionally, the differences in attenuation (ΔA_{max} and ΔA_{avg}) decreased at higher RP contents, suggesting the need to consider both parameters for practical applications. Notably, at RP contents ≥ 55% and 90% RH, $t_{A > 85\%}$ exceeded 200s, highlighting optimal and sustained screening performance (Table 4).

Based on these experimental results, the optimal RP content for achieving effective camouflage depends on the humidity level. Specifically, at 65% RH (Figure 4a), an RP content of 60–65% is recommended to maximize attenuation and ensure sustained performance, compensating

for lower moisture conditions. In contrast, at 90% RH (Figure 4b), an RP content of 55–60% is sufficient to provide robust and prolonged attenuation, optimizing material efficiency under elevated humidity.

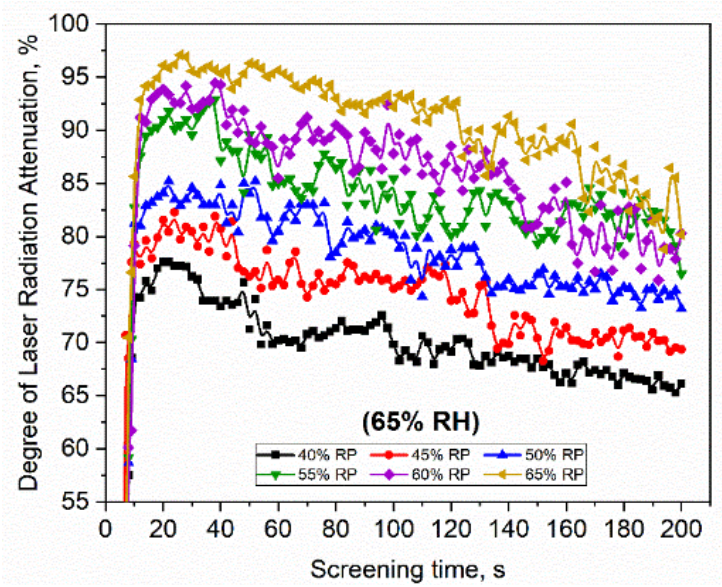

(a)

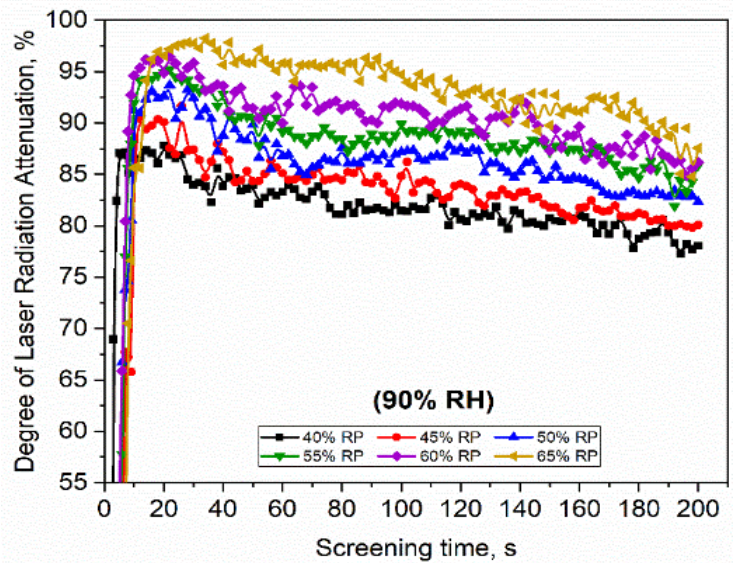

(b)

Figure 4 - The degree of laser radiation attenuation at 65% RH (a) and 90% RH (b)

Table 4 - The degree of laser radiation attenuation as a function of RP content and RH

Samples	RP, %	RH, %	Amax, %	ΔAmax, %	Aavg, %	ΔAavg, %	tA > 85%, s
M1	40	65	77.60	10.23	69.99	11.64	0
		90	87.84		81.63		30
M2	45	65	82.29	9.35	74.48	9.15	0
		90	91.64		83.64		30
M3	50	65	85.18	8.52	78.74	7.60	0
		90	93.70		86.34		60
M4	55	65	92.92	2.32	84.22	4.40	90
		90	95.24		88.61		>200
M5	60	65	94.44	2.01	86.30	4.21	150
		90	96.45		90.51		>200
M6	65	65	97.11	1.13	90.89	2.57	>200
		90	98.24		93.46		>200

Effect of sample mass on the obscuration characteristics

The effect of sample mass m_p on the degree of laser radiation attenuation of the M5 sample under different relative humidity is presented in Figure 5 and Table 5.

It can be seen that the combination of increased sample mass m_p and elevated RH is critical for sustaining effective laser radiation attenuation. When $m_p \leq 0.3$ g, RH exhibits a significant impact on the degree of laser radiation attenuation, as evidenced by the changes in ΔA_{max} and ΔA_{avg}. As a result, the smoke screen is unstable and fails to maintain coverage above 85%. However, the influence of RH on the degree of laser radiation attenuation becomes negligible when $m_p \geq 0.5$ g. The samples exhibit high $t_{A>85\%}$ values (> 200s), particularly at 90% RH (Figure 5b and Table 5). A notable observation is that once the optimal mass threshold is reached (m_p = 0.7 g at 65% RH and m_p = 0.5 g at 90% RH), further increases in m_p result in negligible improvements in laser attenuation. Based on the experimental results, the optimal m_p for a 1 m^3 smoke chamber at different RH levels can be estimated as follows: m_p = 3.25 g at 65% RH and m_p = 2.30 g at 90% RH.

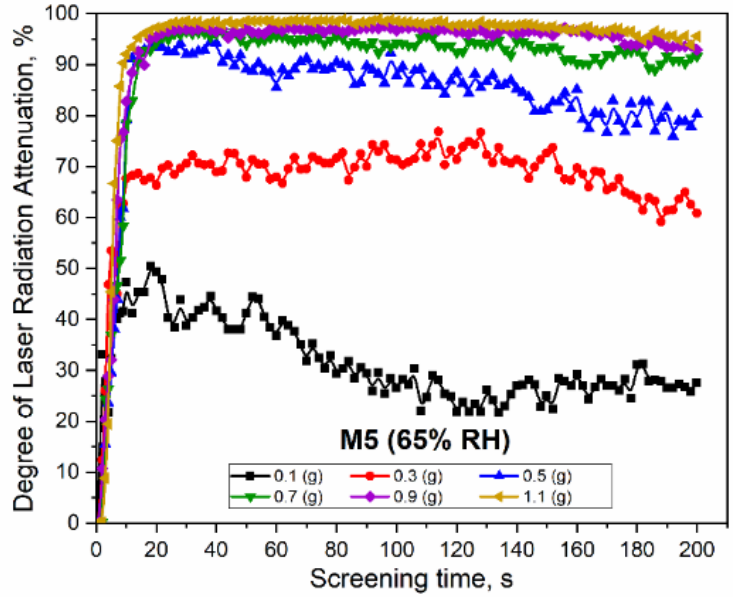

(a)

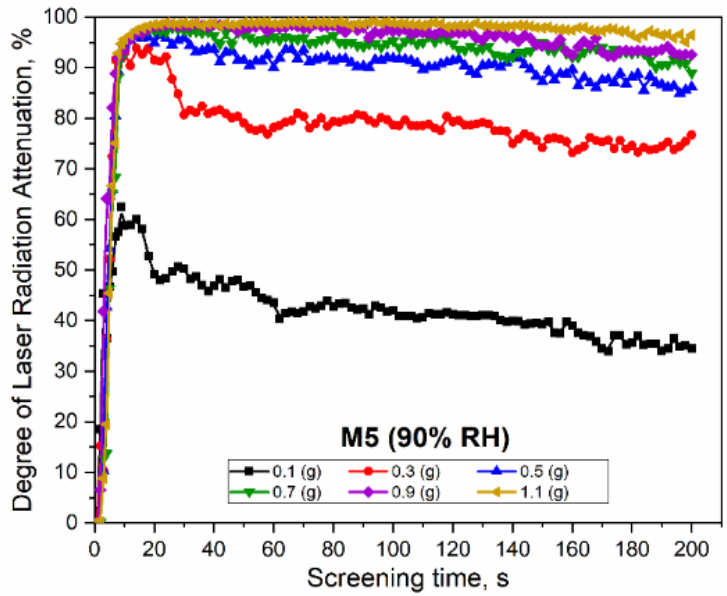

(b)

Figure 5 - Effect of sample mass on the degree of laser radiation attenuation of M5 sample at 65 %RH (a) and 90% RH (b)

Table 5 - The degree of laser radiation attenuation as a function of mp and RH

m_p, g	RH, %	A_{max}, %	ΔA_{max}, %	A_{avg}, %	ΔA_{avg}, %	$t_{A > 85\%}$, s
0.1	65	50.41	12.00	31.67	10.53	0
	90	62.41		42.20		0
0.3	65	76.87	16.98	69.48	9.67	0
	90	93.86		79.16		30
0.5	65	94.44	2.01	86.47	4.31	150
	90	96.45		90.78		>200
0.7	65	96.49	1.37	93.35	1.16	>200
	90	97.86		94.51		>200
0.9	65	97.58	1.05	95.90	0.39	>200
	90	98.63		96.28		>200
1.1	65	98.92	0.22	97.52	0.58	>200
	90	99.14		98.11		>200

Infrared radiation properties

The average IR radiance values of the RP/Mg-Al-based smoke composition were measured using the SR-5000N Radiometer, with the $L_{(\lambda 1-\lambda 2)}$ values calculated according to Eq. (6), and the results are presented in Table 6 and Figure. 6.

The experimental results indicate that all samples (M1-M6) emit IR radiation in both *β* band (3-5 μm) and *γ* band (8-14 μm). However, the intensity distribution of IR radiation shows a clear inverse relationship between the two wavelength bands, which is fundamentally influenced by the compositional characteristics of the sample.

It can be noted that increasing the Mg-Al content leads to an increase in IR radiation in the *β* band, while the IR radiation in the *γ* band decreases. Table 6 shows that M1 has the highest IR radiation in the *β* band at 8.266 (10^{-2} .W.sr^{-1}.cm^{-2}), while M6 has the lowest at 2.195 (10^{-2}.W.sr^{-1}.cm^{-2}). Conversely, in the *γ* band, M6 achieves the highest radiation emission at 4.435 (10^{-2}.W.sr^{-1}.cm^{-2}), while M1 records the lowest at 1.270 (10^{-2}.W.sr^{-1}.cm^{-2}). This observation can be explained by the fact that M1 has higher Mg-Al content, resulting in stronger IR radiation in the *β* band, while M6, with higher RP content, shows higher *γ* band radiation (Toan et al., 2022). This variation indicates that chemical constituents affect IR emission.

Table 6 - The radiance distribution of MATV-RP samples

Samples	RP, %	Mg-Al, %	$L_{(\lambda 1-\lambda 2)}$, ($10^{-2}$.W.sr^{-1}.cm^{-2})		
			β band (3-5 μm)	*γ* band (8-14 μm)	*γ/β* band ratio
M1	40	35	8.266	1.270	0.154
M2	45	30	6.987	1.528	0.219
M3	50	25	5.171	2.557	0.494
M4	55	20	4.394	3.434	0.782
M5	60	15	2.879	3.717	1.291
M6	65	10	2.195	4.435	2.021

The γ/β ratio increases markedly from 0.154 for M1 to 2.201 for M6 (Figure 6a). This highlights that compositional changes impact both the intensity of radiation and its distribution (Figure 6b) between the two spectral regions, suggesting that optimizing the Mg-Al to RP ratio could yield smoke compositions with desired IR properties for specific applications. Notably, the γ/β band ratio observed in the M5 sample (γ/β = 1.291) aligns closely with the value (γ/β = 1.270) previously reported for a composition consisting of 59% RP, 21% Zr, 15% KNO_3, and 5% polyacrylate binder (Koch, 2022).

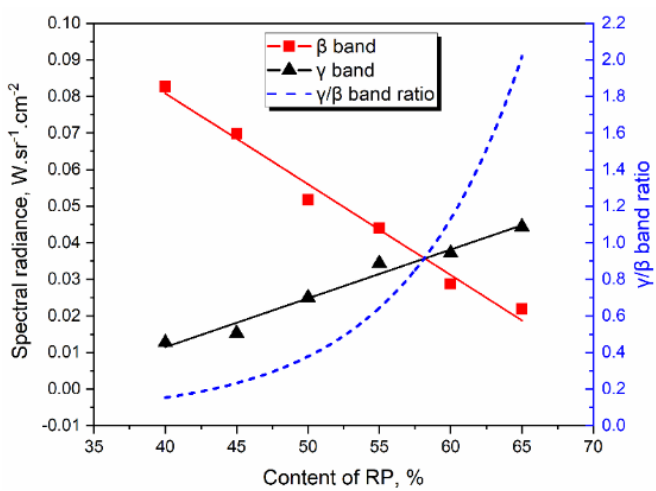

(a)

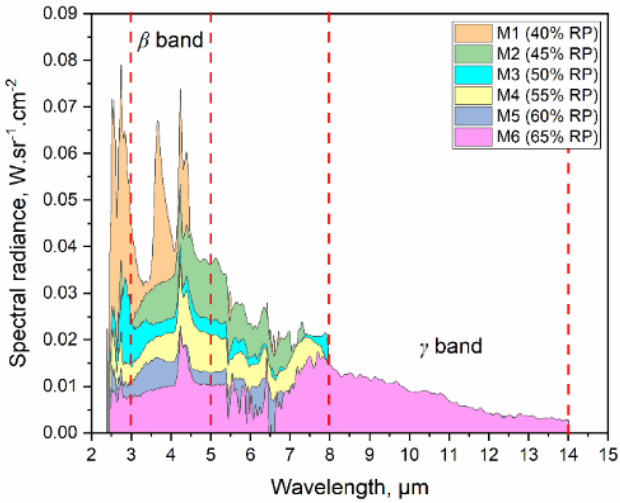

(b)

Figure 6 - Effect of RP and Mg-Al content on the intensity of radiation (a) and its distribution (b) in the β and γ band

Conclusions

The laser obscuration characteristics of RP/Mg-Al-based smoke compositions can be effectively controlled by optimizing the content of RP/Mg-Al and RH levels. Increasing RP content enhances the mass extinction coefficient α_λ, the Yield factor Y_f, and the Figure of Merit F_m, while reducing the transmittance T. At high humidity (90% RH), the degree of laser attenuation significantly improves with the screening time for maintaining over 85% attenuation exceeding 200 seconds, superior to low humidity conditions (65% RH). The initial sample mass m_p greatly influences laser radiation attenuation. For a 1 m^3 smoke chamber, the estimated optimal sample masses are 3.25 g and 2.30 g at 65% and 90% RH, respectively.

In addition to providing effective laser attenuation, the RP/Mg-Al-based compositions demonstrate strong IR radiation characteristics, which are also influenced by the content of RP and Mg-Al. All samples emit IR radiation in both the β (3-5 μm) and γ (8-14 μm) bands. The γ/β ratio exhibits an increase from M1 to M6, demonstrating the capacity to optimize IR radiation through the RP/Mg-Al ratio.

Future research should focus on evaluating the obscuration characteristics of the RP/Mg-Al-based composition in the near and far-IR regions.

References

Arecchi, A. V., Koshel, R. J. & Messadi, T. 2007. *Field guide to illumination*, SPIE Bellingham, WA, USA. Available at: https://doi.org/10.1117/3.764682

Belov, G. V. 1998. Thermodynamic analysis of combustion products at high temperature and pressure. *Propellants, explosives, pyrotechnics,* 23**,** pp.86-89. Available at: https://doi.org/https://doi.org/10.1002/(SICI)1521-4087(199804)23:2<86::AID-PREP86>3.0.CO;2-2

Cudziło, S. 2001. Studies of IR-Screening Smoke Clouds. *Propellants, Explosives, Pyrotechnics,* 26**,** pp.12-16. Available at: https://doi.org/10.1002/1521-4087(200101)26:1

Cudziło, S. & Papliński, A. 1999. An Influence of the Chemical Structure of Smoke-Generating Mixtures on Laser Radiation Attenuation at 1.06-μm and 10.6-μm Wavelengths. *Propellants, Explosives, Pyrotechnics,* 24**,** pp.242-245. Available at: https://doi.org/10.1002/(SICI)1521-4087(199908)24:4

Cudziło, S. & Trzcinski, W. 1999. Comparison investigations of camouflage capability of different pyrotechnic smoke compositions in IR region. 7th International Seminar EURPOPYRO'99, pp 7-11.

Gautam, G., Joshi, A., Joshi, S., Arya, P. & Somayajulu, M. 2006. Radiometric screening of red phosphorus smoke for its obscuration characteristics. *Defence Science Journal,* 56**,** pp.377-381. Available at: https://doi.org/10.14429/dsj.56.1903

Harmata, W. 2018. Smoke as a component of military camouflage systems. *Bulletin of the Military University of Technology,* 67**,** pp.83-113. Available at: https://doi.org/10.5604/01.3001.0012.6600

Kiteto, M. & Mecha, C. 2024. Insight into the Bouguer-Beer-Lambert Law: A review. *Sustainable Chemical Engineering***,** pp.567-587. Available at: https://doi.org/10.37256/sce.5220245325

Klusáček, L. & Navrátil, P. 2004. The Use and Application of Red-Phosphorous Pyrotechnic Composition for camouflage in the infrared region of radiation. *Propellants, Explosives, Pyrotechnics,* 22**,** pp.74-77. Available at: https://doi.org/10.1002/prep.19970220205

Koch, E.-C. 2008. Special Materials in Pyrotechnics: V. Military Applications of Phosphorus and its Compounds. *Propellants, Explosives, Pyrotechnics,* 33**,** pp.165-176. Available at: https://doi.org/10.1002/prep.200700212

Koch, E.-C. 2012. Obscurants. *Metal-Fluorocarbon Based Energetic Materials.* pp.197-199. Available at: https://doi.org/10.1002/9783527644186.ch11

Koch, E.-C. 2022. Radiative Properties of a Red Phosphorus Based Combustion Flame. *Central European Journal of Energetic Materials,* 19**,** pp.5-17. Available at: https://doi.org/10.22211/cejem/147623

Li, J., Chen, X., Wang, Y., Shi, Y. & Shang, J. 2017. Burning and radiance properties of red phosphorus in Magnesium/PTFE/Viton (MTV)-based compositions. *Infrared Physics & Technology,* 85**,** pp.109-113. Available at: https://doi.org/10.1016/j.infrared.2017.06.002

Lyubomir, L., Edmunds, T. & Risham Singh, G. 2021. Applications of laser technology in the army. *Journal of Defense Management,* 11**,** pp.1-8. Available at: https://doi.org/10.35248/2167-0374.21.11.210

Milham, M. E., Anderson, D. & Frickel, R. H. 1982. Infrared optical properties of phosphorus-derived smoke. *Applied Optics,* 21**,** pp.2501-2507. Available at: https://doi.org/10.1364/AO.21.002501

Smit, K., Lee, A. & Burridge, M. Smoke countermeasure testing for the M1A1 Abrams. Proc. Land Warfare Conference, Adelaide, South Australia, 2007. Available at: https://www.researchgate.net/publication/340684654

Smit, K., Lee, A. & Burridge, M. Smoke Countermeasures for Army in the Visual and Infrared. 36th International Pyrotechnics Seminar, 2009 Rotterdam, The Netherlands. Available at: : https://www.researchgate.net/publication/340684572

Suliman, H. M. & Kivrak, S. 2023. Anti-Tank Guided Missile System Design Based on an Object Detection Model and a Camera. *International Journal of Computational Intelligence Systems,* 16**,** pp.20. Available at: https://doi.org/10.1007/s44196-023-00198-6

Suzuki, Y. M., K. & Suzuki, Y. 2002. IR-Screening properties of red phosphorus smoke. *Kayaku Gakkaishi,* 63**,** pp.185-190. Available at: https://www.jes.or.jp/mag_eng/stem/Vol.63/documents/Vol.63,No.4,p.185-190

Toan, N. T., Tinh, N. V. & Sang, D. Q. 2022. Obscurant and Radiation Characteristics of Infrared Screening Smoke Composition Based on Red Phosphorus. *Defence Science Journal,* 72**,** pp.353-358. Available at: https://doi.org/10.14429/dsj.72.17676

Karakteristike zaklanjanja lasera i emisije infracrvenog zračenja dimne smeše na bazi crvenog fosfora i legure Mg-Al

Thang D. Pham, *Nhan* D. Phan, *Toan* T. Nguyen, **autor za prepisku**
Le Quy Don Technical University, Faculty of Special Equipment,
Hanoi, Socialist Republic of Vietnam

OBLAST: pirotehnički materijali, hemijske tehnologije
KATEGORIJA (TIP) ČLANKA: originalni naučni rad

Sažetak:

Uvod/cilj: Sposobnost prigušivanja laserskog zračenja i emisije infracrvenog zračenja predstavlja jednu od ključnih karakteristika koje utiču na kamuflažnu efikasnost multispektralnih dimnih zavesa na bojnom polju. Ovaj rad ispituje uticaje sadržaja crvenog fosfora i legure Mg-Al, početne mase dimnog sastava i relativne vlažnosti vazduha na karakteristike zaklanjanja dimnog oblaka, uključujući stepen prigušenja lasera, masu koeficijenta ekstinkcije, faktor efikasnosti generisanja aerosola i faktor kvaliteta. Takođe, u radu su analizirane i osobine infracrvenog zračenja dimnih zavesa na bazi crvenog fosfora i legura Mg-Al (RP/Mg-Al).

Metode: Prigušenje laserskog zračenja određivano je upoređivanjem početne snage lasera sa snagom izmerenom nakon prolaska kroz dimnu zavesu. Kroz ispitnu komoru emitovan je kontinuirani laser talasne dužine 1,064 μm i izlazne snage 11,0 mW, a snaga je merena pomoću laserskog merača snage. Infracrvene osobine dimnih oblaka analizirane su spektralnim radiometrom SR-5000N u opsegu talasnih dužina od 2,5 do 14,0 μm.

Rezultati: Rezultati pokazuju da povećanje sadržaja crvenog fosfora, mase uzoraka i relativne vlažnosti vazduha poboljšava karakteristike laserskog zaklanjanja. Za komoru dimnog oblaka zapremine 1 m³, procenjene optimalne mase uzorka su 3,25 g i 2,30 g pri nivoima relativne vlažnosti od 65% i 90%. Takođe, povećanjem sadržaja legure Mg-Al povećava se emisija infracrvenog zračenja u β opsegu (3–5 μm), dok emisija u γ opsegu (8–14 μm) opada.

Zaključak: Karakteristike zaklanjanja lasera dimnih smeša na bazi RP/Mg-Al mogu se efikasno kontrolisati optimizacijom sadržaja RP/Mg-Al i nivoa relativne vlažnosti. Takođe, smeše na bazi RP/Mg-Al pokazuju izražene karakteristike infracrvenog zračenja koje su takođe pod uticajem sadržaja crvenog fosfora i legure Mg-Al. Težište budućih istraživanja bi trebalo biti usmereno na ispitivanje karakteristika zaklanjanja smeša na bazi RP/Mg-Al u bliskom i dalekom infracrvenom opsegu.

Ključne reči: multispektralni dim, performanse zaklanjanja, karakteristike infracrvenog zračenja, crveni fosfor, legura Mg-Al.

Paper received on: 22 April 2025.
Manuscript corrections submitted on: 16 May 2025.
Paper accepted for publishing on: 4 June 2025.

© 2026 The Authors. Published by Vojnotehnički glasnik / Military Technical Courier (www.vtg.mod.gov.rs). This article is an open access article distributed under the terms and conditions of the Creative Commons Attribution license (http://creativecommons.org/licenses/by/4.0/rs/).

Sustainable fibre-concrete reinforcement using manufacturing by-products

Ilyes Irki[a], *Mohamed* Kesseir[b], *Farid* Debieb[c], *Chafika* Settari[d]

[a] University Centre of Tipaza, Civil Engineering Department, Faculty of Science, Tipaza, People's Democratic Republic of Algeria + Laboratory of Civil Engineering and Protection of Environment (LCEPE), Medea, People's Democratic Republic of Algeria,
e-mail: Irki.ilyes@cu-tipaza.dz, **corresponding author**,
ORCID iD: https://orcid.org/0000-0003-0152-2559

[b] University of Medea, Laboratory of Civil Engineering and Protection of Environment (LCEPE), Medea,
People's Democratic Republic of Algeria,
e-mail: kesseirmohamed@gmail.com,
ORCID iD: https://orcid.org/0009-0002-4578-7460

[c] University of Medea, Laboratory of Civil Engineering and Protection of Environment (LCEPE), Medea,
People's Democratic Republic of Algeria,
e-mail: f_debieb@yahoo.com,
ORCID iD: https://orcid.org/0000-0002-3898-7037

[d] University of Medea, Laboratory of Civil Engineering and Protection of Environment (LCEPE), Medea,
People's Democratic Republic of Algeria,
e-mail: chafika.settari@gmail.com,
ORCID iD: https://orcid.org/0000-0002-2970-5472

https://doi.org/10.5937/vojtehg74- 58016

FIELD: materials
ARTICLE TYPE: original scientific paper

Abstract:

Introduction/purpose: Concrete is a material with very high compressive strength compared to very low tensile strength, which makes it brittle under tensile and bending stresses, with premature failure manifested by cracking. These stresses can be improved by reinforcing concrete with different types of fibres derived from industrial or other wastes.

Methods: In this context, this work aims to use industrial metal waste in concrete and compare it with metal fibre concrete to overcome this tensile strength deficiency. Two types of industrial fibres and two other types of waste were used, aluminium and steel waste (in the form of shavings) re-

ACKNOWLEDGEMENT: All tests were carried out at the Civil Engineering Laboratory - University of Medea, Algeria. The authors express gratitude to the engineer who contributed to this experimental program; this work was supported by the General Directorate for Scientific Research and Technological Development (DGRSDT) in Algeria.

covered from mechanical milling plants. The properties of the different fibre concretes in the fresh and hardened states are analysed and compared with natural non-fibre concrete.

Results: The experimental results suggest that incorporating such waste in concrete reduces the workability of concrete mixtures, improves the tensile strength of concrete, and reduces considerably its shrinkage without affecting its compressive strength.

Conclusion: Following a rigorous analysis of the obtained results, it was determined that the optimum percentage of recycled fibre in steel is 15%. The tensile strength at this level is comparable to that of industrial fibre-reinforced concrete. This finding is very relevant to the sustainable development strategy of the Algerian government, which promotes the improvement of characteristics and the conservation of natural resources.

Key words: fibre concrete, industrial fibres, dimensional variation, mechanical characteristics, metal waste, recovery.

Introduction

For more than half a century, fibre-reinforced concrete has been the focus of major research efforts in the construction industry. Cement-fibre and concrete-fibre composites represent a major technological advance in many areas of construction and public works (Blazy and Blazy, 2021). In this context, one of the most important ways of improving the performance of concrete is to distribute fibres evenly throughout its volume, resulting in a material known as fibre-reinforced concrete. Several research projects aimed at developing high-performance cementitious matrices have stimulated interest in the use of all types of fibre-reinforced cementitious composites, as studied (BERNIER, 1991).

Several types of fibres of different sizes and shapes, made from many different materials are used; steel fibres are most commonly used, but glass, polypropylene, graphite or Kevlar fibres can also be used (Shah & Ribakov, 2011). A combination of factors, such as the properties of the fibre material, the ability to form bonds between the matrix and the fibres, the content and concentration of fibres in the composite, and the way in which the fibre-reinforced concrete is produced, determines the effectiveness of the fibre action and the resulting mechanical properties of the material (Zollo, 1997). The effectiveness of steel fibres is significantly influenced by their shape and proportions; the aspect ratio is the most important parameter describing the geometrical proportions of the fibres.

A further important factor is the shape of the fibre anchor, which prevents the fibre from being pulled out of the matrix. Fibres with hooked

or small heads at their ends are commonly used (Martinie et al, 2010; Shah & Ribakov, 2011). The addition of industrial or certain types of recycled fibres to concrete has a beneficial effect on several of its mechanical properties, such as tensile strength, shrinkage, crack resistance and ductility (Borg et al, 2016; Irki et al, 2017; Mohammadi et al, 2008; Pešić et al, 2016). As well as using industrial fibres to reinforce concrete, certain fibres can be recovered from by-products, and a number of researchers have investigated the mechanical behaviour of fibre-reinforced concrete (FRC) made from both industrial steel fibres and recycled steel fibres recovered from scrap tyres (Martinelli et al, 2015; Onuaguluchi & Banthia, 2018). In addition, the thinner and shorter fibres recovered from tyres were found to be significantly more rigid, giving the fibre-reinforced concrete (FRC) better mechanical parameters (Li et al, 2004a; 2004b). The result is more ductile products capable of limiting the propagation of damage while ensuring greater durability. These materials are very recent for a sector such as civil engineering, where innovation is difficult (BERNIER, 1991; Rossi & Harrouche, 1990).

There is a wide range of literature on the use of fibres to modify the properties of concrete. Fibres have different effects on the mechanical parameters of concrete - they can improve or deteriorate the properties, depending on the geometry and material of the fibres. It's important to study how the incorporation of recycled fibres affects the concrete and mortars' behaviour in order to explore their effective use as fibre reinforcement (Irki et al, 2018). A number of studies have tested cementitious and polymer matrices reinforced with natural recycled fibres (Abdelaziz et al, 2016; Fiore et al, 2014; Hbib et al, 2011; Irki et al, 2018), while Grzymski et al. (2019) investigated the mechanical properties of concrete incorporating recycled fibres derived from machining waste.

This paper investigates the use of recycled aluminium and steel scrap from mechanical milling in the form of chips, incorporated into conventional vibrated concrete to ensure sufficient water tightness, avoiding high humidity or the presence of water which can cause corrosion of aluminium scrap in alkaline environments (CSTB, 2008), and describes the basic mechanical properties and compares them with industrial fibres. These studies are consistent with the current trend towards sustainable development, and, like other recycled fibres, may help to make effective use of machining waste.

Experimental materials and methods

Materials

In the present study, all mortar mixtures employed a local commercial Portland cement CEM II/B 42.5 sourced from Msila, Algeria. This cement has a Blaine fineness of 385 m²/kg, a density of 3.15, and an average compressive strength of 42.5 MPa at 28 days. It exhibits a low hydration rate and contains a limited amount of sulphides. Table 1 provides a summary of the cement's chemical composition.

Table 1 – Chemical analysis of *the* cement used in the experimental program

Chemical composition (wt %)						
SiO2	Al2O3	Fe2O3	SO3	CaO	MgO	LOI
20.92	5.33	3.43	1.83	61.74	1.58	1.65

The coarse aggregates consisted of natural crushed limestone, with a maximum size of 20 mm and a specific gravity of 2530 kg/m3. For the fine aggregates, a blend comprising 40.17% fine roller sand with a fineness modulus of 1.00 and 59.83% coarse limestone crushed quarry sand was used, with a fineness modulus of 3.35. The overall fineness modulus of this combination was 2.80. These aggregates had a specific gravity of 2550 kg/m3 and a water absorption rate of 1.52%. The physical and mechanical characteristics of the sands are shown in Table 2. Table 3 shows the characteristics of the fibres used for this purpose.

Table 2 – Aggregate characteristics

Characteristics	Fine aggregate		Coarse aggregate	
	roller sand (0/3)	crushed sand (0/5)	8/15	15/25
Finesse modulus	1.00	3.35	/	/
Bulk density (g/cm^3)	2.48	2.54	2.50	2.53
Absolute density (g/cm^3)	1.42	1.49	1.29	1.27
Sand equivalent test SE (%)	69.52	90.60	/	/
Water absorption (%)	1	1.8	0.70	0.80

The recycled fibres are incorporated into the concrete at a rate of 5, 10, 15, 20 and 25% by mass of the cement paste. These rates correspond to 0.5, 1, 2 and 3% by volume of recycled steel fibres and 0.25, 0.75, 1

and 1.25% by concrete volume of recycled aluminium fibres. On the other hand, the industrial fibres are incorporated at 1% by concrete volume.

Table 3 – Mechanical properties of the used fibres

Type of Fibre	FI50 (F1)	T30/50 (F2)	RS	RA
L (mm)	35	30	20	20
D /Thick (mm)	0.60	0.50	0.30	0.30
Width (± 0.1mm)	/	/	3	3
Aspect ratio (l/d)	58	60	66	66
Form	Wavy	hooked	spiral	spiral
Modulus of elasticity[GPa]	210	210	150	69
Elongation at break (%)	4	3.40	0.8	3
Tensile resistance [MPa]	1180	1000	890	120

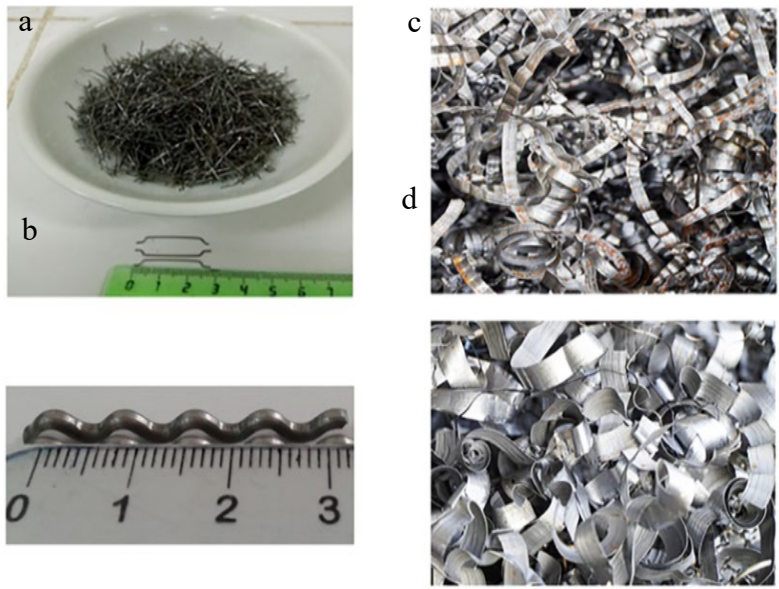

Figure 1 – (a) Industrial fibre (F1), (b) Industrial fibre (F2), (c) Recycled fibre (RS) and (d) Recycled fibre (RA)

Method

The composition of the concrete, with a cement dosage of 350 kg/m3, was based on the BARON-LESAGE method developed at the Laboratoire des Ponts et Chaussées, Paris (Baron & Lesage, 1976), based on the

optimisation of the granular skeleton in the concrete by varying the dosage of fine aggregate in relation to coarse aggregate. The flow time is measured by the LCPC Manibilimeter. This optimisation is shown in Figure 2.

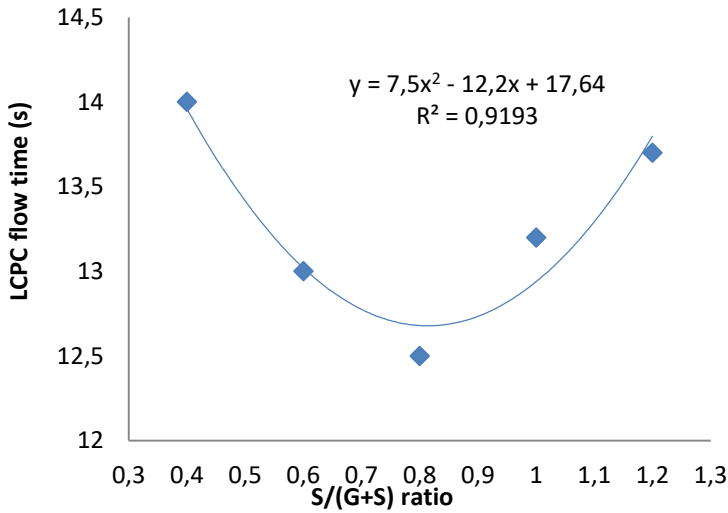

Figure 2 – Granular skeleton optimization

For all mixes, the fine aggregate/total aggregate ratio is kept constant at 0.8, by applying the recommendations of the Baron-Lesage method, summarised as follows:

- A constant W/C ratio for all mixtures is mantained; in this study this ratio is set at W/C= 0.4;
- Flow time is maintained between 8 and 13 seconds, measured with an LCPC maniabilimeter;
- To achieve the last condition, it is necessary to use a plasticizing adjuvant to obtain the desired workability. Table 4 shows the composition of the mixtures studied.

While RC represents the Reference Concrete, RS-C is the recycled steel concrete, and RA-C is the recycled aluminium concrete, whereas F1-C and F2-C are concretes based on fI50 and T30/50 fibres respectively.

Table 4 – Concrete composition

	RC	F1-C	F2-C	RS-C (%)				RA-C (%)			
				5	10	15	20	5	10	15	20
Cement (kg)	350										
Roller sand. (kg)	326.77										
Crushed sand (Kg)	470.23										
8/15 (Kg)	106.33										
15/25 (Kg)	890										
Water (kg)	140										
W/C	0.40										
S/(G+S)	0.80										
Fibre (kg)	0	20		17.5	30	52.5	87.5	17.5	30	52.5	70
Plasticizer (kg)	1.75	2.45	2.10	2.10	2.275	2.450	2.62	2.27	2.45	2.45	2.62

Experimental results and discussion

The results of the various tests on fresh and hardened concrete are shown below, representing the average of at least three test results.

The mixes must have practically constant workability in order to compare the results of the different types of concrete. A third generation plasticiser based on ether polycarbocxylate, supplied by Granitex Algerie (Medaflow 30), was introduced to optimise a consistent flow time interval.

Workability of concrete

In accordance with the recommendations of Standard NF P18-452 (AFNOR, 2017), the workability of the concretes produced is measured using an LCPC workability meter. A constant workability was optimised in order to compare the results in the hardened state, with the flow time considered to be between 10 and 12 seconds (±0.5s). The results of this stage are shown in Figure 3.

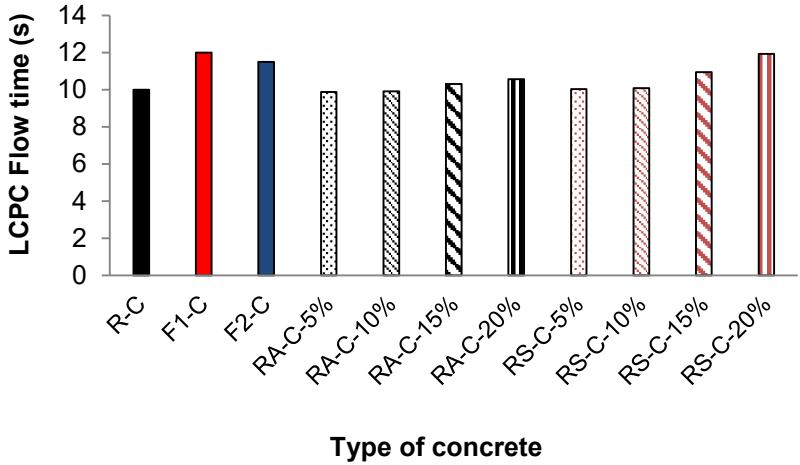

Figure 3 – Flow times for different types of concrete

The results show that the workability of the concrete decreases as the fibre incorporation dosage increases. For this test, the plasticizer dosage was varied to achieve comparable workability between the concretes. For low fibre dosages, workability comparable to the control concrete was recorded, but the higher the fibre dosage, the lower the workability and the concrete required a higher percentage of plasticiser, varying between 30% and 55% compared to the reference concrete. We can also see that the two types of recycled fibres show the same variation.

This finding has been confirmed by other researchers who have incorporated fibres and/or by-products as fibres in high-performance and self-compacting concretes (Borg et al, 2016; Centonze et al, 2012; Corinaldesi & Moriconi, 2011; Irki et al, 2017; Irki et al, 2018; Swamy & Mangat, 1974; Westerholm et al, 2008). On the other hand, industrial fibres affect workability more than recycled fibres, which may be due to the shape of the fibres and their high stiffness (Martinie et al, 2010).

Occluded air

Incorporating fibres can change some properties in the fresh and cured state, including air content, which is measured in this study according to EN 12350-7 (CEN, 2009).

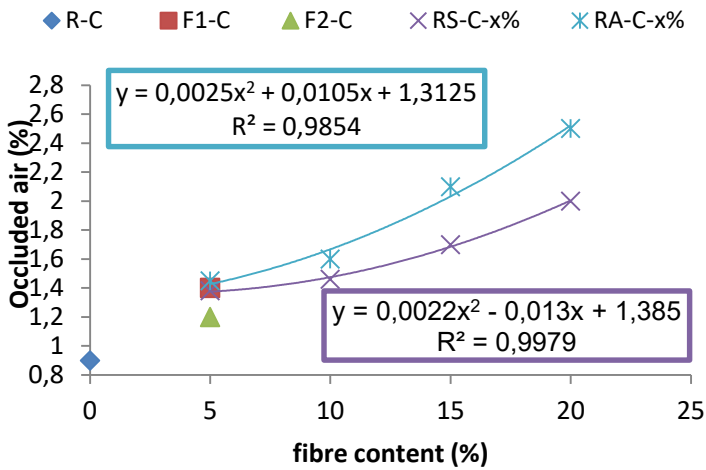

Figure 4 – Occluded air of concrete mixtures

It can be seen that for all the blends the entrapped air varies between 1.4 and 2.6%, which are considered reasonable values (Ortega-Lopez et al, 2021). The percentage of spherical pores in the blends increases as the recycled fibre dosage increases; the spiral shape of the recycled fibres favours the formation of micro-bubbles, and the formation of voids at the fibre/solid matrix interface as a result of air bubbles being entrapped by the fibres during the mixing process (d'Almeida et al, 2006; Pons Ribera et al, 2023; Sakami et al, 2020).

It is very important to investigate whether concrete properties improve by increasing air entrainment. Entrained air can improve freeze-thaw resistance, but it can also reduce the concrete density and decrease compressive strength as seen in Figures 5 and 6 (de Oliveira & Castro-Gomes, 2011; Irki et al, 2017; Irki et al, 2018; Savastano et al, 1999).

Bulk density

The density of fresh concrete was calculated in accordance with Standard NF EN 12350-6 (12350-6, 2019), using the receptacle of the occluded air apparatus.

From the results obtained for density, a decrease in density was observed with increasing fibre dosage. Since the variation is in the order of 0.42% to 2.50%, this decrease is considered a moderate variation (Pons Ribera et al, 2023).

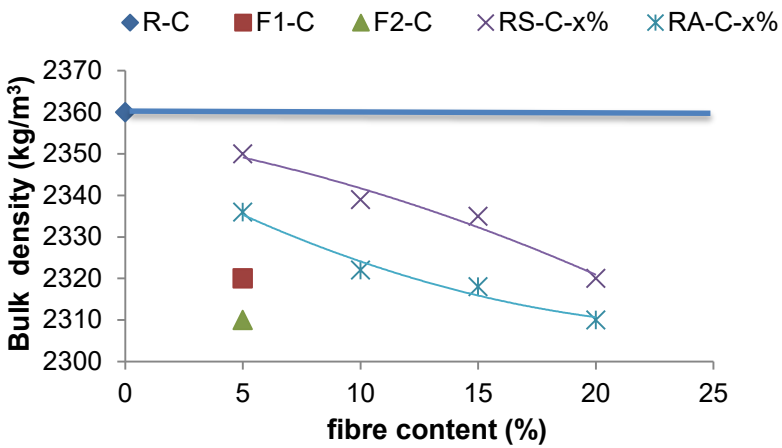

Figure 5 – Bulk density of concretes

The spiral shape of the fibres, which allows the cement paste to penetrate, may be responsible for this small reduction. Moreover, RAC-C-x% blends have a lower density than RS-C-x% blends because steel is known to have a higher density than aluminium. However, incorporating both types of fibre reduces concrete density.

The incorporation of fibres generates more voids at fibre/ matrix interface during the mixing process, causing an increase in porosity and a decrease in bulk density (Abani et al, 2015). Similar results were observed by Sakami et al. (2020), who reported a reduction in bulk density of up to 14.68% when 5% Alfa fibre reinforcement by mass was used.

Compressive strength

The compressive strength of hardened mortar was measured using 100 mm cubic specimens at the age of 28 days, as per References EN12390-1 and EN12390-2 (EN, 2000, 2009b; EN, 2009b). The specimens were covered with plastic sheets, stored in the laboratory for 24 hours, and then cured in water at 20°C. Figure 6 presents the results for 7, 28, and 90 days of curing.

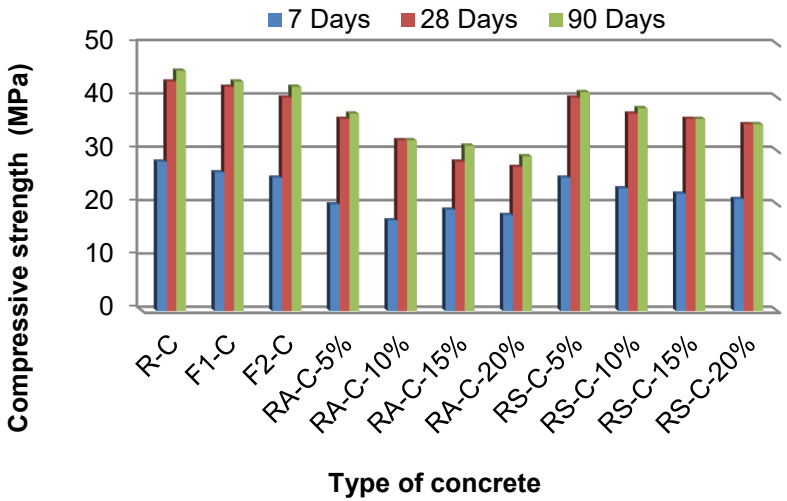

Figure 6 – Variation of the compressive strength with fibre type and amount

The results show that the incorporation of fibres (all types) affects the compressive strength of concrete (Irki et al, 2017; Irki et al, 2018; Savastano et al, 1999). The average reduction is from 7 to 10% for industrial fibres, from 16 to 35% for the RAC-C-x% series and from around 7% to 15% for RS-C-x% series, which is probably due to the decrease in compactness concretes by the increase of occurred air.

It should also be noted that the strength of concrete based on aluminium scrap is more affected. This may be due to the flexibility of this type of waste, whereas steel scrap shows a slight decrease in strength due to better mechanical properties.

Similarly, other researchers have reported that the decrease in compressive strength of SFRCs is due to the decrease in ductility and workability as the volume fraction of fibres increases. The inclusion of fibres leads to a change in failure mode from brittle to ductile failure (Borg et al, 2016; Centonze et al, 2012; Corinaldesi & Moriconi, 2011; Ferrara et al, 2007; Irki et al, 2017)

Flexural strength

The splitting tensile strength was measured at 7, 28 and 90 days of age by a 3-point flexure test using a testing machine with a maximum load capacity of 30 kN according to EN 12390-5 (EN, 2009a). All moulds were covered with plastic sheeting and stored in the laboratory for 24 hours before demoulding. The moulds were cured in water at 20 °C.

The results show that the incorporation of industrial fibres significantly improves the flexural tensile strength. This improvement ranges from 34 to 45% and is due to the shape of the fibres (corrugated and hooked), which ensures better load transmission and adhesion to the concrete (Irki et al, 2017).

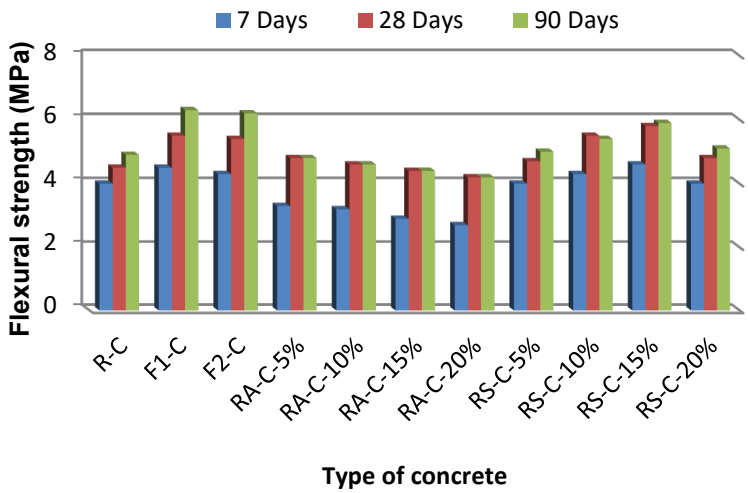

Figure 7 – Variation of the flexural strength with fibre type and amount

Looking at the strengths of the concrete series containing aluminium and steel waste, it can be seen that the RAC-C-x% series shows an inverse relationship with the incorporation of waste (fibres): the flexural tensile strength decreases as the percentage of waste increases. This variation is in the order of 4 to 16%. This is due to reduced concrete compaction resulting from increased porosity (Savastano et al, 1999). Contrary to the RS-C-x% series, the flexural tensile strength is comparable to the reference concrete at a low dosage (5%). After this amount, the strength is improved by 10 and 16% for the RS-C-10% and RS-C-15% mixes, respectively; above this percentage (RS-C-20%), the strength decreases. The increase in the flexural tensile strength confirms the good adhesion between the steel waste and the cementitious matrix, which allows a favourable load transfer up to the saturation level (20%), where the matrix becomes heterogeneous and begins to lose its mechanical properties (Bledzki & Gassan, 1999; Irki et al, 2018; Li et al, 2006).

Conclusion

The use of recycled fibres in the reinforcement of concrete has the effect of modifying some of the properties of Fibre Reinforced concrete:

(a) The granular skeleton of the concrete must be optimised before formulating fibre reinforced concrete.
(b) In order to guarantee the workability of the fibre-reinforced concrete, the higher the fibre content, the greater the need for plasticiser, indicating a reduction in workability with increasing fibre content.
(c) The incorporation of steel and aluminium fibres as well as industrial fibres reduces the density of the concrete. As the density of aluminium is lower than that of steel, concretes based on aluminium fibres have a lower density than those based on steel fibres.
(d) The amount of occluded air generated during the mixing process increases as the recycled fibre content is increased, but is generally acceptable according to the standard.
(e) The compressive strength of concrete reinforced with recycled fibres decreases with increasing fibre content. On average, this decrease is estimated to be 16 to 35% for concrete made from aluminium waste and 7 to 16% for concrete reinforced with steel waste. The strength of concrete made from steel is comparable to that of concrete reinforced with industrial fibres.
(f) Contrary to the compressive strength, the tensile strength of SFR-C increases for industrial fibres (by about 20%).
(g) Two phenomena were observed for the recycled fibre concretes: on the one hand, a gradual decrease in the flexural tensile strength for aluminium fibre concretes (from 2 to 12%) as the percentage is increased.
(h) On the other hand, a gradual improvement of this strength up to 15% of the incorporation dosage (2 to 20% gain in strength), after this amount, the strength decreases.
(i) The optimum percentage of recycled fibre in steel is 15%. the tensile strength at this level is comparable to that of industrial fibre-reinforced concrete.

The use of steel waste is very effective at a dosage of 15% by weight of cement and can be used for the reinforcement of non-structural elements that are subject to simple bending, such as manhole slabs, and sustainable pavements.

The results presented in this paper are part of a research project focusing on the valorisation of industrial waste by-products in civil engineering sector.

References

12350-6, E. 2019. Testing Fresh Concrete. Density. European Committee for Standardization (CEN) Brussels, Belgium. [online]. Available at: https://cdn.standards.iteh.ai/samples/64407/d6e4d96fe65c4643b6369b92b72b4273/SIST-EN-12350-6-2019.pdf

ABANI, S., HAFSI, F., KRIKER, A. & BALI, A. 2015. Valorisation of date palm fibres in Sahara constructions. Energy Procedia, 74, 289-293. Available at: https://doi.org/10.1016/j.egypro.2015.07.608

ABDELAZIZ, S., GUESSASMA, S., BOUAZIZ, A., HAMZAOUI, R., BEAUGRAND, J. & SOUID, A. A. 2016. Date palm spikelet in mortar: Testing and modelling to reveal the mechanical performance. Construction and Building Materials, 124, 228-236. Available at: https://doi.org/10.1016/j.conbuildmat.2016.07.039

AFNOR, N. 2017. P 18-452, Concretes-Measuring the flow time of concretes and mortars using a workability meter. AFNOR, Paris. . [online]. Available at: https://www.boutique.afnor.org/en-gb/standard/nf-p18452/concretes-measuring-the-flow-time-of-concretes-and-mortars-using-a-workabil/fa171358/58582

BARON, J. & LESAGE, R. La composition du béton hydraulique du laboratoire au chantier. 1976. LCPC. [online]. Available at: https://www.ifsttar.fr/fileadmin/user_upload/editions/lcpc/RapportsDeRecherche/RapportDeRecherche-LCPC-RR64.pdf

BERNIER, G. Caractérisation et contrôle des bétons renforcés de fibres. Annales de l'Institut technique du bâtiment et des travaux publics, 1991. [online]. Available at: http://worldcat.org/issn/00202568

BLAZY, J. & BLAZY, R. 2021. Polypropylene fiber reinforced concrete and its application in creating architectural forms of public spaces. Case Studies in Construction Materials, 14, e00549. Available at: https://doi.org/10.1016/j.cscm.2021.e00549

BLEDZKI, A. & GASSAN, J. 1999. Composites reinforced with cellulose based fibres. Progress in polymer science, 24, 221-274. Available at: https://doi.org/10.1016/S0079-6700(98)00018-5

BORG, R. P., BALDACCHINO, O. & FERRARA, L. 2016. Early age performance and mechanical characteristics of recycled PET fibre reinforced concrete. Construction and Building Materials, 108, 29-47. Available at: https://doi.org/10.1016/j.conbuildmat.2016.01.029

CEN 2009. EN 12350-7. Testing fresh concrete–Part 7: Air content–pressure methods. CEN Brussels, Belgium. . [online]. Available at: https://standards.iteh.ai/catalog/standards/cen/a9a40cf5-59cc-4ccd-8b0b-

f3398af736a2/en-12350-7-2009?srsltid=AfmBOopCXx_3YSIcJto9wDj5xJzhTm6NcnjQ1laGo-Y8FsS0xi3LcCRs

CENTONZE, G., LEONE, M. & AIELLO, M. 2012. Steel fibers from waste tires as reinforcement in concrete: a mechanical characterization. Construction and Building Materials, 36, 46-57. Available at: https://doi.org/10.1016/j.conbuildmat.2012.04.088

CORINALDESI, V. & MORICONI, G. 2011. Characterization of self-compacting concretes prepared with different fibers and mineral additions. Cement and Concrete Composites, 33, 596-601. Available at: https://doi.org/10.1016/j.cemconcomp.2011.03.007

CSTB 2008. Comportement de l'aluminium et ses alliages utilisés dans le bâtiment en contact avec le plâtre ou le ciment ainsi que d'autres matériaux. In: CEBT, VERITAS, B., INT., C. A., CONSTRUCTION, N., SOCOTEC, QUALICONSULT & SNFA (eds.) Fiche Technique N° 40 - A. [online]. Available at: https://www.fenetrealu.com/uploads/documents/fiche-technique-40-comportement-aluminium-contact-platre-ciment-75.pdf

D'ALMEIDA, J., AQUINO, R. & MONTEIRO, S. 2006. Tensile mechanical properties, morphological aspects and chemical characterization of piassava (Attalea funifera) fibers. Composites Part A: Applied Science and Manufacturing, 37, 1473-1479. Available at: https://doi.org/10.1016/j.compositesa.2005.03.035

DE OLIVEIRA, L. A. P. & CASTRO-GOMES, J. P. 2011. Physical and mechanical behaviour of recycled PET fibre reinforced mortar. Construction and Building Materials, 25, 1712-1717. https://doi.org/10.1016/j.conbuildmat.2010.11.044

EN, B. 2009a. 12390–5 Testing hardened concrete–Part 5: Flexural strength of test specimens. British Standards Institution-BSI and CEN European Committee for Standardization. [online]. Available at: https://standards.iteh.ai/catalog/standards/cen/275df2f9-c466-4bb1-b41c-b8dfa9fc6d89/en-12390-5-2009?srsltid=AfmBOoqhs9jw2HZ_-JzJ7Yn4vB3zpQbdbZoBpznoFubiasbjKAIyAFXP

EN, C. 2000. 12390-1 Testing hardened concrete–Part 1: Shape, dimensions and other requirements for specimens and moulds. European Committee for Standardization. [online]. Available at: https://standards.iteh.ai/catalog/standards/cen/d1c9ccee-2e5a-425e-a964-961da95d2f99/en-12390-1-2021?srsltid=AfmBOorR30AMbdfc8t1epjwLcjCXgb4Wy0SKZBxjNvkqFIUXdF-Opq5y

EN, T. 2009b. 12390-2,"Testing hardened concrete-Part 2: Making and curing specimens for strength tests". Brussels, Belgium: European Committee for Standardization. [online]. Available at: https://standards.iteh.ai/catalog/standards/cen/ae7e6a86-1cbc-455e-8b2a-8964be9087f9/en-12390-2-2019?srsltid=AfmBOooi0JX5FSZ7DDHXOW6U3YkK7kWxBzhYe1J-7gNFdrbCqbb6NwZG

FERRARA, L., PARK, Y.-D. & SHAH, S. P. 2007. A method for mix-design of fiber-reinforced self-compacting concrete. Cement and Concrete Research, 37, 957-971. Available at: https://doi.org/10.1016/j.cemconres.2007.03.014

FIORE, V., SCALICI, T. & VALENZA, A. 2014. Characterization of a new natural fiber from Arundo donax L. as potential reinforcement of polymer composites. Carbohydrate polymers, 106, 77-83. Available at: https://doi.org/10.1016/j.carbpol.2014.02.016

GRZYMSKI, F., MUSIAŁ, M. & TRAPKO, T. 2019. Mechanical properties of fibre reinforced concrete with recycled fibres. Construction and Building Materials, 198, 323-331. Available at: https://doi.org/10.1016/j.conbuildmat.2018.11.183

HBIB, M., GUESSASMA, S., BASSIR, D. & BENSEDDIQ, N. 2011. Interfacial damage in biopolymer composites reinforced using hemp fibres: finite element simulation and experimental investigation. Composites Science and Technology, 71, 1419-1426. Available at: https://doi.org/10.1016/j.compscitech.2011.05.015

IRKI, I., DEBIEB, F., KADRI, E.-H., BOUKENDAKDJI, O., BENTCHIKOU, M. & SOUALHI, H. 2017. Effect of the length and the volume fraction of wavy steel fibers on the behavior of self-compacting concrete. Journal of adhesion science and Technology, 31, 735-748. Available at: https://doi.org/10.1080/01694243.2016.1231394

IRKI, I., EULDJI, M., BENSABER, H. & SETTARI, C. 2018. Characterization of stem phoenix fibres as potential reinforcement of self compacting mortar. Journal of adhesion science and Technology, 32, 1629-1642. Available at: https://doi.org/10.1080/01694243.2018.1442654

LI, G., GARRICK, G., EGGERS, J., ABADIE, C., STUBBLEFIELD, M. A. & PANG, S.-S. 2004a. Waste tire fiber modified concrete. Composites Part B: Engineering, 35, 305-312. Available at: https://doi.org/10.1016/j.compositesb.2004.01.002

LI, G., STUBBLEFIELD, M. A., GARRICK, G., EGGERS, J., ABADIE, C. & HUANG, B. 2004b. Development of waste tire modified concrete. Cement and Concrete Research, 34, 2283-2289. Available at: https://doi.org/10.1016/j.cemconres.2004.04.013

LI, Z., WANG, L. & WANG, X. 2006. Flexural characteristics of coir fiber reinforced cementitious composites. Fibers and Polymers, 7, 286-294. Available at: https://doi.org/10.1007/BF02875686

MARTINELLI, E., CAGGIANO, A. & XARGAY, H. 2015. An experimental study on the post-cracking behaviour of Hybrid Industrial/Recycled Steel Fibre-Reinforced Concrete. Construction and Building Materials, 94, 290-298. Available at: https://doi.org/10.1016/j.conbuildmat.2015.07.007

MARTINIE, L., ROSSI, P. & ROUSSEL, N. 2010. Rheology of fiber reinforced cementitious materials: classification and prediction. Cement and Concrete Research, 40, 226-234. Available at: https://doi.org/10.1016/j.cemconres.2009.08.032

MOHAMMADI, Y., SINGH, S. & KAUSHIK, S. 2008. Properties of steel fibrous concrete containing mixed fibres in fresh and hardened state. Construction

and Building Materials, 22, 956-965. Available at: https://doi.org/10.1016/j.conbuildmat.2006.12.004

ONUAGULUCHI, O. & BANTHIA, N. 2018. Scrap tire steel fiber as a substitute for commercial steel fiber in cement mortar: Engineering properties and cost-benefit analyses. Resources, Conservation and Recycling, 134, 248-256. Available at: https://doi.org/10.1016/j.resconrec.2018.03.014

ORTEGA-LOPEZ, V., GARCIA-LLONA, A., REVILLA-CUESTA, V., SANTAMARÍA, A. & SAN-JOSE, J. T. 2021. Fiber-reinforcement and its effects on the mechanical properties of high-workability concretes manufactured with slag as aggregate and binder. Journal of Building Engineering, 43, 102548. Available at: https://doi.org/10.1016/j.jobe.2021.102548

PEŠIĆ, N., ŽIVANOVIĆ, S., GARCIA, R. & PAPASTERGIOU, P. 2016. Mechanical properties of concrete reinforced with recycled HDPE plastic fibres. Construction and building materials, 115, 362-370. Available at: https://doi.org/10.1016/j.conbuildmat.2016.04.050

PONS RIBERA, S., HAMZAOUI, R., COLIN, J., BESSETTE, L. & AUDOUIN, M. 2023. Valorization of vegetal fibers (Hemp, Flax, Miscanthus and Bamboo) in a fiber reinforced screed (FRS) formulation. Materials, 16, 2203. Available at: https://doi.org/10.3390/ma16062203

ROSSI, P. & HARROUCHE, N. 1990. Mix design and mechanical behaviour of some steel-fibre-reinforced concretes used in reinforced concrete structures. Materials and Structures, 23, 256. Available at: https://doi.org/10.1007/BF02472199

SAKAMI, S., BOUKHATTEM, L., BOUMHAOUT, M. & BENHAMOU, B. 2020. Development of alfa fiber-based mortar with improved thermo-mechanical properties. Applied Sciences, 10, 8021. Available at: https://doi.org/10.3390/app10228021

SAVASTANO, H., AGOPYAN, V., NOLASCO, A. M. & PIMENTEL, L. 1999. Plant fibre reinforced cement components for roofing. Construction and Building Materials, 13, 433-438. Available at: https://doi.org/10.1016/S0950-0618(99)00046-X

SHAH, A. A. & RIBAKOV, Y. 2011. Recent trends in steel fibered high-strength concrete. Materials & Design, 32, 4122-4151. Available at: https://doi.org/10.1016/j.matdes.2011.03.030

SWAMY, R. & MANGAT, P. 1974. Influence of fibre-aggregate interaction on some properties of steel fibre reinforced concrete. Materials and Structures, 7, 307-314. Available at: https://doi.org/10.1007/BF02473840

WESTERHOLM, M., LAGERBLAD, B., SILFWERBRAND, J. & FORSSBERG, E. 2008. Influence of fine aggregate characteristics on the rheological properties of mortars. Cement and Concrete Composites, 30, 274-282. Available at: https://doi.org/10.1016/j.cemconcomp.2007.08.008

ZOLLO, R. F. 1997. Fiber-reinforced concrete: an overview after 30 years of development. Cement and concrete composites, 19, 107-122. Available at: https://doi.org/10.1016/S0958-9465(96)00046-7

Održivo ojačavanje betona vlaknima upotrebom nusproizvoda iz proizvodnje

Ilyes Irki[a], **autor za prepisku**, *Mohamed* Kesseir[b], *Farid* Debieb[b], *Chafika* Settari[b]

[a] University Centre of Tipaza, Civil Engineering Department, Faculty of Science, Tipaza, People's Democratic Republic of Algeria + Laboratory of Civil Engineering and Protection of Environment (LCEPE), Medea, People's Democratic Republic of Algeria

[b] Laboratory of Civil Engineering and Protection of Environment (LCEPE), Medea, People's Democratic Republic of Algeria

OBLAST: materijali
KATEGORIJA (TIP) ČLANKA: originalni naučni rad

Sažetak:

Uvod/cilj: Beton je materijal sa veoma visokom kompresivnom, ali veoma niskom zateznom čvrstoćom, što ga čini krtim pri delovanju zateznih i savojnih naprezanja, pri čemu se prevremeni lom manifestuje pojavom pukotina. Ova naprezanja mogu se smanjiti ojačavanjem betona različitim vrstama vlakana dobijenih iz industrijskog ili drugog otpada.

Metode: U tom kontekstu, cilj ovog rada je primena industrijskog metalnog otpada u sastav betona i njegovo poređenje sa betonom ojačanim metalnim vlaknima radi prevazilaženja nedostatka zatezne čvrstoće. Korišćene su dve vrste industrijskih vlakana i dve vrste otpada, aluminijumski i čelični otpad (u obliku strugotina) dobijen iz postrojenja za mehaničku obradu. Svojstva svežih i očvrslih betona sa različitim vlaknima analizirana su i upoređena sa prirodnim betonom koji ne sadrži vlakna.

Rezultati: Na osnovu eksperimentalnih rezultata može se zaključiti da primena ovakvog otpada u sastav betona dovodi do smanjenja obradivosti betonskih mešavina, poboljšanja zatezne čvrstoće i značajnog smanjenja skupljanja betona, bez uticaja na kompresivnu čvrstoću.

Zaključak: Nakon detaljne analize dobijenih rezultata, utvrđeno je da je optimalni procenat recikliranih čeličnih vlakana 15%. Zatezna čvrstoća na ovom nivou uporediva je sa čvrstoćom betona koji je ojačan industrijskim vlaknima. Ovo otkriće je posebno značajno za strategiju održivog razvoja Vlade Alžira koja promoviše unapređenje karakteristika materijala i očuvanje prirodnih resursa.

Ključne reči: beton ojačan vlaknima, industrijska vlakna, dimenzionalne promene, mehaničke karakteristike, metalni otpad, oporavak.

Paper received on: 7 April 2025.
Manuscript corrections submitted on: 9 April 2025.
Paper accepted for publishing on: 6 August 2026.

© 2026 The Authors. Published by Vojnotehnički glasnik / Military Technical Courier (www.vtg.mod.gov.rs). This article is an open access article distributed under the terms and conditions of the Creative Commons Attribution license (http://creativsecommons.org/licenses/by/4.0/rs/).

CALL FOR PAPERS AND ARTICLE FORMATTING INSTRUCTIONS

The instructions to authors about the article preparation for publication in the *Military Technical Courier* are based on the Regulations on categorization and ranking of scientific journals of the Ministry of Education, Science and Technological Development of the Republic of Serbia (Official Gazette of the Republic of Serbia, No 159/20). This Regulations aims at improving the quality of national journals and raising the level of their compliance with the international system of scientific information exchange.

The Military Technical Courier / Vojnotehnički glasnik (www.vtg.mod.gov.rs/index-e.html, ISSN 0042-8469 – print issue, e-ISSN 2217-4753 – online, UDC 623+355/359, DOI: 10.5937/VojnotehnickiGlasnik; https://doi.org/10.5937/VojnotehnickiGlasnik), is an peer-reviewed scientific journal.

The owners of the journal are the Ministry of Defence of the Republic of Serbia and the Serbian Armed Forces. The publisher and financier of the *Military Technical Courier* is the University of Defence in Belgrade (Military Academy).

The program of the journal is based on the annual classification of journals performed by a relevant Ministry as well as on its indexing in international indexing databases.

The journal covers scientific and professional fields within the educational-scientific field of **Natural-Mathematical Sciences**, as well as within the educational-scientific field of **Technical-Technological Sciences**, and especially the field of **defense sciences and technologies**. It publishes theoretical and practical achievements leading to professional development of all members of Serbian, regional and international academic communities as well as members of the military and ministries of defence in particular. It publishes papers with balanced coverage of analytical, experimental, and applied research as well as numerical simulations from various disciplines. The material published is of high quality and relevance, written in a manner that makes it accessible to a wider readership. The journal welcomes papers reporting original theoretical and/or practice-oriented research as well as extended versions of already published conference papers. Manuscripts for publication are selected through a double-blind peer-review process to validate their originality, relevance, and readability. This being so, the objective is not only to keep the quality of published papers high but also to provide a timely, thorough, and balanced review process.

The editorial policy of the *Military Technical Courier* is based on the COPE Core Practices, common COPE, DOAJ, OASPA and WAME Principles of Transparency and Best Practice in Scholarly Publishing as well as on the best accepted practices in scientific publishing. The Military Technical Courier has been a COPE (Committee on Publication Ethics) member since 2nd May 2018 and a member of OASPA (Open Access Scholarly Publishers Association) since 27th November 2015.

The Ministry of Science, Technological Development and Innovation of the Republic of Serbia classified the *Military Technical Courier* for the year 2025, on December, 2025:

- **on the list of periodicals for computer sciences,**
  category: reputed national journal **(M51)**,
- **on the list of periodicals for electronics, telecommunications and IT,**
  category: reputed national journal **(M51)**,
- **on the list of periodicals for mechanical engineering,**
  category: reputed national journal **(M51)**,
- **on the list of periodicals for materials and chemical technology,**
  category: national journal of international importance **(M24)**.

The approved lists of national periodicals for the year 2025 can be viewed on the website of the *Military Technical Courier*, page *Journal categorization*.

More detailed information can be found on the website of the Ministry of Education, Science and Technological Development of the Republic of Serbia.

The information on the categorization can be also found on the website of KOBSON (Consortium of Libraries of Serbia for Unified Acquisition).

The periodical is categorized in compliance with the Regulations on categorization and ranking of scientific journals of the Ministry of Education, Science and Technological Development of the Republic of Serbia (Official Gazette of the Republic of Serbia, No 159/20). More detailed information can be found on the website of the Ministry of Education, Science and Technological Development.

The journal is in the Serbian Citation Index – SCIndex (data base of national scientific journals), in the Scientific Information System Redalyc, and in the Russian Index of Science Citation/Российский индекс научного цитирования (RINC/РИНЦ) and is constantly monitored depending on the impact within the bases themselves. More detailed information can be viewed on the website of the *Military Technical Courier*, page *Journal indexing*.

The *Military Technical Courier*, in terms of its content, offers the possibility of open access (DIAMOND OPEN ACCESS) and applies the Creative Commons Attribution (CC BY) licence on copyright. The copyright details can be found on the *Copyright notice and Self-archiving policy* page of the journal's website.

Manuscripts are submitted online, through the electronic editing system ASSISTANT, developed by the Center for Evaluation in Education and Science – CEON.

The access and the registration are through the *Military Technical Courier* site http://www.vtg.mod.gov.rs/index-e.html, on the page *ASSISTANT* or the page *SCINDEKS* or directly through the link (aseestant.ceon.rs/index.php/vtg).

The detailed instructions about the registration for the service are on the website http://www.vtg.mod.gov.rs/index-e.html, on the page *Instructions for ASSISTANT*.

All authors submitting a manuscript for publishing in the *Military Technical Courier* should register for an ORCID ID following the instructions on the web page *Registration for an ORCID identifier*.

The *Military Technical Courier* publishes articles in English, using Arial and a font size of 11pt with Single Spacing.

The procedures of article preparation, writing and editing should be in accordance with the *Publication ethics statement* (http://www.vtg.mod.gov.rs/publication-ethics-statement.html).

The article should contain an abstract with keywords, introduction (motivation for the work), body (adequate overview of the representative work in the field, a clear statement of the novelty in the presented research, suitable theoretical background, one or more examples to demonstrate and discuss the presented ideas), conclusion, and references (without heading and subheading enumeration). The article length should not normally exceed 16 pages of the A4 paper format with single spacing, up to a maximum of 24 pages with references and supplementary material included.

The article should be formatted following the instructions in the Article Form which can be downloaded from website page *Article form*.

Title

The title should be informative. It is in both Journal's and author's best interest to use terms suitable for indexing and word search. If there are no such terms in the title, the author is strongly advised to add a subtitle.

Letterhead title

The letterhead title is given at a top of each page for easier identification of article copies in an electronic form in particular. It contains the author's surname and first name initial (for multiple authors add "et al"), article title, journal title and collation (year, volume, issue, first and last page). The journal and article titles can be given in a shortened form.

Author's name

Full name(s) of author(s) should be used. It is advisable to give the middle initial. Names are given in their original form (with diacritic signs if in Serbian).

Author's affiliation

The full official name and seat of the author's affiliation is given, possibly with the name of the institution where the research was carried out. For organizations with complex structures, give the whole hierarchy (for example, University of Defence in Belgrade, Military Academy, Department for Military Electronic Systems). At least one organization in the hierarchy must be a legal entity. When some of multiple authors have the same affiliation, it must be clearly stated, by special signs or in other way, which department exactly they are affiliated with. The affiliation follows the author's name. The function and title are not given.

Contact details

The postal addresses or the e-mail addresses of the authors are given in the first page.

Type of articles

Classification of articles is a duty of the editorial staff and is of special importance. Referees and the members of the editorial staff, or section editors, can propose a category, but the editor-in-chief has the sole responsibility for their classification.

The *Military Technical Courier* publishes scientific articles.

Scientific articles:

– Original scientific papers (giving the previously unpublished results of the author's own research based on scientific methods);

– Review papers (giving an original, detailed and critical view of a research problem or an area to which the author has made a contribution demonstrated by self-citation);

– Short communications or Preliminary communications (original scientific full papers but shorter or of a preliminary character);

– Scientific commentaries or discussions (discussions on a particular scientific topic, based exclusively on scientific argumentation) and opinion pieces.

Exceptionally, in particular areas, a scientific paper in the Journal can be in a form of a monograph or a critical edition of scientific data (historical, archival, lexicographic, bibliographic, data survey, etc.) which were unknown or hardly accessible for scientific research.

Papers classified as scientific must have at least two positive reviews.

If the journal contains non-scientific contributions as well, the section with scientific papers should be clearly denoted in the first part of the Journal.

Short communications are usually 4-7 pages long, research articles and case studies 10-14 pages, while reviews can be longer. Page number limits are not strict and, with

appropriate reasoning, submitted manuscripts can also be longer or shorter. If extended versions of previously published conference papers are submitted, Editors will check if sufficient new material has been added to meet the journal standards and to qualify such manuscripts for the review process. The added material must not have been previously published. New results are desired but not necessarily required; however, submissions should contain expansions of key ideas, examples, elaborations, etc. of conference papers.

Language

The language of the article should be English. The grammar and style of the article should be of good quality. The systematized text should be without abbreviations (except standard ones). All measurements must be in SI units. The sequence of formulae is denoted in Arabic numerals in parentheses on the right-hand side.

Abstract and summary

An abstract is a concise informative presentation of the article content for fast and accurate evaluation of its relevance. It contains the terms often used for indexing and article search. A 100- to 250-word abstract has the following parts: introduction/purpose of the research, methods, results and conclusion.

Keywords

Keywords are terms or phrases showing adequately the article content for indexing and search purposes. They should be allocated heaving in mind widely accepted international sources (index, dictionary or thesaurus), such as the Web of Science keyword list for science in general. The higher their usage frequency is, the better. Up to 10 keywords immediately follow the abstract and the summary, in respective languages. For this purpose, the ASSISTANT system uses a special tool KWASS for the automatic extraction of key words from disciplinary thesauruses/dictionaries by choice and the routine for their selection, i.e. acceptance or rejection by author and/or editor.

Article acceptance date

The date of the reception of the article, the dates of submitted corrections in the manuscript (optional) and the date when the Editorial Board accepted the article for publication are all given in a chronological order at the end of the article.

Acknowledgements

The name and the number of the project or programme within which the article was realised is given in a separate note at the bottom of the first page together with the name of the institution which financially supported the project or programme.

Article preliminary version

If an article preliminary version has appeared previously at a meeting in a form of an oral presentation (under the same or similar title), this should be stated in a separate note at the bottom of the first page. An article published previously cannot be published in the *Military Technical Courier* even under a similar title or in a changed form.

Tables and illustrations

All the captions should be in the original language as well as in English, together with the texts in illustrations if possible. Tables are typed in the same style as the text and are denoted by Arabic numerals at the top. Photographs and drawings, placed

appropriately in the text, should be clear, precise and suitable for reproduction. Drawings should be created in Word or Corel.

For figures and graphs, proper data plot is recommended i.e. using a data analysis program such as Excel, Matlab, Origin, SigmaPlot, etc. It is not recommended to use a screen capture of a data acquisition program as a figure or a graph.

Citation in the text

Citation in the text must be uniform. The *Military Technical Courier* applies the Harvard Referencing System given in the Harvard Style Manual. When citing sources within your paper, i.e. for in-text references of the works listed at the end of the paper, place the year of publication of the work in parentheses and optionally the number of the page(s) after the author's name, e.g. (Petrovic, 2012, pp.10-12). A detailed guide on citing, with examples, can be found on *Military Technical Courier* website on the page *Instructions for Harvard Style Manual*. In-text citations should follow its guidelines. For checking in-text citations, the ASSISTANT system uses a special tool CiteMatcher to find out quotes left out within papers and in reference lists.

Footnotes

Footnotes are given at the bottom of the page with the text they refer to. They can contain less relevant details, additional explanations or used sources (e.g. scientific material, manuals). They cannot replace the cited literature.

Reference list (Literature)

The cited literature encompasses bibliographic sources such as articles and monographs and is given in a separate section in a form of a reference list. References are not translated to the language of the article.

In compiling the reference list and bibliography, the *Military Technical Courier* applies the Harvard System – Harvard Style Manual. All bibliography items should be listed alphabetically by author's name, without numeration. A detailed guide for listing references, with examples, can be found on *Military Technical Courier* website on the page *Instructions for Harvard Style Manual*. Reference lists at the end of papers should follow its guidelines. In journal evaluation systems, non-standard, insufficient or inconsequent citation is considered to be a sufficient cause for denying the scientific status to a journal.

Authorship Statement

The Authorship statement, submitted together with the paper, states authors' individual contributions to the creation of the paper. In this statement, the authors also confirm that they followed the guidelines given in *the Call for papers* and the *Publication ethics and malpractice statement of the journal*.

All articles are peer reviewed.

The list of referees of the *Military Technical Courier* can be viewed at website page *List of referees*. The article review process is described on the *Peer Review Process* page of the website.

Editorial Team

Address of the Editorial Office:
Vojnotehnički glasnik / Military Technical Courier
Veljka Lukića Kurjaka 33
11042 Belgrade, Republic of Serbia
e-mail: vojnotehnicki.glasnik@mod.gov.rs,
tel.: +381 11 3603 260

POZIV I UPUTSTVO AUTORIMA O NAČINU PRIPREME ČLANKA

Uputstvo autorima o načinu pripreme članka za objavljivanje u *Vojnotehničkom glasniku* urađeno je na osnovu Pravilnika o kategorizaciji i rangiranju naučnih časopisa Ministarstva prosvete, nauke i tehnološkog razvoja Republike Srbije („Službeni glasnik RS“, broj 159/20). Primena ovog Pravilnika prvenstveno služi unapređenju kvaliteta domaćih časopisa i njihovog potpunijeg uključivanja u međunarodni sistem razmene naučnih informacija.

Vojnotehnički glasnik / Military Technical Courier (www.vtg.mod.gov.rs, ISSN 0042-8469 – štampano izdanje, e-ISSN 2217-4753 – online, UDC 623+355/359, DOI: 10.5937/VojnotehnickiGlasnik; https://doi.org/10.5937/VojnotehnickiGlasnik), jeste recenzirani naučni časopis.

Vlasnici časopisa su Ministarstvo odbrane Republike Srbije i Vojska Srbije. Izdavač i finansijer časopisa je Univerzitet odbrane u Beogradu (Vojna akademija).

Programska orijentacija časopisa zasniva se na godišnjoj kategorizaciji časopisa, koju vrši nadležno državno ministarstvo u određenim oblastima, kao i na njegovom indeksiranju u međunarodnim indeksnim bazama.

Časopis obuhvata naučne, odnosno stručne oblasti u okviru obrazovno-naučnog polja **prirodno-matematičkih nauka**, kao i u okviru obrazovno-naučnog polja **tehničko-tehnoloških nauka**, a naročito oblasti **odbrambenih nauka i tehnologija**. Objavljuje teorijska i praktična dostignuća koja doprinose usavršavanju svih pripadnika srpske, regionalne i međunarodne akademske zajednice, a posebno pripadnika vojski i ministarstava odbrane. Publikuje radove sa uravnoteženim izveštavanjem o analitičkim, eksperimentalnim i primenjenim istraživanjima, kao i numeričkim simulacijama, obuhvatajući različite discipline. Objavljeni materijali su visokog kvaliteta i relevantnosti, napisani na način koji ih čini dostupnim širokoj čitalačkoj publici. Svi radovi koji izveštavaju o originalnim teorijskim i/ili praktično orijentisanim istraživanjima ili proširenim verzijama već objavljenih radova sa konferencija su dobrodošli. Radovi za objavljivanje odabiru se dvostruko slepim postupkom recenzije kako bi se osigurala originalnost, relevantnost i čitljivost. Pritom cilj nije samo da se kvalitet objavljenih radova održi visokim već i da se obezbedi pravovremeni, temeljni i uravnoteženi postupak recenzije.

Uređivačka politika *Vojnotehničkog glasnika zasniva* se na preporukama Odbora za etičnost u izdavaštvu (COPE Core Practices) i zajedničkim principima transparentnosti i najbolje prakse u izdavaštvu COPE, DOAJ, OASPA i WAME, kao i na najboljim prihvaćenim praksama u naučnom izdavaštvu. Vojnotehnički glasnik je član COPE (Committee on Publication Ethics) od 2. maja 2018. godine i član OASPA (Open Access Scholarly Publishers Association) od od 27. novembra 2015. godine.

Ministarstvo nauke, tehnološkog razvoja i inovacija Republike Srbije utvrdilo je decembra 2025. godine kategorizaciju Vojnotehničkog glasnika, za 2025. godinu:

- **na listi časopisa za računarske nauke:**
  kategorija vrhunski časopis nacionalnog značaja **(M51),**
- **na listi časopisa za elektroniku, telekomunikacije i informacione tehnologije:**
  kategorija vrhunski časopis nacionalnog značaja (**M51),**
- **na listi časopisa za mašinstvo:**
  kategorija vrhunski časopis nacionalnog značaja **(M51),**
- **na listi časopisa za materijale i hemijske tehnologije:**
  kategorija nacionalni časopis međunarodnog značaja (**M24).**

Usvojene liste domaćih časopisa za 2025. godinu mogu se videti na sajtu *Vojnotehničkog glasnika*, stranica *Kategorizacija časopisa*.

Detaljnije informacije mogu se pronaći i na sajtu Ministarstva prosvete, nauke i tehnološkog razvoja Republike Srbije.

Podaci o kategorizaciji mogu se pratiti i na sajtu KOBSON-a (Konzorcijum biblioteka Srbije za objedinjenu nabavku).

Kategorizacija časopisa izvršena je prema Pravilniku o kategorizaciji i rangiranju naučnih časopisa Ministarstva prosvete, nauke i tehnološkog razvoja Republike Srbije („Službeni glasnik RS", broj 159/20).

Časopis se prati u kontekstu Srpskog citatnog indeksa – SCindeks (baza podataka domaćih naučnih časopisa), Naučno-informacionog sistema Redalyc i Ruskog indeksa naučnog citiranja (RINC). Podvrgnut je stalnom vrednovanju (monitoringu) u zavisnosti od uticajnosti (impakta) u samim bazama. Detalji o indeksiranju mogu se videti na sajtu *Vojnotehničkog glasnika*, stranica *Indeksiranje časopisa*.

Vojnotehnički glasnik, u pogledu svog sadržaja, pruža mogućnost otvorenog pristupa (DIAMOND OPEN ACCESS) i primenjuje Creative Commons (CC BY) odredbe o autorskim pravima. Detalji o autorskim pravima mogu se videti na sajtu časopisa, stranica *Autorska prava i politika samoarhiviranja*.

Radovi se predaju putem onlajn sistema za elektronsko uređivanje ASISTENT, koji je razvio Centar za evaluaciju u obrazovanju i nauci (CEON).

Приступ и регистрација за сервис врше се на сајту www.vtg.mod.gov.rs, преко странице *АСИСТЕНТ* или *СЦИНДЕКС*, односно директно на линку aseestant.ceon.rs/index.php/vtg.

Detaljno uputstvo o registraciji i prijavi za servis nalazi se na sajtu www.vtg.mod.gov.rs, stranica *Uputstvo za ASISTENT*.

Potrebno je da se svi autori koji podnose rukopis za objavljivanje u *Vojnotehničkom glasniku* registruju u registar ORCID (Open Researcher and Contributor ID), prema uputstvu na stranici sajta *Registracija za dobijanje ORCID identifikacione šifre*.

Vojnotehnički glasnik objavljuje članke na engleskom jeziku (arial, veličina slova 11 pt, prored Single).

Postupak pripreme, pisanja i uređivanja članka treba da bude u saglasnosti sa *Izjavom o etičkom postupanju* (http://www.vtg.mod.gov.rs/izjava-o-etickom-postupanju.html).

Članak treba da sadrži sažetak sa ključnim rečima, uvod (motivaciju za rad), razradu (adekvatan pregled reprezentativnosti rada u njegovoj oblasti, jasnu izjavu o novini u predstavljenom istraživanju, odgovarajuću teorijsku pozadinu, jedan ili više primera za demonstriranje i diskusiju o predstavljenim idejama), zaključak i literaturu (bez numeracije naslova i podnaslova). Obim članka treba da bude do jednog autorskog tabaka (16 stranica formata A4 sa proredom Single), a najviše 24 stranice.

Članak treba da bude napisan na obrascu za pisanje članka, koji se u elektronskoj formi može preuzeti sa sajta na stranici *Obrazac za pisanje članka*.

Naslov

Naslov treba da odražava temu članka. U interesu je časopisa i autora da se koriste reči prikladne za indeksiranje i pretraživanje. Ako takvih reči nema u naslovu, poželjno je da se pridoda i podnaslov.

Tekući naslov

Tekući naslov se ispisuje sa strane svake stranice članka radi lakše identifikacije, posebno kopija članaka u elektronskom obliku. Sadrži prezime i inicijal imena autora (ako autora ima više, preostali se označavaju sa „et al." ili „i dr."), naslove rada i časopisa i

kolaciju (godina, volumen, sveska, početna i završna stranica). Naslovi časopisa i članka mogu se dati u skraćenom obliku.

Ime autora

Navodi se puno ime i prezime (svih) autora. Veoma je poželjno da se navedu i srednja slova autora. Imena i prezimena domaćih autora uvek se ispisuju u originalnom obliku (sa srpskim dijakritičkim znakovima), nezavisno od jezika na kojem je napisan rad.

Naziv ustanove autora (afilijacija)

Navodi se pun (zvanični) naziv i sedište ustanove u kojoj je autor zaposlen, a eventualno i naziv ustanove u kojoj je autor obavio istraživanje. U složenim organizacijama navodi se ukupna hijerarhija (npr. Univerzitet odbrane u Beogradu, Vojna akademija, Katedra prirodno-matematičkih nauka). Bar jedna organizacija u hijerarhiji mora biti pravno lice. Ako autora ima više, a neki potiču iz iste ustanove, mora se, posebnim oznakama ili na drugi način, naznačiti iz koje od navedenih ustanova potiče svaki od navedenih autora. Afilijacija se ispisuje neposredno nakon imena autora. Funkcija i zvanje autora se ne navode.

Kontakt podaci

Adresa ili e-adresa svih autora daje se pored imena i prezimena autora.

Kategorija (tip) članka

Kategorizacija članaka obaveza je uredništva i od posebne je važnosti. Kategoriju članka mogu predlagati recenzenti i članovi uredništva, odnosno urednici rubrika, ali odgovornost za kategorizaciju snosi isključivo glavni urednik.

Vojnotehnički glasnik objavljuje naučne članke.

Naučni članak je:

– originalan naučni rad (rad u kojem se iznose prethodno neobjavljeni rezultati sopstvenih istraživanja naučnim metodom);

– pregledni rad (rad koji sadrži originalan, detaljan i kritički prikaz istraživačkog problema ili područja u kojem je autor ostvario određeni doprinos, vidljiv na osnovu autocitata);

– kratko ili prethodno saopštenje (originalni naučni rad punog formata, ali manjeg obima ili preliminarnog karaktera);

– naučna kritika, odnosno polemika (rasprava na određenu naučnu temu, zasnovana isključivo na naučnoj argumentaciji) i osvrti.

Izuzetno, u nekim oblastima, naučni rad u časopisu može imati oblik monografske studije, kao i kritičkog izdanja naučne građe (istorijsko-arhivske, leksikografske, bibliografske, pregleda podataka i sl.), dotad nepoznate ili nedovoljno pristupačne za naučna istraživanja.

Radovi klasifikovani kao naučni moraju imati bar dve pozitivne recenzije.

Ako se u časopisu objavljuju i prilozi vannaučnog karaktera, naučni članci treba da budu grupisani i jasno izdvojeni u prvom delu sveske.

Poželjno je da obim kratkih saopštenja bude 4 do 7 stranica, naučnih članaka i studija slučaja 10 do 14 stranica, dok pregledni radovi mogu biti i duži. Broj stranica nije strogo ograničen i, uz odgovarajuće obrazloženje, prijavljeni članci takođe mogu biti duži ili kraći.

Ako su radovi koji su prethodno objavljeni na konferenciji prošireni, urednici će proveriti da li je dodato dovoljno novog materijala koji ispunjava standarde časopisa i kvalifikuje podnesak za postupak recenzije. Dodati materijal ne sme biti prethodno objavljen. Novi rezultati nisu nužno potrebni, ali su poželjni. Međutim, podnesak treba da sadrži proširene

ključne ideje, primere, razrade, itd., koji su prethodno bili sadržani u podnesku sa konferencije.

Jezik rada

Jezik rada treba da bude engleski.

Tekst mora biti jezički i stilski doteran, sistematizovan, bez skraćenica (osim standardnih). Sve fizičke veličine moraju biti izražene u Međunarodnom sistemu mernih jedinica – SI. Redosled obrazaca (formula) označava se rednim brojevima, sa desne strane u okruglim zagradama.

Sažetak

Sažetak jeste kratak informativan prikaz sadržaja članka koji čitaocu omogućava da brzo i tačno oceni njegovu relevantnost. U interesu je uredništava i autora da sažetak sadrži termine koji se često koriste za indeksiranje i pretragu članaka. Sastavni delovi sažetka su uvod/cilj istraživanja, metodi, rezultati i zaključak. Sažetak treba da ima od 100 do 250 reči i treba da se nalazi između zaglavlja (naslov, imena autora i dr.) i ključnih reči, nakon kojih sledi tekst članka.

Ključne reči

Ključne reči su termini ili fraze koje adekvatno predstavljaju sadržaj članka za potrebe indeksiranja i pretraživanja. Treba ih dodeljivati oslanjajući se na neki međunarodni izvor (popis, rečnik ili tezaurus) koji je najšire prihvaćen ili unutar date naučne oblasti. Za npr. nauku uopšte, to je lista ključnih reči Web of Science. Broj ključnih reči ne može biti veći od 10, a u interesu je uredništva i autora da učestalost njihove upotrebe bude što veća. U članku se pišu neposredno nakon sažetka.

Sistem ASISTENT u tu svrhu koristi specijalnu alatku KWASS: automatsko ekstrahovanje ključnih reči iz disciplinarnih tezaurusa/rečnika po izboru i rutine za njihov odabir, tj. prihvatanje odnosno odbacivanje od strane autora i/ili urednika.

Datum prihvatanja članka

Datum kada je uredništvo primilo članak, datum kada je uredništvo konačno prihvatilo članak za objavljivanje, kao i datumi kada su u međuvremenu dostavljene eventualne ispravke rukopisa navode se hronološkim redosledom, na stalnom mestu, po pravilu na kraju članka.

Zahvalnica

Naziv i broj projekta, odnosno naziv programa u okviru kojeg je članak nastao, kao i naziv institucije koja je finansirala projekat ili program, navodi se u posebnoj napomeni na stalnom mestu, po pravilu pri dnu prve strane članka.

Prethodne verzije rada

Ako je članak u prethodnoj verziji bio izložen na skupu u vidu usmenog saopštenja (pod istim ili sličnim naslovom), podatak o tome treba da bude naveden u posebnoj napomeni, po pravilu pri dnu prve strane članka. Rad koji je već objavljen u nekom časopisu ne može se objaviti u *Vojnotehničkom glasniku* (preštampati), ni pod sličnim naslovom i izmenjenom obliku.

Tabelarni i grafički prikazi

Poželjno je da naslovi svih prikaza, a po mogućstvu i tekstualni sadržaj, budu dati dvojezično, na jeziku rada i na engleskom jeziku.

Tabele se pišu na isti način kao i tekst, a označavaju se rednim brojevima sa gornje strane. Fotografije i crteži treba da budu jasni, pregledni i pogodni za reprodukciju. Crteže treba raditi u programu word ili corel. Fotografije i crteže treba postaviti na željeno mesto u tekstu.

Za slike i grafikone ne sme se koristiti snimak sa ekrana računara programa za prikupljanje podataka. U samom tekstu članka preporučuje se upotreba slika i grafikona neposredno iz programa za analizu podataka (kao što su Excel, Matlab, Origin, SigmaPlot i drugi).

Navođenje (citiranje) u tekstu

Način pozivanja na izvore u okviru članka mora biti jednoobrazan.

Vojnotehnički glasnik za referenciranje (citiranje i navođenje literature) primenjuje Harvardski sistem referenci, odnosno Harvardski priručnik za stil (Harvard Referencing System, Harvard Style Manual). U samom tekstu, u običnim zagradama, na mestu na kojem se vrši pozivanje, odnosno citiranje literature nabrojane na kraju članka, obavezno u običnoj zagradi napisati prezime citiranog autora, godinu izdanja publikacije iz koje citirate i, eventualno, broj stranica. Npr. (Petrović, 2012, pp.10–12).

Detaljno uputstvo o načinu citiranja, sa primerima, dato je na stranici sajta *Uputstvo za Harvardski priručnik za stil*. Potrebno je da se pozivanje na literaturu u tekstu uradi u skladu sa pomenutim uputstvom.

Sistem ASISTENT u svrhu kontrole navođenja (citiranja) u tekstu koristi specijalnu alatku CiteMatcher: otkrivanje izostavljenih citata u tekstu rada i u popisu referenci.

Napomene (fusnote)

Napomene se daju pri dnu strane na kojoj se nalazi tekst na koji se odnose. Mogu sadržati manje važne detalje, dopunska objašnjenja, naznake o korišćenim izvorima (na primer, naučnoj građi, priručnicima), ali ne mogu biti zamena za citiranu literaturu.

Lista referenci (literatura)

Citirana literatura obuhvata, po pravilu, bibliografske izvore (članke, monografije i sl.) i daje se isključivo u zasebnom odeljku članka, u vidu liste referenci. Reference se ne prevode na jezik rada i nabrajaju se u posebnom odeljku na kraju članka.

Vojnotehnički glasnik, kao način ispisa literature, primenjuje Harvardski sistem referenci, odnosno Harvardski priručnik za stil (Harvard Referencing System, Harvard Style Manual).

Literatura se obavezno piše na latiničnom pismu i nabraja po abecednom redosledu, navodeći najpre prezimena autora, bez numeracije.

Detaljno uputstvo o načinu popisa referenci, sa primerima, dato je na stranici sajta *Uputstvo za Harvardski priručnik za stil.* Potrebno je da se popis literature na kraju članka uradi u skladu sa pomenutim uputstvom..

Nestandardno, nepotpuno ili nedosledno navođenje literature u sistemima vrednovanja časopisa smatra se dovoljnim razlogom za osporavanje naučnog statusa časopisa.

Sistem ASISTENT u svrhu kontrole pravilnog ispisa liste referenci koristi specijalnu alatku RefFormatter: kontrola oblikovanja referenci u skladu sa Harvardskim priručnikom za stil.

Izjava o autorstvu

Pored članka dostavlja se Izjava o autorstvu u kojoj autori navode svoj pojedinačni doprinos u izradi članka. Takođe, u toj izjavi potvrđuju da su članak uradili u skladu sa Pozivom i uputstvom autorima i Izjavom o etičkom postupanju časopisa.

Svi radovi podležu stručnoj recenziji.

Spisak recenzenata *Vojnotehničkog glasnika* može se videti na stranici sajta *Spisak recenzenata*. Proces recenziranja objašnjen je na stranici sajta *Recenzentski postupak*.

Uredništvo

Adresa redakcije:
Vojnotehnički glasnik
Veljka Lukića Kurjaka 33
11042 Beograd
e-mail: vojnotehnicki.glasnik@mod.gov.rs
telefon: 011/3603-260

The list of the referees of the *Military Technical Courier* engaged during 2025. is available on the journal's website
http://www.vtg.mod.gov.rs/list-of-referees.html
as well as on the *Military Technical Courier* page in the Serbian Citation Index
https://scindeks.ceon.rs/EditorialBoard.aspx?issn=0042-8469&lang=en.

Spisak recenzenata Vojnotehničkog glasnika koji su angažovani tokom 2025. godine dostupan je na stranici sajta časopisa
http://www.vtg.mod.gov.rs/spisak-recenzenata.html
kao i na stranici Vojnotehničkog glasnika u Srpskom citatnom indeksu
https://scindeks.ceon.rs/EditorialBoard.aspx?issn=0042-8469.

STATEMENT OF THE *MILITARY TECHNICAL COURIER*

ON ETHICAL CONDUCT

NOTE: The editorial policy of the Military Technical Courier is based on the COPE Core Practices, common COPE, DOAJ, OASPA and WAME Principles of Transparency and Best Practice in Scholarly Publishing as well as on the best accepted practices in scientific publishing. The Military Technical Courier has been a COPE (Committee on Publication Ethics) member since 2nd May 2018 and a member of OASPA (Open Access Scholarly Publishers Association) since 27th November 2015. The editorial office applies Checklist for open access publishers on implementing the UNESCO Recommendation on Open Science. This document is part of the UNESCO Open Science Toolkit, designed to support implementation of the UNESCO Recommendation on Open Science. It has been produced in partnership with OASPA.

The main scope of the Military Technical Courier scientific journal is publishing scientific articles after peer reviewing. In the editing process leading to publishing scientific articles, it is necessary to reach an agreement on ethical principles in the behavior of all parties involved (Editorial Office i.e. Editor, members of the Editorial Board, reviewers, and authors alike). The aforementioned principles and practices are defined by this Statement of the Military Technical Courier on Ethical Conduct.

Measures, activities, responsibilities, and duties of the Military Technical Courier Editorial Office

The Editorial Office of the Military Technical Courier does not charge for submitting manuscripts from their authors nor from third parties. The whole process of processing and publishing is completely free of charge for authors – from the manuscript submission services through processing to the article publishing services. There are no hidden costs whatsoever.

The Editorial Office decides finally which manuscripts are to be published. Decisions are based only on manuscript values. In making decisions, there is no discrimination on the basis of race, sex/gender, religion, ethnic origin or political beliefs. In making decisions, the Editorial Office is guided by the Journal's policy, complying with legal regulations dealing with libel, copyright infringement and plagiarism.

Manuscripts are kept as confidential material. No information and/or ideas from manuscripts are to be used for private purposes without authors' explicit consent in writing.

In its work, following the recommendations of the Centre for Evaluation in Education and Science (CEON/CEES), the Editorial Office uses the Serbian Citation Index (SCIndeks) ASSISTANT electronic editing system which provides full transparency of the publishing process (developed on the basis of the OJS platform) while being fully responsible for accepting and publishing articles.

The editing process in the Military Technical Courier consists of the following steps of the Editorial Office:

1. After receiving manuscripts, the Office asks the authors to fill in the Authorship Statement in which they: specify their contribution to the manuscript; confirm that they are familiar with the Journal's policy regarding the retraction of already published articles; confirm that the submitted manuscript is an original paper written and signed by its authors, not previously published, not considered for publication elsewhere and not concurrently sent for review to other journals; confirm that the manuscript and the additional material contain neither any false statements that could be considered defamation, any false claims nor material that in any way endangers personal or property rights of natural or legal persons; confirm that they do not have a conflict of interest that could cast doubt on the

article's integrity and the credibility of the results published in it; confirm that they have obtained permission from copyright holders to use all content from copyright-protected works and other copyright-protected material used in the manuscript; and confirm that they have acknowledged the sources in the manuscript and supplementary material.

2. Before the Editor attends to the manuscript, the Editorial Office checks the manuscript content for plagiarism in order to establish the originality of submitted papers and prevent plagiarism and duplication. The Military Technical Courier does not publish plagiarized papers. The Editorial Office is of the opinion that plagiarism i.e. using another's ideas, words or other creative ways of contributing without acknowledging their source and presenting them as one's own is serious violation of research and publication ethics. Plagiarism may also involve copyright infringement which is violation of law.

Plagiarism involves:

- Verbatim or nearly verbatim copying or paraphrasing parts of other authors' texts without clear citing of the source purposefully, in order to hide the source;
- Copying equations, data or graphical presentations from documents of others without clearly acknowledging the source and/or without the authorization of the original author or copyright holder;

A manuscript showing obvious signs of plagiarism is rejected automatically. In case plagiarism is found in an already published article, the article is revoked (retracted) following the procedure given in point 6.

In order to prevent plagiarism, the Journal uses the iThenticate/CrossRef system within the SCIndeks Assistant service for checking manuscripts. The results obtained by such checking are verified by the Editorial Office in accordance with the COPE guidelines and recommendations.

The Military Technical Courier does not allow the use of generative AI nor AI-assisted technologies such as Large Language Models for writing papers. The use of these technologies is allowed exclusively for improving the language and readability of papers but only under strong supervision of authors. The Editorial Office of the Military Technical Courier may use forensic tools and special software to identify unethical writing of papers with the help of generative artificial intelligence and AI-assisted technologies. Papers found to have used these technologies unethically will be rejected during the editing and review process or they will be subsequently retracted if these malpractices are found in already published articles.

3. After being checked for plagiarism, a manuscript is dealt with by the Editor who continues the publishing process by choosing peer reviewers. Neither the Editorial Team nor the Editor in charge of the particular manuscript are allowed to be in a conflict of interest in the case of the manuscript in question.

If there is a conflict of interest, it is up to the Editorial Board to decide on peer reviewers and further actions regarding the manuscript. The Editorial Board members who might be in a conflict of interest are also excluded from the decision-making process in the case of the manuscript in question.

4. Manuscripts are sent to reviewers only after the initial assessment stating that, based on their form and content scope, they are eligible for publication in the Military Technical Courier. Special care is taken that the initial assessment does not last longer than necessary.

The Military Technical Courier makes use of double-blind peer review of all papers.

It is mandatory for the Editor-in-Chief and the Editorial Team members to take appropriate measures that authors and reviewers remain anonymous to each other during and after the reviewing process, in accordance with the double-blind peer review method.

The Editorial Team of the Military Technical Courier can give information on the submitted manuscript only to the author, reviewers or potential reviewers if necessary.

Every manuscript has to be reviewed by at least two reviewers who are not aware of each other's identity and who review the manuscript independently of each other. Reviewers are chosen solely based on whether they have relevant knowledge for the particular paper review. They must not have the same affiliation as the paper author(s) and they are not allowed to have been co-authors with them in the recent past. Possible suggestions of manuscript authors on engaging particular reviewers are not accepted.

The purpose of a review is to help the Editorial Team make a decision whether the paper should be accepted or rejected and to improve the quality of the manuscript through the process of communication with the Editor, authors and other reviewers. During the reviewing process, the Editor-in-Chief may ask the author to submit additional information, including raw data, if it is necessary for assessing the manuscript. The Editor and the reviewers should treat such information as confidential and should not use it for any other purpose.

The reviewing process usually lasts for four weeks maximum, and only exceptionally up to three months. The period of time from the manuscript submission to its publishing is approximately 90 days.

If authors have some serious and justifiable concern with reviews, the Office checks whether the reviews in question are objective and of academic standard. If the objectivity or quality of these reviews are questionable, the Editor engages additional peer reviewers.

Additional reviewers are also engaged when the decisions of the assigned reviewers are contradictory (accept/reject) or somehow incompatible.

The final decision on the acceptance of a manuscript for publication is made exclusively by the Editorial Team.

5. In extreme cases, especially when the choice of journals is limited due to the paper's narrow subject field, it is acceptable that the members of the Editorial Team of the Military Technical Courier may also be authors of scientific articles published in it. However, in this case, the Editorial Team ensures that the double-blind review process is even more transparent and more rigorous. This means that the Editorial Office will make every effort to maintain the integrity of the review and to minimize any bias by having another associate editor handle the review procedure independently of the editor – author in a completely transparent process. The Editorial Team will take special care that a reviewer does not recognize the author's identity. As an extra precaution, if and when such an article is published, the Editorial Team may accompany the article with a note about a high level of transparency of the editing and reviewing processes in question.

6. In case of the violation of the rights of the Military Technical Courier, copyright holders or authors as well as in case of multiple publication, fake authorship, plagiarism, data manipulation or any other malpractice, the published article must be retracted.

Articles can also be retracted for correcting numerous and/or fundamental flaws which cannot be dealt with by post-publication corrections. Retractions are issued by the Editorial Team, the author(s) or by both parties based on mutual agreement.

A retraction notice has a form of a separate paper listed in the Contents of an issue, classified as "Retraction".

Retractions are published in accordance with the COPE Guidelines elaborated by the CEON/CEES in its database where the Military Technical Courier is primarily indexed.

The CEON/CEES publishes the national citation index where the metadata of retraction notices and related retracted articles must be clearly and appropriately marked and mutually cross-linked. An electronic version of the original article (the one being retracted) is provided with a HTML link to the retraction notice. Retracted articles are

retained in their original form but with a watermark on each page of the PDF document indicating that the article in question is RETRACTED.

7. The Editorial Office is open to academic, scientifically based, collegial and productive exchange of opinions and critiques as well as for expressing possible disagreements regarding the results in articles published in the Military Technical Courier by enabling polemics and reactions to be published in the Journal's section "Letters to the Editor".

Measures, activities, responsibilities, and duties of the Military Technical Courier reviewers

Reviewers are required to assess the scientific and professional values of manuscripts in a qualified and timely manner. They have to focus especially on the genuine contribution and originality of manuscripts. A review should be completely unbiased and the reviewer's assessment unambiguous and backed with arguments.

Reviewers assess manuscripts with regard to the compliance of the content with the Journal's character, importance and effectiveness of the content, convenience of the methods applied, scientific value of the presented information as well as with regard to the style, tone and form of the text. A review has a standard form which comprises assessment of particular elements of a manuscript, general assessment and final recommendation. Personal criticism of the author is unacceptable.

Reviewers must not be in a conflict of interest with authors or research funders. If such a conflict exists, the reviewer is obliged to inform the Editor about it in due time. Reviewers should not accept to review papers out of the scope of their full competence.

They should notify the Editor-in-Chief if they have a reasonable doubt about the author violating ethical standards. A duty of reviewers is to call to the editor's attention any substantial similarity or overlap between the manuscript under consideration and any other published paper of which they have personal knowledge. Also, hey should recognize relevant sources which have not been taken into account in the manuscript. They may recommend citing particular references but must not insist on citing articles published in the Military Technical Courier or their own papers if there is no justification for doing so.

Their suggestions should aim at improving the manuscript's quality. If they conclude the paper deserves to be published but with corrections, they are required to provide detailed instructions.

Manuscripts sent to reviewers must be treated as confidential documents. The material from manuscripts must not be used for reviewers' own research without the author's explicit consent in writing.

The Editorial Office of The Military Technical Courier encourages reviewers to verify their reviews on their personal profile pages on the Web of Science (WoS) platform. When reviewers submit their peer reviews to The Military Technical Courier, they will be asked whether they would like to track, verify and showcase them on the WoS platform. Reviewers can further use their verified peer reviews as evidence of their contribution to the scientific community in applications for promotion, grants, etc.

The reviewing policy of the journal:

- allows visibility of the review in public (**only after the article has been published**),
- shows titles of reviewed articles to reviewers (**only after the article has been published**).

Measures, activities, responsibilities and duties of the Military Technical Courier authors

Authors undertake that the manuscripts are their original contribution, that they have not been published before, and that they are not considered for publication elsewhere.

Parallel submission represents violation of ethical codes which eliminates the manuscript in question from being further considered for publication in the Military Technical Courier. A paper already published elsewhere cannot be published in the Military Technical Courier.

Authors are fully responsible for the complete content of their manuscripts. The manuscript should not contain unfunded or illegal statements nor infringe on the rights of others.

When writing their papers, authors are not allowed to use generative AI nor AI-assisted technologies such as Large Language Models. These technologies are not to be used for the realization of the key authors' task which is to draw scientifically based conclusions and recommendations. Artificial intelligence tools can be used in the process of research to analyze and draw conclusions from data.

Authors are required to make sure that their team mentioned in the manuscript consisits only of individuals whose contribution to the content of the manuscript is significant. If there were other individuals who participated in some other important moments of the research project or in the manuscript preparation, their contribution is to be mentioned in a footnote or in a separate note (Acknowledgement).

The name and the code number of the research project from which the paper originates must be given in a note, as well as the full name of the funding institution. In case the paper has been presented orally elsewhere with the same title or a similar one, the details of such a communication have to be metioned in a note as well.

Authors' duty is to correctly and completely quote the sources which had a significant influence on the content of the research and the manuscript. Fragments of the manuscript, including the text, equations, graphical presentations, figures and tables, directly included from the works of others, must be clearly marked e.g. by quotation marks with a precise reference to the original source (page number) or in a separate paragraph if they are bigger in size.

Full references of all citations in the main text must be given in a separate section (References) in a uniform way, complying with the citation style used in the Military Technical Courier (Harvard Style Manual). The Reference Section contains only the cited sources, not all sources used in the preparation of the manuscript.

In case authors find an error in their article after its publication, they are obliged to promptly notify the Editor-in-Chief (or the Editorial Office) and cooperate in the process of retracting or correcting the article.

Authors are under the obligation to declare in their manuscript whether there is a financial or any other conflict of interest that may influence the results or interpretations of the results.

If the research involves chemicals, activities or equipment posing risk to the health of humans or animals, this must be clearly stated in the manuscript.

When submitting their manuscript, authors agree to comply with the editorial policy of the Military Technical Courier and they confirm such compliance by submitting the Authorship Statement.

Handling allegations of misconduct

Any individual or institution may notify the Editor and/or Editorial Team of ethical malpractice and other misconduct by supplying undisputed information/evidence to start an enquiry. The procedure for investigating the case raised with the supplied evidence is as follows:

- Editor-in-Chief determines to start investigation;
- all evidence is considered confidential during investigation and is available only to those directly involved in the case;
- individuals suspected of ethical breaches are given a chance to respond to the allegations;
- if a misconduct is confirmed, it is further established whether there is a minor or a major violation of publication ethics.
- Minor issues not affecting either the integrity of the paper or that of the Journal, e.g. misunderstanding or misapplication of publication standards, are dealt with by directly communicating authors and reviewers, without third parties involved, in one of the following ways:
- authors and/or reviewers are sent a letter of warning;
- a correction notice is published, e.g. when a source, otherwise properly cited within the main text, has been omitted from the Reference List;
- an erratum is published, e.g. when an error is made by the Editorial staff. Serious, major violations of the ethical code may lead to different measures:
- a separate note or a leading article is published, describing the case;
- afilliate institution of the author/reviewer is officially notified;
- the published article is retracted;
- publishing in the Journal is prohibited for a defined period of time;
- relevant organisations and regulatory bodies are informed about the case for taking course of actions within their competence.

These measures may be taken separately or jointly. In the process of handling the case, relevant expert organisations, bodies or individuals are consulted when necessary.

In resolving ethically controversial issues, the Editorial Team follows the guidelines of the Committee on Publication Ethics (COPE).

Disclaimer

The views in the published articles do not represent the views of the Editor, the Editorial Office, the Editorial Team or the Editorial Board of the Military Technical Courier journal. Authors take full legal and moral responsibility for the information and opinions expressed in their articles. The publisher will not be held liable in any way for any claims or damages.

Conflict of interest

The Military Technical Courier adheres to the conflict of interest policy recommended by COPE and/or other international research publishing regulatory authorities (ICMJE, EASE). The authors must declare their conflicts of interest in the Conflict of Interest Statement (CoIS). In the CoIS, each named author of the article is required to provide: (1) A statement of any potential conflicts of interest relevant to the content or a statement that there are no such conflicts. (2) Disclosure of how the article is funded, including specific disclosure of any and all company funding (partial or total), or a statement that there was no such involvement (if applicable). (3) A comprehensive

explanation of the role of sponsors in article preparation if the article is sponsored in part or whole.

Advertising

Advertising in the Military Technical Courier is not permitted.

Details on the ethical conduct of the Military Technical Courier are also available on the Journal pages: ***Publication Policy, Journal Quality Management and Article Quality Support*** *via the website of the Serbian Citation Index (SCIndex) – publisher of the national citation index, i.e. publisher of the base in which the Military Technical Courier is primarily indexed.*

IZJAVA VOJNOTEHNIČKOG GLASNIKA O ETIČKOM POSTUPANJU

NAPOMENA: Uređivačka politika Vojnotehničkog glasnika zasniva se na preporukama Odbora za etičnost u izdavaštvu (COPE Core Practices) i zajedničkim principima transparentnosti i najbolje prakse u izdavaštvu COPE, DOAJ, OASPA i WAME, kao i na najboljim prihvaćenim praksama u naučnom izdavaštvu. Vojnotehnički glasnik je član COPE (Committee on Publication Ethics) od 2. maja 2018. godine i član OASPA (Open Access Scholarly Publishers Association) od od 27. novembra 2015. godine. Uredništvo primenjuje Kontrolnu listu za izdavače otvorenog pristupa o sprovođenju Preporuke UNESKO-a o otvorenoj nauci. Ovaj dokument je deo Uneskovog kompleta alata za otvorenu nauku, osmišljenog da podrži implementaciju Preporuke Uneska o otvorenoj nauci. Proizveden je u partnerstvu sa OASPA.

Osnovna delatnost naučnog časopisa Vojnotehnički glasnik je objavljivanje članaka nakon stručne recenzije. U procesu uređivanja, koji ima za cilj objavljivanje naučnih članaka, neophodno je postići saglasnost o etičkim načelima u postupcima svih učesnika (redakcije, tj. urednika, članova Uređivačkog odbora i recenzenata časopisa, kao i samih autora). Pomenuta načela i postupci definisani su ovom Izjavom Vojnotehničkog glasnika o etičkom postupanju.

Mere, radnje, odgovornosti i obaveze redakcije Vojnotehničkog glasnika

Uredništvo Vojnotehničkog glasnika ne traži od autora, niti od trećih strana, plaćanje naknade za apliciranje članka za objavljivanje. Čitav postupak uređivanja i objavljivanja članka za autore je potpuno besplatan, kako usluge prijavljivanja rukopisa i njihove obrade, tako i usluge publikovanja članaka. Ne postoje bilo kakvi skriveni troškovi.

Uredništvo Vojnotehničkog glasnika donosi konačnu odluku o tome koji će se rukopisi objaviti. Odluke se donose isključivo na osnovu vrednosti rukopisa. Moraju biti oslobođene rasnih, polnih/rodnih, verskih, etničkih ili političkih predrasuda. Prilikom donošenja odluke o objavljivanju uredništvo se rukovodi uređivačkom politikom, vodeći računa o zakonskim propisima koji se odnose na klevetu, kršenja autorskih prava i plagiranje.

Rukopisi se čuvaju kao poverljiv materijal. Informacije i ideje sadržane u rukopisima ne smeju se koristiti u lične svrhe bez izričite pisane dozvole autora.

U svom radu, prema preporuci Centra za evaluaciju u obrazovanju i nauci (CEON), Redakcija koristi elektronski sistem uređivanja časopisa SCIndeks (Srpski citatni indeks) ASISTENT (razvijen na bazi platforme OJS), koji omogućava transparentnost i javnost rada, podrazumevajući punu odgovornost za prihvatanje i objavljivanje članka.

Proces uređivanja članka u Vojnotehničkom glasniku podrazumeva sledeće obaveze Redakcije:

1. Nakon prijema članka, Redakcija od autora pribavlja Izjavu o autorstvu u kojoj autori: navode svoj pojedinačni doprinos u izradi članka; potvrđuju da su upoznati sa politkom časopisa u vezi sa povlačenjem već objavljenih radova; potvrđuju da poslati rukopis predstavlja originalan rad koji su napisali i potpisali navedeni autori i koji nije objavljen ranije na nekom drugom mestu, te da se rukopis ne razmatra za objavljivanje na drugom mestu i nije istovremeno poslat na recenziju u druge časopise; potvrđuju da članak i dodatni materijali ne sadrže tvrdnje koje bi se mogle smatrati klevetom ili bilo kakve nezakonite tvrdnje i ne sadrže materijal koji na bilo koji način ugrožava lična ili vlasnička prava fizičkih ili pravnih lica; potvrđuju da nemaju sukob interesa koji bi mogao da dovede u pitanje integritet i verodostojnost rezultata koji su objavljeni u članku, kao i da su dobili saglasnost od nosilaca autorskih prava za korišćenje svih izvoda iz dela zaštićenih

autorskim pravima i drugih materijala zaštićenih autorskim pravima koji su korišćeni u rukopisu i da su naveli izvore u rukopisu i dodatnim materijalima.

2. Pre dodele rukopisa uredniku Redakcija proverava da li je sadržaj rukopisa plagijat, radi provere originalnosti prispelih radova i sprečavanja publikovanja plagijata i duplikata. Vojnotehnički glasnik ne objavljuje plagirane radove. Uredništvo polazi od stava da je plagiranje, odnosno preuzimanje tuđih ideja, reči ili drugih oblika kreativnog doprinosa i njihovo predstavljanje kao sopstvenih, grubo kršenje naučne i izdavačke etike. Plagiranje može da uključuje i kršenje autorskih prava, što je zakonom kažnjivo.

Plagiranje obuhvata:

- doslovno (reč po reč) ili gotovo doslovno preuzimanje ili smišljeno, radi prikrivanja izvora, parafraziranje delova tekstova drugih autora bez jasnog naznačavanja izvora;
- kopiranje jednačina, podataka ili tabela iz drugih dokumenata bez pravilnog naznačavanja izvora i/ili bez dozvole izvornog autora ili nosioca autorskog prava.Рукопис у којем се утврде јасне индиције да је плагиран биће аутоматски одбијен. У случају да се плагијаризам открије у већ објављеном раду, чланак ће бити опозван (повучен) у складу са процедуром описаном у тачки 6.

Radi sprečavanja plagijata u časopisu rukopisi se podvrgavaju proveri uz pomoć sistema iThenticate/CrossRef u okviru servisa SCIndeks ASISTENT. Rezultate dobijene proverom verifikuje uredništvo časopisa u skladu sa smernicama i preporukama Komiteta za etiku publikovanja (COPE).

Vojnotehnički glasnik ne dozvoljava upotrebu generativne veštačke inteligencije (engl. generative AI), kao ni tehnologija podržanih veštačkom inteligencijom (engl. AI-assisted), kao što su veliki jezički modeli (engl. Large Language Models), za pisanje rada. Upotreba ovih tehnologija dozvoljena je jedino za unapređenje jezika i čitljivosti rada, ali uz strogu kontrolu autora. Redakcija Vojnotehničkog glasnika može koristiti forenzičke alate i specijalne softvere za identifikaciju neregularnog pisanja rada pomoću generativne veštačke inteligencije i tehnologija podržanih veštačkom inteligencijom. Radovi kod kojih se utvrdi neregularno korišćenje ovih tehnologija biće odbijeni u procesu uređivanja i recenzije ili naknadno opozvani ako se ovi nedostaci utvrde u već objavljenim člancima.

3. Nakon provere na plagijarizam Redakcija dodeljuje prispeli rukopis uredniku koji će nadalje voditi uređivački proces i odabrati recenzente. Uredništvo i urednik kojem je dodeljen prispeli članak ne smeju biti u sukobu interesa u vezi sa rukopisom koji razmatraju.

Ako takav sukob interesa postoji, o izboru recenzenata i sudbini rukopisa odlučuje Uređivački odbor. Članovi Uređivačkog odbora za koje se pretpostavi da bi mogli biti u sukobu interesa takođe ne učestvuju u postupku odlučivanja o određenom rukopisu.

4. Rukopisi se upućuju na recenziju tek nakon inicijalne ocene da li su, s obzirom na formu i tematski delokrug, podobni za objavljivanje u Vojnotehničkom glasniku. Posebna se vodi računa da inicijalna ocena ne traje duže nego što je neophodno.

Vojnotehnički glasnik primenjuje postupak „dvostrukog anonimnog recenziranja svih radova".

Glavni urednik i članovi uredništva dužni su da preduzmu odgovarajuće mere da autori i recenzenti ostanu međusobno anonimni tokom i nakon procesa recenzije, u skladu sa dvostrukim slepim procesom recenzije. Pored toga, uredništvo Vojnotehničkog glasnika može pružiti informaciju o pristiglom rukopisu samo autoru, recenzentima ili potencijalnim recenzentima, ukoliko je to potrebno.Сваки рукопис рецензирају бар два рецензента, независно један од другог, а њихов идентитет је међусобно непознат. Рецензенти се бирају искључиво према томе да ли располажу релевантним знањима за оцену рукописа. Не смеју бити из исте институције као аутори рукописа, нити бити њихови

коаутори у скоријој прошлости. Евентуални предлози аутора рукописа да се ангажују одређени рецензенти не уважавају се.

Cilj recenzije jeste da uredništvu pomogne u donošenju odluke da li rad treba prihvatiti ili odbiti, kao i da se u procesu komunikacije s urednikom, autorima i drugim recenzentima poboljša kvalitet rukopisa.

Tokom postupka recenzije glavni urednik može da zahteva od autora da dostave dodatne informacije, uključujući i primarne podatke, ako su one neophodne za donošenje suda o rukopisu. Urednik i recenzenti moraju da čuvaju takve informacije kao poverljive i ne smeju ih upotrebiti u druge svrhe.

U redovnim okolnostima postupak recenziranja traje najviše četiri nedelje, a samo izuzetno do tri meseca. Period od prijema rada do njegovog objavljivanja traje, u proseku, 90 dana.

U slučaju da autori imaju ozbiljne i osnovane zamerke na recenziju, uredništvo proverava da li je ona objektivna i da li zadovoljava akademske standarde. Ako se posumnja u objektivnost ili kvalitet recenzije, urednik angažuje dodatne recenzente.

Dodatni recenzenti se angažuju i u slučaju kada su odluke postojeća dva recenzenta međusobno oprečne (odbiti/prihvatiti) ili na drugi način nepomirljive.

Konačnu odluku o prihvatanju rukopisa za objavljivanje donosi isključivo uredništvo.

5. U izuzetnim slučajevima, a posebno u onim okolnostima kada je izbor časopisa ograničen zbog specifične tematike članka, članovi uredništva časopisa Vojnotehnički glasnik mogu biti i autori njegovih naučnih radova. Ipak, u ovom slučaju uredništvo sprovodi dodatno transparentniji i rigorozniji dvostruko slepi proces recenzije. To podrazumeva da će Redakcija časopisa uložiti napor da održi integritet recenzije i neobjektivnost svede na najmanju moguću meru, tako što će drugi urednik saradnik voditi proceduru recenzije nezavisno od urednika autora, pri čemu će taj proces biti apsolutno transparentan. Uredništvo će posebno voditi računa da recenzent ne prepozna ko je napisao rad. Kao dodatnu meru predostrožnosti, ako i kada se takav članak objavi, uredništvo može objaviti propratni komentar koji pokazuje koliko je proces uređivanja i recenzije bio transparentan.

6. U slučaju kršenja prava Vojnotehničkog glasnika, nosilaca autorskih prava ili samih autora, objavljivanja istog rukopisa u više časopisa, lažnog autorstva, plagijata, manipulacije podacima radi prevare ili bilo koje druge zloupotrebe, objavljeni rad se mora opozvati.

Članak se može opozvati i zato da bi se ispravile ozbiljne i brojne omaške koje nije moguće obuhvatiti objavljivanjem ispravke. Opoziv objavljuje uredništvo, autor(i) ili obe strane sporazumno.

Opoziv ima oblik zasebnog rada koji se prikazuje u sadržaju sveske i urednički klasifikuje kao Opoziv ili Retrakcija.

Opozivi se publikuju prema zahtevima COPE koje je razradio CEON, kao izdavač baze u kojoj se Vojnotehnički glasnik primarno indeksira, odnosno izdavač nacionalnog citatnog indeksa gde se metapodaci opoziva i opozvanih radova moraju označiti odgovarajućim upozorenjima i međusobno povezati unakrsnim linkovima:

U elektronskoj verziji izvornog članka (onog koji se povlači) uspostavlja se veza (HTML link) sa obaveštenjem o povlačenju. Povučeni članak se čuva u izvornoj formi, ali sa vodenim žigom na PDF dokumentu, na svakoj stranici, koji ukazuje da je članak povučen (RETRACTED).

7. Redakcija je otvorena za akademsku, naučno zasnovanu, kolegijalnu i podsticajnu razmenu mišljenja i kritiku, odnosno za iznošenje eventualnih neslaganja u vezi sa rezultatima objavljenim u člancima Vojnotehničkog glasnika, time što će pružiti mogućnost učesnicima da njihovi predmetni dopisi ili polemike budu objavljeni u rubrici časopisa „Pisma uredniku”.

Mere, radnje, odgovornosti i obaveze recenzenata Vojnotehničkog glasnika

Recenzenti su dužni da kvalifikovano i u zadatim rokovima dostave uredniku ocenu naučne, odnosno stručne vrednosti rukopisa. Recenzent vodi posebnu brigu o stvarnom doprinosu i originalnosti rukopisa. Recenzija mora biti sasvim objektivna, a sud recenzenta jasan i potkrepljen argumentima.

Recenzenti ocenjuju rukopise u odnosu na usklađenost sadržaja s profilom Vojnotehničkog glasnika, značaj i korisnost sadržaja, adekvatnost primenjenih metoda, naučnu vrednost sadržanih informacija, stil izlaganja i opremljenost teksta. Recenzija ima standardni format koji obuhvata ocene pojedinih dimenzija rada, opštu ocenu i zaključnu preporuku. Neprihvatljiva je lična kritika autora.

Recenzent ne sme biti u sukobu interesa sa autorima ili finansijerom istraživanja. Ukoliko takav sukob postoji, recenzent je dužan da o tome pravovremeno obavesti urednika. Recenzent ne prihvata na recenziju radove izvan oblasti za koju se smatra potpuno kompetentnim.

Recenzenti treba da upozore glavnog urednika ako osnovano sumnjaju ili imaju saznanje o povredama etičkih standarda od strane autora rukopisa. Dužnost recenzenta jeste da skrene pažnju uredniku na značajna podudaranja ili sličnost rukopisa sa već objavljenim radom, ukoliko o tome ima lična saznanja. Takođe, treba da prepozna relevantne izvore koji u radu nisu uzeti u obzir. Može da preporuči citiranje određenih referenci, ali ne sme da zahteva citiranje radova objavljenih u časopisu Vojnotehnički glasnik ili svojih radova, ako za to ne postoji opravdanje.

Od recenzenata se očekuje da svojim sugestijama unaprede kvalitet rukopisa. Ako ocene da rad zaslužuje objavljivanje uz korekcije, dužni su da preciziraju način na koji to može da se ostvari.

Rukopisi koji su poslati recenzentu moraju se smatrati poverljivim dokumentima. Recenzenti ne smeju da koriste materijal iz rukopisa za svoja istraživanja bez izričite pisane dozvole autora.

Redakcija Vojnotehničkog glasnika podstiče recenzente da recenzije verifikuju na svojim personalizovanim stranicama na platformi Web of Science (WoS). Kada recenzent uradi recenziju članka za Vojnotehnički glasnik biće pitan da li želi da prati, potvrdi i dobije priznanje za svoj rad na platformi WoS. Recenzent zatim može koristiti svoju verifikovanu recenziju kao dokaz o svojim doprinosima naučnoj zajednici u aplikacijama za promociju, finansiranje i sl.

Recenzentska politika časopisa:

– omogućava javno prikazivanje recenzije (isključivo nakon objavljivanja članka),

– recenzentima prikazuje naslove recenziranog članka (isključivo nakon objavljivanja članka).

Mere, radnje, odgovornosti i obaveze autora koji pišu članke za Vojnotehnički glasnik

Autori garantuju da rukopis predstavlja njihov originalan doprinos, da nije objavljen ranije i da se ne razmatra za objavljivanje na drugom mestu. Istovremeno predavanje istog rukopisa u više časopisa predstavlja kršenje etičkih standarda, što ga isključuje iz daljeg razmatranja za objavljivanje u Vojnotehničkom glasniku. Rad koji je već objavljen na nekom drugom mestu ne može biti preštampan u časopisu Vojnotehnički glasnik.

Autori snose svu odgovornost za celokupni sadržaj rukopisa. Rukopis ne sme da sadrži neosnovane ili nezakonite tvrdnje, niti da krši prava drugih lica.

Prilikom pisanja rada, autori ne smeju koristiti generativne veštačke inteligencije (engl. generative AI), kao ni tehnologije podržane veštačkom inteligencijom (engl. AI-assisted), kao što su veliki jezički modeli (engl. Large Language Models). Ove tehnologije se ne mogu koristiti za realizaciju ključnog zadatka autora, a to je izvođenje zaključaka i

preporuka koji su naučno zasnovani. Alati veštačke inteligencije se mogu koristiti u procesu istraživanja za analizu i izvođenje zaključaka iz podataka.

Autori su dužni da obezbede da njihov autorski tim naveden u rukopisu obuhvati samo ona lica koja su značajno doprinela sadržaju rukopisa. Ako su u bitnim aspektima istraživačkog projekta i pripreme rada učestvovala i druga lica, njihov doprinos treba navesti u fusnoti ili posebnoj napomeni (Zahvalnica, Acknowledgements).

Obaveza je autora da u napomeni navedu naziv i kodnu oznaku naučnoistraživačkog projekta u okviru kojeg je rad nastao, kao i pun naziv finansirajuće institucije. U slučaju da je rad pod istim ili sličnim naslovom bio izložen na nekom skupu u vidu usmenog saopštenja, detalji o tome treba da budu navedeni na istom mestu.

Autori su dužni da potpuno i pravilno citiraju izvore koji su značajno uticali na sadržaj istraživanja i rukopisa. Delovi rukopisa, uključujući tekst, jednačine, slike ili tabele, koji su doslovno preuzeti iz drugih radova, moraju biti jasno označeni posebnom napomenom, npr. znacima navoda sa preciznom oznakom mesta preuzimanja (broja stranice) ili, ako su obimniji, navedeni u zasebnom paragrafu.

Pune reference svih navoda u tekstu (citata) moraju biti navedene u zasebnom odeljku (Literatura) i to na jednoobrazan način, u skladu sa citatnim stilom koji Vojnotehnički glasnik koristi (Harvard Style Manuel). U odeljku Literatura navode se samo citirani, a ne i ostali izvori korišćeni prilikom pripreme rukopisa.

U slučaju da autori otkriju važnu grešku u svom radu nakon njegovog objavljivanja, dužni su da odmah o tome obaveste glavnog urednika (ili Redakciju Vojnotehničkog glasnika) i da sarađuju u procesu povlačenja ili ispravljanja rada.

Obaveza je autora da u rukopisu navedu da li su u finansijskom ili bilo kom drugom bitnom sukobu interesa koji bi mogao da utiče na njihove rezultate ili interpretaciju rezultata.

Ako se u autorovom istraživanju pojavljuju hemijska jedinjenja, postupci ili oprema koji su opasni po zdravlje ljudi ili životinja, to mora biti jasno naznačeno u rukopisu.

Predavanjem rukopisa autori se obavezuju na poštovanje uređivačke politike časopisa Vojnotehnički glasnik, što potvrđuju dostavljanjem Izjave o autorstvu.

Razrešavanje spornih situacija

Svaki pojedinac ili institucija mogu uredniku i/ili uredništvu prijaviti saznanja o kršenju etičkih standarda i drugim nepravilnostima i o tome dostaviti verodostojne informacije/dokaze radi pokretanja istrage. Postupak provere iznetih dokaza odvija se na sledeći način:

– glavni urednik donosi odluku o pokretanju istrage;
– tokom tog postupka svi dokazi se smatraju poverljivim materijalom i predočavaju samo onim licima koja su direktno obuhvaćena slučajem;
– osumnjičenim licima pruža se prilika da odgovore na iznete optužbe;
– ako se utvrdi da je zaista došlo do nepravilnosti, ocenjuje se da li je reč o manjem prekršaju ili grubom kršenju etičkih standarda.

Manji prekršaji, bez posledica po integritet rada i Vojnotehničkog glasnika, na primer kada je reč o nerazumevanju ili pogrešnoj primeni publicističkih standarda, razrešavaju se u direktnoj komunikaciji s autorima i recenzentima, bez uključivanja trećih lica, na neki od sledećih načina:

– autorima i/ili recenzentima upućuje se pismo upozorenja;
– objavljuje se ispravka rada, na primer u slučaju kada se sa spiska referenci izostave izvori koji su u samom tekstu citirani na propisan način;
– objavljuje se eratum, na primerukoliko se ispostavi da je greška nastala omaškom uredništva.

U slučaju grubog kršenja etičkih standarda, uredništvo može da preduzme različite mere:

– objavljuje saopštenje ili uvodnik u kojem se slučaj opisuje;
– službeno obaveštava afilijativnu organizaciju autora/recenzenta;
– povlači objavljeni rada;
– izriče zabranu objavljivanja u časopisu na određeni period;
– predočava slučaj nadležnim organizacijama i regulatornim telima radi preduzimanja mera iz njihove nadležnosti.

Ove mere mogu se primenjivati pojedinačno ili istovremeno. U procesu razrešavanja slučaja po potrebi se konsultuju relevantne ekspertske organizacije, tela ili pojedinci.

Prilikom razrešavanja etički spornih postupaka uredništvo se rukovodi smernicama Komiteta za etiku publikovanja (COPE).

Odricanje odgovornosti

Izneseni stavovi u objavljenim radovima ne izražavaju stavove urednika, članova Redakcije i Uređivačkog odbora časopisa Vojnotehnički glasnik. Autori preuzimaju pravnu i moralnu odgovornost za ideje iznesene u svojim radovima.

Izneseni stavovi u objavljenim radovima ne izražavaju stavove urednika, članova Redakcije i Uređivačkog odbora časopisa Vojnotehnički glasnik. Autori preuzimaju pravnu i moralnu odgovornost za ideje iznesene u svojim radovima. Izdavač neće snositi nikakvu odgovornost u slučaju ispostavljanja bilo kakvih zahteva za naknadu štete.

Sukob interesa

Vojnotehnički glasnik se pridržava politike sukoba interesa koju preporučuju COPE i/ili druga međunarodna regulatorna tela (ICMJE, EASE). Od autora se traži da se izjasne o svom sukobu interesa u Izjavi o sukobu interesa. U Izjavi su autori dužni da navedu: 1) izjavu o svim potencijalnim sukobima interesa za svakog imenovanog autora relevantnu za sadržaj članka ili izjavu da nemaju takve sukobe; 2) tvrdnja o načinu na koji je članak finansiran, konkretno o finansiranju, delimično ili potpuno, od strane neke kompanije ili, alternativno, tvrdnja da nije bilo tog učešća i 3) sveobuhvatno objašnjenje uloge sponzora u pripremi članka ako je članak sponzorisan, bilo u celini ili delimično.

Reklamiranje

Nije dozvoljeno reklamiranje u Vojnotehničkom glasniku.

Detalji o etičkom postupanju Vojnotehničkog glasnika dostupni su i na stranicama časopisa: Uređivačka politika, Upravljanje kvalitetom časopisa, Podrška kvalitetu radova u Srpskom citatnom indeksu – izdavaču baze u kojoj se Vojnotehnički glasnik primarno indeksira, odnosno izdavaču nacionalnog citatnog indeksa.

Graphic design editor
Marija Marić, e-mail: marija.maric@mod.gov.rs

Proofreading,
English translation and language editing
Maja Hristić, e-mail: maja.hristic@hotmail.com

CIP – Cataloguing in the publication
National Library of Serbia, Belgrade

623+355/359

VOJNOTEHNIČKI glasnik : naučni časopis Ministarstva odbrane i Vojske Srbije = Military Technical Courier : Scientific Journal of the Ministry of Defence and Serbian Armed Forces / glavni i odgovorni urednik Dragan Trifković. - God. 1, br. 1 (1953)- . - Beograd : Univerzitet odbrane u Beogradu, Vojna akademija, 1953- (Beograd : Vojna štamparija). - 23 cm

Tromesečno. - Glavni stvarni naslov od br. 1 (2026) Military Technical Courier. - Tekst na engl. jeziku. - Drugo izdanje na drugom medijumu: Vojnotehnički glasnik (Online) = ISSN 2217-4753
ISSN 0042-8469 = Војнотехнички гласник
COBISS.SR-ID 4423938

Price: 600.00 RSD

Printed in 100 copies

According to the Opinion of the Ministry of Science and Technological Development No. 413-00-1201/2001-01 of 12 September 2001, *Military Technical Courier* is a publication of special interest for science.

UDC: National Library of Serbia, Belgrade

Address: Vojnotehnički glasnik/Military Technical Courier,
Veljka Lukića Kurjaka 33, 11042 Belgrade, Republic of Serbia

https://www.scopus.com/sourceid/21101207440
http://www.vtg.mod.gov.rs/index-e.html
http://aseestant.ceon.rs/index.php/vtg/issue/current
http://scindeks.nb.rs/journaldetails.aspx?issn=0042-8469
https://www.redalyc.org/revista.oa?id=6617
http://elibrary.ru/title_about.asp?id=53280
https://doaj.org/toc/2217-4753

Military Technical Courier has entered into an electronic licensing agreement with EBSCO Publishing. The full text of *Military Technical Courier* can be found in EBSCO Publishing databases.

e-mail: vojnotehnicki.glasnik@mod.gov.rs, X: @MilTechCourier
Subscription to print edition: e-mail: vojnotehnicki.glasnik@mod.gov.rs;

The journal is published quarterly.

The first printed issue of the *Military Technical Courier* was published on 1 January 1953.
The first electronic edition of the *Military Technical Courier* was published online on 1 January 2011.

Printed by Vojna štamparija, Belgrade, Ratka Resanovica 1,
e-mail: vojna.stamparija@mod.gov.rs

Likovno-grafički urednik
Marija Marić, e-mail: marija.maric@mod.gov.rs

Prevodilac i lektor za engleski jezik
Maja Hristić, e-mail: maja.hristic@hotmail.com

CIP – Katalogizacija u publikaciji
Narodna biblioteka Srbije, Beograd

6623+355/359

VOJNOTEHNIČKI glasnik : naučni časopis Ministarstva odbrane i Vojske Srbije = Military Technical Courier : Scientific Journal of the Ministry of Defence and Serbian Armed Forces / glavni i odgovorni urednik Dragan Trifković. - God. 1, br. 1 (1953)- . - Beograd : Univerzitet odbrane u Beogradu, Vojna akademija, 1953- (Beograd : Vojna štamparija). - 23 cm

Tromesečno. - Glavni stvarni naslov od br. 1 (2026)
Military Technical Courier. - Tekst na engl. jeziku. -
Drugo izdanje na drugom medijumu:
Vojnotehnički glasnik (Online) = ISSN 2217-4753
ISSN 0042-8469 = Војнотехнички гласник
COBISS.SR-ID 4423938

Cena: 600,00 dinara

Tiraž: 100 primeraka

Na osnovu mišljenja Ministarstva za nauku, tehnologiju i razvoj Republike Srbije, broj 413-00-1201/2001-01 od 12. 9. 2001. godine, časopis „Vojnotehnički glasnik" je publikacija od posebnog interesa za nauku.

UDK: Narodna biblioteka Srbije, Beograd

Adresa redakcije: Vojnotehnički glasnik,
Veljka Lukića Kurjaka 33,11042 Beograd

https://www.scopus.com/sourceid/21101207440
http://www.vtg.mod.gov.rs
http://aseestant.ceon.rs/index.php/vtg/issue/current
http://scindeks.nb.rs/journaldetails.aspx?issn=0042-8469
https://www.redalyc.org/revista.oa?id=6617
http://elibrary.ru/title_about.asp?id=53280
https://doaj.org/toc/2217-4753

Vojnotehnički glasnik je licenciran kod EBSCO Publishing-a.

Kompletan tekst *Vojnotehničkog glasnika* dostupan je u bazama podataka EBSCO Publishing-a.

e-mail: vojnotehnicki.glasnik@mod.gov.rs; X: @MilTechCourier

Pretplata na štampano izdanje: e-mail: vojnotehnicki.glasnik@mod.gov.rs;

Časopis izlazi tromesečno.

Prvi štampani broj Vojnotehničkog glasnika objavljen je 1.1.1953. godine.

Prvo elektronsko izdanje Vojnotehničkog glasnika na Internetu objavljeno je 1.1.2011. godine

Štampa: Vojna štamparija, Beograd, Ratka Resanovica 1,
e-mail: vojna.stamparija@mod.gov.rs

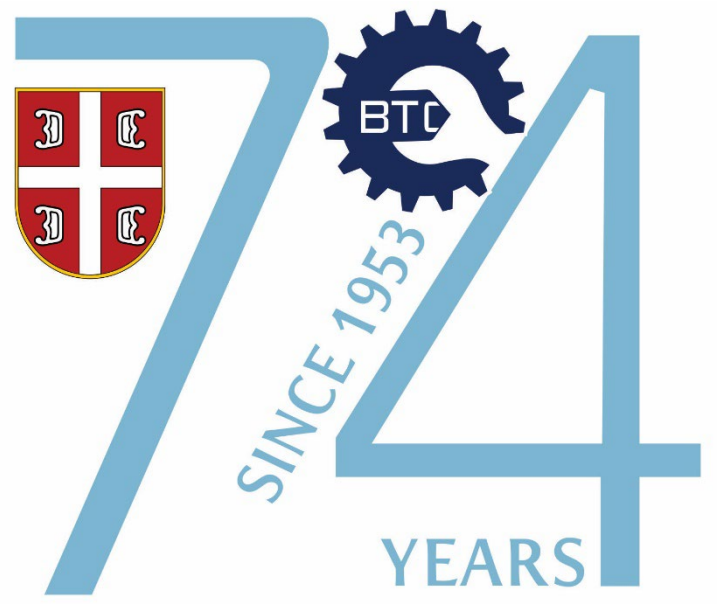
BTC
SINCE 1953
74
YEARS

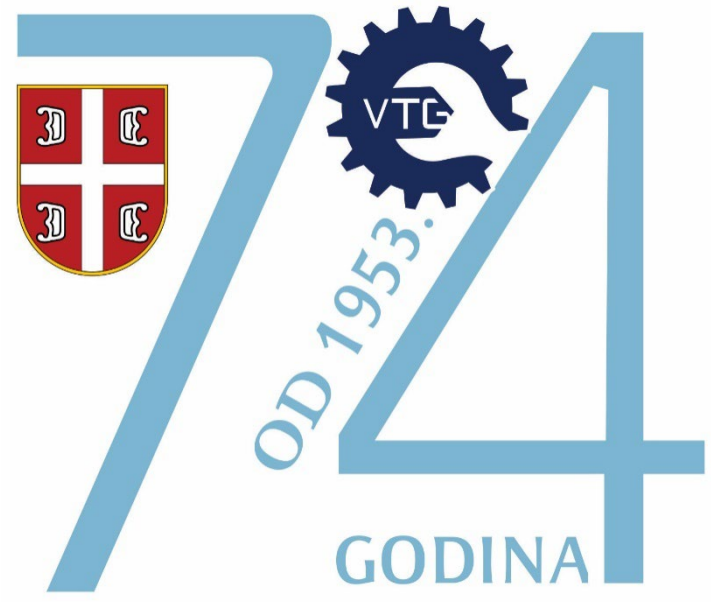
VTC
OD 1953.
74
GODINA

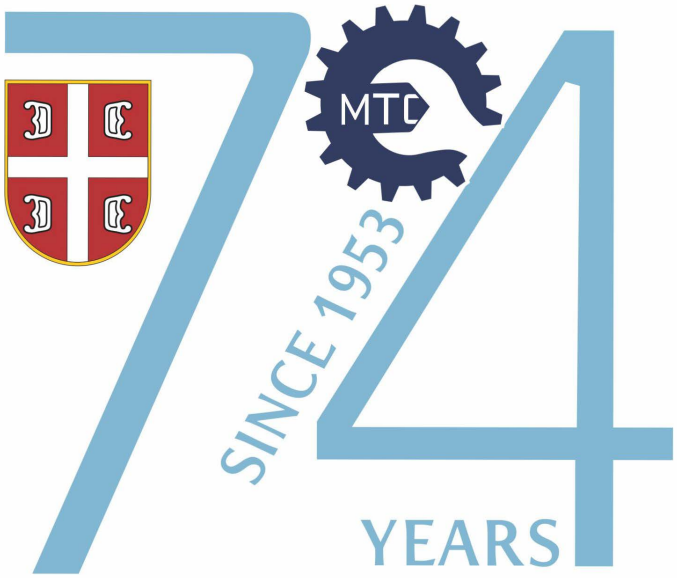
MTC
SINCE 1953
74
YEARS


VTC
OD 1953.
74
GODINA

ISSN 0042-8469
e-ISSN 2217-4753
UDC 623 + 355/359

SCIENTIFIC JOURNAL OF THE MINISTRY OF DEFENCE AND SERBIAN ARMED FORCES

MILITARY TECHNICAL COURIER

VOLUME 74 • NUMBER 1 • JANUARY – MARCH 2026.

NAUČNI ČASOPIS MINISTARSTVA ODBRANE I VOJSKE SRBIJE

VOJNOTEHNIČKI GLASNIK

VOLUMEN 74 • BROJ 1 • JANUAR – MART 2026.

www.vtg.mod.gov.rs
COBISS.SR-ID 4423938
DOI: 10.5937/VojnotehnickiGlasnik